Poly(ethylene glycol) Hydrogels to Engineer the Mesenchymal Stromal Cell Secretome

By

Varsha Vinay Rao

B.S., Montana State University, 2015

A thesis submitted to the

Faculty of the Graduate School of the

University of Colorado in partial fulfillment

of the requirements for the degree of

Doctor of Philosophy

Department of Chemical and Biological Engineering

2021

Committee Members:

Kristi Anseth

Stephanie Bryant

Jeffrey Stansbury

Wei Tan

Seth Donahue

Abstract

Rao, Varsha Vinay (Ph.D., Chemical Engineering)

Poly(ethylene glycol) hydrogels to engineer the mesenchymal stromal cell secretome

Thesis directed by Dr. Kristi Anseth

Bone marrow derived mesenchymal stem/stromal cells (MSCs) are widely used in clinical trials. In addition to their multipotency, MSC therapeutic efficacy relies on their secretory abilities; specifically, their secretion of growth factors, chemokines, and cytokines can influence endogenous cell behaviors and direct wound healing. Because MSCs only constitute 0.001-0.01% of all mononuclear cells in the bone marrow, their *in vitro* expansion is required to achieve clinically relevant cell numbers. Unfortunately, expansion of MSCs on tissue culture polystyrene (TCPS) can significantly reduce their *in vivo* regenerative capacities. Additionally, when injected intravenously or delivered carrier-free to a defect site, MSCs have low survival and engraftment. To begin to address these challenges, this thesis focused on developing hydrogel platforms to direct and maintain MSC secretory properties during *in vitro* expansion and *in vivo* delivery. We used PEG-based synthetic macromers reacted via bio-click reactions to create hydrogel environments to direct matrix mechanics, MSC-matrix interactions, and MSC-MSC contacts.

First, by controlling MSC exposure to matrix mechanics, we designed a 2D soft hydrogel intervention to increase MSC cytokine secretion during *in vitro* TCPS expansion. Next, we designed a granular hydrogel system, comprised of micron-scale PEG-based hydrogels, to promote MSC secretion in 3D. By modulating scaffold porosity and including integrin and cadherin binding epitopes, we controlled MSC cell-cell and cell-matrix interactions. Pore-directed cell clustering

increased MSC trophic factor secretion, specifically through N-cadherin mediated interactions. Exploiting our understanding of the influence of cell clustering and the inclusion of N-cadherin peptide mimetics on MSC secretion, we next evaluated the capacity of MSC-laden porous scaffolds to direct bone regeneration in critical-sized rat calvarial defects. Finally, we used these scaffolds to better understand how MSC secretion is changed in osteoporotic environments. Large clusters of osteoporotic MSCs had a pro-resorptive secretory profile, which was reduced by blocking N-cadherin interactions. Overall, we designed multiple hydrogel platforms to exert precise control over the *in vitro* MSC microenvironment and increased our understanding of how biophysical factors can be tuned to influence MSC secretory properties.

Acknowledgements

This work would not have been possible without the support of my colleagues, family, and friends. First and foremost, I would like to thank my advisor, Dr. Kristi Anseth. Kristi, thank you for all your advice, your support, and your thoughtful edits. I have grown so much as a scientist in your group. I would also like to thank my committee members, Drs. Stephanie Bryant, Jeffrey Stansbury, Wei Tan, and Seth Donahue for their guidance. Seth, this thesis would not have been possible without your collaboration. Thank you to Dr. Joseph Dragavon for his patience, his dedication, and his microscopy wizardry. Additionally, I would like to thank my other collaborators—Cole Ferreira, Auden Balouch, Dr. Sam Wojda, and Dr. Doug Peters—for their time and expertise.

I am so grateful for the continued support of the members of the Anseth research group, both past and present. Thank you to Kyle Kyburz for introducing me to MSCs, mechanical memory, and Kristi. Thank you to Andrea González Rodríguez, whose charm and candor over the visit weekend convinced me to come to CU. Thank you to Andrea and Megan Schroeder for being so welcoming, for listening, for hosting, and for offering advice and encouragement, both inside lab and out. Thank you to Alex Caldwell for being my microgel mentor and for always sharing the food on your table. Anouk Killaars, thank you for setting an example with your elegant science and for navigating collaborations with me. Ben Carberry, your resilience, positive attitude, and friendship has given me strength. Ben Richardson, thank you for sparking my interest in the future of food. Thank you to Max Yavitt and Laura Macdougall for always being up for a distracting conversation and for all the chemistry help. I am grateful to Marissa Weschler for her support and friendship during lockdown and after. Michael Blatchley, my writing, my data, and my lunches

Finally, I would like to express a heartfelt thank you to my partner, Ankur. You have filled my grad school experience with laughter, adventure, and a true sense of belonging. Thank you for being there. Thank you for loving me. Kill the turkey.

Table of Contents

List of Tables

List of Figures

Chapter 6

Chapter 7

<div align="center">

Chapter 1

Introduction and Background

Sections as published in Advanced Healthcare Materials, 2021, 2001948

</div>

1.1 Introduction

Originally isolated from the bone marrow in the 1970s, mesenchymal stromal cells (MSCs) were thought to be a new stem cell line capable of differentiating into multiple lineages.[1] In 2006, the International Society for Cellular Therapy (ISCT) defined a set of characteristics to identify MSCs based on their adherence to plastic, their spindle-like morphology, cell surface marker profile, and their trilineage differentiation potential (i.e., chondrogenic, osteogenic, and adipogenic).[2] Since these early discoveries, MSCs have been found in many tissues, including adipose, muscle, dental pulp, Wharton's jelly, and umbilical cord, and have been differentiated into additional pathways, such as cardiogenic, neurogenic, and myogenic.[3,4]

Due to their ease of isolation, proliferation capacity, and multipotency, MSCs have been widely explored for use in various cell-based therapies.[4,5] However, studies tracking in vivo cell fate found the therapeutic benefits of exogenously delivered MSCs were not primarily related to their differentiation, but instead their secretory properties.[6–8] Specifically, MSC secrete factors that can signal to endogenous cells and influence proliferation, resolve inflammation, deposit matrix, and heal wounds.[6–8] As a result, recent academic and clinical efforts have focused on MSC-secreted trophic factors and understanding their role as potent modulators of tissue regeneration.[4,6,7,9–11]

1.1.1 MSC secreted factors are key regulators of regeneration

MSCs secrete cytokines, chemokines, inflammatory factors, growth factors, exosomes and microvesicles filled with proteins and genetic material, collectively referred to as the

MSC secretome.[4,9,12] These factors signal to endogenous cells in a manner that can increase proliferation,[13] direct migration,[14] initiate differentiation,[15] and even modulate activation[16] or polarization[17,18] of immune cells. Based on these findings, in 2019, the ISCT updated the definition of MSCs to include functional assays, such as the trophic factor secretion, modulation of immune cells, and promotion of angiogenesis.[19] The potent, yet versatile secretion profiles of MSCs, has led to their use in treating a diverse range of diseases. For example, since 2010, ten MSC therapies have been approved around the world to treat Graft Versus Host disease (e.g., Canada, New Zealand, Japan), critical limb ischemia (e.g., India), and complex perianal fistulas to treat Chron's Disease (e.g., Europe).[5] In the United States, a query of clinical trials (NIH, clincaltrials.gov) mentioning mesenchymal stem cells found over 1200 trials. Approximately 25% of trials focused on treating musculoskeletal diseases, ~20% on autoimmune diseases, and ~10% on diseases related to the cardiovascular, neurological, or respiratory systems (Figure 1.1a). Of further note, the MSCs were predominantly sourced from bone marrow, followed by isolation from adipose tissue and the umbilical cord (Figure 1.1b).

The use of MSCs as a therapeutic continues to grow, as evidenced by the growth in the number of US clinical trials utilizing MSCs over the past ten years (Figure 1.1c). In fact, the largest increase occurred in 2020, with over 230 new trials documented through October (many associated with the COVID-19 pandemic). While the number of early Phase (Phases 1-2) clinical trials has consistently increased, many trials fail to progress to Phase 3 or beyond (Figure 1.1d). This significant drop is just one indication of the many challenges to ensure the efficacy of MSC-based therapies. Looking how MSCs have been delivered, >90% of trials directly inject MSCs into the body, either locally or systemically (Figure 1.1e), but evidence and intuition has shown that this leads to low MSC survival and retention upon delivery. As a result, several

research groups have been engineering scaffolds for MSC delivery, but to date, only 6% of clinical trials combined MSCs with biomaterials (Figure 1.1e). Clearly, there are many opportunities to improve on MSC therapies and advance the technology to latter stages of clinical trials and regulatory approval.
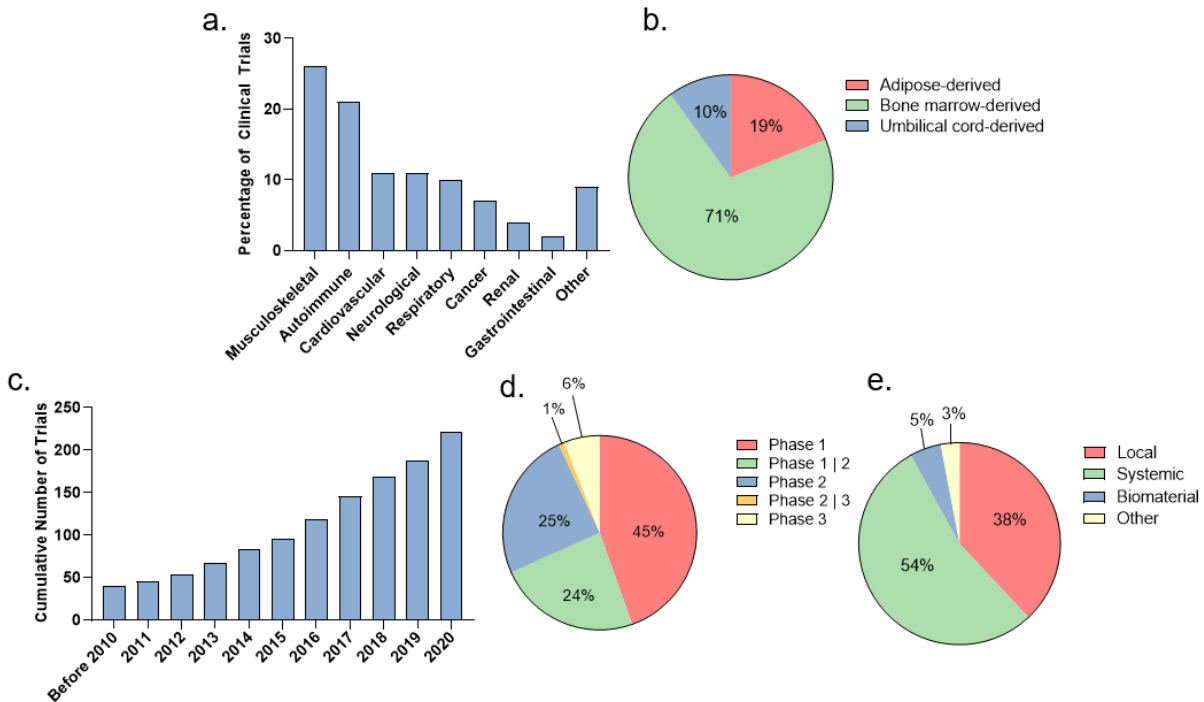
Figure 1.1 Mesenchymal stem cell-based clinical trials in the United States between 2010-2020. a) MSC clinical trials based on the organ system affected by the disease. b) Source of MSCs used in clinical trials. c) Number of clinical trials using MSCs over time. d) MSC clinical trials categorized by phase. e) Methods of delivering MSCs in clinical trials. Local refers to direct injection into the targeted tissue; systemic refers to intravenous infusion; and biomaterial refers to its combination with MSC delivery. These data were obtained from clinicaltrials.gov and searching for "Mesenchymal Stem Cell" in the "Other" category, limited to the United States. Data was collected on October 11, 2020.

1.1.2 Challenges hindering MSC clinical success

A large discrepancy remains between the number of MSCs that can be easily and reliably isolated from the bone marrow, and the number of cells needed for a clinical dose. For example, one milliliter of bone marrow contains only 10-100 MSCs; however, most clinically relevant treatments require 1-200 million cells per dose. These calculations highlight the fact that

after their isolation, MSCs must be expanded ex vivo.[5,20,21] Large-scale MSC expansion is typically performed in bioreactors that rely on materials such as tissue culture plastic (TCPS) (e.g., multilayered flasks) or silica and dextran microspheres (e.g., microcarriers).[22,23] However, expansion of MSCs on these substrates, as well as enzymatic passaging methods, can bias MSCs towards an osteogenic fate,[24] cause loss of multipotency (e.g., chondrogenic differentiation),[25,26] hinder DNA repair,[27] induce replicative senescence,[26,28,29] and even decrease expression of surface markers (e.g., CD105, CD90, CD73) that are associated with the MSC undifferentiated phenotype. Others have also shown that two-dimensional (2D) culture is not as effective in maintaining MSC secretory properties compared to three-dimensional (3D) culture methods.[30,31]

Following expansion, MSCs can be delivered locally, at the site of injury, or systemically throughout the body.[32–34] However, upon injection into a tissue site, many MSCs are washed away, phagocytosed, or necrose.[33,35] In fact, studies have shown that < 5% of administered MSCs are present in the tissue a few hours after transplantation.[36] Similarly, systemic administration of MSCs, typically through intravenous injection, can lead to accumulation in the lungs and clearance by monocytes within 24 hours.[37–40] This rapid clearance requires multiple doses of MSCs for clinical efficacy, resulting in greater reliance on in vitro expansion.[41]

Despite their high innate paracrine activity, the method used to expand MSCs ex vivo can further enhance or alter their secretory function. For example, biochemical priming methods (e.g., exposure to specific biochemical factors), hypoxic microenvironments,[42,43] pro-inflammatory cytokines,[44] small molecules,[45,46] and various growth factors[5,47] have all been shown to enhance MSC secretory properties. Depending on the disease context, specific factors secreted can be important (e.g., angiogenic factors for vascularization); however, an overall increase in the

secretion of all factors may also be detrimental (e.g., pro-inflammatory factors that exacerbate inflammation in rheumatoid arthritis treatments). In the end, while priming methods provide promising strategies to alter MSC's secretory profiles, the altered profile can be short lived, as the cells revert back to their steady state once the cue is removed.[48]

1.1.3 Designing hydrogels to improve MSC clinical translation

Advances in MSC biology and bioengineering have led to the identification of strategies which have the potential to address many of the limitations related to MSC-based therapies. Specifically, researchers have focused on two general approaches. The first alters MSCs directly, using strategies such as genetic engineering, cell surface modifications, or intracellular nanoparticle delivery to alter MSC functions. For example, advances in gene editing technologies have been used to increase MSC secretion of specific therapeutic factors, especially those relevant for treatment in a specific disease scenario where one factor can make a large therapeutic impact. Cellular approaches, though, do not directly improve the in vivo retention time of MSCs and their protection from immune clearance in vivo. Thus, a second, complementary approach is to control the MSCs environment using biomaterials, during expansion and/or after delivery. Biomaterials can provide matrix interactions to improve MSC survival, local retention, or even influence secretory properties via outside-in signaling (e.g., mechanosensing).

Biomaterials play critical roles in current MSC-based engineering approaches, as they allow user control of the biophysical and biochemical extracellular matrix signal that can influence a cell's behavior and function. To date, many biomaterials have been investigated to control MSC functions, ranging from natural to synthetic materials, polymers, ceramics, metals, including those with complex 2D and 3D architectures. While a vast assortment of biomaterials exists to date this thesis focuses on hydrogels, and their wide applications for MSC expansion and delivery. We

direct the reader to other reviews which carefully evaluate the broader range of biomaterials used for tissue engineering applications.[49–51]

Hydrogels can be synthesized from synthetic or natural homopolymers, copolymers, or macromolecular monomers that readily dissolve in water, but are physical or chemically crosslinked to render them insoluble.[52,53] The resulting network imbibes large amounts of water, but the crosslinks impart structural integrity along with unique material properties.[54,55] Depending on the chemistry, hydrogels can be engineered to degrade via cell-directed mechanisms (e.g., enzyme cleavable crosslinkers), environmental mechanisms (e.g., hydrolysis, pH changes), user-directed mechanisms (e.g., light), or a combination of the three. The use of hydrogels offers a highly tunable material platform which allows for temporal and spatial control over cell-matrix and cell-cell interactions. In addition, cells can be expanded on the surface of hydrogels (i.e., 2D culture) or encapsulated within a hydrogel (i.e., 3D culture). To promote MSC attachment, proliferation, differentiation, and secretory properties, hydrogels can be functionalized with integrin-binding peptides,[56,57] degradable peptide sequences,[58] small molecules,[59,60] nanoparticles,[61] or even chemokines and growth factors.[44,62]

Some of the barriers to the success of clinical therapies might be overcome by designing hydrogel culture platforms capable of promoting MSC secretory properties during expansion and delivery (Figure 1.2). Specifically, hydrogels systems could be engineering to: (i) promote MSC proliferation and maintain regenerative properties (i.e., stemness and secretion) during ex vivo expansion, (ii) improve MSC survival, retention, and engraftment in vivo, and/or (iii) direct the MSC secretory profile using tailored biochemical and biophysical cues.

	TCPS	2D hydrogel	3D bulk gel	microsphere	porous scaffold	spheroid
Increases proliferation	↑↑	↑	↑	–	↑	↑↑
Promotes secretory properties	–	↑	↑	↑	↑↑	↑↑
Facilitates cell-cell interactions	–	–	↑	↑	↑↑	↑↑
Provides user control over cellular microenvironment	–	↑	↑↑	↑↑	↑	–
Improves in vivo survival	–	–	↑↑	↑↑	↑	↑
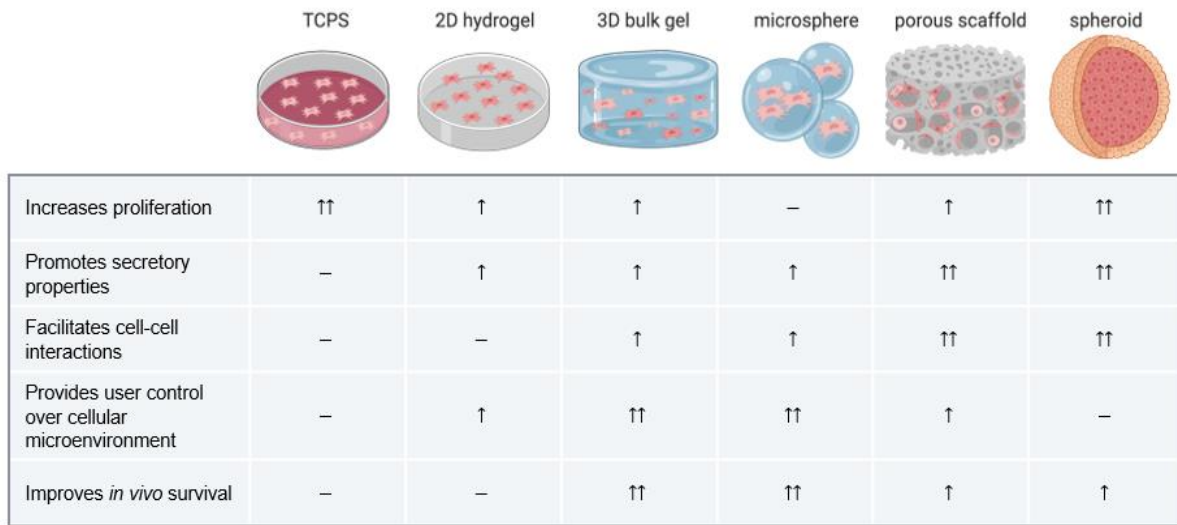
Figure 1.2 Culture systems to expand and deliver MSCs.
A variety of material platforms are used to expand and deliver MSCs, including tissue culture polystyrene (TCPS), hydrogels (either on 2D surfaces or 3D encapsulation), microspheres, porous scaffolds, and or multi-cellular spheroids. Each of these systems has the ability to influence MSC proliferation, secretory properties, and survival upon delivery. Strategies that encapsulate cells (e.g., hydrogels, microspheres) lead to higher levels of cell-matrix interactions compared to 2D surfaces. Porous scaffolds and multi-cellular spheroids lead to more cell-cell interactions. As a qualitative assessment, minus sign (-) indicates a system that does not improve the corresponding property, while the single up arrow (↑) indicates a slight improvement, and the double arrow (↑↑) indicates a higher level of improvement.

This introduction highlights some of the current strategies being developed in the biomaterial community to understand and direct MSC secretion, with a significant focus on influencing the cytokine, chemokines, inflammatory factors, and growth factors secreted by MSCs. While examples herein focus specifically on the aforementioned MSC secretions, we acknowledge that microvesicles and exosomes are also key components of the MSC secretome. However, the influence of cell culture methods on MSC exosomes and microvesicles has been thoroughly reviewed elsewhere.[63–65] Instead, this contribution reviews how material properties, such as the matrix modulus, viscoelasticity, dimensionality, cell adhesion, and porosity, influence MSC secretion. Emphasis is placed on how hydrogel culture platforms can be engineered to

control MSC cell-matrix and cell-cell interactions and increase overall secretion. In addition, examples are selected to highlight how biochemical cues, such as peptides, small molecules, and proteins, can improve and direct the MSC secretory profile. Finally, we posit on future directions to fill gaps with respect to understanding how microenvironment can influence the MSC secretome and designing the next generation of biomaterials, with optimized biophysical and biochemical cues, to direct the MSC secretome for improved clinical translation outcomes.

1.2 Biochemical compounds to direct the MSC secretome

MSC culture within hydrogels enables modulation of the local cellular environment to maintain MSC phenotypes during cell expansion, provide protection upon delivery, and promote paracrine secretion. However, the sole use of a material environment is not always sufficient to sustain MSC secretion. In the tissue engineering field, combining hydrogels with biochemical compounds in cell culture is ubiquitous. Numerous biochemical compounds (i.e., small molecules, peptides, and proteins) are known to influence MSC functions (e.g., adhesion, migration, proliferation, and differentiation), and these molecules can be introduced into hydrogels through bulk adsorption or matrix-immobilization (Figure 1.3a). A subset of these factors has already have been shown to influence and direct the MSC secretory profile. For this reason, combining biochemical priming methods with optimal hydrogel properties that predictably direct MSC secretion may prove especially beneficial in the translation of cell-based therapies.

1.2.1 Directing MSC secretion using small molecules

Small molecules (<1000 Da) are advantageous for cell-therapy applications because their characteristic properties (i.e., small size, high stability, non-immunogenicity, and low cost) minimize, and even overcome, many of the downsides associated with protein-based biofactors (such as, high cost, poor shelf-life, and recombinant manufacturing

considerations).[66,67] Specific to regenerative medicine, advances in stem cell biology have shown the promise of small molecules to control MSC fate. Examples include: purmorphamine (for osteogenic differentiation),[68] phenamil (for osteogenic differentiation),[69] and kartogenin (for chondrogenic differentiation) for MSCs.[70]
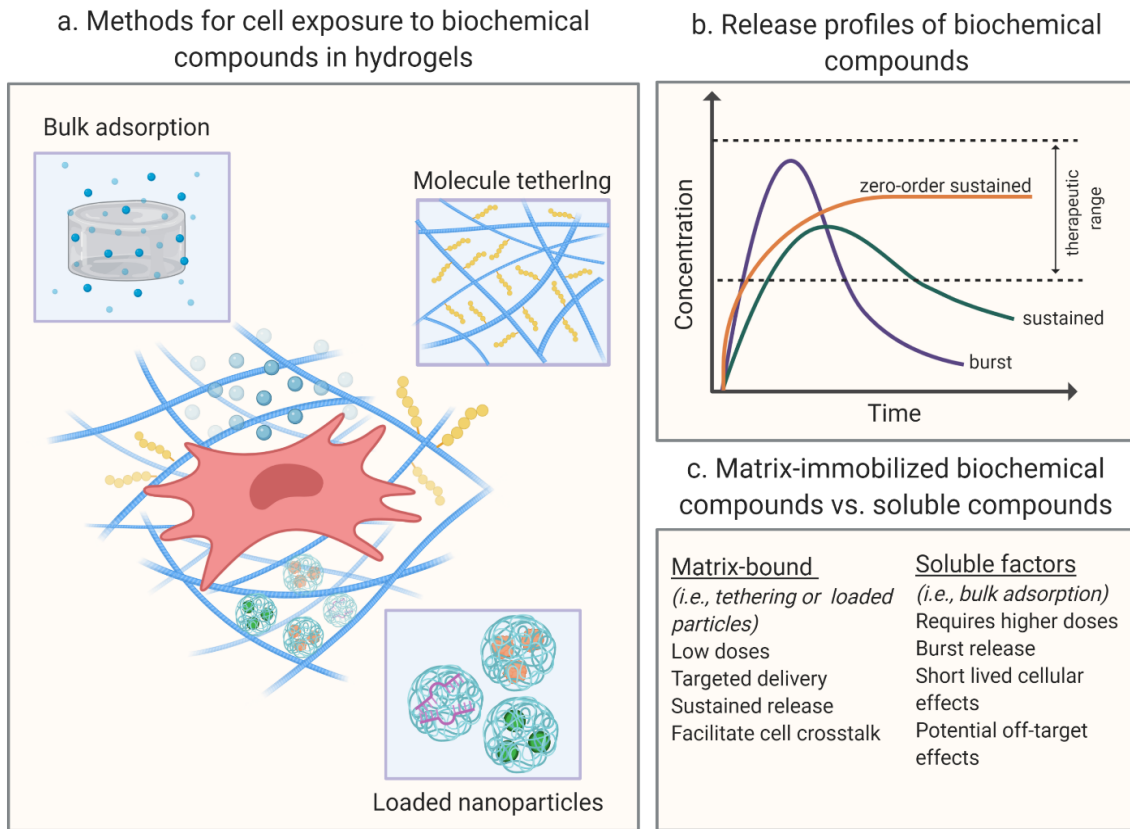
Figure 1.3 Biochemical microenvironmental modifications to influence MSC secretion.
a) Biochemical compounds such as small molecules, peptides, or proteins, can be incorporated into hydrogels by a variety of methods focused on either bulk adsorption or immobilization to the matrix. b) Release profiles of biochemical compounds will vary depending on how the compound is incorporated into the hydrogel and can be tailored for immediate or prolonged release and cell exposure over time. c) Immobilization of biochemical compounds to hydrogel matrices enables slower release profiles to be obtained, compared to bulk adsorption, which results in the need for lower biochemical doses. Bulk adsorption of biochemical factors is the simplest method for incorporation; however, burst release profiles often result, necessitating higher concentrations of the bioactive factor.

Purmorphamine was discovered by Wu et al. who demonstrated the use of this molecule to differentiate mouse embryonic mesoderm fibroblasts into an osteoblast lineage.[71] Later, it was revealed that delivery of adsorbed purmorphamine throughout porous calcium phosphate beads resulted in increased trabecular bone formation when implanted in a chick embryo femur.[72] Park et al. identified phenamil as a molecule that induced osteogenic differentiation and mineralization of mMSCs.[73] Delivery of phenamil in vitro has been achieved either by adsorption or entrapment of the drug in biodegradable poly(lactide-co-glycolide acid) (PLGA) scaffolds.[74,75] In another study, Fan et al. used a combination of phenamil and BMP-2 with PLGA scaffolds to induce in vitro osteogenesis of MSCs and regenerate bone in a mouse calvarial defect.[60] To promote chondrogenic differentiation of hMSCs, Johnson et al. identified kartogenin, which also demonstrated chondroprotective effects in vitro.[70]

While the aforementioned small molecules were identified primarily for inducing MSC differentiation, control of other MSC functions is often necessary in therapeutic interventions. For example, adhesion, migration, and homing of cells to their target organ for regeneration and repair is highly sought-after; however, poor homing to disease sites is often observed when MSCs are systemically infused.[76] For the first time, a study by Levy et al. used a screen to identify small molecules to improve targeting of systemically infused MSCs.[46] Specifically, 9,000 signal-transduction modulators were screened to identify hits that increase MSC surface expression of homing ligands, such as CD11a, that bind to intercellular adhesion molecule 1 (ICAM-1). When MSCs were treated with Ro-31-8425 (an identified hit from this screen), increased cell adhesion to an ICAM-1-coated substrate was observed in vitro. Targeted delivery of systemically administered MSCs to inflamed sites in vivo was also achieved in an ICAM-1-binding domain-dependent manner. Pre-treatment of MSCs with Ro-31-8425 prior to delivery in vivo resulted in

an increased anti-inflammatory response through decreased expression of TNF-α at the site of inflammation. This use of Ro-31-8425 represents a new paradigm for engineering MSC homing to enhance their therapeutic efficacy.

Modulating the immune response upon MSC delivery is another desirable aspect to control for improving patient outcomes and decreasing adverse effects. For this reason, Yang et al. developed a high-throughput screening method which evaluated a library of 1402 FDA-approved bioactive compounds to activate the secretion of PGE2, an inflammatory mediator secreted by MSCs that can reduce foreign body responses after implantation.[45] The authors identified tetrandrine (a calcium channel blocker) as a potential candidate to increase MSC secretion of PGE2 through the NF-κB/COX-2 signaling pathway. When co-cultured with murine macrophages, tetrandrine-primed MSCs diminished the level of TNF-α secreted by the macrophages, and when delivered into a murine ear skin inflammation model, a significant reduction in TNF-α levels were observed. These results indicate that tetrandrine-primed MSCs, with enhanced secretion of PGE2, achieved stronger immunosuppressive effects in vivo compared to unprimed MSCs. In addition, the study highlights how small molecule priming can be utilized to increase anti-inflammatory signaling by MSCs. Further identification of small molecules that perform similar functions are needed to develop a library of compounds that influence the MSC secretome.

Other molecules known to have significant effects on many cell functions are hormones. For example, the hormone estrogen can influence cell growth, metabolism, and differentiation in various tissues via estrogen receptors (ER)-α and ER-β, both of which MSCs possess. Hong et al. reported that supplementation of 17-β estradiol (E2), a form of estrogen, significantly increased the proliferation of hMSCs in vitro; however, the dose range over which MSCs responded varied by donor sex.[77] More specifically, a wider range of E2 concentrations (10^{-8} to 10^{-12} M) was observed

to significantly increase male MSC proliferation compared to female MSCs (10^{-8} to 10^{-10} M). E2 supplementation maintained the native MSC phenotype during in vitro expansion by expression of MSC surface markers and their ability to differentiate into osteogenic and adipogenic lineages. These results demonstrate that estrogen supplementation may play an important role in maintaining hMSC phenotype during expansion in vitro, which may help produce the large numbers of undifferentiated MSCs often required for cell-based therapies. The effect of E2 supplementation on the MSC secretome has yet to be investigated.

Another avenue which warrants further exploration is examination of small molecules that are known inhibitors of pathways involved in MSC secretion. For example, inhibitors of NF-κB, TGF-β, and Wnt/β-catenin signaling pathways. Although these pathways regulate multiple cell functions, targeted inhibition would identify specific regulatory proteins that may control crucial MSC secreted factors. For example, the small molecules ML-10B, an inhibitor of NF-κB signaling, was able to suppresses TNF-α induced expression of CCL2 and IL-6 in MSCs, indicating that this signaling pathway is required for MSC pro-inflammatory factor priming.[56] Further exploration of small molecule inhibitors would provide valuable insight towards developing methods to modulate the MSC secretome mechanistically.

The molecules discussed herein are a small sample of recently identified compounds that target specific MSC functions namely, cell expansion, homing, differentiation, and anti-inflammatory secretion. Most of the studies described include incorporation of small molecules into the cell culture media to modulate specific cell functions in vitro. It is important to note that MSC priming is often short-lived (on the scale of hours to several days).[5] After delivered in vivo, MSCs frequently lose their directed secretion that was previously obtained in vitro. However, to overcome such challenges, hydrogels can be utilized as delivery vehicles to provide sustained

release of biochemical compounds (Figure 1.3b and 1.3c), in addition to controlling the local MSC environment.

1.2.2   Use of pro-inflammatory cytokines to direct the MSC secretory profile

Many studies have demonstrated that MSCs possess a broad range of immunoregulatory abilities that influence both the adaptive and innate immune responses.[78] In addition, MSCs expanded ex vivo have been shown to suppress the activity of many immune cells, such as, macrophages, T cells, B cells, dendritic cells, and various white blood cells.[79] Though it is clear that MSCs exhibit immunosuppressive effects, the underlying cellular and molecular mechanisms responsible for such actions have yet to be fully elucidated. However, much evidence points to secretion of soluble factors by MSCs to be the culprit for select immunomodulation functions.

During the inflammatory phase of the wound healing process, neutrophils and macrophages are chemoattracted to the site of injury by bioactive compounds (i.e., various growth factors and cytokines). Once the immune cells arrive, they secrete pro-inflammatory factors such as TNF-α, IL-1β, or IFN-γ to induce inflammation. While this inflammatory step is crucial to initiate the wound healing process, it is quickly succeeded by a more regenerative stage, where endogenous cells deposit matrix and ensure vascularization. A prolonged inflammatory stage can lead to longer wound healing times and can even be responsible for the development of various diseases.

Secretion of anti-inflammatory cytokines by MSCs is highly sought-after towards the development of cell-based therapies. MSC soluble factors, which have been shown to suppress select immune cell functions and transition cells from pro- to anti-inflammatory polarizations, include TGF-β1, HGF, PGE2, IL-6, and IL-10.[78,80] In addition, MSCs have been shown to alter the cytokine secretion profile of select immune cells by upregulating regulatory cytokines (i.e., IL-10) and downregulating inflammatory cytokines (i.e., IFN-γ, IL-12, and TNF-

α), inducing greater anti-inflammatory effects.[79,81] This characteristic of MSCs makes them extremely powerful to potentially mitigate inflammation and reduce adverse effects upon cellular delivery in vivo.[81–83] However, this anti-inflammatory factor secretion does not occur naturally for MSCs, rather, they must be probed with pro-inflammatory factors (such as, IFN-γ, TNF-α, IL-1α, and IL-1β) from their surrounding environment in order to direct their secretion profile.[84–86]

The most common immunomodulatory agents used to direct specific MSC factor secretion are TNF-α and IFN-γ.[87,88] IFN-γ is often studied because preliminary activation of MSCs by immune cells in vivo can be accomplished by secretion of IFN-γ alone, or in combination with additional cytokines.[89,90] Alone, or in combination with IFN-γ, TNF-α (a pro-inflammatory cytokine produced by macrophages/monocytes during acute inflammation) is responsible for a diverse range of cell signaling events.[91] In a study by Chinnadurai et al., MSC treatment with IFN-γ (50 ng/mL) inhibited proliferation of activated T cells and blocked cytokine production by T cells (specifically, IFN-γ, IL-2, and TNF-α).[62] This inhibition of T cell effector function was found to be through upregulation of programmed cell death-1 ligands (PDL-1). Using media from mMSCs primed with IFN-γ (10 ng/mL), Vigo et al. found the immunosuppressive properties of these cells to be mediated by early phosphorylation of signal transducer and activator of transcription (STAT) 1 and STAT3, as well as inhibition of mTOR activity, leading to inhibition of T cell proliferation.[44] These results provide insight, demonstrating IFN-γ mediated manipulation of MSCs, and providing an understanding of the intracellular pathways affected by IFN-γ. It is important to note, however, INF-γ stimulation of MSCs is often dose dependent (requiring doses > 10 ng/mL) and short-lived (on the scale of hours to days). MSC priming with TNF-α is known to promote upregulation of select immunoregulatory factors, specifically, PGE2, CCL2, and HGF.[47] Combinatory preconditioning of MSCs with TNF-α and IFN-γ can increase factor H (a

regulator protein in the alternative complement pathway) production by MSCs, thus inhibiting complement activation in both dose and time dependent manners.[92] In a study by François et al., MSCs primed with TNF-α and IFN-γ suppressed T cell proliferation in vitro due to IFN-mediated indoleamine 2,3-dioxygenase (IDO) upregulation.[93] This increase in IDO activity in MSCs led to the differentiation of monocytes into IL-10 secreting M2 immunosuppressive macrophages. These M2 macrophages were then responsible for suppression of T cell proliferation in an IL-10-independent manner. These results showcase the immunosuppressive properties of TNF-α and IFN-γ primed MSCs.

In another study, Redondo-Castro et al. pre-treated hMSCs with inflammatory cytokines to prime the cells towards an anti-inflammatory and pro-trophic phenotype in vitro.[94] hMSCs from three different donors were cultured in vitro and treated with either IL-1α, IL-1β, TNF-α, or IFN-γ. MSCs primed with either IL-1α or IL-1β resulted in increased trophic factor secretion of granulocyte-colony stimulating factor (G-CSF) mediated through an IL-1 receptor type 1 (IL-1R1) mechanism.[94] To further confirm the anti-inflammatory potential of MSCs, immortalized mouse microglial cells (a population of macrophages found in the central nervous system) were treated with bacterial lipopolysaccharide and exposed to conditioned media of IL-1-primed MSCs. The authors showed that IL-1-primed MSC conditioned media added to inflamed microglial cells resulted in decreased secretion of inflammation markers (specifically, IL-6, G-CSF and TNF-α), and an increase in the microglial-derived anti-inflammatory mediator IL-10. These results highlight the ability of primed MSCs to orchestrate other cells to induce a more effective anti-inflammatory response, demonstrating the potential use of priming inflammatory treatments to enhance the beneficial actions of MSCs for future stroke therapies.

1.3 Directing MSC secretion using hypoxic culture conditions

A common element of tissue injury is the presence of hypoxia, a reduction in oxygen to levels of less than 5%. This reduction in oxygen tension leads to activation of several factors and chemoattractants (such as, stromal cell-derived factor 1, secreted by endogenous stromal cells), which cause MSCs to migrate to areas of hypoxia. Upon MSC migration, it has been demonstrated that production of various therapeutic paracrine mediators (i.e., VEGF, FGF-2, and IL-6 by MSCs) are increased.[95,96] These in vivo phenomena can be recapitulated in vitro through the use of hypoxic culture conditions ($<5\%$ O_2). Many studies have demonstrated that hypoxic conditioning of MSCs results in secretion of various angiogenic (i.e., VEGF, FGF-2, HGF, and IGF-1) and anti-apoptotic factors (BCL-2 mediated) from MSCs isolated from various sources (bone marrow, adipose tissue, and placenta).[97,98] Hypoxic culture conditions not only increase growth factor secretion from MSCs, but also promote MSCs to retain their stemness and an undifferentiated cell phenotype.[99] Collectively, hypoxic conditioning of cultured MSCs may result in increased production and secretion of trophic factors and augmentation of angiogenic effects from the conditioned cells relative to normoxic ($\sim21\%$ O_2) culture conditioning.[95]

Kim et al. demonstrated that MSCs cultured in hypoxic conditions of 3% O_2 for 5 days show enhanced stemness and immunomodulatory functions. Specifically, hypoxic-conditioned MSCs were resistant to passage-dependent senescence mediated by the monocyte chemoattractant protein-1 (MCP-1) and p53/p21 cascade, and secreted large amounts of pro-angiogenic and immunomodulatory factors, resulting in suppression of T cell proliferation in vitro.[42] Administration of MSCs primed with hypoxia in a humanized rat model of graft-versus-host disease significantly augmented symptoms and improved survival outcomes.[42]

In a study by Antebi et al., human and porcine bone marrow MSC functions were evaluated after short (48 hours) and long term (10 days) exposure to hypoxic environments.[43] Specifically,

MSCs were evaluated for their metabolic activity, proliferation, viability, clonogenicity, gene expression, and secretory capacity. The authors demonstrated that hypoxia augments the therapeutic characteristics of both porcine and human MSCs. Short-term (48 hours) hypoxia (2% O_2) offered the greatest benefit overall, exemplified by the increase in proliferation, self-renewing capacity, and modulation of key genes (i.e., VEGF, HMGB1 and NANOG) and the inflammatory milieu (i.e., IFN-γ and IL-18) as compared to normoxia (21% O_2). These results are important indications that hypoxic conditioning of MSCs augments cellular functions desired for clinical applications.

It is well known that cell-cell contacts can increase MSC survival and trophic factor secretion, as showcased by MSCs cultured in spheroids compared to dispersed cells. In addition to promoting cellular contacts, it is hypothesized that spheroids improve MSC secretion by the formation of a hypoxic core.[100,101] However, in a study by Murphy et al., it was found that while a small (<10%) gradient of oxygen tension was observed in spheroids of approximately 350 µm, the enhanced function of MSC spheroids is not oxygen mediated at this size.[100] In a follow up to this study, the same group investigated short-term hypoxic preconditioning of MSCs prior to spheroid formation to increase cell viability, proangiogenic potential, and resultant bone formation. Ho et al., exposed hMSCs in a monolayer either to 1% O_2 or ambient air for 3 days prior to spheroid formation of varying cell densities and encapsulation in alginate hydrogels. Hypoxia-preconditioned MSC spheroids were more resistant to apoptosis, secreted increased levels of VEGF compared to ambient air controls, and high cell density spheroids (15,000 cells) exhibited the greatest osteogenic potential in vitro.[101] When hypoxia-preconditioned MSC spheroids in gels were transplanted into a rat critical-sized femoral segmental defect, increased bone healing was observed compared to gels containing preconditioned individual MSCs or acellular gels. These

results demonstrate that hypoxic preconditioning enhances the therapeutic potential of MSC spheroids for tissue engineering applications. Further investigations of hypoxic environments on the MSC secretory profile are necessary to elucidate the underlying mechanisms responsible for the increased cell secretion. While biochemical factors can influence the secretory profile of MSCs, the changes to the secretome are dependent on the presence priming factors, inherently making them short-lived and incompatible after delivery. Thus, developing biomaterials capable of maintaining cues during and after delivery can be advantageous.

1.4   Tailoring hydrogel network properties to direct MSC secretion

Designing biomaterials to direct MSC secretory profiles first requires a basic understanding as to how cells interact with their matrix. In the body, cells are surrounded by an extracellular matrix (ECM) that provides a structural basis for the tissue, providing a foundation for cell adhesion and an environment for cell-cell and cell-matrix signaling interactions. The composition of the ECM is tissue specific and can vary greatly; however, its main components are structural proteins, such as collagen and branched glycosaminoglycans. In addition to providing binding sites for cell adhesion, these proteins sequester bioactive molecules making the ECM capable of directing cell behaviors.[102] Countless studies have confirmed the crucial role of the ECM in directing cell growth, differentiation, and disease progression.[102–104] Cell-matrix interactions are largely facilitated through integrins; receptors on the cell surface that are internally connected to the cytoskeleton. Integrin receptors span the cell membrane and are comprised of an alpha and beta subunit. In mammals, 18 distinct alpha domains and eight distinct beta domains have been identified. In humans, combinations of these subunits result in 24 integrin receptors that each bind to specific amino acid sequences found in various ECM proteins. For example, the sequence RGD (arginine – glycine – aspartic acid), present in fibronectin, laminin, and vitronectin, is bound by

α5β1, α8β1, αVβ1, αVβ3, αVβ5, αVβ6, αVβ8, and αIIbβ3 integrins. Upon binding, multiple integrin receptors cluster together with other cytosolic proteins to initiate the formation of a focal adhesion complex, which ultimately mature and facilitate cell spreading and migration.[105]

With this information in mind, biomaterial researchers often incorporate ECM components into engineered matrices to promote cell attachment and to ensure cell responsive behaviors due to changes in matrix mechanics). Incorporation of ECM components into biomaterials can be accomplished by either using specific ECM proteins as scaffolding materials, such as in collagen-based gels or decellularized tissues, or by incorporating bioactive peptide sequences, such as RGD (a fibronectin mimic) or GFOGER (a collagen mimic), into scaffolds created with bioinert polymers (Figure 1.4a). While these proteins are critical to ensuring cell adhesion, ECM proteins can also independently participate in initiating downstream cell signaling, specifically by influencing the MSC secretory profile.

1.4.1 ECM composition

In 2014, De Lisio et al. showed that expression of paracrine factors, such as Interleukin (IL)-6, granulocyte-macrophage colony-stimulating factor (GM-CSF), vascular endothelia growth factor (VEGF), transforming growth factor beta-1 (TGF-β1), and tumor necrosis factor-alpha (TNF-α), were altered between murine MSCs (mMSCs) cultured on plates coated with collagen or laminin, in which different integrins mediate cell attachment.[106] Generally, the gene expression of the aforementioned growth factors was downregulated when mMSCs were grown on collagen. Abdeen et al. compared the effects of fibronectin, collagen, and laminin coatings on human MSC (hMSC) angiogenic factor secretion.[107] Human microvascular endothelial cells (HMVECs) treated with hMSC conditioned media from cells cultured on fibronectin coated polyacrylamide hydrogels (E~40 kPa) resulted in increased tubulogenesis compared to HMVECs

treated with media from hMSCs cultured on collagen I and laminin coated gels. However, this effect was fully dependent on the stiffness of the gels, and no differences in HMVEC tubulogenesis was observed with hMSC conditioned media treatment from 0.5 kPa and 10 kPa gels coated with different ECM proteins. In another study, monocyte chemotaxis towards MSC conditioned media was enhanced by MSC culture on hydrogels containing hyaluronic acid.[108]

With respect to ECM mimicking peptide incorporation, in vitro encapsulation of hMSCs in poly(ethylene glycol) (PEG) hydrogels modified with the peptide GFOGER, a collagen I mimic that binds to integrin α5β1, improved secretion of inflammatory factors, IL-8 and IL-6, and chemotactic factor monocyte chemoattractant protein-1 (MCP-1) compared to hydrogels modified with RGD alone.[109] When hMSCs in GFOGER gels were delivered to a murine radial segmental defect, μCT revealed significantly higher levels of new bone formation was observed at both 4 and 8 weeks, compared to defects treated with hMSCs in the absence of GFOGER.[109] Collectively, these results show that ECM composition can be a powerful tool to direct MSC secretion.

1.4.2 Matrix modulus

In addition to the biochemical components present in the ECM, the mechanical cues present in a cell's surroundings can also influence their activity. Utilizing biomaterial culture platforms, researchers can easily modify several bulk material properties, such as stiffness, viscoelasticity, porosity, and degradability, all of which can direct MSC fate and secretory behavior (Figure 1.4b).

For example, increased matrix stiffness can lead to increased cytoskeletal tension, resulting in a more open nucleus and the translocation of key transcriptional regulators, which initiate downstream gene expression. Specific to hMSCs, stiff and soft mechanical cues are known to

direct cell fate, proliferation, and apoptosis. Prolonged exposure of hMSCs to soft or stiff matrices can result in an irreversible commitment of the cells to the lineages specified by the matrix elasticity of their substrate, despite contradictory soluble differentiation cues; a phenomenon dubbed mechanical memory. This memory is often thought to be determinantal in the context of culturing, as serial passaging of MSCs is known to cause a loss of multipotency, increased DNA damage, and eventual senescence.[26,110]
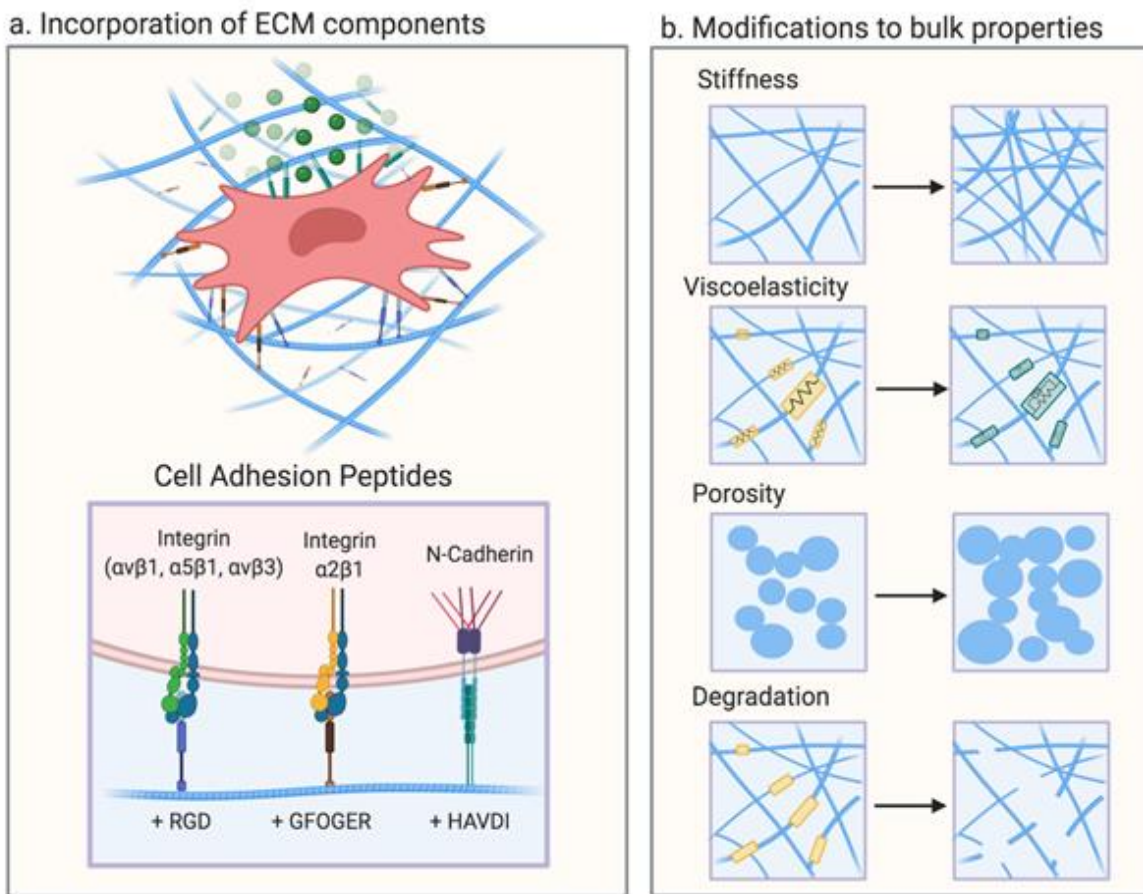
Figure 1.4 Matrix composition and physical properties influence MSC secretion.
a) To promote cell adhesion, bioactive cell adhesion molecules are often incorporated in hydrogel formulations. Integrins, present on the cell surface, bind to amino acid sequences found in ECM adhesion proteins. For example, RGD and GFOGER peptides, fibronectin and collagen mimics respectively, have been shown to differentially influence MSC secretory profiles. Similarly, peptides derived from N-cadherins (e.g., HAVDI) can mimic cell-cell interactions and influence MSC secretory properties. b) Bulk hydrogel properties (e.g., stiffness, viscoelasticity) influence

MSC interactions and global secretory properties. Porosity and degradation properties can direct MSC clustering and promote secretion through increased cell-cell contacts.

Compared to differentiation studies using MSCs, a smaller number of investigations have explored the influence of matrix stiffness on MSC cytokine secretion. hMSCs cultured on 2D polyacrylamide gels (E~40 kPa) coated with fibronectin (i.e., α3β1, αVβ1) resulted in increased VEGF and insulin-like growth factor (IGF) secretion compared to hMSCs on soft (E~500 Pa) gels with the same coating. To determine if hMSC secreted factors could cause changes in a functional cellular output, conditioned media from hMSCs was used to promote human microvascular endothelial cell (HMVEC) tubulogenesis.[107] Results from this study revealed the highest tube area in cultures with media collected from hMSCs cultured on 40 kPa gels.[107]

Expanding on the influence of matrix stiffness on MSC secretory factors, Ogle et al. cultured MSCs on 30 kPa and 100 kPa on PEG-diacrylate (PEGDA) hydrogels functionalized with peptides targeting integrins or cadherins or on PEGDA hydrogels containing hyaluronic acid or heparin.[108] Regardless of the functionalization, MSCs cultured on 30 kPa gels exhibited an overall abundance of immunomodulatory factors relative to MSCs cultured on 100 kPa PEGDA gels or TCPS.[108] Further, conditioned media from MSCs cultured on 30 kPa gels enabled promotion of vessel network formation in human umbilical cord endothelial cells (HUVECs). However, the 30 kPa gels were not able to promote MSC proliferation as much as stiffer hydrogel conditions relative to TCPS, indicating that a combination approach might be necessary to achieve high numbers of secretory MSCs.

A potential combinatorial approach would be to use hydrogel culture post TCPS expansion to rescue MSC secretory phenotypes. Rao et al. observed that hMSCs serially passaged on TCPS lose their secretory properties over time.[31] In late passage hMSCs, a significant decrease was observed in the secretion of factors related to cell proliferation and differentiation, such as TGF-

β1, VEGF, glial cell-derived neurotrophic factor (GDNF), and epidermal growth factor (EGF). However, simply transferring hMSCs to soft hydrogels, at either early or late passages, can restore the secretion of key chemokines, growth factors, and inflammatory factors. Collectively, these results indicate that hydrogel interventions could be employed during ex vivo expansion to instruct MSCs to secrete factors before they are delivered in vivo. Additionally, factors from MSCs cultured on 2D biomaterial substrates could be collected and delivered cell-free into patients.

Although tuning matrix stiffness might prove advantageous when harvesting MSC-secreted factors or priming MSCs before intravenous delivery, embedding MSCs in biomaterial matrices for in vivo delivery is often efficacious. For example, Won et al. suggested that a soft ECM may enhance the effect of the inflammatory stimuli, TNF-α, on MSC secretion. hMSCs were encapsulated within soft (E~2 kPa) and stiff (E~35 kPa) RGD-functionalized alginate hydrogels.[56] hMSCs in soft matrices secreted higher levels of chemokines involved in monocyte recruitment (CCL2, IL-6) upon treatment with TNF-α, which was attributed to an increased clustering of TNF receptors and redistribution of actin polymerization mediated by lipid rafts. Both led to NF-κB activation and upregulation of downstream genes (e.g., CCL2 and IL-6).[56]

1.4.3   Viscoelasticity

Viscoelastic hydrogels are synthesized using covalent adaptable linkers, hydrophobic interactions that increase with temperature, and guest-host interactions. Viscoelastic hydrogels are of growing interest within the field of tissue engineering, as they can better recapitulate aspects of the mechanical properties of soft tissues and are often injectable. To investigate the influence of a viscoelastic material on the MSC secretome, Liu et al. cultured MSCs on polydimethylsiloxane (PDMS) surfaces with varying shear storage moduli (~1-100 kPa) and viscoelastic properties

((G"/G') = tan (δ) ~0.2-1.2).[111] MSCs cultured on low stiffness (~1 kPa) substrates with the highest tan (δ) (>1) had a >3-fold increase in osteopontin expression, relative to other conditions. Similar increases were observed for IL-8, MCP-1, IL-21, brain-derived neurotrophic factor (BNDF), and stromal cell-derived factor (SDF)-1a for MSCs on compliant substrates.

Viscoelastic, shear-thinning hydrogels have also been developed as injectable MSC delivery system and to test the influence of viscoelasticity on the MSC secretome.[112]. Human adipose derived stem cells (hASCs) cultured in gels with intermediate stiffnesses (100-300 Pa) and relaxation time constants (12-13 seconds) resulted in increased secretion of angiogenic factors (VEGF, ANG, HGF) compared to cells cultured in gels with lower or higher stiffnesses and relaxation times. While further secretory studies need to be conducted using MSCs, viscoelastic materials show promise as injectable cell delivery systems for clinical use.

Biophysical and biochemical cues delivered to MSCs through their matrix environment, such as stiffness, viscoelasticity, and ECM proteins, can direct both their constitutive factor secretion and their responsive factor section. However, it is clear that the influence of matrix stiffness on MSC secretome is factor dependent and thus, clear conclusions cannot be drawn as is possible with matrix stiffness and MSC differentiation. Additionally, other types of mechanical stimuli, such as strain, compression, or tension, and other material properties, such as viscoelasticity and topography, need further experimentation to fully determine their influence on MSC secretion.

1.5   Material design strategies to increase MSC cell-cell interactions

Beyond cell-matrix interactions, MSCs are also dependent on cell-cell signaling cues, mediated in part through N-cadherins present on the cell surface. N-cadherins contain both an extracellular domain, that dimerizes with N-cadherins present on neighboring cells, and an intracellular domain, linked to actin cytoskeleton which is capable of facilitating downstream

signaling. Specifically, the cytoplasmic domain binds to β-catenin, a transcriptional regulator involved in Wnt and NF-κB pathways. In vivo, bone marrow derived MSCs reside in N-cadherin expressing clusters in their native niche which help to maintain their stemness.[4] In vitro, N-cadherin expression has been confirmed on MSC cell membranes,[113] and its expression has been shown to be elevated in MSC clusters.[114]

Relevant for MSC therapies, N-cadherin signaling can directly upregulate MSC secretion. MSCs residing in cell aggregates or clusters, with increased N-cadherin expression, also exhibit increased secretion of growth factors.[113] Further validating this observation, several groups have observed a loss of MSC secretory abilities when cells are cultured in the presence of N-cadherin blocking antibodies.[30,115] In one example, an N-cadherin blocking antibody was administered to aggregated MSCs (~40 cells/clusters) in a porous PEG-based microgel scaffold with average pore diameters of 200 μm. Over a ten-fold decrease was observed for 45% of the measured cytokines when N-cadherin signaling was blocked for three days in MSC clusters.[114] This points to increased cellular contacts and N-cadherin signaling as a valuable tool to sustainably increase MSC secretion.

1.5.1 Culture of MSCs as spheroids

To increase MSC cell-cell contacts and better mimic their physiological niche, researchers have employed the use of MSC spheroids, or large cell aggregates, produced by hanging drop culture or centrifugal aggregation techniques.[116] Spheroid culture has been shown to improve MSC survival, multipotency, and secretory potential. Specifically, Leach has shown that MSCs in spheroid culture have distinct transcriptomes compared to adherent cells, with a marked increase in genes associated with ontologies for wound healing and inflammatory responses.[57,117] Bartosh et al. found that MSCs in spheroids (25,000 cells/spheroid) secreted high levels of potent anti-

inflammatory factors, such as tumor necrosis factor-α-stimulated protein 6 (TSG-6) and stanniocalcin-1 (STC-1), and were able to decrease activation of macrophages in vitro, and inflammation in vivo using a peritonitis mouse model.[88]

In addition, spheroid size can affect MSC secretion. MSCs in large spheroids (40,000 cells/spheroid) have elevated secretion of several important cytokines involved in inflammatory signaling, including growth-regulated oncogene (GRO), interferon gamma (IFN-γ), and IL-10, compared to MSCs in smaller spheroids (10,000 cells/ spheroid).[118] However, apoptosis and necrosis can increase at the center of very large spheroids (>100,000 cells) due to nutrient deficiencies.[88]

While spheroid culture alone can improve MSC secretion, encapsulating aggregates in biomaterials may further improve and control secretion. Even though matrix interactions are limited to the peripheral cells, these signals can be amplified throughout the aggregate. For example, MSC spheroids encapsulated in RGD modified alginate hydrogels resulted in elevated secretion levels of VEGF, TGF-β, GRO, and EGF compared to spheroids in unmodified gels.[57] Once encapsulated, the stiffness of the matrix can also influence cell secretion. MSC spheroids encapsulated in stiff fibrin gels (G'~1200 Pa) had higher VEGF secretion, while spheroids in soft gels (G'~100Pa) secreted higher levels of PGE2.[119] Using multifactorial statistical analysis, the researchers were able to a predict an optimal intermediate gel formulation (G'~ 400Pa) in which both VEGF and PGE2 levels were highest.[119]

1.5.2   3D porous biomaterials

In lieu of spheroid culture to increase MSC cell-cell contacts, recent studies have focused on the use of porous biomaterial environments to cluster MSCs. Porous scaffolds can be synthesized using various methods, including dissolution of embedded porogens by solvents,[120,121] in situ

degradation of soft materials,[122] cell-mediated degradation of bulk single-phase hydrogels,[123] 3D printing and extrusion,[124] and lyophilization.[30] Additionally, individual hydrogel building blocks on micron length scales, termed "microgels", have been used to create porous scaffolds. Monodisperse microgels have been synthesized using microfluidic devices[125,126] or on a bulk scale using suspension polymerization[127] techniques. Once synthesized, the microgels can then be assembled in the presence of cells to create 3D porous networks where cells reside in the void spaces.

Compared to bulk scaffolds where cells are embedded in hydrogels with nanometer-sized pores, Qazi et al. observed that rat MSCs (rMSCs) embedded in lyophilized alginate scaffolds (average pore size of 122 ± 29 µm) secreted higher levels of cytokines and regenerative factors (e.g., hepatocyte growth factor (HGF), fibroblast growth factor-2 (FGF-2), and IGF) compared to those encapsulated in bulk alginate gels.[30]

In porous systems, a material characteristic (i.e., pore size) can be used to direct cell cluster size, albeit in much smaller numbers than those used in typical spheroid cultures. Caldwell and Rao et al. used microgels networks to control cluster size[114] MSC clusters (~40 cells/cluster) in the 200 µm scaffolds expressed elevated cytokine secretion as measured by cytokine array. In another example, extrusion printing was used to fabricate gelatin scaffold with three pore sizes: ~200 µm, ~300 µm, and ~400 µm. After 3 days of culture, hMSCs in the ~300 µm scaffolds had significantly higher expression of angiopoietin (ANGPT) and HGF, compared to MSCs in other pore sizes. In addition, increased expression of VEGF and FGF was observed after 7 days of MSC culture in scaffolds with pore sizes of ~300 µm, relative to results obtained in 200 µm and 400 µm pores.[124]

In a similar manner used to incorporate integrin binding peptide epitopes, biomaterial scientists have also included N-cadherin peptide mimics into scaffolds to mimic cell-cell interactions. For example, the amino acid sequence HAVDI (Histidine – Alanine – Valine – Aspartic Acid – Isoleucine) binds to N-cadherins,[129,130] and has led to a >10-fold increase in GNDF and IGF by MSCs. In one study, inclusion of HAVDI resulted in increased secretion of 96% of all measured cytokines by clustered MSCs relative to RGD only conditions. Most notably, the inclusion of HAVDI elevated secretion of non-clustered cells to levels similar to MSCs in clusters.[114,131] Just as the inclusion of ECM peptide mimics drastically improves cellular adhesion to synthetic biomaterials, the inclusion of HAVDI can be used to radically increase MSC secretion in biomaterials where MSC clustering cannot be induced, thereby decreasing the numbers of MSCs needed per dose.

1.5.3 Microencapsulation

Another method to achieve hydrogel encapsulated MSC aggregates is through microencapsulation, where cells are encapsulated within individual microgels using a microfluidic device. In one example, mMSCs were encapsulated within alginate microgels, which was later crosslinked with poly-D-lysine and resulted in aggregates of 2-7 cells. The multicellular aggregates had increased expression of anti-inflammatory genes (e.g., IL-10, TSG-6, and TGF-β1) relative to mMSCs on TCPS.[132] Intravenous delivery of the MSC microspheres intravenously results in an in vivo half-life of over 50 hours, a 5x increase compared the half-life of unencapsulated MSCs.

In addition to increased constitutive factor expression, MSCs in multicellular aggregates respond to pro-inflammatory stimulants more effectively than their single cell counterparts. This heightened response has been observed by MSCs in microporous environments or in spheroids; all of which promote cell-cell contacts.[88,133] Exogeneous IGF-1 amplified MSC paracrine secretion

in a microporous environment (pore size ~120 µm) relative to MSCs in nanoporous gels (pore size~10 nm).[30] These effects were abrogated in the presence of an N-cadherin blocking antibody, confirming that cell-cell contacts are necessary for MSC reactive responses. Similarly, MSCs in spheroids have increased immunomodulatory paracrine section in the presence of IFN-γ and TNF-α relative to disassociated cells.[88,134]

Overall, material properties significantly influence MSC secretion, mediated both by cell-matrix and cell-cell interactions. However, these factors are highly interdependent, making it difficult to reach definitive conclusions as to how each individual material properties can be used to direct MSC secretion. Generally, properties, such as matrix stiffness and viscoelasticity in materials with integrin binding domains, instruct MSC secretion though direct cell-matrix interactions. Soft substrates can broadly increase secretion of MSCs cultured on them, but receptor clustering in 3D can be different (e.g., allowing MSCs to respond more effectively to TNF-α treatment). Numerous studies have reported the effectiveness of cell-cell interactions on MSC secretion in an N-cadherin dependent manner. Complementary, material properties, such as porosity, can be used to direct MSCs clustering, thereby increasing secretion. Lastly, as bioactive components are incorporated into materials (e.g., integrin- or cadherin-biding peptides), cell-matrix interactions can further direct the MSC secretion profile, or simply increase total factor secretion, without relying on large cell numbers or exogenous delivery of biochemical factors.

1.6   MSC cytotherapy for bone regeneration in critical sized defects

As seen in Figure 1.1a, the majority of MSC clinical trials focus on treating diseases and ailments of the musculoskeletal system, including bone regeneration. One 2010 study estimated the U.S. market for bone trauma was over $3 billion[135]. While most fractures heal on their own, 5-10% of all fractures have unresolved healing, sometimes termed non-unions. Non

healing can result critical sized defects that are particularly prevalent in patients that undergo tumor resections, are born with congenital defects, or undergo a traumatic event. Additionally, diseases, such as osteoporosis, can add compounding effects and reduce bone healing even further. When proper fracture healing does not occur, whether due to disease or large sized bone resection or injury, delivery of mesenchymal stem/stromal cells (MSCs) has been used extensively in pre-clinical settings to aid in bone regeneration[136–140].

MSCs secrete trophic factors that can influence various stages of wound healing. Specifically, MSCs secrete factors that can influence cell infiltration (e.g., MCP-1), immunomodulation (e.g., TNF-α, IL-10), vascularization (e.g., Angiogenin, VEGF), and matrix remodeling (e.g., TGF-β), all important steps required for bone healing[141,142]. *In vitro*, treatment of inflammatory or M1 macrophages with MSC conditioned media can repolarization them to a regenerative, M2 macrophages[143]. However, MSCs can also secrete pro-inflammatory factors, such as TNF-α, that promote M1 macrophage polarization and can potentially impaired inflammation resolution. MSC secreted factors also include chemotactic cues that promote macrophage migration *in vitro*[144]. *In vivo*, while macrophage infiltration is a crucial step in fracture healing, this could potentially lead solely to an inflammatory wound healing response, which does not promote bone regeneration. Proangiogenic factors secreted by MSCs caused endothelial cell tubulogenesis[145,146] *in vitro*, a potential indicators of *in vivo* defect vascularization. Other studies have explored the effects of MSC conditioned media on osteoblastic functions[146–148]. Specifically, exposure to MSC conditioned media supplemented with osteogenic induction factors resulted in increased ALP expression and higher matrix deposition by osteogenic progenitors compared to treatment with osteogenic media conditions alone[146]. Co-cultures of hMSCs and human osteoblasts caused elevated gene expression of ALP and Collagen 1a in

osteoblasts[149]. However, MSC secretion of TNF-α can reduce osteoblast mineralization[56]. While many *in vitro* studies suggest that MSC secreted factors may be beneficial to wound healing, further research is needed to understand how *in vivo* MSC delivery affects bone regeneration.

In addition to *in vitro* experiments assessing the effects of MSC secreted factors on osteogenesis, several *in vivo* studies have delivered biomaterials in critical-sized defects to promote bone regeneration. In one example, alginate gels were soaked in condition media containing MSC secreted factors and then implanted into a critical sized calvarial defects in rats[8]. After 8 weeks, gels containing MSC conditioned media demonstrated improved defect closure relative to gels soaked in standard cell culture media. As a follow up, antibody depletion studies determined that IGF-1, VEGF, and TGF-beta were primarily responsible for angiogenesis and bone formation while MCP-1 and MCP-3 signaled to endogenous mMSCs and endothelial cell infiltration[15,145]. While biomaterials allow localized delivery that can be controlled over time, they will eventually be depleted from the depot. In contrast, implantation of MSCs directly can allow for a more sustained release or dynamic reciprocity, depending on the local bone microenvironment.

To this end, other bone regeneration approaches deliver MSCs, often using biomaterials carriers modified to promote survival and manipulate their secretory properties. In one example, MSCs were clustered into spheroids and exposed to three days of hypoxic conditioning (1% oxygen) to elevate their secretion[147]. Before implantation, MSCs secreted pro-angiogenic factors, specifically VEGF, after exposure to hypoxia. *In vivo*, hypoxic preconditioning improved angiogenesis, as evidenced by increased neovessel formation in defects treated with preconditioned MSCs compared to control defects after 2 weeks. Additionally, critical sized femoral defects treated with MSC spheroids entrapped in alginate gels exhibited

significantly elevated bone formation compared to defects treated with gels containing individual MSCs after 12 weeks. In another study, bone formation was improved in critical sized femoral defects in mice treated with MSCs in hydrogels modified with a collagen mimic peptide, GFOGER, compared to treatment with MSC-laden gels functionalized with RGD only[148]. Micro-array gene expression analysis revealed increased expression of inflammation (TNF-α, IL-1β), vascularization (VEGFR1/2), and bone formation (RUNX2) related genes in the host animals treated with MSCs in GFOGER functionalized gels compared to animals treated with RGD control gels. *In vitro*, MSCs encapsulated in GFOGER functionalized gels had elevated secretion of IL-6, IL-8, and VEGF relative to MSCs in RGD only gels.

1.7   Research Overview

The goal of this thesis is to design hydrogel microenvironments to control MSC secretory properties during *in vitro* expansion and *in vivo* delivery. Using poly(ethylene glycol) based hydrogels crosslinked with bio-click chemistries, we alter material parameters—such as matrix mechanics, inclusion of integrin and cadherin binding epitopes, and porosity—to impart control over MSCs cell-matrix and cell-cell interactions. Overall, we seek to understand the how biophysical cues can be tuned to direct MSC secretion.

First, to achieve clinically relevant numbers, MSCs must be expanded *in vitro.* Currently, *in vitro* expansion protocols rely on supraphysiologically stiff substrates such as tissue culture polystyrene (TCPS) or dextran microcarriers. Therefore, in Chapter 3, we first aim to understand the effects of TCPS expansion on MSC regenerative properties. We characterize changes to MSC proliferation, mechanosening ability, stemness, and secretion during serial expansion on TCPS. As matrix mechanics can influence MSC stemness properties, we then hypothesize that soft

hydrogel culture (post TCPS expansion) can be used to rescue secretory properties lost during serial passaging.

After *in vitro* expansion, MSC delivered *in vivo* without a biomaterial protection show poor retention, survival, and engraftment. While encapsulation in bulk hydrogels can increase MSC in vivo retention, bulk encapsulation in hydrogels does not increase MSC secretory properties. To address this limitation, in Chapter 4, we design a porous granular scaffold to promote MSC secretion during *in vivo* delivery. By modulating scaffold porosity, we control MSC cell-cell interactions to elucidate the effects of cell clustering on MSC secretion. We further sought to modify the granular scaffolds with integrin and cadherin mimetic peptides to understand how cadherin signaling affects MSC secretion.

Chapters 5 and 6 investigate the utility of our 3D granular porous hydrogels in clinically relevant applications. We first evaluate the capacity for these material systems to direct bone regeneration in a critical sized rat calvarial defect (Chapter 5). We design degradable granular hydrogels and formulate them to increase rMSC secretion. We implant these materials into 6 mm calvarial defects in rats and monitor microgel degradation, rMSC survival, and bone formation over 8 weeks. In Chapter 6, we study the secretome of MSCs isolated from a diseased bone environment, specifically a model of postmenopausal osteoporosis. By utilizing granular hydrogels, we exert precise control over the MSC microenvironment and characterize differences between osteoporotic and healthy MSC secretion as a function of cell clustering and N-cadherin signaling.

Finally, Chapter 7 summarizes the key findings of this thesis and suggests future directions to engineer the next generation of hydrogels to direct MSC secretome.

1.8 References

(1)   Friedenstein, A. J.; Gorskaja, U. F.; Kulagina, N. N. Fibroblast Precursors in Normal and Irradiated Mouse Hematopoietic Organs. *Experimental Hematology* **1976**, *4* (5), 267–274.

(2)   Dominici, M.; Blanc, K. le; Mueller, I.; Marini, F. C.; Krause, D. S.; Deans, R. J.; Keating, A.; Prockop, D. J.; Horwitz, E. M. Minimal Criteria for Defining Multipotent Mesenchymal Stromal Cells . The International Society for Cellular Therapy Position Statement. *Cytotherapy* **2006**, *8* (4), 315–317. https://doi.org/10.1080/14653240600855905.

(3)   Hass, R.; Kasper, C.; Böhm, S.; Jacobs, R. Different Populations and Sources of Human Mesenchymal Stem Cells (MSC): A Comparison of Adult and Neonatal Tissue-Derived MSC. *Cell Communication and Signaling* **2011**, *9*. https://doi.org/10.1186/1478-811X-9-12.

(4)   Pittenger, M. F.; Discher, D. E.; Péault, B. M.; Phinney, D. G.; Hare, J. M.; Caplan, A. I. Mesenchymal Stem Cell Perspective: Cell Biology to Clinical Progress. *npj Regenerative Medicine*. Nature Research December 1, 2019. https://doi.org/10.1038/s41536-019-0083-6.

(5)   Levy, O.; Kuai, R.; Siren, E. M. J.; Bhere, D.; Milton, Y.; Nissar, N.; De Biasio, M.; Heinelt, M.; Reeve, B.; Abdi, R.; Alturki, M.; Fallatah, M.; Almalik, A.; Alhasan, A. H.; Shah, K.; Karp, J. M. Shattering Barriers toward Clinically Meaningful MSC Therapies. *Science advances*. NLM (Medline) July 1, 2020, p eaba6884. https://doi.org/10.1126/sciadv.aba6884.

(6)   Murray, I. R.; Péault, B. Q&A: Mesenchymal Stem Cells - Where Do They Come from and Is It Important? *BMC Biology* **2015**, *13* (1). https://doi.org/10.1186/s12915-015-0212-7.

(7)   Caplan, A. I. Why Are MSCs Therapeutic? New Data: New Insight. *Journal of Pathology*. J Pathol January 2009, pp 318–324. https://doi.org/10.1002/path.2469.

(8)   Osugi, M.; Katagiri, W.; Yoshimi, R.; Inukai, T.; Hibi, H.; Ueda, M. Conditioned Media from Mesenchymal Stem Cells Enhanced Bone Regeneration in Rat Calvarial Bone Defects. *Tissue Engineering - Part A* **2012**, *18* (13–14), 1479–1489. https://doi.org/10.1089/ten.tea.2011.0325.

(9)   Fontaine, M. J.; Shih, H.; Schäfer, R.; Pittenger, M. F. Unraveling the Mesenchymal Stromal Cells' Paracrine Immunomodulatory Effects. *Transfusion Medicine Reviews*. W.B. Saunders January 1, 2016, pp 37–43. https://doi.org/10.1016/j.tmrv.2015.11.004.

(10)   English, K.; French, A.; Wood, K. J. Mesenchymal Stromal Cells: Facilitators of Successful Transplantation? *Cell Stem Cell*. Cell Stem Cell October 8, 2010, pp 431–442. https://doi.org/10.1016/j.stem.2010.09.009.

(11)   da Silva Meirelles, L.; Fontes, A. M.; Covas, D. T.; Caplan, A. I. Mechanisms Involved in the Therapeutic Properties of Mesenchymal Stem Cells. *Cytokine & Growth Factor Reviews* **2009**, *20* (5–6), 419–427. https://doi.org/10.1016/j.cytogfr.2009.10.002.

(12)   da Silva Meirelles, L.; Fontes, A. M.; Covas, D. T.; Caplan, A. I. Mechanisms Involved in the Therapeutic Properties of Mesenchymal Stem Cells. *Cytokine & Growth Factor Reviews* **2009**, *20* (5–6), 419–427. https://doi.org/10.1016/j.cytogfr.2009.10.002.

(13)   Herrera, M. B.; Bussolati, B.; Bruno, S.; Morando, L.; Mauriello-Romanazzi, G.; Sanavio, F.; Stamenkovic, I.; Biancone, L.; Camussi, G. Exogenous Mesenchymal Stem Cells

Localize to the Kidney by Means of CD44 Following Acute Tubular Injury. *Kidney International* **2007**, *72* (4), 430–441. https://doi.org/10.1038/sj.ki.5002334.

(14)   Ogata, K.; Osugi, M.; Kawai, T.; Wakayama, Y.; Sakaguchi, K.; Nakamura, S.; Katagiri, W. Secretomes of Mesenchymal Stem Cells Induce Early Bone Regeneration by Accelerating Migration of Stem Cells. *Journal of Oral and Maxillofacial Surgery, Medicine, and Pathology* **2018**, *30* (5), 445–451. https://doi.org/10.1016/j.ajoms.2018.04.002.

(15)   Katagiri, W.; Sakaguchi, K.; Kawai, T.; Wakayama, Y.; Osugi, M.; Hibi, H. A Defined Mix of Cytokines Mimics Conditioned Medium from Cultures of Bone Marrow-Derived Mesenchymal Stem Cells and Elicits Bone Regeneration. *Cell Proliferation* **2017**, *50* (3), e12333. https://doi.org/10.1111/cpr.12333.

(16)   Nicola, M. Di; Carlo-Stella, C.; Magni, M.; Milanesi, M.; Longoni, P. D.; Matteucci, P.; Grisanti, S.; Gianni, A. M. Human Bone Marrow Stromal Cells Suppress T-Lymphocyte Proliferation Induced by Cellular or Nonspecific Mitogenic Stimuli. *Blood* **2002**, *99* (10), 3838–3843. https://doi.org/10.1182/blood.V99.10.3838.

(17)   Zinöcker, S.; Vaage, J. T. Rat Mesenchymal Stromal Cells Inhibit T Cell Proliferation but Not Cytokine Production Through Inducible Nitric Oxide Synthase. *Frontiers in Immunology* **2012**, *3* (APR), 62. https://doi.org/10.3389/fimmu.2012.00062.

(18)   Corcione, A.; Benvenuto, F.; Ferretti, E.; Giunti, D.; Cappiello, V.; Cazzanti, F.; Risso, M.; Gualandi, F.; Mancardi, G. L.; Pistoia, V.; Uccelli, A. Human Mesenchymal Stem Cells Modulate B-Cell Functions. *Blood* **2006**. https://doi.org/10.1182/blood-2005-07-2657.

(19)   Viswanathan, S.; Shi, Y.; Galipeau, J.; Krampera, M.; Leblanc, K.; Martin, I.; Nolta, J.; Phinney, D. G.; Sensebe, L. Mesenchymal Stem versus Stromal Cells: International

Society for Cell & Gene Therapy (ISCT®) Mesenchymal Stromal Cell Committee Position Statement on Nomenclature. *Cytotherapy* **2019**, *21* (10), 1019–1024. https://doi.org/10.1016/j.jcyt.2019.08.002.

(20)   Galderisi, U.; Squillaro, T.; Peluso, G. Clinical Trials With Mesenchymal Stem Cells: An Update. *Cell Transplantation* **2016**, *25*, 829–848. https://doi.org/10.3727/096368915X689622.

(21)   Chen, Y.-S. Mesenchymal Stem Cell: Considerations for Manufacturing and Clinical Trials on Cell Therapy Product. *International Journal of Stem cell Research & Therapy* **2016**, *3* (1), 1–12. https://doi.org/10.23937/2469-570X/1410029.

(22)   Squillaro, T.; Peluso, G.; Galderisi, U. Review Clinical Trials With Mesenchymal Stem Cells : An Update. *Cell Transplantation* **2016**, *25*, 829–848.

(23)   Chen, Y.-S. Mesenchymal Stem Cell: Considerations for Manufacturing and Clinical Trials on Cell Therapy Product. *International Journal of Stem cell Research & Therapy* **2016**, *3* (1), 1–12. https://doi.org/10.23937/2469-570X/1410029.

(24)   Wagner, W.; Horn, P.; Castoldi, M.; Diehlmann, A.; Bork, S.; Saffrich, R.; Benes, V.; Blake, J.; Pfister, S.; Eckstein, V.; Ho, A. D. Replicative Senescence of Mesenchymal Stem Cells: A Continuous and Organized Process. *PLoS ONE* **2008**, *3* (5). https://doi.org/10.1371/journal.pone.0002213.

(25)   Jiang, T.; Xu, G.; Wang, Q.; Yang, L.; Zheng, L.; Zhao, J.; Zhang, X. In Vitro Expansion Impaired the Stemness of Early Passage Mesenchymal Stem Cells for Treatment of Cartilage Defects. *Cell Death and Disease* **2017**, *8* (6). https://doi.org/10.1038/cddis.2017.215.

(26)   Wagner, W.; Horn, P.; Castoldi, M.; Diehlmann, A.; Bork, S.; Saffrich, R.; Benes, V.; Blake, J.; Pfister, S.; Eckstein, V.; Ho, A. D. Replicative Senescence of Mesenchymal Stem Cells: A Continuous and Organized Process. *PLoS ONE* **2008**, *3* (5). https://doi.org/10.1371/journal.pone.0002213.

(27)   Wu, P. K.; Wang, J. Y.; Chen, C. F.; Chao, K. Y.; Chang, M. C.; Chen, W. M.; Hung, S. C. Early Passage Mesenchymal Stem Cells Display Decreased Radiosensitivity and Increased DNA Repair Activity. *Stem Cells Translational Medicine* **2017**, *6* (6), 1504–1514. https://doi.org/10.1002/sctm.15-0394.

(28)   Banfi, A.; Bianchi, G.; Notaro, R.; Luzzatto, L.; Cancedda, R.; Quarto, R. Replicative Aging and Gene Expression in Long-Term Cultures of Human Bone Marrow Stromal Cells. *Tissue Engineering* **2002**, *8* (6), 901–910. https://doi.org/10.1089/107632702320934001.

(29)   Rao, V. v.; Vu, M. K.; Ma, H.; Killaars, A. R.; Anseth, K. S. Rescuing Mesenchymal Stem Cell Regenerative Properties on Hydrogel Substrates Post Serial Expansion. *Bioengineering & Translational Medicine* **2018**, No. June, 1–10. https://doi.org/10.1002/btm2.10104.

(30)   Qazi, T. H.; Mooney, D. J.; Duda, G. N.; Geissler, S. Biomaterials That Promote Cell-Cell Interactions Enhance the Paracrine Function of MSCs. *Biomaterials* **2017**, *140*, 103–114. https://doi.org/10.1016/j.biomaterials.2017.06.019.

(31)   Rao, V. V.; Vu, M. K.; Ma, H.; Killaars, A. R.; Anseth, K. S. Rescuing Mesenchymal Stem Cell Regenerative Properties on Hydrogel Substrates Post Serial Expansion. *Bioengineering & Translational Medicine* **2018**, No. June, 1–10. https://doi.org/10.1002/btm2.10104.

(32) Madl, C. M.; Heilshorn, S. C.; Blau, H. M. Bioengineering Strategies to Accelerate Stem Cell Therapeutics. *Nature*. Nature Publishing Group May 17, 2018, pp 335–342. https://doi.org/10.1038/s41586-018-0089-z.

(33) Burdick, J. A.; Mauck, R. L.; Gerecht, S. To Serve and Protect: Hydrogels to Improve Stem Cell-Based Therapies. *Cell Stem Cell* **2016**, *18* (1), 13–15. https://doi.org/10.1016/j.stem.2015.12.004.

(34) Führmann, T.; Tam, R. Y.; Ballarin, B.; Coles, B.; Elliott Donaghue, I.; van der Kooy, D.; Nagy, A.; Tator, C. H.; Morshead, C. M.; Shoichet, M. S. Injectable Hydrogel Promotes Early Survival of Induced Pluripotent Stem Cell-Derived Oligodendrocytes and Attenuates Longterm Teratoma Formation in a Spinal Cord Injury Model. *Biomaterials* **2016**. https://doi.org/10.1016/j.biomaterials.2015.12.032.

(35) Hofmann, M.; Wollert, K. C.; Meyer, G. P.; Menke, A.; Arseniev, L.; Hertenstein, B.; Ganser, A.; Knapp, W. H.; Drexler, H. Monitoring of Bone Marrow Cell Homing into the Infarcted Human Myocardium. *Circulation* **2005**, *111* (17), 2198–2202. https://doi.org/10.1161/01.CIR.0000163546.27639.AA.

(36) Levit, R. D.; Landázuri, N.; Phelps, E. A.; Brown, M. E.; García, A. J.; Davis, M. E.; Joseph, G.; Long, R.; Safley, S. A.; Suever, J. D.; Lyle, A. N.; Weber, C. J.; Taylor, W. R. Cellular Encapsulation Enhances Cardiac Repair. *Journal of the American Heart Association* **2013**, *2* (5). https://doi.org/10.1161/JAHA.113.000367.

(37) Ullah, M.; Liu, D. D.; Thakor, A. S. Mesenchymal Stromal Cell Homing: Mechanisms and Strategies for Improvement. *iScience*. Elsevier Inc. May 31, 2019, pp 421–438. https://doi.org/10.1016/j.isci.2019.05.004.

(38) Kraitchman, D. L.; Tatsumi, M.; Gilson, W. D.; Ishimori, T.; Kedziorek, D.; Walczak, P.; Segars, W. P.; Chen, H. H.; Fritzges, D.; Izbudak, I.; Young, R. G.; Marcelino, M.; Pittenger, M. F.; Solaiyappan, M.; Boston, R. C.; Tsui, B. M. W.; Wahl, R. L.; Bulte, J. W. M. Dynamic Imaging of Allogeneic Mesenchymal Stem Cells Trafficking to Myocardial Infarction. *Circulation* **2005**, *112* (10), 1451–1461. https://doi.org/10.1161/CIRCULATIONAHA.105.537480.

(39) Wagner, B.; Henschler, R. Fate of Intravenously Injected Mesenchymal Stem Cells and Significance for Clinical Application. In *Advances in biochemical engineering/biotechnology*; Springer, Berlin, Heidelberg, 2012; Vol. 130, pp 19–37. https://doi.org/10.1007/10_2012_155.

(40) Scarfe, L.; Taylor, A.; Sharkey, J.; Harwood, R.; Barrow, M.; Comenge, J.; Beeken, L.; Astley, C.; Santeramo, I.; Hutchinson, C.; Ressel, L.; Smythe, J.; Austin, E.; Levy, R.; Rosseinsky, M. J.; Adams, D. J.; Poptani, H.; Park, B. K.; Murray, P.; Wilm, B. Non-Invasive Imaging Reveals Conditions That Impact Distribution and Persistence of Cells after in Vivo Administration. *Stem Cell Research and Therapy* **2018**, *9* (1). https://doi.org/10.1186/s13287-018-1076-x.

(41) Ozeki, N.; Muneta, T.; Koga, H.; Nakagawa, Y.; Mizuno, M.; Tsuji, K.; Mabuchi, Y.; Akazawa, C.; Kobayashi, E.; Matsumoto, K.; Futamura, K.; Saito, T.; Sekiya, I. Not Single but Periodic Injections of Synovial Mesenchymal Stem Cells Maintain Viable Cells in Knees and Inhibit Osteoarthritis Progression in Rats. *Osteoarthritis and Cartilage* **2016**, *24* (6), 1061–1070. https://doi.org/10.1016/j.joca.2015.12.018.

(42) Kim, Y. H.; Jin, H. J.; Heo, J.; Ju, H.; Lee, H. Y.; Kim, S.; Lee, S.; Lim, J.; Jeong, S. Y.; Kwon, J. H.; Kim, M.; Choi, S. J.; Oh, W.; Yang, Y. S.; Hwang, H. H.; Yu, H. Y.; Ryu, C.

M.; Jeon, H. B.; Shin, D. M. Small Hypoxia-Primed Mesenchymal Stem Cells Attenuate Graft-versus-Host Disease. *Leukemia* **2018**, *32* (12), 2672–2684. https://doi.org/10.1038/s41375-018-0151-8.

(43) Antebi, B.; Rodriguez, L. A.; Walker, K. P.; Asher, A. M.; Kamucheka, R. M.; Alvarado, L.; Mohammadipoor, A.; Cancio, L. C. Short-Term Physiological Hypoxia Potentiates the Therapeutic Function of Mesenchymal Stem Cells. *Stem Cell Research and Therapy* **2018**, *9* (1). https://doi.org/10.1186/s13287-018-1007-x.

(44) Vigo, T.; Procaccini, C.; Ferrara, G.; Baranzini, S.; Oksenberg, J. R.; Matarese, G.; Diaspro, A.; Kerlero de Rosbo, N.; Uccelli, A. IFN-γ Orchestrates Mesenchymal Stem Cell Plasticity through the Signal Transducer and Activator of Transcription 1 and 3 and Mammalian Target of Rapamycin Pathways. *Journal of Allergy and Clinical Immunology* **2017**, *139* (5), 1667–1676. https://doi.org/10.1016/j.jaci.2016.09.004.

(45) Yang, Z.; Concannon, J.; Ng, K. S.; Seyb, K.; Mortensen, L. J.; Ranganath, S.; Gu, F.; Levy, O.; Tong, Z.; Martyn, K.; Zhao, W.; Lin, C. P.; Glicksman, M. A.; Karp, J. M. Tetrandrine Identified in a Small Molecule Screen to Activate Mesenchymal Stem Cells for Enhanced Immunomodulation. *Scientific Reports* **2016**, *6*. https://doi.org/10.1038/srep30263.

(46) Levy, O.; Mortensen, L. J.; Boquet, G.; Tong, Z.; Perrault, C.; Benhamou, B.; Zhang, J.; Stratton, T.; Han, E.; Safaee, H.; Musabeyezu, J.; Yang, Z.; Multon, M.-C.; Rothblatt, J.; Deleuze, J.-F.; Lin, C. P.; Karp, J. M. A Small-Molecule Screen for Enhanced Homing of Systemically Infused Cells. *Cell Reports* **2015**, *10* (8), 1261–1268. https://doi.org/10.1016/j.celrep.2015.01.057.

(47)   Noronha Nc, N. D. C.; Mizukami, A.; Caliári-Oliveira, C.; Cominal, J. G.; Rocha, J. L. M.; Covas, D. T.; Swiech, K.; Malmegrim, K. C. R. Priming Approaches to Improve the Efficacy of Mesenchymal Stromal Cell-Based Therapies. *Stem Cell Research and Therapy*. BioMed Central Ltd. May 2, 2019. https://doi.org/10.1186/s13287-019-1224-y.

(48)   Ranganath, S. H.; Tong, Z.; Levy, O.; Martyn, K.; Karp, J. M.; Inamdar, M. S. Controlled Inhibition of the Mesenchymal Stromal Cell Pro-Inflammatory Secretome via Microparticle Engineering. *Stem Cell Reports* **2016**, *6* (6), 926–939. https://doi.org/10.1016/j.stemcr.2016.05.003.

(49)   Lutolf, M. P.; Hubbell, J. A. Synthetic Biomaterials as Instructive Extracellular Microenvironments for Morphogenesis in Tissue Engineering. *Nature Biotechnology*. Nature Publishing Group January 1, 2005, pp 47–55. https://doi.org/10.1038/nbt1055.

(50)   Hubbell, J. A. Biomaterials in Tissue Engineering. *Bio/Technology*. Nature Publishing Group 1995, pp 565–576. https://doi.org/10.1038/nbt0695-565.

(51)   Place, E. S.; Evans, N. D.; Stevens, M. M. Complexity in Biomaterials for Tissue Engineering. *Nature Materials* **2009**, *8* (6), 457–470. https://doi.org/10.1038/nmat2441.

(52)   Slaughter, B. V; Khurshid, S. S.; Fisher, O. Z.; Khademhosseini, A.; Peppas, N. A. Hydrogels in Regenerative Medicine. *Advanced materials (Deerfield Beach, Fla.)* **2009**, *21* (32–33), 3307–3329. https://doi.org/10.1002/adma.200802106.

(53)   Peppas, N. A. *Hydrogels in Medicine and Pharmacy*; CRC Press, 1986.

(54)   Peppas, N. A.; Hilt, J. Z.; Khademhosseini, A.; Langer, R. Hydrogels in Biology and Medicine: From Molecular Principles to Bionanotechnology. *Advanced Materials* **2006**, *18* (11), 1345–1360. https://doi.org/10.1002/adma.200501612.

(55)   Peppas, N. A.; Bures, P.; Leobandung, W.; Ichikawa, H. Hydrogels in Pharmaceutical Formulations. *European Journal of Pharmaceutics and Biopharmaceutics* **2000**, *50* (1), 27–46. https://doi.org/10.1016/S0939-6411(00)00090-4.

(56)   Wong, S. W.; Lenzini, S.; Cooper, M. H.; Mooney, D. J.; Shin, J. W. Soft Extracellular Matrix Enhances Inflammatory Activation of Mesenchymal Stromal Cells to Induce Monocyte Production and Trafficking. *Science Advances* **2020**, *6* (15). https://doi.org/10.1126/sciadv.aaw0158.

(57)   Ho, S. S.; Murphy, K. C.; Binder, B. Y. K.; Vissers, C. B.; Leach, J. K. Increased Survival and Function of Mesenchymal Stem Cell Spheroids Entrapped in Instructive Alginate Hydrogels. *Stem Cells Translational Medicine* **2016**, *5*, 773–781.

(58)   Sridhar, B. V.; Brock, J. L.; Silver, J. S.; Leight, J. L.; Randolph, M. A.; Anseth, K. S. Development of a Cellularly Degradable PEG Hydrogel to Promote Articular Cartilage Extracellular Matrix Deposition. *Advanced Healthcare Materials* **2015**, *4* (5), 702–713. https://doi.org/10.1002/adhm.201400695.

(59)   Park, K. W.; Waki, H.; Kim, W.-K.; Davies, B. S. J.; Young, S. G.; Parhami, F.; Tontonoz, P. The Small Molecule Phenamil Induces Osteoblast Differentiation and Mineralization. *Molecular and Cellular Biology* **2009**, *29* (14), 3905–3914. https://doi.org/10.1128/MCB.00002-09.

(60)   Fan, J.; Im, C. S.; Cui, Z. K.; Guo, M.; Bezouglaia, O.; Fartash, A.; Lee, J. Y.; Nguyen, J.; Wu, B. M.; Aghaloo, T.; Lee, M. Delivery of Phenamil Enhances BMP-2-Induced Osteogenic Differentiation of Adipose-Derived Stem Cells and Bone Formation in Calvarial Defects. *Tissue engineering. Part A* **2015**, *21* (13–14), 2053–2065. https://doi.org/10.1089/ten.tea.2014.0489.

(61)   Fan, W.; Yuan, L.; Li, J.; Wang, Z.; Chen, J.; Guo, C.; Mo, X.; Yan, Z. Injectable Double-Crosslinked Hydrogels with Kartogenin-Conjugated Polyurethane Nano-Particles and Transforming Growth Factor B3 for in-Situ Cartilage Regeneration. *Materials Science and Engineering C* **2020**, *110*, 110705. https://doi.org/10.1016/j.msec.2020.110705.

(62)   Chinnadurai, R.; Copland, I. B.; Patel, S. R.; Galipeau, J. IDO-Independent Suppression of T Cell Effector Function by IFN-γ–Licensed Human Mesenchymal Stromal Cells. *The Journal of Immunology* **2014**, *192* (4), 1491–1501. https://doi.org/10.4049/jimmunol.1301828.

(63)   Tsiapalis, D.; O'Driscoll, L. Mesenchymal Stem Cell Derived Extracellular Vesicles for Tissue Engineering and Regenerative Medicine Applications. *Cells*. NLM (Medline) April 16, 2020. https://doi.org/10.3390/cells9040991.

(64)   Park, K. S.; Bandeira, E.; Shelke, G. V.; Lässer, C.; Lötvall, J. Enhancement of Therapeutic Potential of Mesenchymal Stem Cell-Derived Extracellular Vesicles. *Stem Cell Research and Therapy*. BioMed Central Ltd. September 23, 2019, pp 1–15. https://doi.org/10.1186/s13287-019-1398-3.

(65)   Brennan, M. Á.; Layrolle, P.; Mooney, D. J. Biomaterials Functionalized with MSC Secreted Extracellular Vesicles and Soluble Factors for Tissue Regeneration. *Advanced Functional Materials* **2020**, 1909125. https://doi.org/10.1002/adfm.201909125.

(66)   Balmayor, E. R. Targeted Delivery as Key for the Success of Small Osteoinductive Molecules. *Advanced Drug Delivery Reviews* **2015**, *94*, 13–27. https://doi.org/10.1016/j.addr.2015.04.022.

(67)   Lo, K. W.-H.; Jiang, T.; Gagnon, K. A.; Nelson, C.; Laurencin, C. T. Small-Molecule Based Musculoskeletal Regenerative Engineering. *Trends in biotechnology* **2014**, *32* (2), 74–81. https://doi.org/10.1016/j.tibtech.2013.12.002.

(68)   Wu, X.; Ding, S.; Ding, Q.; Gray, N. S.; Schultz, P. G. A Small Molecule with Osteogenesis-Inducing Activity in Multipotent Mesenchymal Progenitor Cells. *Journal of the American Chemical Society* **2002**, *124* (49), 14520–14521. https://doi.org/10.1021/ja0283908.

(69)   Lo, K. W.-H.; Ulery, B. D.; Kan, H. M.; Ashe, K. M.; Laurencin, C. T. Evaluating the Feasibility of Utilizing the Small Molecule Phenamil as a Novel Biofactor for Bone Regenerative Engineering. *Journal of Tissue Engineering and Regenerative Medicine* **2014**, *8* (9), 728–736. https://doi.org/10.1002/term.1573.

(70)   Johnson, K.; Zhu, S.; Tremblay, M. S.; Payette, J. N.; Wang, J.; Bouchez, L. C.; Meeusen, S.; Althage, A.; Cho, C. Y.; Wu, X.; Schultz, P. G. A Stem Cell-Based Approach to Cartilage Repair. *Science* **2012**, *336* (6082), 717–721. https://doi.org/10.1126/science.1215157.

(71)   Wu, X.; Ding, S.; Ding, Q.; Gray, N. S.; Schultz, P. G. A Small Molecule with Osteogenesis-Inducing Activity in Multipotent Mesenchymal Progenitor Cells. *Journal of the American Chemical Society* **2002**, *124* (49), 14520–14521. https://doi.org/10.1021/ja0283908.

(72)   Gellynck, K.; Shah, R.; Parkar, M.; Young, A.; Buxton, P.; Brett, P. Small Molecule Stimulation Enhances Bone Regeneration but Not Titanium Implant Osseointegration. *Bone* **2013**, *57* (2), 405–412. https://doi.org/10.1016/j.bone.2013.09.012.

(73)   Park, K. W.; Waki, H.; Kim, W.-K.; Davies, B. S. J.; Young, S. G.; Parhami, F.; Tontonoz, P. The Small Molecule Phenamil Induces Osteoblast Differentiation and Mineralization. *Molecular and Cellular Biology* **2009**, *29* (14), 3905–3914. https://doi.org/10.1128/MCB.00002-09.

(74)   Lo, K. W.-H.; Kan, H. M.; Laurencin, C. T. Short-Term Administration of Small Molecule Phenamil Induced a Protracted Osteogenic Effect on Osteoblast-like MC3T3-E1 Cells. *Journal of Tissue Engineering and Regenerative Medicine* **2016**, *10* (6), 518–526. https://doi.org/10.1002/term.1786.

(75)   Lo, K. W.-H.; Ulery, B. D.; Kan, H. M.; Ashe, K. M.; Laurencin, C. T. Evaluating the Feasibility of Utilizing the Small Molecule Phenamil as a Novel Biofactor for Bone Regenerative Engineering. *Journal of Tissue Engineering and Regenerative Medicine* **2014**, *8* (9), 728–736. https://doi.org/10.1002/term.1573.

(76)   Zhao, D.; Lei, L.; Wang, S.; Nie, H. Understanding Cell Homing-Based Tissue Regeneration from the Perspective of Materials. *Journal of Materials Chemistry B*. Royal Society of Chemistry July 22, 2015, pp 7319–7333. https://doi.org/10.1039/c5tb01188d.

(77)   Hong, L.; Zhang, G.; Sultana, H.; Yu, Y.; Wei, Z. The Effects of 17-β Estradiol on Enhancing Proliferation of Human Bone Marrow Mesenchymal Stromal Cells in Vitro. *Stem Cells and Development* **2011**, *20* (5), 925–931. https://doi.org/10.1089/scd.2010.0125.

(78)   Zhao, Q.; Ren, H.; Han, Z. Mesenchymal Stem Cells: Immunomodulatory Capability and Clinical Potential in Immune Diseases. *Journal of Cellular Immunotherapy*. Shanghai Hengrun Biomedical Technology Research Institute March 2016, pp 3–20. https://doi.org/10.1016/j.jocit.2014.12.001.

(79)   Abdi, R.; Fiorina, P.; Adra, C. N.; Atkinson, M.; Sayegh, M. H. Immunomodulation by Mesenchymal Stem Cells: A Potential Therapeutic Strategy for Type 1 Diabetes. *Diabetes*. American Diabetes Association July 2008, pp 1759–1767. https://doi.org/10.2337/db08-0180.

(80)   Abdi, R.; Fiorina, P.; Adra, C. N.; Atkinson, M.; Sayegh, M. H. Immunomodulation by Mesenchymal Stem Cells: A Potential Therapeutic Strategy for Type 1 Diabetes. *Diabetes*. American Diabetes Association July 2008, pp 1759–1767. https://doi.org/10.2337/db08-0180.

(81)   Song, N.; Scholtemeijer, M.; Shah, K. Mesenchymal Stem Cell Immunomodulation: Mechanisms and Therapeutic Potential. *Trends in Pharmacological Sciences*. Elsevier Ltd September 1, 2020, pp 653–664. https://doi.org/10.1016/j.tips.2020.06.009.

(82)   Ghannam, S.; Bouffi, C.; Djouad, F.; Jorgensen, C.; Noël, D. Immunosuppression by Mesenchymal Stem Cells: Mechanisms and Clinical Applications. *Stem Cell Research and Therapy*. BioMed Central March 2010, p 2. https://doi.org/10.1186/scrt2.

(83)   Wang, M.; Yuan, Q.; Xie, L. Mesenchymal Stem Cell-Based Immunomodulation: Properties and Clinical Application. *Stem Cells International*. Hindawi Limited 2018. https://doi.org/10.1155/2018/3057624.

(84)   Cicchese, J. M.; Evans, S.; Hult, C.; Joslyn, L. R.; Wessler, T.; Millar, J. A.; Marino, S.; Cilfone, N. A.; Mattila, J. T.; Linderman, J. J.; Kirschner, D. E. Dynamic Balance of Pro- and Anti-Inflammatory Signals Controls Disease and Limits Pathology. *Immunological Reviews* **2018**, *285* (1), 147–167. https://doi.org/10.1111/imr.12671.

(85)   Saldaña, L.; Bensiamar, F.; Vallés, G.; Mancebo, F. J.; García-Rey, E.; Vilaboa, N. Immunoregulatory Potential of Mesenchymal Stem Cells Following Activation by

Macrophage-Derived Soluble Factors. *Stem Cell Research & Therapy* **2019**, *10* (1), 58. https://doi.org/10.1186/s13287-019-1156-6.

(86)   Kyurkchiev, D. Secretion of Immunoregulatory Cytokines by Mesenchymal Stem Cells. *World Journal of Stem Cells* **2014**, *6* (5), 552. https://doi.org/10.4252/wjsc.v6.i5.552.

(87)   Sivanathan, K. N.; Gronthos, S.; Rojas-Canales, D.; Thierry, B.; Coates, P. T. Interferon-Gamma Modification of Mesenchymal Stem Cells: Implications of Autologous and Allogeneic Mesenchymal Stem Cell Therapy in Allotransplantation. *Stem Cell Reviews and Reports* **2014**, *10* (3), 351–375. https://doi.org/10.1007/s12015-014-9495-2.

(88)   Bartosh, T. J.; Ylöstalo, J. H.; Mohammadipoor, A.; Bazhanov, N.; Coble, K.; Claypool, K.; Lee, R. H.; Choi, H.; Prockop, D. J. Aggregation of Human Mesenchymal Stromal Cells (MSCs) into 3D Spheroids Enhances Their Antiinflammatory Properties. *Proceedings of the National Academy of Sciences of the United States of America* **2010**, *107* (31), 13724–13729. https://doi.org/10.1073/pnas.1008117107.

(89)   Krampera, M.; Cosmi, L.; Angeli, R.; Pasini, A.; Liotta, F.; Andreini, A.; Santarlasci, V.; Mazzinghi, B.; Pizzolo, G.; Vinante, F.; Romagnani, P.; Maggi, E.; Romagnani, S.; Annunziato, F. Role for Interferon-γ in the Immunomodulatory Activity of Human Bone Marrow Mesenchymal Stem Cells. *Stem Cells* **2006**, *24* (2), 386–398. https://doi.org/10.1634/stemcells.2005-0008.

(90)   Ghannam, S.; Bouffi, C.; Djouad, F.; Jorgensen, C.; Noël, D. Immunosuppression by Mesenchymal Stem Cells: Mechanisms and Clinical Applications. *Stem Cell Research and Therapy*. BioMed Central March 2010, p 2. https://doi.org/10.1186/scrt2.

(91)   Idriss, H. T.; Naismith, J. H. TNFα and the TNF Receptor Superfamily: Structure-Function Relationship(s). *Microscopy Research and Technique* **2000**, *50* (3), 184–195. https://doi.org/10.1002/1097-0029(20000801)50:3<184::AID-JEMT2>3.0.CO;2-H.

(92)   Tu, Z.; Li, Q.; Bu, H.; Lin, F. Mesenchymal Stem Cells Inhibit Complement Activation by Secreting Factor h. *Stem Cells and Development* **2010**, *19* (11), 1803–1809. https://doi.org/10.1089/scd.2009.0418.

(93)   François, M.; Romieu-Mourez, R.; Li, M.; Galipeau, J. Human MSC Suppression Correlates with Cytokine Induction of Indoleamine 2,3-Dioxygenase and Bystander M2 Macrophage Differentiation. *Molecular Therapy* **2012**, *20* (1), 187–195. https://doi.org/10.1038/mt.2011.189.

(94)   Redondo-Castro, E.; Cunningham, C.; Miller, J.; Martuscelli, L.; Aoulad-Ali, S.; Rothwell, N. J.; Kielty, C. M.; Allan, S. M.; Pinteaux, E. Interleukin-1 Primes Human Mesenchymal Stem Cells towards an Anti-Inflammatory and pro-Trophic Phenotype in Vitro. *Stem Cell Research and Therapy* **2017**, *8* (1). https://doi.org/10.1186/s13287-017-0531-4.

(95)   Madrigal, M.; Rao, K. S.; Riordan, N. H. A Review of Therapeutic Effects of Mesenchymal Stem Cell Secretions and Induction of Secretory Modification by Different Culture Methods. *Journal of Translational Medicine*. BioMed Central Ltd. December 11, 2014, p 260. https://doi.org/10.1186/s12967-014-0260-8.

(96)   Gnecchi, M.; Zhang, Z.; Ni, A.; Dzau, V. J. Paracrine Mechanisms in Adult Stem Cell Signaling and Therapy. *Circulation Research*. Lippincott Williams & Wilkins November 21, 2008, pp 1204–1219. https://doi.org/10.1161/CIRCRESAHA.108.176826.

(97) Song, N.; Scholtemeijer, M.; Shah, K. Mesenchymal Stem Cell Immunomodulation: Mechanisms and Therapeutic Potential. *Trends in Pharmacological Sciences*. Elsevier Ltd September 1, 2020, pp 653–664. https://doi.org/10.1016/j.tips.2020.06.009.

(98) Li, J. H.; Zhang, N.; Wangi, J. A. Improved Anti-Apoptotic and Anti-Remodeling Potency of Bone Marrow Mesenchymal Stem Cells by Anoxic Pre-Conditioning in Diabetic Cardiomyopathy. *Journal of Endocrinological Investigation* **2008**, *31* (2), 103–110. https://doi.org/10.1007/BF03345575.

(99) Hawkins, K. E.; Sharp, T. V.; Mckay, T. R. The Role of Hypoxia in Stem Cell Potency and Differentiation. *Regenerative Medicine*. Regen Med November 2013, pp 771–782. https://doi.org/10.2217/rme.13.71.

(100) Murphy, K. C.; Hung, B. P.; Browne-Bourne, S.; Zhou, D.; Yeung, J.; Genetos, D. C.; Leach, J. K. Measurement of Oxygen Tension within Mesenchymal Stem Cell Spheroids. *Journal of the Royal Society Interface* **2017**, *14* (127). https://doi.org/10.1098/rsif.2016.0851.

(101) Ho, S. S.; Hung, B. P.; Heyrani, N.; Lee, M. A.; Leach, J. K. Hypoxic Preconditioning of Mesenchymal Stem Cells with Subsequent Spheroid Formation Accelerates Repair of Segmental Bone Defects. *Stem Cells* **2018**, *36* (9), 1393–1403. https://doi.org/10.1002/stem.2853.

(102) Kyburz, K. A.; Anseth, K. S. Synthetic Mimics of the Extracellular Matrix: How Simple Is Complex Enough? *Annals of Biomedical Engineering* **2015**, *43* (3), 489–500. https://doi.org/10.1007/s10439-015-1297-4.

(103) Humphrey, J. D.; Dufresne, E. R.; Schwartz, M. A. Mechanotransduction and Extracellular Matrix Homeostasis. *Nature Reviews Molecular Cell Biology*. Nature Publishing Group December 11, 2014, pp 802–812. https://doi.org/10.1038/nrm3896.

(104) Tibbitt, M. W.; Anseth, K. S. Hydrogels as Extracellular Matrix Mimics for 3D Cell Culture. *Biotechnology and Bioengineering* **2009**, *103* (4), 655–663. https://doi.org/10.1002/bit.22361.

(105) Karimi, F.; O'Connor, A. J.; Qiao, G. G.; Heath, D. E. Integrin Clustering Matters: A Review of Biomaterials Functionalized with Multivalent Integrin-Binding Ligands to Improve Cell Adhesion, Migration, Differentiation, Angiogenesis, and Biomedical Device Integration. *Advanced Healthcare Materials* **2018**, *1701324*, 1–28. https://doi.org/10.1002/adhm.201701324.

(106) De Lisio, M.; Jensen, T.; Sukiennik, R. A.; Huntsman, H. D.; Boppart, M. D. Substrate and Strain Alter the Muscle-Derived Mesenchymal Stem Cell Secretome to Promote Myogenesis. *Stem Cell Research and Therapy* **2014**, *5* (3), 74. https://doi.org/10.1186/scrt463.

(107) Abdeen, A. A.; Weiss, J. B.; Lee, J.; Kilian, K. A. Matrix Composition and Mechanics Direct Proangiogenic Signaling from Mesenchymal Stem Cells. *Tissue engineering. Part A* **2014**, *20* (19–20), 2737–2745. https://doi.org/10.1089/ten.tea.2013.0661.

(108) Ogle, M. E.; Doron, G.; Levy, M. J.; Temenoff, J. S. Hydrogel Culture Surface Stiffness Modulates Mesenchymal Stromal Cell Secretome and Alters Senescence. *Tissue Engineering Part A* **2020**, ten.tea.2020.0030. https://doi.org/10.1089/ten.tea.2020.0030.

(109) Clark, A. Y.; Martin, K. E.; García, J. R.; Johnson, C. T.; Theriault, H. S.; Han, W. M.; Zhou, D. W.; Botchwey, E. A.; García, A. J. Integrin-Specific Hydrogels Modulate

Transplanted Human Bone Marrow-Derived Mesenchymal Stem Cell Survival, Engraftment, and Reparative Activities. *Nature Communications* **2020**, *11* (1). https://doi.org/10.1038/s41467-019-14000-9.

(110) Wu, P. K.; Wang, J. Y.; Chen, C. F.; Chao, K. Y.; Chang, M. C.; Chen, W. M.; Hung, S. C. Early Passage Mesenchymal Stem Cells Display Decreased Radiosensitivity and Increased DNA Repair Activity. *Stem Cells Translational Medicine* **2017**, *6* (6), 1504–1514. https://doi.org/10.1002/sctm.15-0394.

(111) Liu, F. D.; Pishesha, N.; Poon, Z.; Kaushik, T.; Van Vliet, K. J. Material Viscoelastic Properties Modulate the Mesenchymal Stem Cell Secretome for Applications in Hematopoietic Recovery. *ACS Biomaterials Science and Engineering* **2017**, *3* (12), 3292–3306. https://doi.org/10.1021/acsbiomaterials.7b00644.

(112) Cai, L.; Dewi, R. E.; Goldstone, A. B.; Cohen, J. E.; Steele, A. N.; Woo, Y. J.; Heilshorn, S. C. Regulating Stem Cell Secretome Using Injectable Hydrogels with In Situ Network Formation. *Advanced Healthcare Materials* **2016**, *5* (21), 2758–2764. https://doi.org/10.1002/adhm.201600497.

(113) Cosgrove, B. D.; Mui, K. L.; Driscoll, T. P.; Caliari, S. R.; Mehta, K. D.; Assoian, R. K.; Burdick, J. A.; Mauck, R. L. N-Cadherin Adhesive Interactions Modulate Matrix Mechanosensing and Fate Commitment of Mesenchymal Stem Cells. *Nature Materials* **2016**, *15* (12), 1297–1306. https://doi.org/10.1038/nmat4725.

(114) Caldwell, A. S.; Rao, V. V.; Golden, A. C.; Anseth, K. S. Porous Bio-Click Microgel Scaffolds Control HMSC Interactions and Promote Their Secretory Properties. *Biomaterials* **2020**, *232* (December 2019), 119725. https://doi.org/10.1016/j.biomaterials.2019.119725.

(115) Caldwell, A. S.; Campbell, G. T.; Shekiro, K. M. T.; Anseth, K. S. Clickable Microgel Scaffolds as Platforms for 3D Cell Encapsulation. *Advanced Healthcare Materials* **2017**, *6* (15), 1–8. https://doi.org/10.1002/adhm.201700254.

(116) Gionet-Gonzales, M. A.; Leach, J. K. Engineering Principles for Guiding Spheroid Function in the Regeneration of Bone, Cartilage, and Skin. *Biomedical Materials (Bristol)* **2018**, *13* (3). https://doi.org/10.1088/1748-605X/aab0b3.

(117) Gionet-Gonzales, M. A.; Leach, J. K. Engineering Principles for Guiding Spheroid Function in the Regeneration of Bone, Cartilage, and Skin. *Biomedical Materials (Bristol)* **2018**, *13* (3). https://doi.org/10.1088/1748-605X/aab0b3.

(118) Murphy, K. C.; Whitehead, J.; Falahee, P. C.; Zhou, D.; Simon, S. I.; Leach, J. K. Multifactorial Experimental Design to Optimize the Anti-Inflammatory and Proangiogenic Potential of Mesenchymal Stem Cell Spheroids. *Stem Cells* **2017**, *35* (6), 1493–1504. https://doi.org/10.1002/stem.2606.

(119) Murphy, K. C.; Whitehead, J.; Zhou, D.; Ho, S. S.; Leach, J. K. Engineering Fibrin Hydrogels to Promote the Wound Healing Potential of Mesenchymal Stem Cell Spheroids. *Acta Biomaterialia* **2017**, *64*, 176–186. https://doi.org/10.1016/j.actbio.2017.10.007.

(120) Peyton, S. R.; Kalcioglu, Z. I.; Cohen, J. C.; Runkle, A. P.; Van Vliet, K. J.; Lauffenburger, D. A.; Griffith, L. G. Marrow-Derived Stem Cell Motility in 3D Synthetic Scaffold Is Governed by Geometry along with Adhesivity and Stiffness. *Biotechnology and Bioengineering* **2011**, *108* (5), 1181–1193. https://doi.org/10.1002/bit.23027.

(121) Madden, L. R.; Mortisen, D. J.; Sussman, E. M.; Dupras, S. K.; Fugate, J. A.; Cuy, J. L.; Hauch, K. D.; Laflamme, M. A.; Murry, C. E.; Ratner, B. D. Proangiogenic Scaffolds as Functional Templates for Cardiac Tissue Engineering. *Proceedings of the National*

Academy of Sciences of the United States of America* **2010**, *107* (34), 15211–15216. https://doi.org/10.1073/pnas.1006442107.

(122) Golden, A. P.; Tien, J. Fabrication of Microfluidic Hydrogels Using Molded Gelatin as a Sacrificial Element. *Lab on a Chip* **2007**, *7* (6), 720–725. https://doi.org/10.1039/b618409j.

(123) Lutolf, M. P.; Weber, F. E.; Schmoekel, H. G.; Schense, J. C.; Kohler, T.; Müller, R.; Hubbell, J. A. Repair of Bone Defects Using Synthetic Mimetics of Collagenous Extracellular Matrices. *Nature Biotechnology* **2003**, *21* (5), 513–518. https://doi.org/10.1038/nbt818.

(124) Qazi, T. H.; Tytgat, L.; Dubruel, P.; Duda, G. N.; Van Vlierberghe, S.; Geissler, S. Extrusion Printed Scaffolds with Varying Pore Size As Modulators of MSC Angiogenic Paracrine Effects. *ACS Biomaterials Science and Engineering* **2019**, *5* (10), 5348–5358. https://doi.org/10.1021/acsbiomaterials.9b00843.

(125) de Rutte, J. M.; Koh, J.; Di Carlo, D. Scalable High-Throughput Production of Modular Microgels for In Situ Assembly of Microporous Tissue Scaffolds. *Advanced Functional Materials* **2019**, *29* (25), 1900071. https://doi.org/10.1002/adfm.201900071.

(126) Zhang, L.; Chen, K.; Zhang, H.; Pang, B.; Choi, C.-H.; Mao, A. S.; Liao, H.; Utech, S.; Mooney, D. J.; Wang, H.; Weitz, D. A. Microfluidic Templated Multicompartment Microgels for 3D Encapsulation and Pairing of Single Cells. *Small* **2018**, *14* (9), 1702955. https://doi.org/10.1002/smll.201702955.

(127) Caldwell, A. S.; Campbell, G. T.; Shekiro, K. M. T.; Anseth, K. S. Clickable Microgel Scaffolds as Platforms for 3D Cell Encapsulation. *Advanced Healthcare Materials* **2017**, *6* (15), 1–8. https://doi.org/10.1002/adhm.201700254.

(128) Qazi, T. H.; Tytgat, L.; Dubruel, P.; Duda, G. N.; Van Vlierberghe, S.; Geissler, S. Extrusion Printed Scaffolds with Varying Pore Size As Modulators of MSC Angiogenic Paracrine Effects. *ACS Biomaterials Science and Engineering* **2019**, *5* (10), 5348–5358. https://doi.org/10.1021/acsbiomaterials.9b00843.

(129) Williams, E.; Williams, G.; Gour, B. J.; Blaschuk, O. W.; Doherty, P. *A Novel Family of Cyclic Peptide Antagonists Suggests That N-Cadherin Specificity Is Determined by Amino Acids That Flank the HAV Motif**; 2000.

(130) Cosgrove, B. D.; Mui, K. L.; Driscoll, T. P.; Caliari, S. R.; Mehta, K. D.; Assoian, R. K.; Burdick, J. A.; Mauck, R. L. N-Cadherin Adhesive Interactions Modulate Matrix Mechanosensing and Fate Commitment of Mesenchymal Stem Cells. *Nature Materials* **2016**, *15* (12), 1297–1306. https://doi.org/10.1038/nmat4725.

(131) Qazi, T. H.; Mooney, D. J.; Duda, G. N.; Geissler, S. Niche-Mimicking Interactions in Peptide-Functionalized 3D Hydrogels Amplify Mesenchymal Stromal Cell Paracrine Effects. *Biomaterials* **2020**, *230*. https://doi.org/10.1016/j.biomaterials.2019.119639.

(132) Mao, A. S.; Özkale, B.; Shah, N. J.; Vining, K. H.; Descombes, T.; Zhang, L.; Tringides, C. M.; Wong, S. W.; Shin, J. W.; Scadden, D. T.; Weitz, D. A.; Mooney, D. J. Programmable Microencapsulation for Enhanced Mesenchymal Stem Cell Persistence and Immunomodulation. *Proceedings of the National Academy of Sciences of the United States of America* **2019**, *116* (31), 15392–15397. https://doi.org/10.1073/pnas.1819415116.

(133) Murphy, K. C.; Hung, B. P.; Browne-Bourne, S.; Zhou, D.; Yeung, J.; Genetos, D. C.; Leach, J. K. Measurement of Oxygen Tension within Mesenchymal Stem Cell Spheroids. *Journal of the Royal Society Interface* **2017**, *14* (127). https://doi.org/10.1098/rsif.2016.0851.

(134) Zimmermann, J. A.; Mcdevitt, T. C. Pre-Conditioning Mesenchymal Stromal Cell Spheroids for Immunomodulatory Paracrine Factor Secretion. *Cytotherapy* **2014**, *16* (3), 331–345. https://doi.org/10.1016/j.jcyt.2013.09.004.

(135) Frost; Sullivan. *U.S. Trauma Fixation Markets*; 2008.

(136) Levy, O.; Kuai, R.; Siren, E. M. J.; Bhere, D.; Milton, Y.; Nissar, N.; de Biasio, M.; Heinelt, M.; Reeve, B.; Abdi, R.; Alturki, M.; Fallatah, M.; Almalik, A.; Alhasan, A. H.; Shah, K.; Karp, J. M. Shattering Barriers toward Clinically Meaningful MSC Therapies. *Science Advances* **2020**, *6*.

(137) Stoddart, M. J.; Salgado, A.; Presen, D. M.; Traweger, A.; Gimona, M.; Redl, H. Mesenchymal Stromal Cell-Based Bone Regeneration Therapies: From Cell Transplantation and Tissue Engineering to Therapeutic Secretomes and Extracellular Vesicles. *Frontiers in Bioengineering and Biotechnology | www.frontiersin.org* **2019**, *1*, 352. https://doi.org/10.3389/fbioe.2019.00352.

(138) Phetfong, J.; Sanvoranart, T.; Nartprayut, K.; Nimsanor, N.; Seenprachawong, K.; Prachayasittikul, V.; Supokawej, A. Osteoporosis: The Current Status of Mesenchymal Stem Cell-Based Therapy. *Cellular & Molecular Biology Letters* **2016**, *21* (1), 12. https://doi.org/10.1186/s11658-016-0013-1.

(139) Antebi, B.; Pelled, G.; Gazit, D. Stem Cell Therapy for Osteoporosis. *Current Osteoporosis Reports* **2014**, *12* (1), 41–47. https://doi.org/10.1007/s11914-013-0184-x.

(140) Murphy, M. P.; Quarto, N.; Longaker, M. T.; Wan, D. C. Calvarial Defects: Cell-Based Reconstructive Strategies in the Murine Model. https://doi.org/10.1089/ten.tec.2017.0230.

(141) Cao, X.; Frenette, P. S.; Mao, J. J.; Robey, P. G.; Simmons, P. J.; Wang, C.-Y.; Bianco, P. The Meaning, the Sense and the Significance: Translating the Science of Mesenchymal Stem Cells into Medicine. *Nature Medicine* **2013**. https://doi.org/10.1038/nm.3028.

(142) Cheung, W. H.; Miclau, T.; Chow, S. K.-H.; Yang, F. F.; Alt, V. Fracture Healing in Osteoporotic Bone. *Injury* **2016**, *47*, S21–S26. https://doi.org/10.1016/S0020-1383(16)47004-X.

(143) Caldwell, A. S.; Rao, V. v.; Golden, A. C.; Bell, D. J.; Grim, J. C.; Anseth, K. S. Mesenchymal Stem Cell-Inspired Microgel Scaffolds to Control Macrophage Polarization. *Bioengineering and Translational Medicine* **2021**, *6* (2). https://doi.org/10.1002/BTM2.10217/FORMAT/PDF.

(144) Gionet-Gonzales, M.; Casella, A.; Diloretto, D.; Ginnell, C.; Griffin, K. H.; Bigot, A.; Leach, J. K. Sulfated Alginate Hydrogels Prolong the Therapeutic Potential of MSC Spheroids by Sequestering the Secretome. *Advanced Healthcare Materials* **2021**, 2101048. https://doi.org/10.1002/ADHM.202101048.

(145) Ando, Y.; Matsubara, K.; Ishikawa, J.; Fujio, M.; Shohara, R.; Hibi, H.; Ueda, M.; Yamamoto, A. Stem Cell-Conditioned Medium Accelerates Distraction Osteogenesis through Multiple Regenerative Mechanisms. **2014**. https://doi.org/10.1016/j.bone.2013.12.029.

(146) Abdeen, A. A.; Weiss, J. B.; Lee, J.; Kilian, K. A. Matrix Composition and Mechanics Direct Proangiogenic Signaling from Mesenchymal Stem Cells. *Tissue Engineering Part A* **2014**, *00* (00), 1–9. https://doi.org/10.1089/ten.tea.2013.0661.

(147) Ho, S. S.; Hung, B. P.; Heyrani, N.; Lee, M. A.; Leach, J. K. Hypoxic Preconditioning of Mesenchymal Stem Cells with Subsequent Spheroid Formation Accelerates Repair of

Segmental Bone Defects. *Stem Cells* **2018**, *36* (9), 1393–1403. https://doi.org/10.1002/STEM.2853.

(148) Clark, A. Y.; Martin, K. E.; García, J. R.; Johnson, C. T.; Theriault, H. S.; Han, W. M.; Zhou, D. W.; Botchwey, E. A.; García, A. J. Integrin-Specific Hydrogels Modulate Transplanted Human Bone Marrow-Derived Mesenchymal Stem Cell Survival, Engraftment, and Reparative Activities. *Nature Communications* **2020**, *11* (1). https://doi.org/10.1038/s41467-019-14000-9.

Chapter 2

Thesis Objectives

2.1 Overview

Bone marrow derived mesenchymal stem/stromal cells (MSCs) are widely used in clinical trials for a variety of applications, including musculoskeletal and cardiovascular disorders, graft-versus-host disease, perianal fistulas, and, recently, COVID-19[1–3]. While the multipotency of MSCs has been well documented[1,2], a growing body of evidence suggests that trophic factors secreted by MSCs play a major role in their therapeutic efficacy[4–6]. MSCs secrete a variety of factors including chemokines to initiate immune cell infiltration, cytokines and growth factors to direct endogenous cell activities, and inflammatory factors to modulate macrophage or lymphocyte polarization[1,7–10]. Delivery of MSCs could be particularly useful in difficult wound healing scenarios, such as critical sized bone defects resulting from non-union healing[11,12].

Because MSCs only constitute 0.001-0.01% of all mononuclear cells in the bone marrow, *in vitro* expansion is needed to achieve clinically relevant cell numbers (~millions of cells/dose)[1–3]. Unfortunately, methods to expand MSCs i*n vitro* can significantly alter their *in vivo* regenerative capacities, such as stemness and proliferation, thereby decreasing their therapeutic efficiency[13–16]. Additionally, when injected intravenously or delivered to the defect site without a carrier, MSCs are often washed away or phagocytosed within hours, reducing their engraftment and potential healing capacity[17]. There is a need to design culture platforms to maintain MSC regenerative properties, specifically their secretion of cytokine and growth factors, both during *in vitro* expansion and *in vivo* delivery.

As strategy to design culture platforms to direct MSC phenotypes, we first sought to understand how cell-matrix and cell-cell interactions control MSC functions. To date, many studies have focused on studying how biophysical factors affect MSC differentiation. Cell matrix cues, such as stiffness, can bias MSCs towards an osteogenic fate irreversibly[18,19]. However, the influence of matrix mechanical cues on MSC secretory properties has not been fully explored. In addition to cell-matrix interactions, cell-cell interactions can influence MSC fate and secretory properties. When cultured as spheroids, or aggregates with a high degree of cellular connections, MSCs show improved stemness and secretory properties[20,21]. However, less is known about the combined influence of cell-cell and cell-matrix interactions on MSCs trophic factor secretion. To explore these questions, there is a need for material systems capable of controllably clustering MSCs while maintaining cell-matrix interactions. With this information in mind, this thesis exploits several hydrogel systems to investigate how the stiffness of the expansion matrix and extent of cell-matrix and cell-cell interactions alter MSC secretory profiles and influence *in vivo* healing outcomes.

2.2   Objectives

This thesis focuses on designing hydrogel systems to control and manipulate MSC secretory properties, both during *in vitro* expansion and *in vivo* delivery. During *in vitro* expansion on traditional TCPS substrates, MSCs lose their stem and secretory properties. Therefore, we develop a hydrogel intervention, with tailored mechanical properties and matrix adhesion cues, to maintain MSC secretory phenotypes during *in vitro* culture and rescue properties lost during expansion on traditional TCPS substrates. Next, noting the significant differences observed in the secretory profiles of single versus spheroid MSC cultures, we develop and explore a granular hydrogel system to control and mimic MSC cell-cell signaling. We hypothesize that these porous material

systems can be engineered to direct MSC secretory profiles through the manipulation of MSC-MSC and MSC-matrix interactions. Next, we exploit the elucidated effects of MSC cell-cell contacts on their secretion to design *in vivo* MSC delivery systems to promote bone regeneration. We test the efficacy of these MSC-laden granular hydrogels systems on bone formation in critical-sized rat calvarial defects. Finally, we harness the precise control over MSC microenvironment afforded by granular hydrogels to better understand the differences in the secretory profiles of MSCs isolated from healthy versus osteoporotic bone, as a function of cell-cell and cell-matrix cues. Throughout this thesis, poly(ethylene glycol) (PEG) based hydrogels crosslinked with bio-click reactions are used to control matrix mechanics, provide cell-matrix cues, and direct cell clustering. To test these hypotheses, the specific objectives of this thesis are to:

> **Aim 1:** Characterize human MSC (hMSC) proliferation, mechanosensing, cell surface marker expression, and secretory properties during serial expansion on tissue culture plastic (TCPS). Investigate the effects of transferring MSCs to hydrogel surfaces after TCPS expansion by measuring surface marker expression and secretory properties;
>
> **Aim 2:** Design PEG-based granular hydrogel scaffolds to control MSC cell-matrix and cell-cell interactions. Elucidate the effects of pore-directed cell clustering and integrin and cadherin binding epitopes on MSC trophic factor secretion;
>
> **Aim 3:** Engineer 3D hydrogel microenvironments to modulate and study the secretory properties of healthy and osteoporotic rat MSCs (rMSCs);
>
> > **Aim 3a:** Synthesize degradable granular scaffolds to tailor the secretory profile of healthy rMSCs by controlling cluster size and incorporating integrin and cadherin binding epitopes. Evaluate the efficacy of rMSC-laden scaffolds to direct bone regeneration in critical-sized rat calvarial defects;

Aim 3b: Utilize granular hydrogel scaffolds to explore the relationship between N-cadherin mediated cell-cell contacts, cell-matrix cues, and the secretory profiles of rMSCs isolated from healthy and osteoporotic bone.

The first aim of this thesis focuses on characterizing the influence of serial passaging on TCPS on hMSC regenerative phenotypes, specifically proliferation rates, mechanosensing ability, stem cell surface marker expression, and secretory properties. hMSCs isolated from bone marrow (18-year-old female) are passaged every three days on TCPS for up to 12 passages (P12). Changes in characteristic cell-surface marker expression or stemness, Yes-associated protein (YAP) associated mechanosening, proliferation, and secretory profiles are characterized using fluorescent activated cell sorting (FACS), immunostaining, and cytokine arrays. We plate Early (P2-P3), middle (P5-P6), and late passage (P11-P12) hMSCs on soft fibronectin (RGD) functionalized PEG-hydrogels synthesized via photoinitiated thiol-ene click chemistry (E~1kPa). The ability of soft hydrogel culture to rescue any drift in MSC properties caused by TCPS expansion is assessed (Chapter 3).

Results from Chapter 3 support the notion that material-directed biophysical cues can rescue MSC secretory properties in 2D expansion systems. However, MSC secreted factors must also be promoted in 3D culture during and after *in vivo* delivery. Inspired by the elevated trophic factor secretion seen in MSCs cultured as spheroids, we next develop granular hydrogel scaffolds, comprised of micron scale PEG-based hydrogel building blocks, to control the cell-cell and cell-matrix interactions of MSCs in 3D. Microgels of varied diameters (~10, ~100, ~200 µm) are created using a strain promoted azide alkyne cycloaddition reaction between multi-arm PEG macromers functionalized with dibenzocyclooctyne and azide groups in an inverse phase

suspension polymerization. Scaffold pore architecture is varied between average pore lengths of ~10 µm, ~100 µm, ~200 µm to create microenvironments where hMSCs reside as mostly single cells to clusters of tens of cells. Additionally, we modify scaffolds with fibronectin (RGD) and N-cadherin (HAVDI) peptide mimetics to assess the role of cell-matrix (integrins) and cell-cell (cadherins) interactions on hMSC secretion. Secreted factors are measured using cytokine arrays and interactions between conditions are determined principal component analysis (Chapter 4).

After understanding how cell-cell contacts and N-cadherin signaling control hMSC secretion, we next sought to rationally engineer hydrogel scaffolds to tailor rat MSC (rMSCs) secretory properties to promote *in vivo* bone regeneration. As MSC secretory properties greatly affect immune cells, we deliver allogenic rMSCs into wildtype rats instead of delivering hMSCs into nude rats. To tolerate cross-species cell delivery, nude rats have genetically altered immune systems which may not fully respond to human MSC secreted factors or accurately recapitulate wound healing cascades. Therefore, before implantation, we conduct experiments to compare the effect of cell clustering and cadherin binding epitopes on healthy rMSC versus hMSC secretion. We next encapsulate rMSCs in scaffolds fabricated from degradable granular hydrogels and implant them into 6 mm critical sized rat calvarial defects. Experimental groups include high and low rMSC secretion conditions and acellular controls. Upon implantation into the calvarial defects, we assess rMSC retention, microgel degradation, and bone regeneration using *in vivo* imaging, microcomputed tomography, and histological analysis (Chapter 5).

While Chapter 5 evaluates the efficacy of rMSC laden microgel scaffolds to regenerate bone *in vivo*, the material systems developed in Chapter 4 can also be used to better understand how MSC secretory profiles change during disease. Specifically, in Chapter 6, we study the secretory profiles of MSCs isolated from a model of postmenopausal osteoporosis, ovariectomized rats

(OVX) and compare the results to healthy rMSCs. Experiments are designed to investigate the influence of cell-cell and cell-matrix interactions on the OVX rMSC secretome. Informed by Chapter 4 results, OVX and SHAM rMSCs are encapsulated in granular hydrogel scaffolds of varied pore dimensions (average major axis pore length ~10, 100, 200 µm) to control their clustering phenotypes. Key differences in secreted proteins, specifically factors known influence bone resorption and deposition, between healthy and OVX rMSCs are quantified using cytokine arrays. Lastly, the role of N-cadherin signaling on the regulation of OVX rMSC secretory profiles is elucidated.

Finally, Chapter 7 discusses the implications of the work presented in this thesis, as well as providing a perspective on future directions that one might explore based on the data presented. Additionally, we outline key challenges and propose ideas to engineer the future generations of precision hydrogels to control MSC secretory properties.

2.3   References

(1) Pittenger, M. F.; Discher, D. E.; Péault, B. M.; Phinney, D. G.; Hare, J. M.; Caplan, A. I. Mesenchymal Stem Cell Perspective: Cell Biology to Clinical Progress. *npj Regenerative Medicine* **2019**, *4* (22). https://doi.org/10.1038/s41536-019-0083-6.

(2) Trounson, A.; Mcdonald, C. Cell Stem Cell Stem Cell Therapies in Clinical Trials: Progress and Challenges. *Stem Cell* **2015**, *17*, 11–22. https://doi.org/10.1016/j.stem.2015.06.007.

(3) Wechsler, M. E.; Rao, V. v; Borelli, A. N.; Anseth, K. S. Engineering the MSC Secretome : A Hydrogel Focused Approach. **2021**, *2001948*, 1–17. https://doi.org/10.1002/adhm.202001948.

(4)   da Silva Meirelles, L.; Fontes, A. M.; Covas, D. T.; Caplan, A. I. Mechanisms Involved in the Therapeutic Properties of Mesenchymal Stem Cells. *Cytokine & Growth Factor Reviews* **2009**, *20* (5–6), 419–427. https://doi.org/10.1016/j.cytogfr.2009.10.002.

(5)   Lian, Q.; Liang, X.; Ding, Y.; Zhang, Y.; Tse, H.-F. Paracrine Mechanisms of Mesenchymal Stem Cell-Based Therapy: Current Status and Perspectives. *Cell Transplantation* **2014**, *23*, 1045–1059. https://doi.org/10.3727/096368913X667709.

(6)   Caplan, A. I.; Correa, D. The MSC: An Injury Drugstore. *Cell Stem Cell* **2011**, *9* (1), 11–15. https://doi.org/10.1016/j.stem.2011.06.008.

(7)   Caplan, A. I.; Correa, D. THE MSC: AN INJURY DRUGSTORE The Mesenchymal Stem Cell (MSC). **2011**. https://doi.org/10.1016/j.stem.2011.06.008.

(8)   Chen, L.; Tredget, E. E.; Wu, P. Y. G.; Wu, Y.; Wu, Y. Paracrine Factors of Mesenchymal Stem Cells Recruit Macrophages and Endothelial Lineage Cells and Enhance Wound Healing. *PLoS ONE* **2008**. https://doi.org/10.1371/journal.pone.0001886.

(9)   Kusuma, G. D.; Carthew, J.; Lim, R.; Frith, J. E. Effect of the Microenvironment on Mesenchymal Stem Cell Paracrine Signaling: Opportunities to Engineer the Therapeutic Effect. https://doi.org/10.1089/scd.2016.0349.

(10)   da Silva Meirelles, L.; Fontes, A. M.; Covas, D. T.; Caplan, A. I. Mechanisms Involved in the Therapeutic Properties of Mesenchymal Stem Cells. *Cytokine & Growth Factor Reviews* **2009**, *20* (5–6), 419–427. https://doi.org/10.1016/j.cytogfr.2009.10.002.

(11)   Phetfong, J.; Sanvoranart, T.; Nartprayut, K.; Nimsanor, N.; Seenprachawong, K.; Prachayasittikul, V.; Supokawej, A. Osteoporosis: The Current Status of Mesenchymal Stem Cell-Based Therapy. **2016**. https://doi.org/10.1186/s11658-016-0013-1.

(12)   Stoddart, M. J.; Salgado, A.; Presen, D. M.; Traweger, A.; Gimona, M.; Redl, H. Mesenchymal Stromal Cell-Based Bone Regeneration Therapies: From Cell Transplantation and Tissue Engineering to Therapeutic Secretomes and Extracellular Vesicles. *Frontiers in Bioengineering and Biotechnology | www.frontiersin.org* **2019**, *1*, 352. https://doi.org/10.3389/fbioe.2019.00352.

(13)   Lambrechts, T.; Sonnaert, M.; Schrooten, J.; Luyten, F. P.; Aerts, J.-M.; Papantoniou, I. Large-Scale Mesenchymal Stem/Stromal Cell Expansion: A Visualization Tool for Bioprocess Comparison. *Tissue engineering. Part B, Reviews* **2016**, *22* (6), 485–498. https://doi.org/10.1089/ten.teb.2016.0111.

(14)   Panchalingam, K. M.; Jung, S.; Rosenberg, L.; Behie, L. A. Bioprocessing Strategies for the Large-Scale Production of Human Mesenchymal Stem Cells: A Review. *Stem Cell Research & Therapy* **2015**, *6* (1), 225. https://doi.org/10.1186/s13287-015-0228-5.

(15)   Trounson, A.; Mcdonald, C. Cell Stem Cell Stem Cell Therapies in Clinical Trials: Progress and Challenges. **2015**. https://doi.org/10.1016/j.stem.2015.06.007.

(16)   Ma, T.; Tsai, A. C.; Liu, Y. Biomanufacturing of Human Mesenchymal Stem Cells in Cell Therapy: Influence of Microenvironment on Scalable Expansion in Bioreactors. *Biochemical Engineering Journal* **2016**, *108*, 44–50. https://doi.org/10.1016/j.bej.2015.07.014.

(17)   A, I.; K, O.; SE, W.; AL, B. Effect of Intra-Medullar and Intra-Venous Infusions of Mesenchymal Stem Cells on Cell Engraftment by *In-Vivo* Cell Tracking and Osteoinductivity in Rabbit Long Bones: A Pilot Study. *Orthopedic & Muscular System : Current Research* **2014**, *3* (3), 172. https://doi.org/10.4172/2161-0533.1000172.

(18)   Engler, A. J.; Sen, S.; Sweeney, H. L.; Discher, D. E. Matrix Elasticity Directs Stem Cell Lineage Specification. *Cell* **2006**, *126* (4), 677–689. https://doi.org/10.1016/j.cell.2006.06.044.

(19)   Yang, C.; Tibbitt, M. W.; Basta, L.; Anseth, K. S. Mechanical Memory and Dosing Influence Stem Cell Fate. *Nature Materials* **2014**, *113*, 645–651. https://doi.org/10.1038/NMAT3889.

(20)   Ho, S. S.; Murphy, K. C.; Binder, B. Y. K.; Vissers, C. B.; Leach, J. K. Increased Survival and Function of Mesenchymal Stem Cell Spheroids Entrapped in Instructive Alginate Hydrogels. *Stem Cells Translational Medicine* **2016**, *5*, 773–781.

(21)   Murphy, K. C.; Whitehead, J.; Falahee, P. C.; Zhou, D.; Simon, S. I.; Leach, J. K. Multifactorial Experimental Design to Optimize the Anti-Inflammatory and Proangiogenic Potential of Mesenchymal Stem Cell Spheroids. *Stem Cells* **2017**, *35* (6), 1493–1504. https://doi.org/10.1002/stem.2606.

Chapter 3

Rescuing mesenchymal stem cell regenerative properties on hydrogel substrates post serial expansion

3.1 Abstract

Human mesenchymal stem cells (hMSCs) are used in numerous clinical trials. Millions of cells/kg are needed for efficacy in treatments, necessitating *ex vivo* expansion. To obtain high cell numbers, hMSCs are expanded on stiff substrates (e.g., tissue culture polystyrene (TCPS), polystyrene microcarriers) which bias the hMSCs towards an osteogenic fate and induce replicative senescence. In this study, we sought to quantify how serial expansion of hMSCs on TCPS influences their proliferation, expression of hMSC-specific surface markers, mechanosensing, and secretory properties. Results show decreased proliferation and hMSC surface marker expression after only 5 passages (P5). Decreased YAP nuclear localization indicates a loss of mechanosensing in hMSCs at later passages (P12). Cytokine secretion is reduced after expansion (P11) compared to fresh isolates. We next investigated the capacity of hydrogels matrices to revert the hMSCs back to their initial regenerative capacity after expansion. During expansion, hMSCs were transferred onto poly(ethylene glycol) hydrogels (E~1kPa) modified with CRGDS (to promote cell attachment). The drift in cell surface marker expression observed at middle passages (P5) on TCPS could be reversed on hydrogels, evidenced by an ~50% increase in CD105+CD90+CD73+ hMSCs after 9 days. Hydrogel culture also increased secretion of cytokines involved in inflammatory signaling, cell growth and trafficking for both early and late passage hMSCs. Collectively, these results show significant changes in functional properties of

hMSCs with TCPS expansion. However, some changes can be rescued by using hydrogels substrates, suggesting that tailoring material properties may be useful for improving *in vitro* methods for serially expanding hMSCs.

3.2 Introduction

Human mesenchymal stem cells (hMSCs) are multipotent cells capable of differentiating into cell types found in tissues of the mesoderm (bone, cartilage, fat), ectoderm (epithelium, neural), and endoderm (muscle, gut, lung)[1]. hMSCs are characterized by a cell surface maker profile, which is constituted by positive expression of CD105, CD90, CD73 and negative expression of CD34, CD45, CD14[1]. They are also capable of secreting various cytokine and chemokines to modulate immune responses and promote wound healing. Due to their myriad capabilities in regenerative therapies, hMSCs are one of the most widely used stem cells in clinical trials with over 800 trials registered worldwide[2]. hMSCs are being tested as cell-based therapies for treatment of graft versus host disease, myocardial infraction, various neurological diseases, and bone and cartilage regeneration. Although the number of trials using hMSCs has increased 3 fold over the past decade, the percentage of these trials that have advanced to Phase III/IV has stagnated around 2-7% for multiple years[3,4]. While the lack of late phase trials is the result of many compounding problems, one contributing factor is a lack of robust, scalable, and reproducible methods that allow efficient *ex vivo* expansion of hMSCs while maintaining their therapeutic properties[4–7]. hMSCs readily adhere to tissue culture plastic surfaces, a property used in their isolation from bone marrow where they make up approximately 0.001-0.01% of mononuclear cells. Isolation alone does not yield enough cells for fundamental studies and/or clinical applications. Thus, hMSCs are expanded *ex vivo*. This is typically done on stiff surfaces like tissue culture polystyrene (TCPS) in laboratory settings. Multilayered TCPS flasks or polystyrene microbeads in bioreactors for clinical scale

expansion. A typical intravenous dose of hMSCs is approximately 1 million cells per kg for each patient. Thus, the clinical use of hMSCs is contingent upon their successful *ex vivo* expansion[8,9].

While regenerative medicine applications exploit the multipotency and differentiation of hMSCs, hMSCs are also known to secrete many trophic factors that impact therapeutic outcomes. hMSCs secrete various cytokines and chemokines involved in immunodulation, especially those related to inflammation signaling, cell trafficking, and lymphocyte differentiation and proliferation[10–13]. Although the precise mechanisms involved in hMSC immunomodulation are largely unknown, several molecules, such as TNF-α and IL-6[14,15], have been cited as potent regulators of initial inflammatory responses, while others, such as VEGF or HGF[10,16,17], can aid in angiogenesis and wound healing.

hMSCs are an adherent cell population as they can sense the mechanics of their environment through integrins that translate extracellular mechanical cues into intracellular biochemical signaling. One output of this mechanotransduction is the nuclear shuttling of Yes-associated protein, YAP, on culture substrates with high moduli[18]. Many studies have used biomaterials with tunable elastic moduli and viscoelasticity to investigate the influence of these mechanical properties on the differentiation of hMSCs. For example, hMSCs have been shown to commit to a cell lineage when cultured on substrates with moduli corresponding to tissue-specific matrix properties (e.g. E~0.1kPa for neurogenesis, E~10kPa for myogenesis, and E>25kPa for osteogenesis)[19]. Following up on this work, Yang *et al.* found that mechanosensing of hMSCs, and ultimately their multipotency, depended on the time of exposure to stiff matrix environments[20]. Long exposure to stiff moduli (E~40kPa) for 10 days caused irreversible YAP nuclear localization, even when the substrate was softened (E~2kPa), but the effects were reversible when the exposure to the stiff microenvironment was shorter (<7 days)[20]. Additionally, cells exposed to longer stiff

mechanical doses were biased towards osteogenesis, losing their multipotency. The time course of matrix stiffness has also been shown to influence angiogenesis[17]. hMSCs cultured on 4kPa hydrogels showed increased mRNA levels of proteins associated with new blood vessel formation compared to hydrogels of lower elasticity[21]. hMSCs primed on soft hydrogels (~2-5kPa) show reduced α smooth muscle actin expression, a marker for a pro-fibrotic response, even after transfer to stiff hydrogels (100kPa), indicating soft mechanical memory[22]. Previous studies have indicated that prolonged culture on traditional tissue culture plates and flasks and use of enzymatic passaging methods can bias hMSCs towards an osteogenic fate[23], cause loss of chondrogenic and adipogenic differentiation ability [23,24], cause loss of DNA repair ability[25], induce replicative senescence, and decrease cell surface markers essential to the MSC phenotype function[26–28]. Less is known about the effect that prolonged expansion on stiff surfaces may have on hMSC mechanosensing and immunomodulation properties. Motivated by the growing body of evidence that hMSCs respond to both the magnitude and dose of their substrate modulus, we sought to further characterize the temporal changes that occur in hMSC properties both under typical expansion conditions and when transferred to hydrogel substrates.

When hMSCs are isolated from their bone marrow niche and expanded *ex vivo*, stimuli from the culture microenvironment can intentionally or unintentionally influence their regenerative properties, ultimately affecting the potency of transplanted hMSCs. This motivated the fundamental studies reported herein, where we sought to characterize and quantify phenotypic drift in hMSCs during their expansion under typical conditions used in research laboratories. The characterization focused on defined *in vitro* criteria based on properties used to characterize freshly isolated hMSCs: proliferation, cell surface marker expression, mechanosensing abilities, and secretome. The drift of each of these properties was quantified during expansion on TCPS with

repeated enzymatic detachment. Uniquely, the experimental design included conditions to investigate the effect of soft PEG-hydrogels substrate usage in the expansion protocol on the hMSC phenotype. hMSCs of early (P1-P2), middle (P5-P7) and late (P11-P12) passages were transferred to PEG-hydrogels (E~1kPa) post TCPS (E~GPa) expansion. Together, we hypothesized that exposure to soft matrix cues after serial passaging on TCPS could recover or maintain the regenerative and multipotency properties of hMSCs lost during expansion.

3.3   Materials and Methods

3.3.1   hMSC isolation and expansion

Fresh human bone marrow aspirate was purchased from Lonza (Donor 18yo black female), and the human mesenchymal stem cells (hMSCs) were isolated based on preferential adhesion to TCPS plates, using previous published protocols[20,29]. Freshly isolated hMSCs (P1) were detached with 0.05% trypsin-EDTA (Sigma) and subsequently centrifuged, counted, and frozen down in 80% fetal bovine serum (FBS) (Invitrogen) and 20% dimethylsulphoxide and stored in liquid nitrogen. For passaging, hMSCs were cultured for 3 days on TCPS at an initial density of 4000 cells/cm^2 using expansion media (low glucose Dulbecco's Modified Eagle Medium (1 ng/mL glucose) (ThermoFisher) supplemented with 10% FBS (ThermoFisher), 1 ng/mL fibroblast growth factor basic (Life Technologies), 50U/ml penicillin (ThermoFisher), 50 µg/ml streptomycin (ThermoFisher), 0.5µg/mL of Amphotericin B (ThermoFisher)) and replated at a density of 4000 cells/cm^2. This method was repeated to generate desired passage numbers. For subsequent analyses, cells at desired passage numbers (P2 for early, P5-P7 for middle, and P11-P12 for late) were frozen in cell freezing medium (Sigma) and stored in liquid nitrogen.

3.3.2   Hydrogel precursors

Eight-arm 40 kDa poly(ethylene glycol) (PEG) was functionalized with norbornene as previously described[30,31]. Briefly, 5-norbornene-2-carboxylic acid was coupled to 8-arm 40kDa poly(ethylene glycol)-amine (Jenkem) in the presence of 1-[Bis(dimethylamino)methylene]-1H-1,2,3-triazolo[4,5-b]pyridinium3-oxid hexafluorophosphate,N-[(Dimethylamino)-1H-1,2,3-triazolo-[4,5-b]pyridin-1-ylmethylene]-N-methylmethanaminium-hexafluorophosphate N-oxide (HATU, Sigma) and N,N-Diisopropylethylamine (DIEA, Sigma), in dimethylformamide (DMF). The reaction was performed overnight at room temperature (RT). The resulting norbornene functionalized PEG (PEG-8NB) was precipitated with cold ethyl ether, resuspended in DI H_2O, dialyzed and lyophilized. The functionality of the PEG-8NB (~95%) was confirmed with ^{1}H NMR by comparing the hydrogen peak associated with norbornene double bound (~6.2 ppm) to the CH_2 groups of PEG backbone (~3.6 ppm). Eight-arm 20kDa PEG-thiol and CRGDS were purchased from Jenkem and Bachem, respectively.

3.3.3   Hydrogel fabrication

Hydrogels were polymerized as described previously described[31]. Briefly, polymer precursor solution was prepared by mixing 500nM 8-arm 40 kDa PEG-NB, 250nM 8-arm 20kDa PEG-thiol (Jenkem) 2 mM photoinitiator lithium phenyl-2,4,6-trimethylbenzoylphosphinate (LAP) and 2mM CRGDS adhesive peptide (Bachem) in PBS at a thiol:ene ratio of 1. The photoinitiator LAP has been used extensively in our group[32,33] and others[34,35] and has been shown to be cytocompatible. After vortexing, 12µL or 50µL of the solution was pipetted onto a hydrophobic Sigmacote (Sigma) treated slide. Sigmacote treated slides were made by flaming glass microscope slides (VWR, 3"x1"x1mm), soaking in Sigmacote for 30 minutes, washing with deionized water, and air drying. A 12 mm or 25 mm thiolated coverslip was placed on top of the droplet and it was allowed to spread fully. Glass coverslips (VWR) were thiolated by vapor

deposition of (3-Mercatopropyl) triethoxy-silane performed overnight at 80°C. The polymer precursor solution was photopolymerized in between a Sigmacote treated glass slide and a thiolated coverslip with exposure to 365nm UV light at 10mW/cm² for 3 minutes to form hydrogels with a diameter of 12 or 25 mm and thickness of 100 μm. Hydrogels were equilibrium swollen in sterile PBS overnight before use.

3.3.4   Rheological characterization

All rheological measurements were performed using a DHR3 rheometer (TA instruments) fitted with a UV light guide accessory with an 8mm parallel plate tool. Optically thin hydrogels with a thickness of 250 μm were formed *in situ* by irradiating with 365 nm light (I_0 = 10mW/cm², Omnicure 1000, Lumen Dynamics) for 30 seconds. The shear storage modulus (G') was characterized at constant strain (1%) and angular frequency (1 rad/s). The Young's modulus, E, was calculated using the following relationship $E = 2G'(1+ v)$, where a Poisson's ratio (v) of 0.5 for the PEG hydrogels was assumed[36].

3.3.5   hMSC culture on hydrogels and TCPS transfer

Frozen down hMSCs were re-suspended in experimental media (low glucose Dulbecco's Modified Eagle Medium (1 ng/mL glucose) (ThermoFisher) supplemented with 10% FBS (ThermoFisher), 50U/ml penicillin (ThermoFisher), 50 μg/ml streptomycin (ThermoFisher), 0.5μg/mL of Amphotericin B (ThermoFisher)). hMSCs were then seeded on the hydrogels at a density of 4,000 cells/cm² for immunostaining and 6,000 cells/cm² for flow cytometry and secretome analysis. Hydrogels were moved into a new well plate 24 h post seeding to eliminate any confounding influence of hMSCs that attached to the TCPS in subsequent analysis. In parallel experiments, hMSCs were also seeded onto TCPS controls for flow cytometry and secretome analysis and glass coverslips for YAP and EdU analysis using the same procedure.

3.3.6   Immunostaining

hMSCs on hydrogels were fixed by treatment with 2% paraformaldehyde (PFA) for 15 min and subsequently fixed with 4% PFA for 30 min. Because of the weaker cell-matrix interactions on hydrogels, hMSCs cultured on hydrogels were initially fixed with 2% paraformaldehyde for 15 minutes before full fixation to prevent their detachment during media aspiration. TCPS samples were only fixed for 30 min with 4% PFA. Samples were washed three times with PBS for 10 minutes at RT and subsequently permeabilized with 0.1% TritonX100 in PBS for 1 hour at RT. Next, samples were blocked with 5% bovine serum albimun (BSA) in PBS for 1 hour at RT. Samples were incubated with anti-YAP antibody (1:400, mouse, Santa Cruz Biotech), anti-CD90 (1:200, rabbit, abcam) or anti-CD105 (1:800, mouse, abcam) primary antibodies in 5% BSA for 1 h at RT or overnight at 4°C. After washing with PBST (0.5 wt% Tween-20 in PBS) three times for 10 min, samples were incubated with secondary antibodies (goat anti-mouse AlexaFlour 647 (1:400, Invitrogen), goat anti-rabbit Alexaflour 488 (1:400, Invitrogen), DAPI (1:500, Sigma), and Rhodamine Phallodin (1:300, Sigma Aldrich) for 1 hour in the dark at RT. Samples were rinsed with PBST two times for 10 min and stored in PBS at 4 °C until imaging. YAP samples were imaged with a spinning disk confocal microscope (Operetta High Content Imaging System, Perkin Elmer). CD90 and CD105 samples were imaged using a laser scanning confocal microscope (Zeiss LSM 710).

3.3.7   Proliferation

A Click-iT EdU Imaging Kit (ThermoFisher) was used to characterize proliferating cells at pre-selected passage conditions (P1, P7, P12). In brief, hMSCs were seeded on either hydrogels or coverslips and treated with 10μM EdU (5-ethynyl-2'-deoxyuridine) one day post seeding. After 24 hours with EdU treatment in growth media, the typical cell cycle for hMSCs, samples were

fixed by treatment with 2% paraformaldehyde (PFA) for 15 min and subsequently fixed with 4%

PFA for 15 min. TCPS samples were only fixed for 30 min with 4% PFA. Samples were washed

three times with PBS for 10 minutes at RT. All samples were permeabilized with 0.1% TritonX100

in PBS for 1 hour at RT and subsequently blocked with 5% bovine serum albimun (BSA) in PBS

for 1 hour at RT. Samples were incubated with the Click-iT reaction cocktail containing

an azide functionalized Alexa Flour 488 dye for 30 min in the dark at RT. Afterward,

immunostaining was continued as described before.

3.3.8   YAP nuclear localization and proliferation quantification

Using the Harmony software (Perkin Elmer), DAPI and Rhodamine Phallodin channels were

used to identify the nuclear and cytoplasmic region of each cell in a single imaging plane. Using

the YAP fluorescent channel, the average YAP intensity in the nuclear and cytoplasmic areas were

calculated for each cell. Next, the YAP nuclear to cytoplasmic ratio was calculated as the average

YAP intensity in the nucleus divided by the average YAP intensity in the cytoplasm. For

proliferation, the number of nuclei was calculated using DAPI staining. Numbers of proliferating

cells were quantified by the nuclei stained EdU+. Percent of proliferating cells was calculated for

each field of view analyzed.

3.3.9   Immunophenotyping

Cells at early (P2), middle (P5), and late passages (P11) were seeded onto TCPS and

hydrogels for 1, 3, or 9 days. A subset of the cells was analyzed for Day 0 cell surface marker

expression. Flow cytometry was performed on a BD FACSCelesta. Cells were trypsinized from

hydrogels or TCPS plates and washed with Cell Staining Buffer (Biolegend) with centrifugation

at 3.5 x g for 5 min twice. The cell pellets were resuspended in 100 μL of Cell Staining Buffer and

stained with antibodies anti-CD105 conjugated with Alexa Flour 488, anti-CD90 conjugated with

Brilliant Violet 421, and anti-CD73 conjugated with PE (BioLegend) using the manufacturer's recommended antibody volume (5 μL/10⁶ cells) by incubation for 20 min on ice in the dark. Samples were washed three times with Cell Staining Buffer, resuspended in 500 μL of Cell Staining Buffer and the manufacturer's recommended volume of 7-AAD Viability Staining Solution (5 μL/ 10⁶ cells) was incubated on ice for 3 min in the dark. Size gates and voltages were set using unstained cells and fluorescence minus one control for each passage sample. UltraComp beads (Fisher) were used as positive controls.

3.3.10 Cytokine secretion analysis

Secretory profiles were assessed for early (P1) and late (P11) passage cells on TCPS and hydrogels using a Human Cytokine Array C5 (RayBiotech) and the manufacturer's protocol was followed. Hydrogels were pooled to ensure sufficient cell numbers for cytokine detection (>200,000 cells). After three days in media with FBS, serum free media was added and cell secreted protein was allowed to accumulate for 2 days. For hydrogel samples, media was concentrated using Pierce Protein Concentrators (ThermoFisher) with a 3kDa MWCO cutoff to ensure all cytokines were retained. In brief, after sample incubation with 1 mL of media from each condition in addition to a cellular control gel and TCPS for 5 hours at RT or overnight at 4°C, each array was washed with manufacturer's washing buffer for 3 times. Next, the membranes were incubated with a biotinylated antibody cocktail for 2 hours at RT or overnight at 4°C, washed with washing buffer 3 times, and incubated with HRP-streptavidin for 2 hours at RT or overnight at 4°C. After incubation of the detection buffers, chemiluminescence was detected using a charge-coupled device (CCD) camera (ImageQuant LAS 4000 GE Healthcare). Exposure and incubation times were kept constant between each condition and its controls. A control hydrogel received the same media treatment as samples in case any components from FBS became trapped in/on the

hydrogel. However, this control did not show increased cytokine detection, indicating hydrogels did not sequester any measurable amount of cytokines and only hMSC secreted factors were analyzed. Raw images were analyzed using the 2D Array feature of ImageQuant (GE Healthcare). Background signal was subtracted, and average intensities were normalized to positive spot controls. Intensities from corresponding spots from control arrays were subtracted and each value was normalized to cell number.

3.3.11 Statistics

All experiments were performed with at least three replicates per condition unless stated otherwise. For proliferation, at least 20 fields of view were analyzed. For YAP analysis, at least 50 cells were analyzed per replicate, and for flow cytometry, conditions were analyzed three times and the % CD90+CD105+CD73+ cells were averaged. Data were compared using one-way ANOVA assuming unequal variances in Prism 6 (GraphPad Software, Inc). Data is presented as mean ± standard deviation.

3.4 Results

3.4.1 Hydrogel fabrication

Peptide-functionalized poly(ethylene glycol) (PEG) hydrogels were synthesized via a thiol-ene photoclick reaction[30]. 8-arm PEG-thiols were co-polymerized with 8-arm PEG-norbornene (equal stoichiometry) to form predominantly elastic hydrogels (E=1- 20kPa), where the final modulus was controlled by the concentration of PEG macromolecules in the initial solution (Figure 3.1 a,b). The fibronectin-derived integrin binding motif, CRGDS, was incorporated into the hydrogels at a 2mM concentration to promote hMSC attachment[20]. While the hydrogels biochemical and biomechanical properties can be further tuned by selection of the initial formulation, all future studies used the 2 w/v% hydrogels (E~1kPa). This elasticity was selected

as prior literature has reported the modulus of bone marrow to be ~300 Pa[37,38]. The gel formulation also provided structural integrity during fabrication, culturing and transferring of cells. Furthermore, hMSCs cultured on hydrogel substrates with this elastic modulus had largely cytoplasmic YAP and remained proliferative.
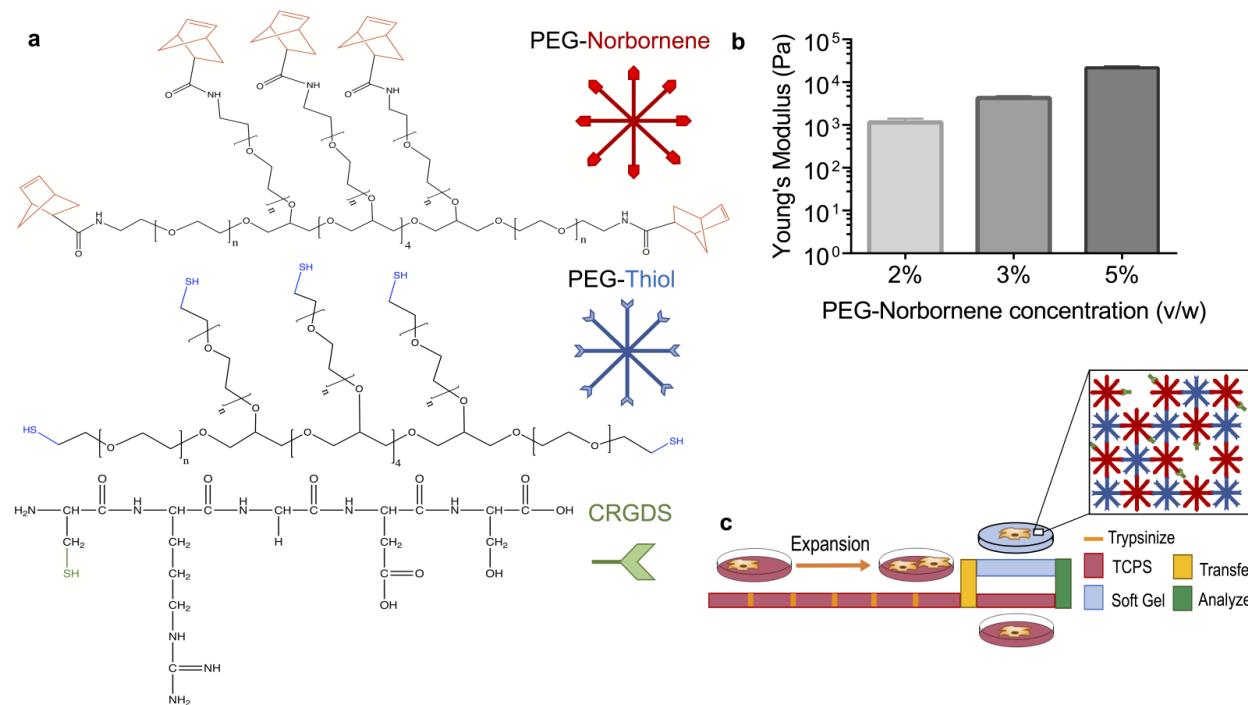
Figure 3.1 Synthesis and rheological characterization of hydrogels.
a) Structures of hydrogel precursors 8-arm 40kDa poly(ethylene glycol) (PEG) functionalized with norbornene, 8 arm 20kDa PEG-Thiol, peptide CRGDS, a fibronectin mimic b) Young's modulus of hydrogels of gels with 2, 3, 5 w/v% PEG-NB and polymerized in the presence of the photoinitiatror lithium phenyl-2,4,6-trimethylbenzoylphosphinate (LAP). Polymer precursor solution was exposed to 365 nm light with an intensity of 10mW/cm^2 for 30 seconds. c) Schematics of experimental protocols. hMSCs are expanded on TCPS and at a pre-selected passage numbers transferred to PEG hydrogels. Key hMSC properties were measured at various stages of TCPS expansion and times on hydrogel materials.

Thus, we aimed to compare the differences between hMSC properties when expanded on TCPS, where YAP nuclear localization predominates, and the modulus is 6 orders of magnitude higher than these PEG hydrogel microenvironments. We were particularly interested in whether or not transfer of hMSCs to the PEG hydrogels post TCPS culture would allow them to recover their initial phenotype that might drift with TPCS expansion (Figure 3.1c).
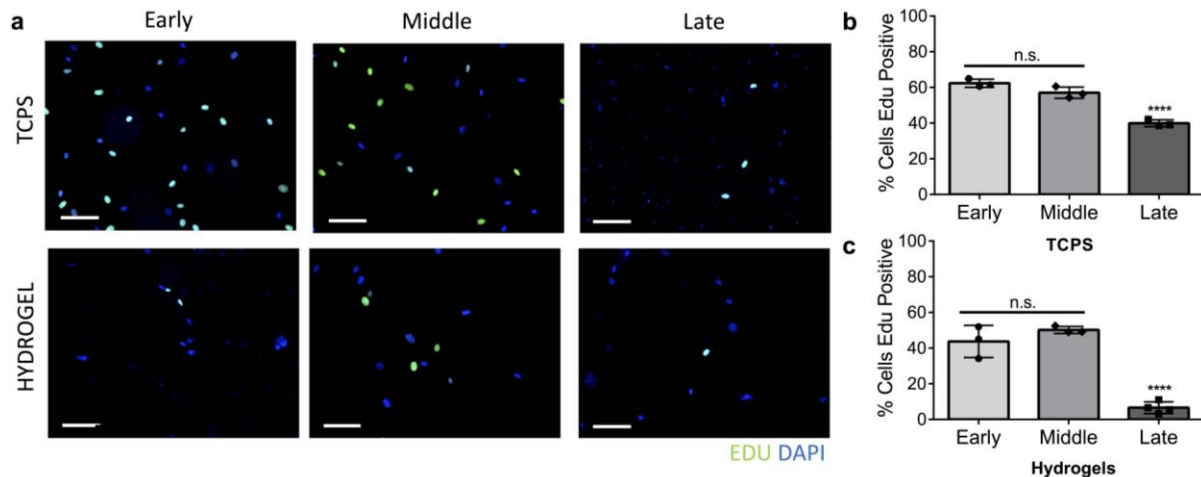
Figure 3.2 hMSCs become less proliferative with expansion.
a) Representative immunofluorescence images of for early (P1), middle (P7) and late (P12) cell nuclei (DAPI, blue). EdU+ cells (green) represent the faction of proliferating hMSCs over a 24 hour period of culture on either TCPS or hydrogels (scale bars = 100µm) b) Quantification of cell proliferation shows decreased proliferation at late passages on TCPS and c) hydrogels (n.s. – not significant compared to early passage, **** p< 0.0001)

3.4.2   TCPS expansion leads to loss of proliferation

hMSC proliferation was quantified under growth conditions using an EdU assay; the effects

of serial expansion on the percentage of proliferating cells are reported in Figure 3.2. Early (P1),

middle (P7), and late (P12) passage cells were exposed to EdU for 24 hours (a typical cell

cycle for hMSCs) to ensure all cells had the opportunity to proliferate. Incorporation

of EdU+ was measured using immunofluorescence staining and imaging; the number of EdU+

positive cells was normalized to all nuclei to determine the percent of proliferating cells for each

condition (Figure 3.2a). On TCPS, high levels of proliferating hMSCs were observed initially,

62±2% at early passages, but this level decreased with culture time and passaging (57±3%, middle

passages, and 39±2%, late passages (Figure 3.2b). In contrast, hMSCs cultured on

soft hydrogels had lower proliferation rates (44±9% at early passages, 50 ± 2% at middle passages,

and 7.0±3% of late passages (Figure 3.2C). Overall, hMSCs show decreased proliferation with expansion, and their proliferation was lower on hydrogels relative to TCPS.

3.4.3 hMSC mechanosensing ability is lost with TCPS expansion

In addition to decreased proliferative capacity, hMSCs mechanosensing ability was assessed at early (P1), middle (P7), and late passages (P12). After 3 days of culture on either hydrogels or TCPS, YAP, a transcriptional co-activator that translocates to the nucleus on stiff substrates, was fluorescently labelled. The nuclear and cytoplasmic intensities were calculated using image analysis described in the methods, Section 3.3 (Figure 3.3a-c). The YAP nuclear to cytoplasmic (nuc/cty) ratio is plotted on a Tukey plot for each cell in the hydrogel or TCPS conditions (Figure 3.3d).

At early passage numbers, hMSCs cultured on TCPS exhibited high YAP nuclear localization (mean YAP nuc/cyt ratio ~4) (Figure 3.3a) compared to hydrogels where YAP remained diffuse in the cytoplasm (mean YAP nuc/cyt ratio ~2). These results indicate a biochemical response of the hMSCs when transferred from TCPS to the lower modulus hydrogels. For middle passage cells, the YAP nuc/cyt ratio remains high on TCPS, and the hMSC similarly sense the difference in substrate stiffness when transferred to the hydrogels (Figure 3.3b). In contrast, the late passage cells (P12) show cytoplasmic YAP in both TCPS and gel condition (Figure 3.3c), which was somewhat unexpected. After image analysis and quantification, no significant difference was observed in the mean YAP nuc/cyt ratios between TCPS and hydrogels for late passage hMSCs. Compared to a difference of ~2 between TCPS and hydrogel mean ratios in early and middle passage cells, no increase in YAP nuc/cyt ratios on TCPS compared to hydrogels indicates an inability of late passage hMSCs to sense their stiff microenvironment (Figure 3.3d).
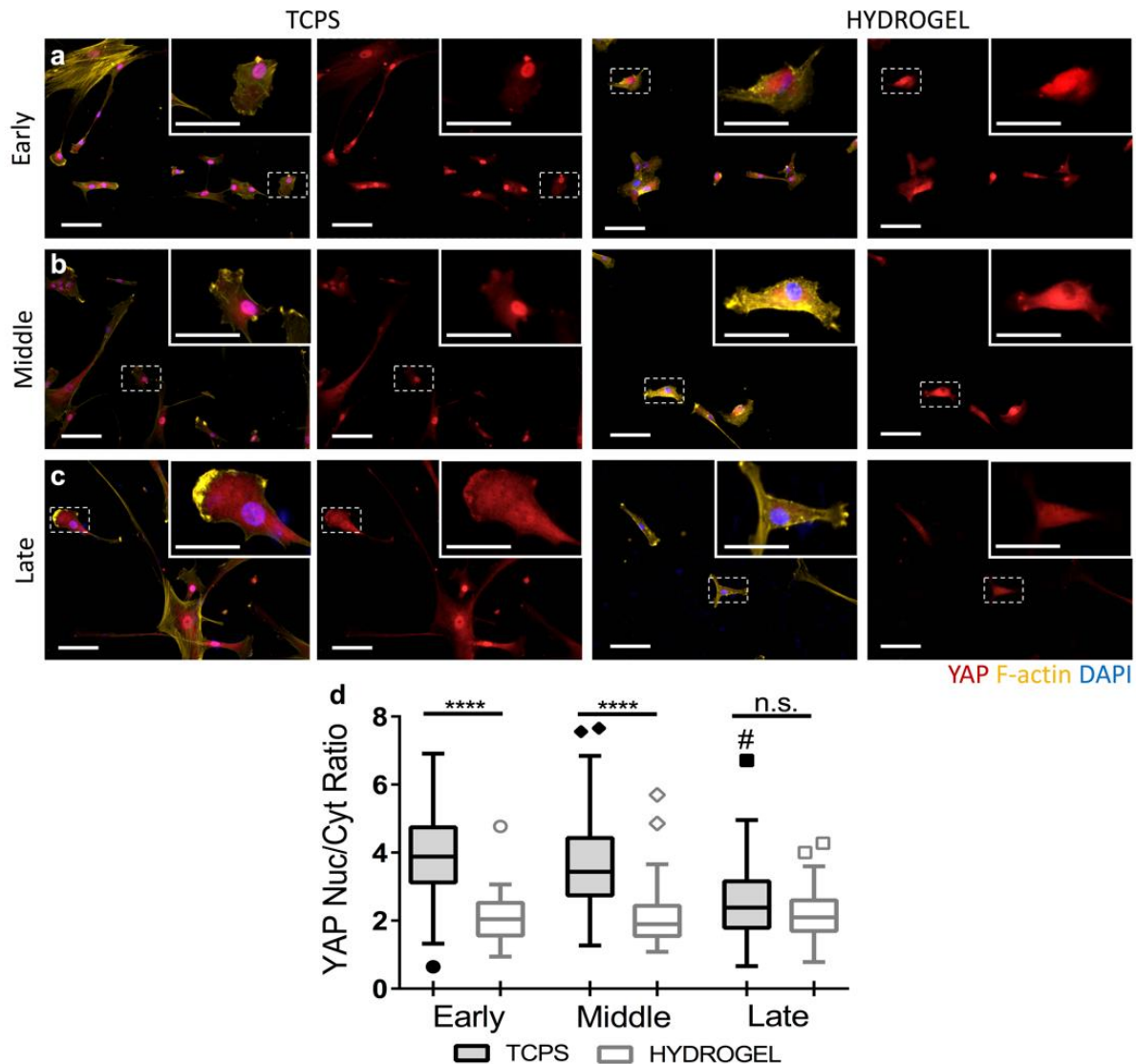
Figure 3.3 hMSC mechanosensing ability becomes lost with expansion on TCPS. Representative immunofluorescence images of a) early (P1), b) middle (P7), and c) late passage hMSCs (P12) on TCPS and hydrogel conditions (scale bars = 100 μm). Insert shows a higher magnification of a single hMSC identified by the boxed with dashed lines (scale bar = 50 μm) d) Tukey plot reporting the YAP nuclear to cytoplastic ratios for each cell cultured on either TCPS or the hydrogel conditions. Statistics were performed on the mean YAP nuclear to cytoplasmic ratio for each condition (n=3) (# - late TCPS relative to early TCPS, **** $p<0.0001$, # $p<0.0001$)

3.4.4   hMSC secretory properties decline with passage number on TCPS

hMSCs are known to secrete various cytokines and chemokines influence the function and

regenerative capacity of multiple immune cell types. Cytokine secretion from early (P1) and late

(P11) passage cells was measured using a Human Cytokine Array C5 (Ray Biotech). Late passage hMSCs show decreased secretion of most cytokines and growth factors compared to early passage cells (Figure 3.4). Chemokine (C-X-C motif) ligand 1 (CXCL1) and chemokine (C-C motif) ligand 4 (CCL4) are both involved in neutrophil trafficking and show decreased expression[39]. Pro-inflammatory cytokines TNF-α and MIF were also reduced, indicating that late passage hMSCs may lose their ability to promote M1 polarization or participate in the initial stages of wound healing[15,40]. Osteopontin (OPN) was one of the few molecules whose secretion increased with passage on TCPS; OPN is known to be involved in osteogenesis and inflammatory signaling[41].
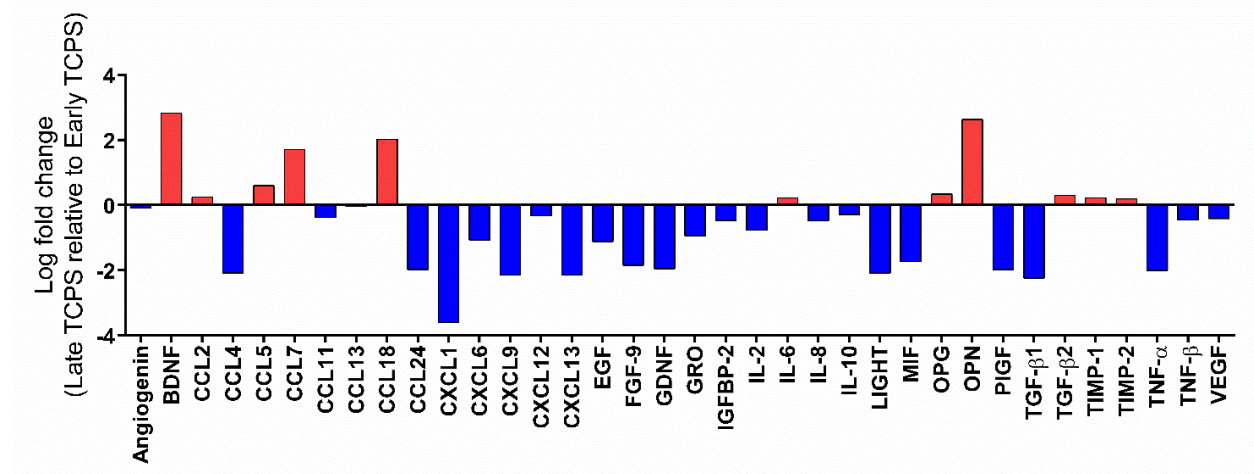
Figure 3.4 Expansion of hMSCs on TCPS decreases their cytokine secretion.
Log fold change in cytokine secretion of late (P11) relative to early (P1) passage hMSCs expanded on TCPS. Cytokines with no significant changes in their secretion are not reported.

3.4.5   Soft hydrogels rescue the hMSC immunophenotype post TCPS expansion

hMSCs' cell identity is defined by their expression of cell surface markers CD90, CD105 and CD73[1]. The expression of these markers are also known to decrease as cells begin differentiating and lose multipotency[42]. hMSC expression of both CD105 and CD90 was first confirmed with P2 cells on TCPS using immunofluorescence imaging (Figure 3.5a), and the population was further characterized using flow cytometry to measure expression of three (CD105, CD90, CD73) hMSC-

specific surface markers. Expression of these makers was characterized for the hMSC populations at early (P2), middle (P5) and late passage (P12), for cells expanded on TCPS, as well as cells transferred to hydrogels. Initially, 88±1% of early passage hMSCs on TCPS were CD90+CD105+CD73+ (Figure 3.7). but this population of cells decreased significantly with passaging on TCPS, middle passages (56±4%) and late passages (52±13%) (Figure 3.5b). When early passage hMSCs were transferred to hydrogels post TCPS expansion, results showed that they maintained their cell surface marker expression over the entire 9 days experimental time course (Figure 3.5c). Strikingly, middle passage hMSCs on TCPS (56±4%) were able to recover their immunophenotype when transferred to soft gels, with 86±3% of the population expressing CD90, CD105 and CD73 after just three days on the hydrogels (Figure 5.5d). This ~50% increase compared to TCPS controls was maintained over the course of 9 days on culture on the hydrogels. In contrast, late passage hMSCs showed no recovery of the immunophenotype when transferred to gels, suggesting an irreversible change in the hMSC population after extended culture times on TCPS (Figure 5.5e).

DAPI F-actin CD105 CD90
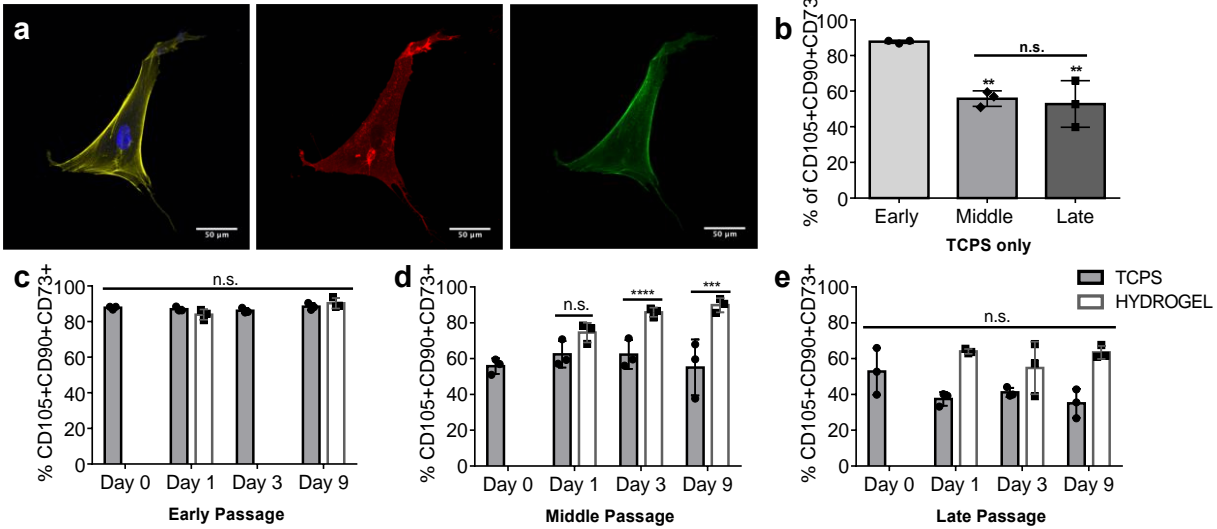
Figure 3.5 Immunophenotypic markers of hMSCs are lost with expansion on TCPS, but can be recovered by soft hydrogel culture for middle passage cells.

a) Immunofluorescence image of early passage (P2) cells on TCPS showing expression of CD105 (red), CD90 (green), F-actin (yellow), DAPI (blue) (scale bar = 50µm) b) Quantification of cell surface marker expression with flow cytometry analysis of early (P2), middle (P5) and late (P12) passage hMSCs on TCPS c,d,e) quantification of cell surface marker expression for early (c), middle (d) and late (e) passage hMSCs cultured on soft hydrogels and TCPS for 1, 3, 9 days (**$p<0.01$, ***$p<0.001$, **** $p<0.0001$, n.s. – nonsignificant)

3.4.6   Enhanced hMSC secretome on hydrogels

Finally, the influence of transferring hMSCs to soft hydrogels on their secretory properties was measured using the cytokine array assay. Compared to their TCPS controls, secretion of most cytokines increased when either early or late passage cells were cultured on hydrogels (Figure 3.6a). TCPS-induced loss of cytokine secretion including GNDF, CXCL1, TNF-α, and MIF, was recovered on hydrogels. Secretion of cytokines involved in cell growth, including EGF, FGF-7, IGF-1, GNDF, PDGF-BB, was increased in both early and late passage cells on hydrogels (Figure 3.6b). Secretion of chemoattracts, involved in macrophage and neutrophil cell trafficking, was also higher for both passages. Pro-inflammatory cytokine secretion, known to be involved in M1 macrophage polarization and wound healing cascades, was also higher on soft gel culture. In

contrast, anti-inflammatory cytokine expression, such as those related to M2 polarization, was largely unchanged. Secretion of cytokines and chemokines involved lymphocyte responses, such as T-cell differentiation and proliferation or B-cell activation, were more variable and no clear trends were observed. Overall, these results indicate that soft gel culture can recover and enhance hMSC secretory properties across multiple passages.

Figure 3.6 Secretory properties of hMSCs is enhanced of soft hydrogels.
a) Heatmap of cytokine secreted by hMSCs on early TCPS, late TCPS relative to TCPS control and early hydrogel, late hydrogel each relative to hydrogel control. b) Relative secretion of cytokines related to cell growth, chemoattractant, pro-inflammatory, anti-inflammatory or lymphocyte response functions.

3.5   Discussion

hMSCs show promise for future cellular therapies as they are relatively easy to isolate and have been implicated in the treatment of a variety of diseases due to their differentiation capacity and secretory properties. As a cell-based therapy they are often administered intravenously. This requires cell numbers on the orders of tens of millions per patient per dose, necessitating expansion *ex vivo*. As hMSCs are found in multiple locations *in vivo*, their *in vivo* properties could be variable based on their specific stem cell niche. To forgo this variability, this study and various others have

chosen to define the hMSC phenotype based on the *in vitro* properties of a population of freshly isolated hMSCs. Compared to early passage cells, results suggest a decrease in proliferative capacity, mechanosensing ability, cell surface marker expression, and secreted cytokines with expansion on TCPS. However, some passages of hMSCs that have been expanded on TCPS can regain immunophenotypic markers and higher levels of cytokine secretion when transferred to soft PEG hydrogel matrices.

Previous studies have shown reduced proliferation, differentiation capacity and onset of replicative senescence for hMSCs expanded on TCPS. As these cell types are further investigated, their mechanosensing and secretory properties have become of interest for their use in tissue engineering and cellular therapies. Loss in mechanosensing with expansion could have widespread implications for integrating biomaterial and scaffold design into hMSC expansion protocols. The mechanical properties of materials have already been tuned to direct stem cell fate. Decreased cytokine expression with expansion would likely lower effectiveness of therapies reliant on factors secreted by hMSCs, such as graft versus host disease. Further, only hMSCs populations positive for CD90, CD105 and CD73 over a specific threshold, usually 90-95%, can be administered to patients[6,43]. In this work, cell surface marker expression could be increased for middle passage hMSCs by transferring them to hydrogels post TCPS expansion. The percent of triple CD90+CD105+CD73+ cells increased from 56% to over 80% after 3 days on hydrogels, compared to their TCPS control (Figure 3.5d). Cell surface marker recovery strategies like this could be of use in hMSC manufacturing, allowing for decreased expansion times while still achieving high cell numbers.

With respect to mechanosensing, significant differences were observed between middle and late passage hMSCs. As indicated by the higher mean YAP nuc/cyt ratios (Figure 3.3b), middle

passage hMSCs remain sensitive to the culture substrate stiffness. Thus, culture on a substrate with

an elasticity similar to their *in vivo* niche may have prompted the cells to begin restoring their cell

surface markers when transferred to hydrogels. In addition, about half of the cells were still able

to proliferate on hydrogels, increasing turnover (Figure 3.2c). In contrast, the late passage hMSCs

lose their responsiveness to the mechanical properties of their microenvironment, and with their

low proliferation rates on hydrogels, are unable to recover their immunophenotype. However,

both differences in the stiffness and biochemical surface properties of the hydrogels and TCPS are

substantially different and influence cell-matrix interactions. The thiol-ene PEG hydrogels system

was formulated to present a single integrin-binding RGDS epitope, while TCPS is a surface that

is highly modified with adsorbed serum proteins. As a result, hMSC-material interactions and the

strength of adhesion vary between the two systems. Increased cytokine secretion on hydrogels for

both early and late passage hMSCs, the first being able to sense stiffness and another unable, could

indicate that the change in surface chemistry from TCPS to hydrogel is involved in promoting

hMSC secretory abilities. Additionally, this increase could indicate a connection to other

mechanical sensing pathways, independent of YAP, that could still be active at late passages.

Overall these results indicate that both expansion time and soft gel cultures have an effect on the

hMSC cytokine secretion. To further increase cytokine production, pre-conditioning strategies

with pro-inflammatory molecules have been employed by other groups[14,44,45]. As cells were not

pre-treated in any way, further experiments help elucidate the effect of IFN-γ , IL-1β or TNF-α

simulation on secretion properties for early or late passage cells. As their immunomodulary and

inflammatory response is better understood and defined, hMSC culturing conditions should be

tailored to ensure maximum therapeutic potency.

Ultimately, it is important to recognize that each component of the hMSC phenotype is linked

to the performance of another. For example, mechanical stiffness of microenvironment, sensed through integrins on the cell surface, can direct differentiation. Additionally, the cell surface marker CD73 has been shown to enhance immunosuppression by reducing inflammatory molecules in both B-cells and hMSCs, useful in treating autoimmune disorders like rheumatoid arthritis[46,47]. In umbilical cord derived hMSCs, loss of CD105 expression has been linked to decreased ability to inhibit Th1 lymphocyte proliferation in co-culture[48]. Decreased hMSC secretory potency and chemokine receptors expression can reduce hMSC homing ability to injured tissues[49]. The results of this study indicate that loss of properties is also linked. Loss in hMSC properties *in vitro* can have detrimental effects during *in vivo* transplantation. The success of stem cell therapies is contingent on the design of biomaterial systems to expand multipotent and regenerative hMSCs. By recovering immunophenotype and improving cytokine secretion during expansion, *in vivo* therapeutics of hMSCs could be improved.

3.6   Conclusion

The goal of this study was two-fold: quantify the phenotypic drift of hMSCs during expansion on TCPS and then assess whether transfer of hMSCs to soft hydrogel matrices could restore lost hMSC phenotype. Expansion solely on TCPS decreased hMSC proliferation rates, mechanosensing ability, cell surface marker expression, and secretory profile. Transfer of middle passage hMSCs to PEG hydrogels formed via a thiol-ene bioclick reaction (E~1 kPa) was able to partially restore expression of CD90, CD105, and CD73, cell surface markers crucial to hMSC definition and function. In contrast, late passage hMSC (P15) lost their YAP-associated mechanosensing and had low proliferation rates, and transfer to hydrogels was unable to recover their immunophenotype. In addition, culture of hMSCs on hydrogel promoted cytokine and chemokine secretion from both early and late passage hMSC populations. The simultaneous

quantification of changes in multiple cell properties with exposure to TCPS and soft hydrogels culture can inform a more optimal expansion time course designed to preserve desired MSC phenotypes.

3.7   Acknowledgements

3.8   Supplemental Information
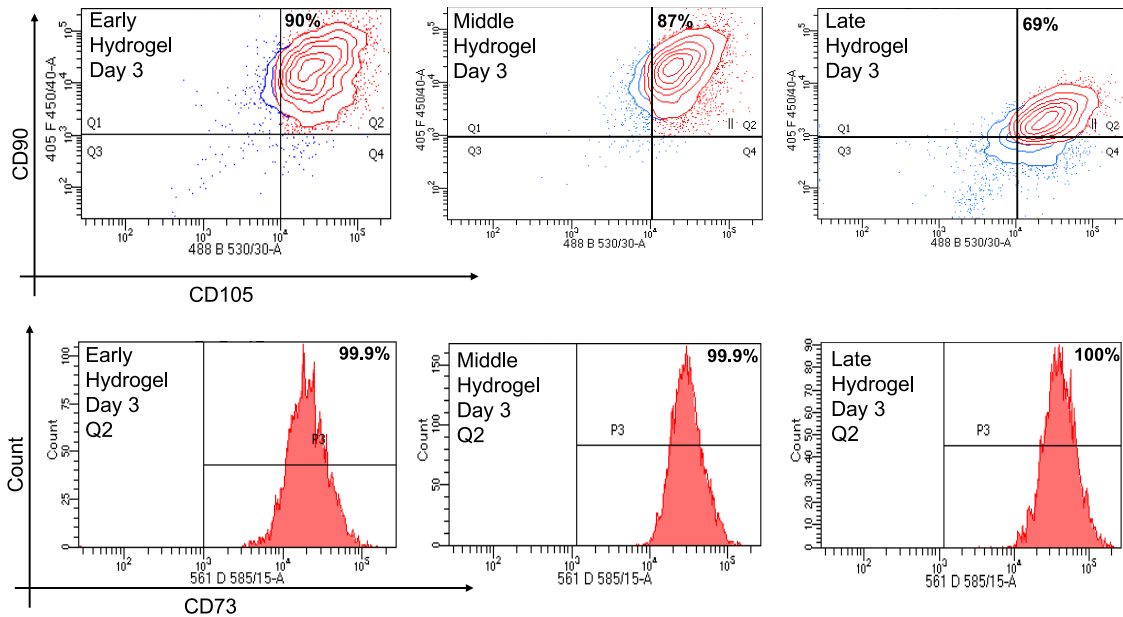
Figure 3.7 Flow cytometry plots of hMSCS on TCPS and hydrogels.
Representative flow cytometry plots used to determine % CD90+CD105+CD73+ cells for early (P2), middle (P5) and late (P12) cell populations for a,b) TCPS and c,d) hydrogels. CD90 was labelled with FITC and CD105 was labelled with Brilliant Violet 421. CD73 expression (labelled with PE) was determined for cells in quadrant 2 from CD90, CD105 plots were assessed for expression. All voltages and gates were set with unstained and single fluorescent controls. Only viable cells were used for analysis. Viability was determined with 7-AAD Viability Stain (BioLegend).

3.9   References

(1)   Dominici M, Blanc K Le, Mueller I, et al. Minimal criteria for defining multipotent

mesenchymal stromal cells . The International Society for Cellular Therapy position statement. *Cytotherapy*. 2006;8(4):315-317. doi:10.1080/14653240600855905

(2)   Billing AM, Ben Hamidane H, Dib SS, et al. Comprehensive transcriptomic and proteomic characterization of human mesenchymal stem cells reveals source specific cellular markers. *Sci Rep*. 2016;6(February):1-15. doi:10.1038/srep21507

(3)   Bunpetch V, Zhang Z-Y, Zhang X, et al. Strategies for MSC expansion and MSC-based microtissue   for   bone   regeneration.   *Biomaterials*.   2017:1-13. doi:10.1016/j.biomaterials.2017.11.023

(4)   Trounson A, Mcdonald C. Cell Stem Cell Stem Cell Therapies in Clinical Trials: Progress and Challenges. 2015. doi:10.1016/j.stem.2015.06.007

(5)   Lambrechts T, Sonnaert M, Schrooten J, Luyten FP, Aerts J-M, Papantoniou I. Large-Scale Mesenchymal Stem/Stromal Cell Expansion: A Visualization Tool for Bioprocess Comparison. *Tissue Eng Part B Rev*. 2016;22(6):485-498. doi:10.1089/ten.teb.2016.0111

(6)   Panchalingam KM, Jung S, Rosenberg L, Behie LA. Bioprocessing strategies for the large-scale production of human mesenchymal stem cells: a review. *Stem Cell Res Ther*. 2015;6(1):225. doi:10.1186/s13287-015-0228-5

(7)   Ma T, Tsai AC, Liu Y. Biomanufacturing of human mesenchymal stem cells in cell therapy: Influence of microenvironment on scalable expansion in bioreactors. *Biochem Eng J*. 2016;108:44-50. doi:10.1016/j.bej.2015.07.014

(8)   Squillaro T, Peluso G, Galderisi U. Review Clinical Trials With Mesenchymal Stem Cells : An Update. *Cell Transplant*. 2016;25:829-848.

(9)   Chen Y-S. Mesenchymal Stem Cell: Considerations for Manufacturing and Clinical Trials on Cell Therapy Product. *Int J Stem cell Res Ther*. 2016;3(1):1-12. doi:10.23937/2469-

570X/1410029

(10) Madrigal M, Rao KS, Riordan NH. A review of therapeutic effects of mesenchymal stem cell secretions and induction of secretory modification by different culture methods. *J Transl Med*. 2014;12:260. doi:10.1186/s12967-014-0260-8

(11) Cheleuitte D, Mizuno S, Glowacki J. *In Vitro* Secretion of Cytokines by Human Bone Marrow: Effects of Age and Estrogen Status. *J Clin Endocrinol Metab*. 1998;83(6):2043-2051. doi:10.1210/jcem.83.6.4848

(12) Zhukareva V, Obrocka M, Houle JD, Fischer I, Neuhuber B. Secretion profile of human bone marrow stromal cells: Donor variability and response to inflammatory stimuli. *Cytokine*. 2010;50:317-321. doi:10.1016/j.cyto.2010.01.004

(13) Kyurkchiev D, Bochev I, Ivanova-Todorova E, et al. Secretion of immunoregulatory cytokines by mesenchymal stem cells. *World J Stem Cells J Stem Cells*. 2014;6(65):552-570. doi:10.4252/wjsc.v6.i5.552

(14) Li C, Li G, Liu M, Zhou T, Zhou H. Paracrine effect of inflammatory cytokine-activated bone marrow mesenchymal stem cells and its role in osteoblast function. *J Biosci Bioeng*. 2016;121(2):213-219. doi:10.1016/j.jbiosc.2015.05.017

(15) Bone RC. Sepsis: A New Hypothesis for Pathogenesis of the Disease Process*. *Chest*. 1997;112(1):235-243. doi:10.1378/chest.112.1.235

(16) Rustad KC, Wong VW, Sorkin M, et al. Enhancement of mesenchymal stem cell angiogenic capacity and stemness by a biomimetic hydrogel scaffold. *Biomaterials*. 2012;33(1):80-90. doi:10.1016/J.BIOMATERIALS.2011.09.041

(17) Kwon HM, Hur SM, Park KY, et al. Multiple paracrine factors secreted by mesenchymal stem cells contribute to angiogenesis. *Vascul Pharmacol*. 2014;63(1):19-28.

doi:10.1016/j.vph.2014.06.004

(18)   Dupont S, Morsut L, Aragona M, et al. Role of YAP/TAZ in mechanotransduction. *Nature*. 2011;474(7350):179-183. doi:10.1038/nature10137

(19)   Engler AJ, Sen S, Sweeney HL, Discher DE. Matrix Elasticity Directs Stem Cell Lineage Specification. *Cell*. 2006;126(4):677-689. doi:10.1016/j.cell.2006.06.044

(20)   Yang C, Tibbitt MW, Basta L, Anseth KS. Mechanical memory and dosing influence stem cell fate. *Nat Mater*. 2014;113:645-651. doi:10.1038/NMAT3889

(21)   Mammoto A, Connor KM, Mammoto T, et al. A mechanosensitive transcriptional mechanism that controls angiogenesis. *Nature*. 2009;457(7233):1103-1108. doi:10.1038/nature07765

(22)   Chen Xi Li1†, Nilesh P. Talele1†, Stellar Boo1†, et al. MicroRNA-21 preserves the fibrotic mechanical memory of mesenchymal stem cells. *Nat Mater*. 2016;16(3).

(23)   Wagner W, Horn P, Castoldi M, et al. Replicative Senescence of Mesenchymal Stem Cells: A Continuous and Organized Process. *PLoS One*. 2008;3(5). doi:10.1371/journal.pone.0002213

(24)   Jiang T, Xu G, Wang Q, et al. In vitro expansion impaired the stemness of early passage mesenchymal stem cells for treatment of cartilage defects. *Nat Publ Gr*. 2017;8. doi:10.1038/cddis.2017.215

(25)   Wu PK, Wang JY, Chen CF, et al. Early passage mesenchymal stem cells display decreased radiosensitivity and increased DNA repair activity. *Stem Cells Transl Med*. 2017;6(6):1504-1514. doi:10.1002/sctm.15-0394

(26)   Wagner W, Horn P, Castoldi M, et al. Replicative Senescence of Mesenchymal Stem Cells: A Continuous and Organized Process. *PLoS One*. 2008;3(5).

doi:10.1371/journal.pone.0002213

(27)   Banfi A, Bianchi G, Notaro R, Luzzatto L, Cancedda R, Quarto R. Replicative Aging and Gene Expression in Long-Term Cultures of Human Bone Marrow Stromal Cells. *TISSUE Eng*. 2002;8(6).

(28)   Blasco MA. Telomere length, stem cells and aging. *Nat Chem Biol*. 2007. doi:10.1038/nchembio.2007.38

(29)   Lech W, Figiel-Dabrowska A, Sarnowska A, et al. Phenotypic, Functional, and Safety Control at Preimplantation Phase of MSC-Based Therapy. *Stem Cells Int*. 2016;2016. doi:10.1155/2016/2514917

(30)   Fairbanks BD, Schwartz MP, Halevi AE, Nuttelman CR, Bowman CN, Anseth KS. A Versatile Synthetic Extracellular Matrix Mimic via Thiol- Norbornene Photopolymerization. *Adv Mater*. 2009;21(48):5005-5010. doi:10.1002/adma.200901808

(31)   Gould ST, Darling NJ, Anseth KS. Small peptide functionalized thiol–ene hydrogels as culture substrates for understanding valvular interstitial cell activation and de novo tissue deposition. *Acta Biomater*. 2012;8:3201-3209. doi:10.1016/j.actbio.2012.05.009

(32)   Fairbanks BD, Schwartz MP, Bowman CN, Anseth KS. Photoinitiated polymerization of PEG-diacrylate with lithium phenyl-2,4,6-trimethylbenzoylphosphinate: polymerization rate and cytocompatibility. *Biomaterials*. 2009;30(35):6702-6707. doi:10.1016/j.biomaterials.2009.08.055

(33)   Lin C-C, Anseth KS. Cell-cell communication mimicry with poly(ethylene glycol) hydrogels for enhancing beta-cell function. *Proc Natl Acad Sci U S A*. 2011;108(16):6380-6385. doi:10.1073/pnas.1014026108

(34)   Fiedler CI, Aisenbrey EA, Wahlquist JA, et al. Enhanced mechanical properties of photo-

clickable thiol–ene PEG hydrogels through repeated photopolymerization of in-swollen macromer. *Soft Matter*. 2016;12(44):9095-9104. doi:10.1039/C6SM01768A

(35) Sawicki LA, Kloxin AM. Design of thiol–ene photoclick hydrogels using facile techniques for cell culture applications. *Biomater Sci*. 2014;2(11):1612-1626. doi:10.1039/C4BM00187G

(36) Chen VJ, Ma PX. *Scaffolding In Tissue Engineering*.; 2006. doi:10.1007/s13398-014-0173-7.2

(37) Shin J-W, Buxboim A, Spinler KR, et al. Contractile Forces Sustain and Polarize Hematopoiesis from Stem and Progenitor Cells. *Cell Stem Cell*. 2014;14(1):81-93. doi:10.1016/J.STEM.2013.10.009

(38) Ivanovska IL, Shin J-W, Swift J, Discher DE. Stem cell mechanobiology: diverse lessons from bone marrow. *Trends Cell Biol*. 2015;25(9):523-532. doi:10.1016/J.TCB.2015.04.003

(39) Griffith JW, Sokol CL, Luster AD. Chemokines and Chemokine Receptors: Positioning Cells for Host Defense and Immunity. *Annu Rev Immunol*. 2014;32:659-702. doi:10.1146/annurev-immunol-032713-120145

(40) Corwin EJ. Understanding Cytokines Part I: Physiology and Mechanism of Action Cytokine Physiology. *Biol Res Nurs Corwin / Underst Cytokines Part I*. 2000;2(1). http://journals.sagepub.com/doi/pdf/10.1177/109980040000200104. Accessed April 9, 2018.

(41) Chen Q, Shou P, Zhang L, et al. An osteopontin-integrin interaction plays a critical role in directing adipogenesis and osteogenesis by mesenchymal stem cells. *Stem Cells*. 2014;32(2):327-337. doi:10.1002/stem.1567

(42) Kloxin AM, Kasko AM, Salinas CN, Anseth KS. Photodegradable hydrogels for dynamic

tuning of physical and chemical properties. *Science*. 2009;324(5923):59-63. doi:10.1126/science.1169494

(43)   Martin C, Olmos É, Collignon M-L, et al. Revisiting MSC expansion from critical quality attributes to critical culture process parameters. *Process Biochem*. 2017;59:231-243. doi:10.1016/j.procbio.2016.04.017

(44)   Pourgholaminejad A, Aghdami N, Baharvand H, Moazzeni SM. The effect of pro-inflammatory cytokines on immunophenotype, differentiation capacity and immunomodulatory functions of human mesenchymal stem cells. *Cytokine*. 2016;85:51-60. doi:10.1016/j.cyto.2016.06.003

(45)   Gnecchi M, Danieli P, Malpasso G, Ciuffreda MC. Paracrine Mechanisms of Mesenchymal Stem Cells in Tissue Repair. In: *Methods in Molecular Biology (Clifton, N.J.)*. Vol 1416. ; 2016:123-146. doi:10.1007/978-1-4939-3584-0_7

(46)   Chen X, Shao H, Zhi Y, et al. CD73 Pathway Contributes to the Immunosuppressive Ability of Mesenchymal Stem Cells in Intraocular Autoimmune Responses. *Stem Cells Dev*. 2016;25(4):337-346. doi:10.1089/scd.2015.0227

(47)   Kaku H, Cheng KF, Al-Abed Y, Rothstein TL. A Novel Mechanism of B Cell–Mediated Immune Suppression through CD73 Expression and Adenosine Production. *J Immunol*. 2014;193(12):5904-5913. doi:10.4049/jimmunol.1400336

(48)   Na T, Liu J, Zhang K, Ding M, Yuan B-Z. The Notch Signaling Regulates CD105 Expression, Osteogenic Differentiation and Immunomodulation of Human Umbilical Cord Mesenchymal Stem Cells. *PLoS One*. 2015:1-19. doi:10.1371/journal.pone.0118168

(49)   Hocking AM. The Role of Chemokines in Mesenchymal Stem Cell Homing to Wounds. *Adv Wound Care*. 2015;4(11):623-630. doi:10.1089/wound.2014.0579

Chapter 4

Porous bio-click microgel scaffolds control hMSC interactions and promote their secretory properties

Sections as published in Biomaterials, 232, 2020, 119725

4.1   Abstract

Human mesenchymal stem/stromal cells (hMSCs) are known to secrete numerous cytokines that signal to endogenous cells and aid in tissue regeneration. However, the role that biomaterial scaffolds can play in controlling hMSC secretory properties has been less explored. Here, microgels were co-assembled with hMSCs using three different microgel populations, with large (190±100µm), medium (110±60µm), and small (13±6µm) diameters, to create distinct porous environments that influenced hMSC clustering. Cells embedded in large diameter microgel networks resided in large clusters (~40 cells), compared to small clusters (~6 cells) observed in networks using medium diameter microgels and primarily single cells in small diameter microgel networks. Using a cytokine microarray, an overall increase in secretion was observed in scaffolds that promoted hMSC clustering, with over 60% of the measured cytokines most elevated in the large diameter microgel networks. N-cadherin interactions were identified as partially mediating these differences, so the microgel formulations were modified with an N-cadherin epitope, HAVDI, to mimic cell-cell interactions. Results revealed increased secretory properties for hMSCs in HAVDI functionalized scaffolds, even the non-clustered cells in small diameter microgel networks. Together, these results demonstrate opportunities for microgel-based scaffold systems for hMSC delivery and tailoring of porous materials properties to promote their secretory potential.

4.2 Introduction

hMSCs are the one of the most commonly used adult stem cells in clinical trials[1]. Extensive research has documented the ability of hMSCs to differentiate into cells of a mesenchymal lineage (e.g., osteoblasts, chondrocytes, adipocytes) and to secrete numerous trophic factors. Specifically, hMSCs secrete a plethora of factors capable of influencing angiogenesis, fibrosis, apoptosis, cell differentiation, immune responses and cardiac, muscle, and neural tissue regeneration[3]. While much is known about the effects of biomaterial scaffold properties (matrix mechanics[4–7], dimensionality[8], porosity[9,10], adhesive ligand tethering[11,12], etc.) on hMSCs differentiation, the influence of these properties on the hMSC secretome is less known. As a result, there is a growing interest in understanding how scaffold delivery systems can be designed to influence their secretory properties and therapeutic outcomes[2,3].

Although cell-matrix interactions, including passage number and substrate mechanics[13,14], significantly affect the hMSC secretory phenotype, studies have documented the influence of cell-cell interactions in promoting increased secretion of cytokines[15]. For example, aggregating hMSCs in spheroid cultures increased survival and upregulated secretion of both VEGF and PGE2 compared to disassociated cells[16]. Spheroid size has also been implicated in directing hMSC secretory properties, with cells in larger spheroids (40,000 cells/spheroid) secreting elevated levels of several cytokines involved in inflammatory signaling, including GRO, IFN-γ, and IL-10 compared to cells in smaller spheroids (10,000 cells/spheroid)[17]. Further, Qazi *et al.* used porous alginate scaffolds to tailor the microenvironment to achieve higher levels of secreted cytokine in rat MSCs (rMSCs)[18]. rMSCs encapsulated in lyophilized alginate scaffolds with a mean pore size of 122±29 µm secreted higher levels of cytokines and regenerative factors, specifically HGF, IGF,

and FGF2, compared to rMSCs encapsulated in bulk alginate hydrogels or plated on TCPS. This work also implicated N-cadherin as a mediator for paracrine signaling in rMSCs; as blocking N-cadherin interactions decreased cytokine secretion in the scaffolds. Collectively, these studies support the notion that cell-cell connections, and particularly N-cadherin, is critical for enhanced paracrine signaling in MSCs. Based on this premise, we designed 3D porous bio-click hydrogel scaffolds to manipulate and control hMSC cell-cell interactions in a systematic manner and then quantified the effect on the secretion of proteins using a cytokine array.

Caldwell *et al*. demonstrated a new method for assembling microgel scaffolds into porous cell laden scaffolds using azide-alkyne bioclick-reactions[19]. hMSCs were embedded in peptide functionalized poly(ethylene glycol) scaffolds with microgels of varying size to create distinct hMSC-material interactions and microenvironments. Changes in particle diameter lead to alterations in overall porosity, pore dimensions, and cell morphology. Building on this initial study, in this paper, microgels with a broader range of diameters and final pore dimensions were used to encapsulate hMSCs and control their cell-matrix versus cell-cell interactions. hMSC secretory properties are significantly altered with increased clustering resulting in higher secretion of several cytokines known to be important in hMSC based cell therapies. Immunostaining and quantitative image analysis suggested that N-cadherin interactions may be contributing to these differences. Thus, an N-cadherin mimicking peptide (HAVDI) was conjugated to the microgel formulations. Previously, HAVDI peptide has been conjugated to hyaluronan gels where it increased chondrogenic differentiation of hMSCs[20]. Here, experiments were designed to test whether HAVDI could mimic cell-cell interactions and promote the secretory properties of single or clustered cells encapsulated in microgel networks. Interestingly, principal component analysis showed that secretory properties were elevated for all HAVDI conditions and the secretory profiles

of cells in different pore sizes were more similar to each other when HAVDI was included in the scaffolds. Overall, the results reported herein demonstrate the design of a porous bio-click hydrogel scaffolds that allow for hMSC encapsulation and manipulation of the secretory profile by controlling cell-cell interactions or incorporating bioactive moieties that promote cell-matrix interactions.

4.3 Materials and methods

4.3.1 Macromer synthesis and microgel polymerization

Eight-arm poly(ethylene glycol) (PEG) amine (JenKem, M_n~20,000 Da) was reacted with dibenzocylcooctyne (DBCO) as previously described[19]. End-group functionalization was confirmed by ^{1}H NMR to be >85%. Four-arm PEG-azide (PEG-N$_3$) was also synthesized as previously described[21]. End-group functionalization was confirmed by ^{1}H NMR to be >95%. A cellularly-adhesive peptide, GRGDS (RGD), and an N-cadherin mimicking peptide, GHAVDI (HAVDI), were synthesized using standard Fmoc chemistry and a Rink Amide MBHA resin (Chempep Inc, USA) on a Protein Technologies Tribute Peptide Synthesizer. An azide modified lysine analog (Fmoc-azide-L-lysine, ChemImpex) was used to synthesize an azide-labeled RGD (N$_3$-KGRGDS) and HAVDI (N$_3$-KGHAVDI). Peptides were purified using reverse phase High Pressure Liquid Chromatography (HPLC) and confirmed using Electrospray Ionization (ESI) mass spectroscopy.

Microgels were synthesized as previously described[19]. Briefly, microgels were fabricated using an inverse suspension polymerization in hexanes with Span-80 (2.25% v/v) and Tween-20 (0.75% v/v) using PEG-DBCO and PEG-N$_3$ macromers while an applied shear force was varied to control microgel size during polymerization. The applied shear was achieved using either magnetic stirring, vortexing, or sonication to create 190±100µm (large), 110±60µm (medium), and

13±6µm (small) microgels, respectively. Two distinct sets of microgels were prepared with 11mM excess of either functional group to allow for subsequent scaffold assembly. N_3-GRGDS, was included in all microgels at a concentration of 1mM, while N_3-HAVDI was included at the same 1mM concentration for selected studies related to mimicking cell-cell interactions by modifying the microgel chemistry. Microgels were washed (under sterile conditions) with isopropanol (4x) and with phosphate buffered saline (PBS) (1x) before resuspension in PBS.

4.3.2   Characterization of porous microgel scaffolds

Microgel size and scaffold porosity were visualized by incorporating an azide labeled fluorophore (AlexaFluor 647 azide, Life Technologies, 0.04mM) during microgel formation. Scaffold porosity was also visualized by swelling the networks with fluorescein isothiocyanate-dextran (Millipore Sigma, 2,000kDa). The resulting porous scaffolds were then imaged on a laser scanning confocal (Zeiss LSM710) using a 10x water objective. The microgel diameter and pore size were quantified using previously published MATLAB codes[19]. Microgel storage moduli were assessed through shear rheology using a DH-R3 rheometer from TA Instruments, while scaffold mechanical properties were assessed through compressive rheology using an MTS Synergie 100.

4.3.3   hMSC isolation and culture

hMSCs were isolated from fresh bone marrow aspirate purchased from Lonza (donor 18-year-old black female). Following previously published protocols[13,22], hMSCs were isolated based on preferential adhesion to tissue culture polystyrene plates. Freshly isolated hMSCs were detached with 0.05% trypsin–EDTA (Sigma) and subsequently centrifuged, counted, and frozen in Cell Freezing Medium (Thermo Fisher). Only passage 2 or 3 cells were used for all encapsulation experiments. Growth media consisted of low glucose (1 ng/mL glucose) Dulbecco's Modified Eagle Medium (ThermoFisher) supplemented with 10% FBS (ThermoFisher), 1 ng/ml

fibroblast growth factor basic (bFGF) (Life Technologies), 50 U/ml penicillin (ThermoFisher), 50 µg/ml streptomycin (ThermoFisher), 0.5µg/ml of Amphotericin B (ThermoFisher). For secretion experiments, the same media was used sans bFGF (referred to as Experimental Media).

4.3.4   Cell encapsulation

Microgel scaffolds were fabricated by combining equal volumes (50µL macromer volume) of DBCO-excess and N_3-excess microgels in 2mL of PBS. The microgel suspensions were then centrifuged at 1000rcf for 10 minutes, followed by 3000 rcf for 2 minutes. Microgel scaffolds were then placed in PBS and allowed to equilibrate in PBS, reaching a final swollen volume of ~200µL in each case. To create cell-laden microgel scaffolds hMSCs (1million cells) were mixed with microgels during network formation (cell density of 5million cells/mL). After centrifugation scaffolds were immediately placed in experimental media.

4.3.5   Immunofluorescent staining

Three days after encapsulation, hMSCs in microgel networks were fixed by treatment with 10% formalin for 30 min at room temperature (RT). Samples were washed three times with PBS for 10 min at RT on shaker plate. Next, samples were permeabilized and blocked with 0.1% TritonX100 and 5% bovine serum albumin (BSA) respectively in PBS for 1 hr at RT. Samples were incubated with anti-N-cadherin antibody (3 µg ml^{-1}, mouse, Invitrogen) in Cell Staining Buffer (Bio-rad) overnight at 4°C. After three washes with PBST (0.5 wt% Tween-20 in PBS) for 10 min on the shaker, samples were incubated with goat anti-rabbit Alexaflour 488 (1:400, Invitrogen), DAPI (1:500, Sigma) and Rhodamine Phalloidin (1:300, Sigma Aldrich) for 1 hr at RT in the dark. For cell cluster analysis, no primary antibody was added and only DAPI and Rhodamine Phalloidin was incubated for 1 hr at RT. Samples were imaged on either a Nikon

Spinning Disc Confocal (40x air or 60x water objective) or a Zeiss Laser Scanning Confocal (20x air objective) microscopes.

4.3.6 Image analysis

Approximately 80 µm z-stack images (with <1 µm intervals between slices) were imported into IMARIS 3D visualization software (Bitplane). For cell cluster analysis, a 3D surface was reconstructed using the F-actin stain in order to define the confines of a cell cluster. Next, nuclei were identified with Spots Analysis. Using a pre-written Matlab code (Split into Surface Objects Xtension) within the IMARIS software, the number of nuclei within each cluster was determined. A cluster was defined as possessing greater than 2 nuclei. The intensity of the N-cadherin punctate was performed using ImageJ. To start, maximum intensity projections of the images were compiled and duplicates converted to binary. Particles analysis was performed on the binary image and the intensities within particles were determined using the original maximum intensity projection. Outlier analysis was conducted using the ROUT method and Q=1%. Over 150 punctate were analyzed for N=3 gels per condition.

4.3.7 Secretory analysis

Global secretory profiles were measured using a Human Cytokine Array C5 (RayBiotech) and the manufacturer's protocol was followed. Briefly, media was collected from microgel samples after three days. Arrays were blocked and incubated with 1 ml of media from each condition and acellular controls for overnight at 4°C. Each array was washed with manufacturer's washing buffer for three times. Next, the membranes were incubated with a biotinylated antibody cocktail for 2 hr at RT, washed, and then incubated with HRP-streptavidin for 2 hr at RT. After incubation of the detection buffers, chemiluminescence was detected using a charge-coupled device camera (ImageQuant LAS 4000 GE Health- care). Exposure and incubation times were kept constant

between each condition and controls. Raw images were analyzed using the 2D Array feature of ImageQuant (GE Healthcare). Background signal was subtracted, and average intensities were normalized to positive spot controls. Intensities from corresponding spots from control arrays were subtracted and each value was normalized to µg DNA as determined by Quant-it Pico Green assay.Before running the assay, microgels scaffolds were homogenized with a TissueLyser II (Qiagen) at 30 Hz for 1 minute and digested in with in 1 mg mL^{-1} Papain enzyme (Sigma) in PBE buffer containing 1.77 mg mL^{-1} L-cysteine overnight at 65°C. DNA concentration per gel was determined using manufacturer's protocol for the Quant-it Pico Green assay.

ELISAs were performed according to the manufacturer's protocol for specific cytokine concentration quantification. VEGF and LIF ELISAs were purchased from R&D systems, GDNF from Thermo Fisher, IGF-1 from Ray Biotech. Concentration values were also normalized to µg DNA.

4.3.8 N-cadherin blocking

Blocking of N-cadherin cell-cell interactions was performed based on previously published protocols[18,23]. Briefly, trypsinized hMSCs were centrifuged, re-suspended in experimental media containing N-cadherin blocking antibody (50 µg ml^{-1}, Sigma-Aldrich GC4), and incubated for 45 min at 4°C. The cells were then washed twice with PBS and encapsulated in microgels networks. 10 ug/mL of the N-cadherin blocking antibody was also included in the media throughout the experiments to ensure sustained blocking.

4.3.9 Statistics and Principal Component Analysis (PCA)

Statistical analysis of data for cell clustering (percentage of cells in a cluster and number of cells per cluster), and specific ELISAs were performed using GraphPad prism. Statistical significance was determined using one-way ANOVAs with Tukey post hoc comparisons. All

conditions represent three independent biological replicates unless otherwise noted. Principle

component analysis (PCA) was used to assess correlations between the secretory profiles of cells

in each scaffold condition. All analysis and PCA plots were made using the software ClustVis.

4.4 Results
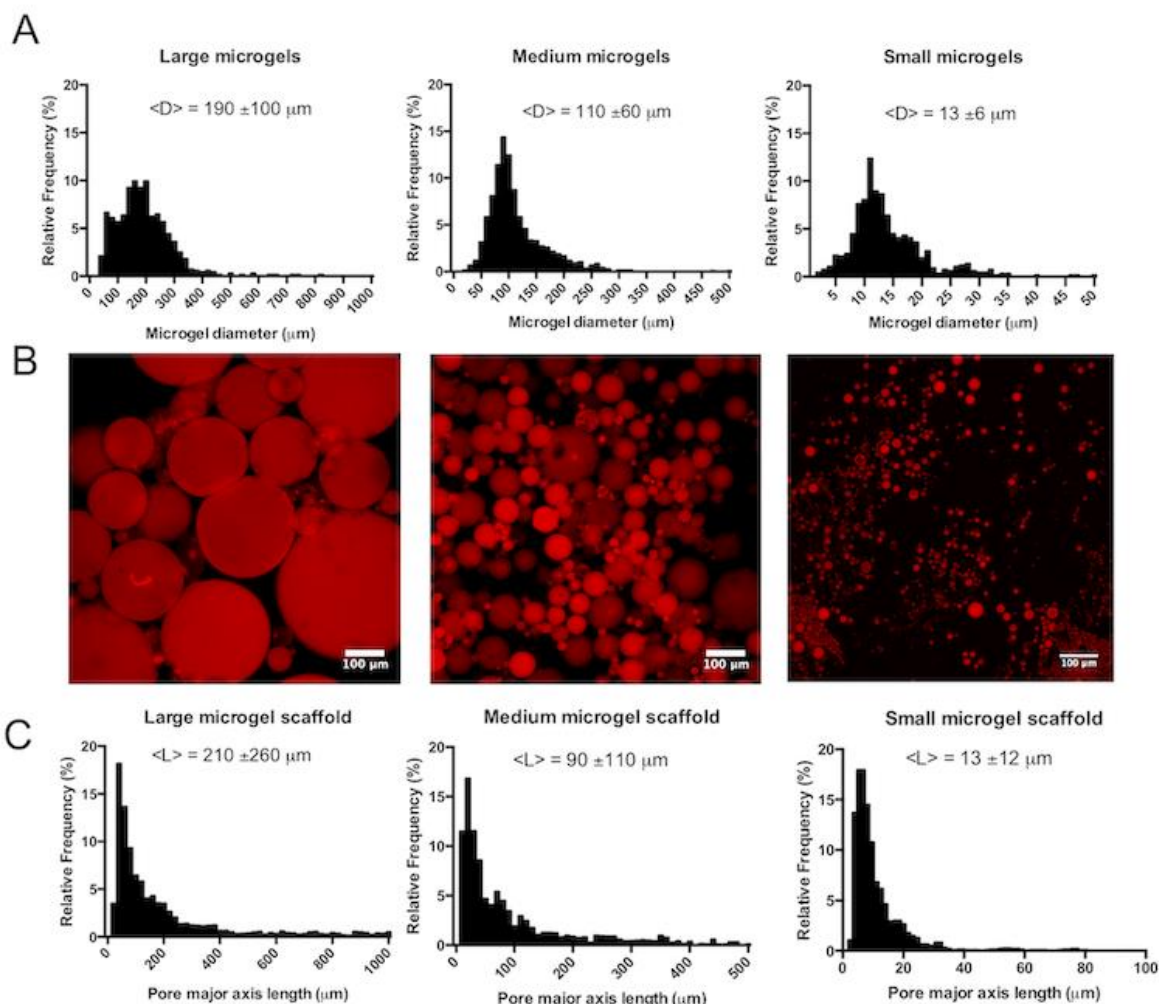
Figure 4.1 Generation of varied porous scaffolds using clickable microgel building blocks.
(A) Clickable microgel building blocks were synthesized using an inverse suspension
polymerization out of 8-arm poly(ethylene glycol) (PEG) functionalized dibenzylcyclooctyne
(DBCO), 4-arm PEG-N3, and an azide functionalized cellularly adhesive peptide (GRGDS).
During the polymerization shear was varied to create microgels with 190±100µm (left), 110±60µm
(middle), and 13±6µm (right) mean particle diameters, termed large, medium, and small,
respectively. (B) Microgel scaffolds were formed by co-assembling DBCO and N3 particles for
each size group (190±100µm (left), 110±60µm (middle), and 13±6µm (right)). Particles were
visualized via incorporation of an azide labeled AlexaFluor 647 dye (C). The resulting microgel

scaffold structures were categorized by measuring the pore mean major axes lengths. Pore lengths correlated with the microgel diameter, with average lengths of 210±260µm (large diameter, left), 90±110µm (medium diameter, middle), and 13±12µm (small diameter, right).

4.4.1 Generation of scaffolds with varying pore dimensions using clickable microgel units

Clickable PEG microgels with excess DBCO or N_3 functional groups were fabricated via an inverse suspension polymerization[19]. Three distinct populations of PEG microgels were synthesized with mean diameters of 190±100µm, 110±60µm, and 13±6µm (Figure 4.1a). These populations will be subsequently referred to as large, medium, and small diameter microgels, respectively.

Microgel storage moduli were measured to be 12.3±2.3kPa and 2.1±0.3kPa for DBCO excess and N_3 excess particles, respectively (Figure 4.7a). Microgel scaffolds were assembled by mixing equal volumes of DBCO and N_3 microgel populations (large (190±100µm), medium (110±60µm), or small (13±6µm) diameters) and centrifuging to induce particle-particle interactions (Figure 4.1b); the resulting porous microgel scaffolds were then characterized by light microscopy. Scaffold compressive moduli were measured to be 1.9±0.3kPa for large, 2.0±0.4kPa for medium, and 2.5±0.2kPa for small diameter microgel scaffolds, with no significant difference between conditions (Figure 4.7b). To improve visualization of the pore size within the microgel scaffolds, scaffolds were swollen with a high molecular weight fluorescent dextran (Figure 4.8). Each network condition maintained a similar three-dimensional structure, with interconnected pores of varying size throughout the microgel network. Pore structure, however, varied significantly between the conditions, with pore dimensions scaling with microgel size (Figure 4.1c). The average pore diameter in large microgel networks was measured to be 210±260µm, 90±110µm in medium microgel networks, and 13±12µm in small microgel networks. The total porosity was similar for large and medium microgel scaffolds at 30.5±0.2% and 28.8±1.0%, respectively, while small microgel scaffolds were less porous with an overall void content of 10.9±0.3% (Table 4.1).
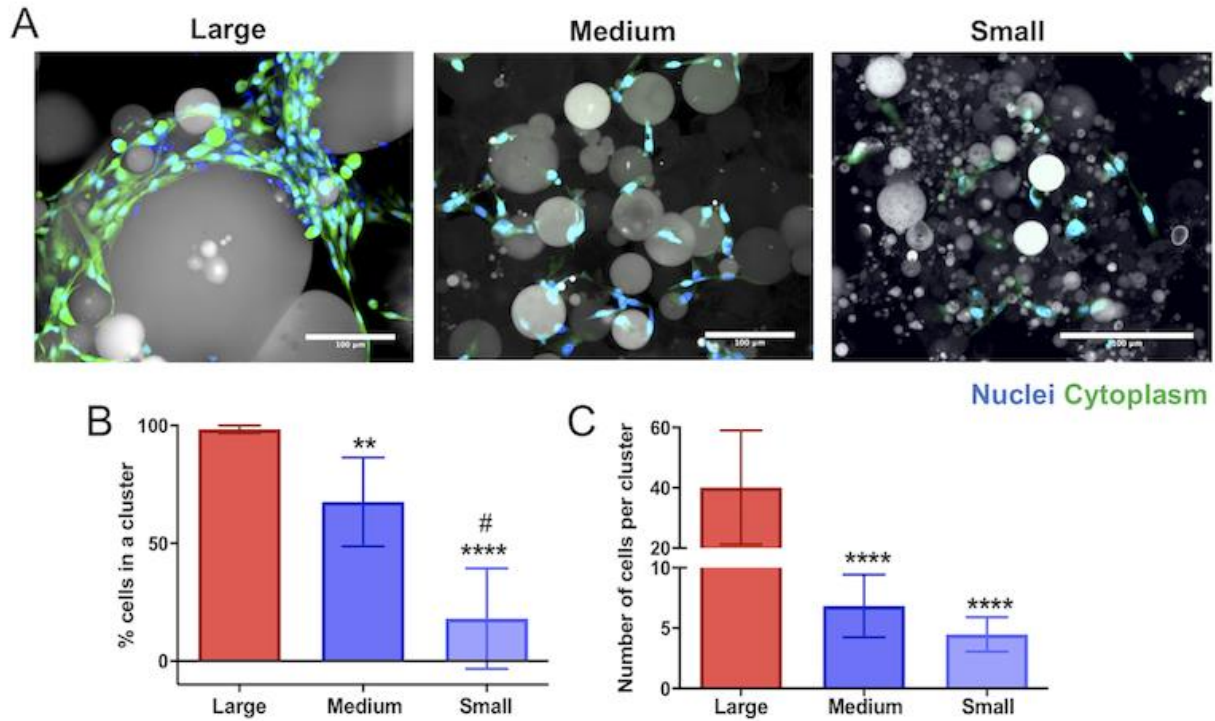
Figure 4.2 Pore dimensions control human mesenchymal stem cell (hMSC) clustering in varied porous scaffolds.
(A) Images of hMSCs cultured in large (190±100µm) diameter (left), medium (110±60µm) diameter (middle), and small (13±6µm) diameter (right) microgel scaffolds for 72 hours. Cells stained for nuclei (blue, DAPI) and cytoplasm (green, Calcien) and particles shown via transmitted light. Scale bars = 100µm. (B) Percent of cells in a cluster in each microgel condition. Cell-cell interactions were quantified by measuring the average number of cells in a cluster (3 or more cells physically touching) in each condition. (C) Average number of cells in a cluster was also quantified for each condition. Average number of cells per cluster between the medium and small microgel scaffolds was not significantly different. Significance determined using a one-way ANOVA. All stars represent significance compared to large microgel condition. ****$p<0.0001$, ** $p<0.01$, # $p<0.001$ (compared to medium diameter).

4.4.2   Human mesenchymal stem cell (hMSC) clustering scales with pore size

The size and frequency of clustered cells was determined using light microscopy and 3D visualization software (IMARIS). hMSCs were encapsulated in porous microgels networks fabricated with large (190±100µm), medium (110±60µm), and small (13±6µm) diameter microgels at a density of 5 million cells/mL. Centrifugation speeds and the encapsulation procedure have been previously optimized and reported as cytocompatible[19], and hMSCs in each

condition were highly viable with no significant difference between conditions (96.3±4.6% in large microgel scaffolds, 92.8±4.0% in medium microgel scaffolds, and 94.2±2.7% in small microgel scaffolds) (Figure 4.9). After three days in culture, samples were fixed, stained with DAPI and rhodamine phalloidin, and imaged on a Nikon spinning disc confocal microscope. Qualitative differences in the cell cluster size are readily observed between the three microgel conditions (Figure 4.2a).

Z-stacks of the cell-laden microgel scaffolds were imported into IMARIS 3D visualization software and a 3D surface was rendered over a cluster by utilizing the cytoplasmic stain. The number of nuclei per cluster was determined using a Matlab code (Split into Surface Objects Xtension) in the IMARIS software. hMSC cluster size was analyzed for N>8 gels for each particle size condition. An increase in pore size, a function of the microgel particle size, led to a higher percentage of cells residing in a cluster, defined as possessing three or more nuclei. This cluster threshold was chosen to assess cell-cell interactions during the microgel scaffold assembly and not as a result of cell division over 72 hours of culture time. In networks fabricated from large (190±100µm) diameter particles, almost all hMSCs resided within a cluster (98±1.6%) (Figure 4.2b). The percentage of cells in a cluster was significantly lower in both the medium (110±60µm) and small (13±6µm) diameter microgel networks, 68±19% and 18±21%, respectively. Each condition was statistically different than the others. Additionally, larger pore sizes caused an increase in the cluster size: ~ 40±18 cells/cluster in the large microgel scaffolds, ~7±3 cells/cluster in the medium and ~5±1 cells/cluster in the small microgel networks. The average hMSC cluster size was not significantly different between the medium and small microgel scaffolds.

4.4.3   hMSC secretory properties vary with scaffold porosity and cluster size

After 72 hours in each culture condition (large (190±100µm), medium (110±60µm), or small (13±6µm) diameter microgel scaffolds), the secreted proteins in the media were measured using a cytokine array and normalized to DNA content to quantify the effect of scaffold properties on the hMSC cytokine secretion. A cytokine array was selected to quantify a broad number of cytokines and chemokines involved in hMSC paracrine signaling. Analyses revealed that the scaffold pore architecture strongly influenced the hMSC secretome (Figure 4.3a).

Figure 4.3 hMSC secretory properties vary with scaffold porosity.
(A) Heatmap of cytokine expression of encapsulated hMSCs in large (190±100µm), medium (110±60µm), and small (13±6µm) diameter microgel networks. Red intensities represent high expression while blue intensities represent low or undetectable expression levels compared to control (cell media). Values were normalized to DNA content. (B) Cytokines that were most elevated in large (left, red), medium (middle, blue), and small microgel scaffolds (right, light blue). (C) List of regenerative factors that were most elevated in large (left, red), medium (middle, blue), and small microgel scaffolds (right, light blue).

Cells encapsulated in the large microgel scaffolds demonstrated a distinct secretory profile, compared to relatively similar secretory profiles between the medium and small diameter microgel scaffolds. In general, hMSCs in the large diameter microgel scaffolds secreted higher concentrations (represented by red intensities on the heatmap) of cytokines compared to the lower concentrations (represented by blue intensities on the heatmap) by cells in the medium and small diameter microgel scaffolds. Of the 72 cytokines secreted at detectable levels, 48 (~60%) were most elevated in the large diameter microgel scaffolds, while only 18 (25%) and 11 (~15%) were highest in the medium and small diameter microgel scaffolds, respectively (Figure 4.3b). Beyond this global screen, a subset of factors was selected based on a literature review of hMSC regenerative therapies[24–27]. Of the 24 factors chosen, a similar trend was observed, with the majority of these regenerative cytokines (65%) being most elevated in networks formed from large microgels, compared to 21% in medium microgels, and 13% in small diameter microgel networks.

4.4.4   N-cadherin interactions increase with increased cell clustering

N-cadherins are a type I classical cadherin responsible for adherence junctions between cells primarily of the mesenchymal lineage. Cadherins are one of several membrane bound proteins that are involved in intercellular communication, with N-cadherins being the most widely expressed on hMSCs[28]. Since differential cell clustering occurred in the porous scaffold conditions, immunofluorescent staining was performed on encapsulated hMSCs to assess differences in cell-cell interactions mediated via N-cadherin. To adequately image and quantify the punctate, the microgels were not stained during imaging. In Figure 4.4a (top), large N-cadherin punctae were observed in hMSC clusters in the large (190±100μm) diameter microgel scaffolds. In contrast, while hMSCs in the medium (110±60μm) diameter microgel scaffolds maintained some cell clustering and elevated N-cadherin staining (Figure 4.4a, middle), the

majority of hMSCs in the small (13±6µm) diameter microgel scaffolds did not reside in clusters and had more diffuse N-cadherin staining (Figure 4.4a, bottom). These differences were further quantified by analysis of the N-cadherin punctate intensity and a significant increase in expression by hMSCs encapsulated in the large microgel scaffolds was observed (Figure 4.4b).

Nuclei F-actin N-cadherin
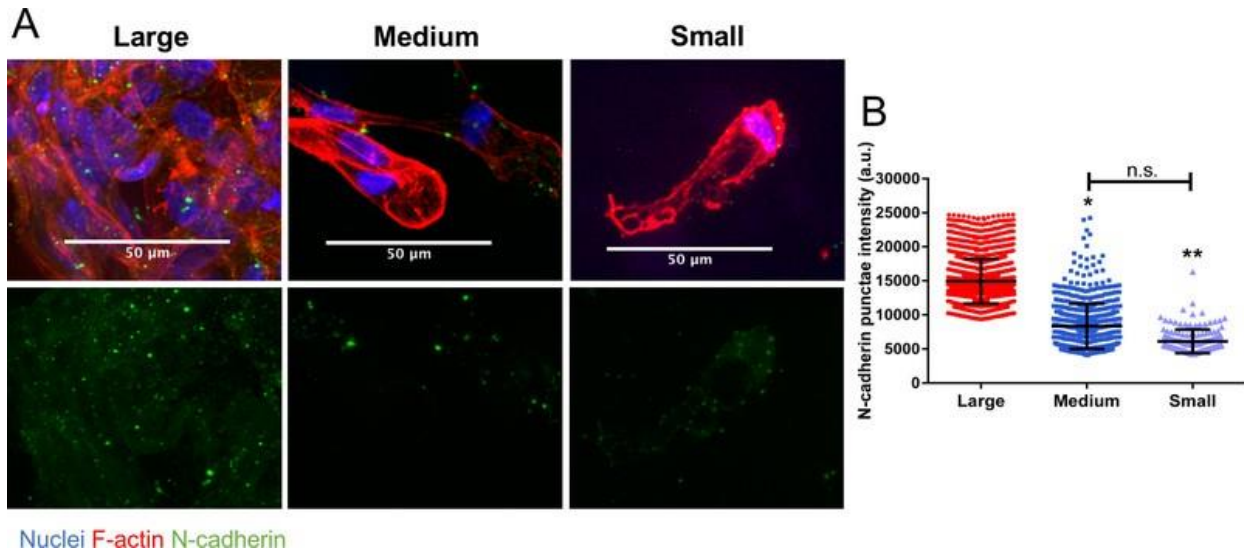
Figure 4.4 N-cadherin interaction and expression increases with increased cell clustering.
(A) hMSCs in large (190±100µm) diameter microgel scaffolds (top, right) with highly clustered cells show more intense staining for N-cadherin punctate compared with smaller clusters in medium (110±60µm) diameter microgel scaffolds (middle, right) and largely single cells in small (13±6µm) diameter microgel scaffolds (bottom, right) Cells stained for nuclei (blue), N-cadherin (green), and F-actin (red). (B) Intensity quantification of the N-cadherin punctate. Stars represent significance relative to large microgel scaffolds. ** $p<0.01$, * $p<0.05$, n.s. – non-significant

4.4.5 Blocking N-cadherin interactions in microgel scaffolds decreases hMSC secretory properties

To further investigate the role of cell-cell interactions mediated via N-cadherin on the hMSC secretory phenotype, hMSCs were incubated with a monoclonal antibody against N-cadherin (αN-Cad) prior to encapsulation. The culture media was also supplemented with αN-Cad during the entire culture period. After 72 hours, the cell media was collected and analyzed with a cytokine array as described above. Results revealed that blocking N-cadherin led to a significant decrease in the secretion of cytokines by hMSCs for all scaffold conditions (Figure 4.5a). Notably, the
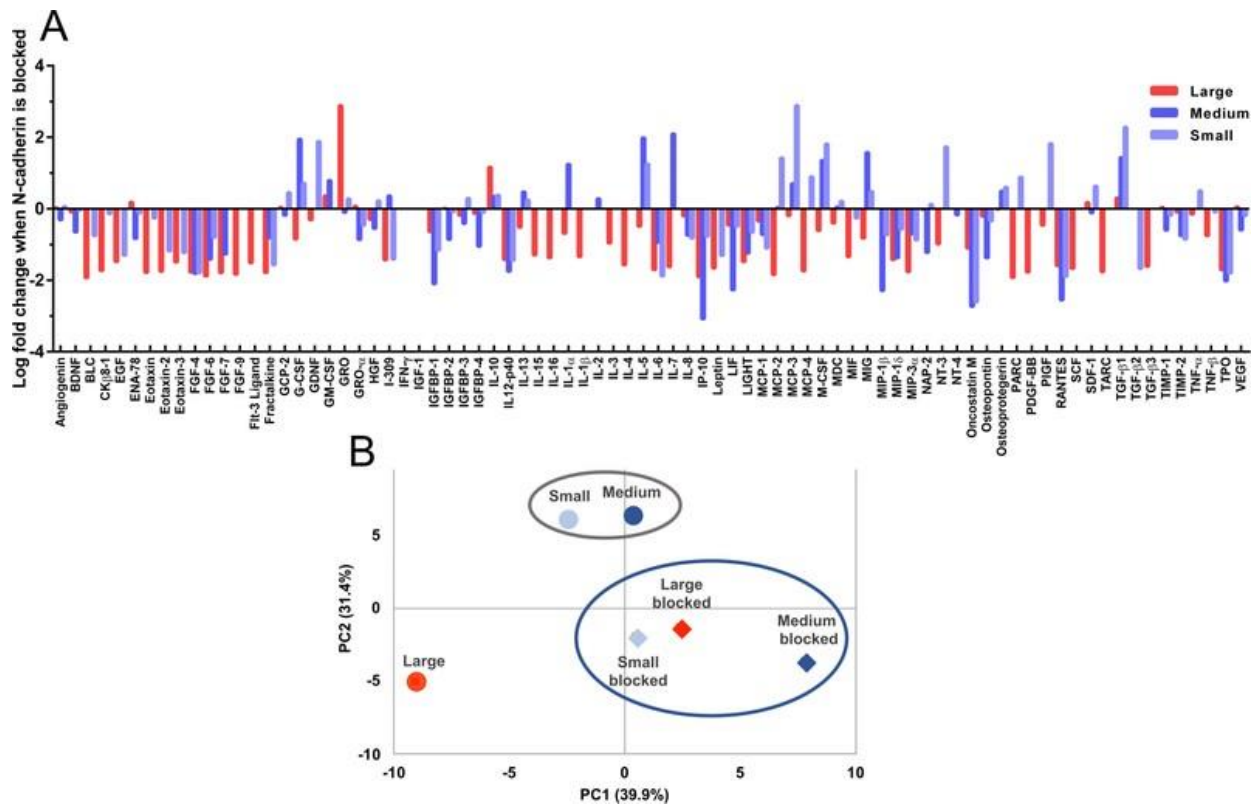
Figure 4.5 Blocking N-cadherin interactions in microgel scaffolds decreases hMSC secretory properties.
(A) Log-fold change in cytokine secretion from hMSCs in large (190±100µm) diameter (red), medium (110±60µm) diameter (blue), and small (13±6µm) diameter (light blue) microgel scaffolds when cultured in the presence of an anti-N-cadherin antibody compared to their respective unmodified conditions. Negative fold change indicates a decreased in cytokine expression in the presence of blocking. (B) Principal component analysis of hMSC secretory profile of standard conditions (circles) and N-cadherin blocked conditions (diamonds). Colors correspond to conditions in (A) PC1 and PC2 explained 39.9% and 31.4% of the variance, respectively.

expression of 78% of all measured cytokines was decreased in the large (190±100µm) diameter

microgel scaffolds, while 44% and 46% of all cytokines were similarly decreased in the medium

(110±60µm) and small (13±6µm) diameter microgel scaffolds, respectively. Over a ten-fold

decrease was observed for 45% of cytokines in the large condition and 20% and 19% for the

medium and small diameter microgel networks respectively. Only two factors in the large diameter

microgel scaffold were upregulated by over ten-fold, while only 7 and 8 of factors were highly

upregulated in medium and small diameter microgel scaffolds, respectively. Principal component

analysis (PCA) was used to evaluate the differential role of N-cadherin interactions on the secretory profiles observed between the microgel networks. PC1 and PC2 explained 39.9% and 31.4% of the variance respectively. When examined this way, the secretory profile of hMSCs encapsulated in large diameter microgel scaffolds under standard culture conditions was distinct from those in medium and small diameter microgel networks (Figure 4.5b). However, when the N-cadherin interactions were blocked, the secretory profile of the hMSCs in all pore conditions became similar. These results help quantify and illustrate the role that N-cadherin interactions and cell-cell clustering play in the dictating the secretory profiles of hMSCs.

4.4.6 HAVDI functionalized microgel scaffolds promote the secretory phenotype of hMSCs

To engineer a microgel assembled scaffold to promote the secretory profile of hMSCs, even in the absence of cell-cell interactions, an N-cadherin mimetic peptide, HAVDI, was conjugated to the microgel formulations. hMSCs were cultured for 3 days in the same porous microgel system and the conditioned media was analyzed via cytokine arrays. The inclusion of the HAVDI peptide drastically increased the hMSC secretory profile in all scaffold conditions (Figure 4.6a). Of all the eighty measured cytokines, 96% of them were increased in large (190±100µm) diameter microgel networks and 86% and 89% were increased in medium (110±60µm) and small (13±6µm) diameter microgel networks respectively (Figure 4.6a). Of the previously identified regenerative cytokines (24), almost all (97%) were increased in large diameter microgel scaffolds, while 23 (96%) and 22 (92%) were elevated in the medium and small diameter microgel conditions respectively. Out of all the elevated cytokines, 33%, 42% and 45% were elevated 10-fold in large, medium, and small diameter microgel networks respectively. It should also be noted that no significant differences in hMSC cluster size or frequency of cells in clusters was observed due to the presence of the HAVDI (Figure 4.10). Thus, the primary effect was attributed to interactions between cells and HAVDI.

Principal component analysis demonstrated that the secretory phenotype of hMSCs in HAVDI networks were more similar to each other compared to their unmodified counterparts (Figure 4.6b). PC1 and PC2 explained 70.4% and 18.3% of the variance respectively.

Currently, the majority of hMSC clinical trials are focused on cardiovascular, neurological, inflammatory diseases, and bone/cartilage regeneration[1,29]. Cytokines secreted by hMSCs are integral to the success of many of these therapeutic applications[2,3]. Based on an analysis of hMSCs clinical trials focused on tissue regeneration, VEGF, GDNF, IGF-1, and LIF were selected for further analysis using ELISAs. Vascular endothelial growth factor (VEGF) is a key signaling cytokine involved in angiogenesis[30] and has been shown to improve MSC survival in infarct hearts where they can help repair cardiac tissue after myocardial infraction[31,32]. hMSCs secreted VEGF in all three pore size conditions (~1000-4000 pg/µg DNA) (Figure 4.6a) but the HAVDI interactions increased secretion in medium and small diameter microgel scaffolds by 1.5-2-fold. A non-significant increase was observed in the large diameter microgel scaffolds (Figure 4.6c). For neurodegenerative applications, glial cell- derived neurotrophic factor (GDNF) has restorative and protective effects on multiple neuronal cell types[33]. MSCs genetically modified to overexpressed GDNF provided local neuroprotection in an inflammatory model of Parkinson's[34]. GDNF was significantly elevated in each condition upon the addition of HAVDI (Figure 4.6d). This was most noticeable in medium and small diameter microgel scaffolds, where GDNF levels rose by two orders of magnitude (~2 pg/µg DNA in unmodified conditions to >250pg/µg DNA in HAVDI conditions). IGF-1 is another anabolic cytokine that plays an important role in cardiac repair, as it can recruit and stimulate the differentiation of endogenous cells in the injured heart[35]. Low levels of IGF-1 secretion were observed in unmodified conditions (1-3pg/µg DNA in large

diameter microgel scaffolds, <1pg/µg DNA in medium and small diameter microgel scaffolds) but was elevated to 20-50pg/µg DNA in HAVDI networks (Figure 4.6e).
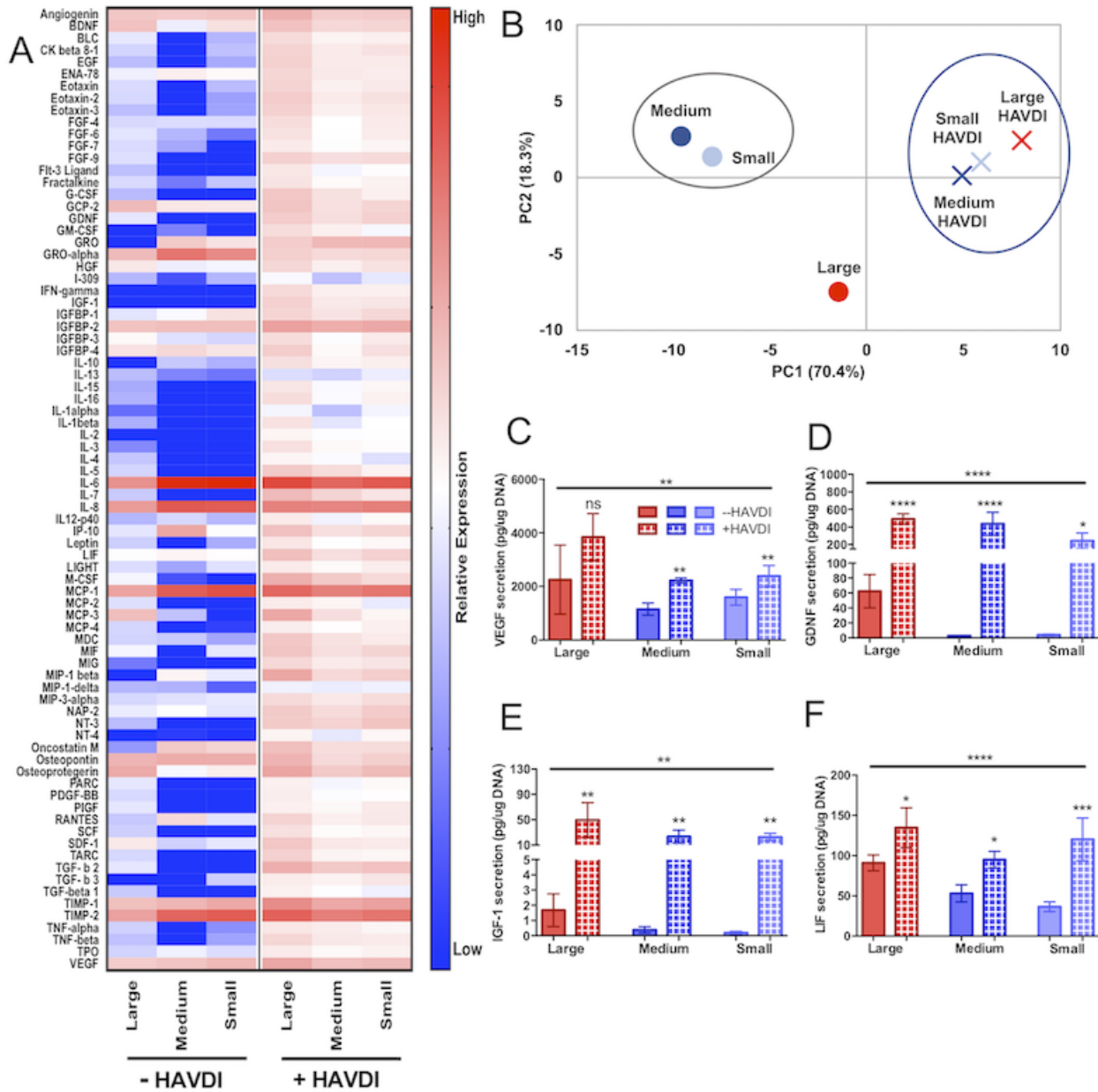
Figure 4.6 HAVDI inclusion in microgel scaffolds increases secretory phenotype of hMSCs. (A) Heatmap of cytokine expression of encapsulated hMSCs in large (190±100µm), medium (110±60µm), and small (13±6µm) diameter microgel scaffolds with and without inclusion of the HAVDI peptide. (B) PCA analysis of hMSC secretory profile between large (red), medium (blue), and small (light blue) microgel scaffolds without (circles) and with HAVDI (X symbol). PC1 and PC2 explained 70.4% and 18.3% of the variance respectively. (C) ELISA quantification of VEGF, (D) GDNF, and (E) IGF-1. HAVDI conditions are represented by hashed bars. Stars represent

significance relative to respective unmodified scaffolds. Overall significance (top bar) determined using a one-way ANOVA with multiple comparisons. ****p<0.0001, ** p<0.01, n.s. – non-significant

Leukemia inhibitory factor (LIF) is involved in myogenic precursor cell recruitment and has also been implicated in myoblast proliferation and differentiation[36]. Significant upregulation in LIF secretion was observed in all scaffolds upon the addition of HAVDI, ranging from a 1.5-fold increase in large diameter microgel scaffolds to over a three-fold upregulation in small diameter microgel scaffold conditions (Figure 4.6f). Combined, these data lend support to the notion that both the HAVDI peptide and cell clustering can promote the secretory properties of encapsulated hMSCs in microgel scaffolds.

4.5   Discussion

Porous scaffolds assembled from individual microgel components have drawn increased interest in the fields of biomaterials research and tissue regeneration. Several groups have demonstrated the versatile nature of this platform, where cross-linking reactions[37], incorporation of bioactive moieties[38,39], and particle size[40] can all be tuned to alter the final scaffold properties[41]. Often, a key design parameter is to create cell-instructive scaffolds, where microgels and cells are assembled together, and scaffold properties can be tuned to control multiple cell functions independently. Some examples include directing matrix deposition[42], controlling cell motility[43], facilitating diffusion and nutrient transport[44], and mitigating immunogenic responses *in vivo*[41]. In this contribution, an assembled microgel scaffold was designed to control hMSC secretory properties via both physical and biochemical means. First, three particle sizes, 190±100µm, 110±60µm, and 13±6µm diameters, were used to created scaffolds with major axis pore lengths of ~210µm, ~90µm, and ~13µm, respectively. Cells encapsulated in networks with 190±100µm (large) diameter particles were more frequently located in clusters (~98%) and the cluster sizes were larger (~40 cell/cluster) compared to less frequent (68% and 18%) and smaller clusters (7

and 5 cells/cluster) in 110±60µm (medium) and 13±6µm (small) diameter microgel scaffolds, respectively (Figure 4.2). Increased cell-cell interactions significantly influenced hMSC secretory properties, where cells in large diameter microgel scaffolds secreted a higher level of a variety of proteins as assessed by a cytokine array. Approximately 60% of all cytokines measured were elevated in the large diameter microgel scaffolds. This data aligns with a growing body of literature demonstrating how scaffold porosity can affect cell function, such as dendritic cell activation[45,46] and hMSC osteogenic differentiation[47]. Of particular note, Qazi *et al.* demonstrated that pore size of gelatin scaffolds affected the angiogenic potential of hMSCs, with optimal secretion of angiogenic cytokines achieved in porous scaffolds that promoted clustering of infiltrating cells[48]. Together, these data demonstrate how pore size alone can be used to control cell-cell clustering and direct cell function.

In addition to manipulating pore size, several biochemical and physical strategies have been developed to improve the secretory properties of hMSCs, typically by exposing cells to exogenously delivered inflammatory molecules (i.e., licensing)[27,49] or by culturing hMSCs in large aggregates termed spheroids[15]. Additionally, it should be noted that MSCs be isolated from multiple tissues and cells can have varied secretory behavior based on their tissue of origin[50,51]. Murphy *et al.* used a hanging drop method to create hMSCs spheroids on the order of thousands of cell per aggregate and observed changes in secretion based on spheroid size[17]. In contrast, in the large microgel scaffolds presented in this study, there were ~1 million cells per gel and an average cluster size of 40 cells. Although it is difficult to compare spheroids directly with cells in porous scaffolds, the central theme of both is that hMSC cell-cell contacts contribute to their enhanced their secretory properties.

hMSCs are known to interact with each other via N-cadherins, which contain an extracellular domain that dimerizes between bound cells and an intracellular domain anchored to the cytoskeleton capable of signal transduction through several catenin mediated pathways[28]. In our centrifugation approach for the scaffold assembly, hMSCs had high levels of N-cadherin expression in the large clusters present in large (190±100µm) diameter microgel scaffolds (Figure 4.4), and decreased expression in the small cell clusters present in the 110±60µm (medium) and 13±6µm (small) diameter microgel scaffolds. The role of the N-cadherin interactions on the hMSC secretory phenotype was further confirmed by blocking the interactions with a monoclonal antibody against N-cadherin. A marked decrease in secretion of a variety of different cytokines was observed in all conditions, but most noticeably in the large diameter microgel scaffolds, secretion was decreased ~78% for all of the measured cytokines (Figure 4.5a). Further implicating the role of N-cadherin in influencing the hMSC secretory phenotype, the profile of hMSCs between conditions was more similar when N-cadherin was blocked compared to standard culture, as determined by principal component analysis (Figure 4.5b). These data align with previous investigations, where the inclusion of a N-cadherin blocking antibody in porous and bulk hydrogels decreased the hMSC secretory phenotype, as assessed via a cytokine array[18].

To test whether cell-matrix interactions could mimic some of the same benefits as cell-cell interactions, an N-cadherin peptide epitope (HAVDI) was introduced into the microgel formulation to promote a secretory phenotype. While its role in hMSC differentiation and mechanosensing has previously been studied[20,23], less is known of its ability to stimulate hMSC secretory properties. The inclusion of HAVDI did not significantly alter hMSC multipotency, as assessed by CD105 expression (Figure 4.10a). However, it boosted cytokine secretion in all pore sizes, including VEGF, GDNF, LIF, and IGF-1 (Figure 4.6) without altering cell cluster

characteristics (Figure 4.10b,c). Additionally, PCA analysis confirmed that the secretory phenotype of cells in HAVDI scaffolds were more similar to each other than when in unmodified conditions. This approach may prove advantageous for design of biomaterial delivery systems for cell transplantation, where cell clustering is prohibited or non-ideal, but a secretory phenotype is beneficial for therapeutic outcomes. Design of scaffolds that can promote not only the survival, but secretion profiles of delivered cells may provide specific benefits for cell-based therapies for regenerative medicine.

4.6 Conclusions

The therapeutic potential of hMSCs paracrine factors is quickly being recognized; necessitating the development of biomaterial systems to deliver and promote secretory hMSCs. In this study, porous bio-click microgel assembled scaffolds were designed to control the secretory phenotype of hMSCs. First, microgel scaffold pore size was used to control hMSC aggregate size, allowing for increased secretory properties with highly clustered cells. Secondly, an N-cadherin mimetic peptide (HAVDI) was included to enhance hMSC cytokine secretion, in both clustered and singly encapsulated cell conditions. The ability to improve cell secretory behavior even when it is limited by other factors (i.e. lack of cell clustering) holds promise for improving cell-based therapies. These findings are relevant for informing biomaterial design both in *in vitro* studies as well the delivery of hMSCs for clinical applications.

4.7 Data Sharing

The raw data used in this study are available from the corresponding author upon reasonable request.

4.8 Acknowledgments

4.9   Supplemental Information

Table 4.1 Overall void fraction for microgel scaffolds. Reported values are averages of three separate gels ± standard deviation.

Condition	Void Fraction
190 ± 100μm diameter microgel scaffold	0.305 ± 0.002
110 ± 60μm diameter microgel scaffold	0.288 ± 0.01
13 ± 6μm diameter microgel scaffold	0.109 ± 0.003
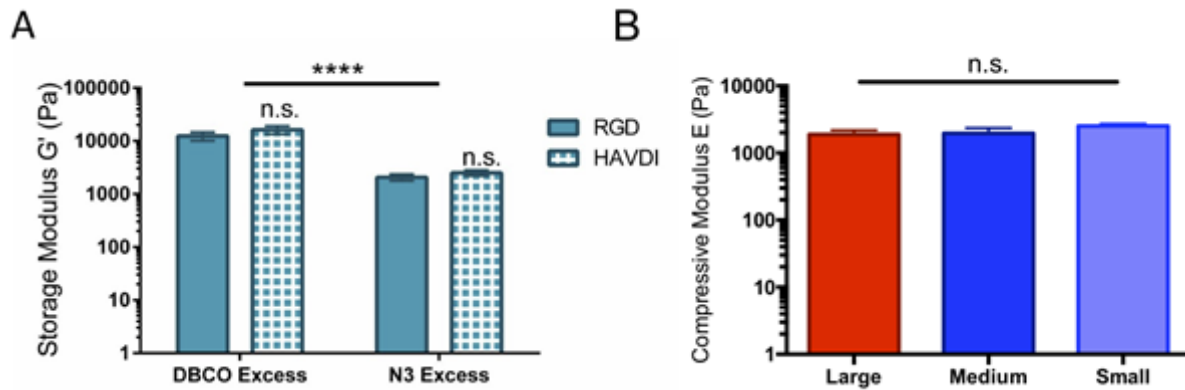
Figure 4.7 Rheological characterization of microgel and microgel scaffolds.
(A) Final *in situ* moduli of bulk gels made with either excess DBCO or azide groups without (solid color) or with (patterned color) the HAVDI peptide. The inclusion of the HAVDI peptide did not significantly alter microgel mechanics. (B) Compressive modulus of large (190 ± 100μm) diameter (red), medium (110 ± 60μm) diameter (blue), and small (13 ± 6μm) diameter (light blue) microgel scaffolds. Overall significance determined using one-way ANOVAs with multiple comparisons. **** $p < 0.0001$, n.s. – not significant
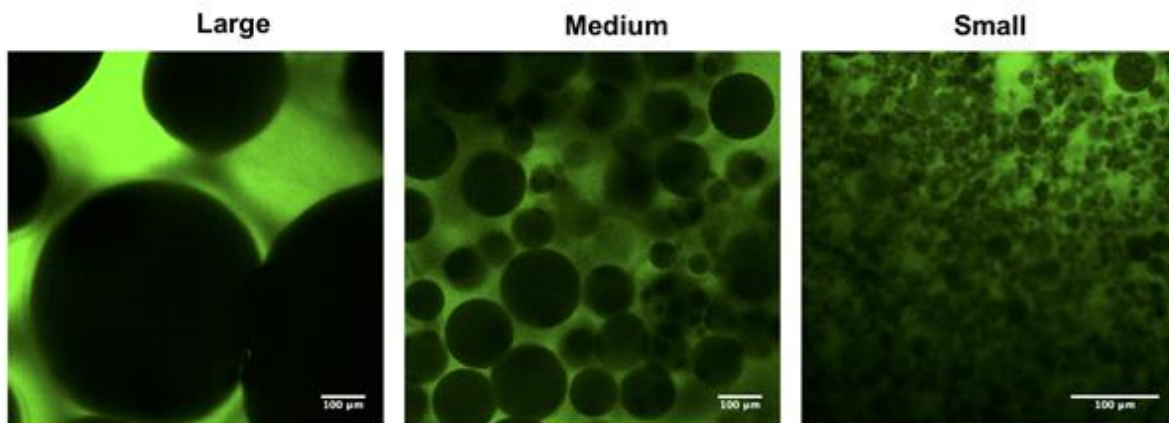
Figure 4.8 Scaffold porosity.
Porosity was visualized by swelling a 2,000kDa fluorescent dextran (green) into the large (190 ± 100µm), medium (110 ± 60µm), and small (13 ± 6µm) diameter microgel networks. Scale bar denotes 100µm.
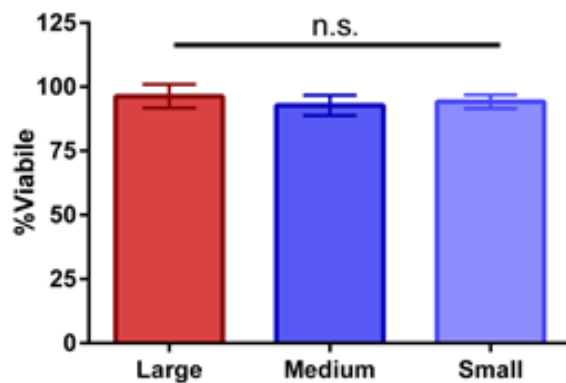
Figure 4.9 hMSC viability.
Viability of encapsulated hMSCs after 72 hours in large (190 ± 100µm), medium (110 ± 60µm), and small (13 ± 6µm) diameter microgel scaffolds as determined by calcein and ethidium homodimer staining. Significance determined using a one-way ANOVA. n.s. – not significant
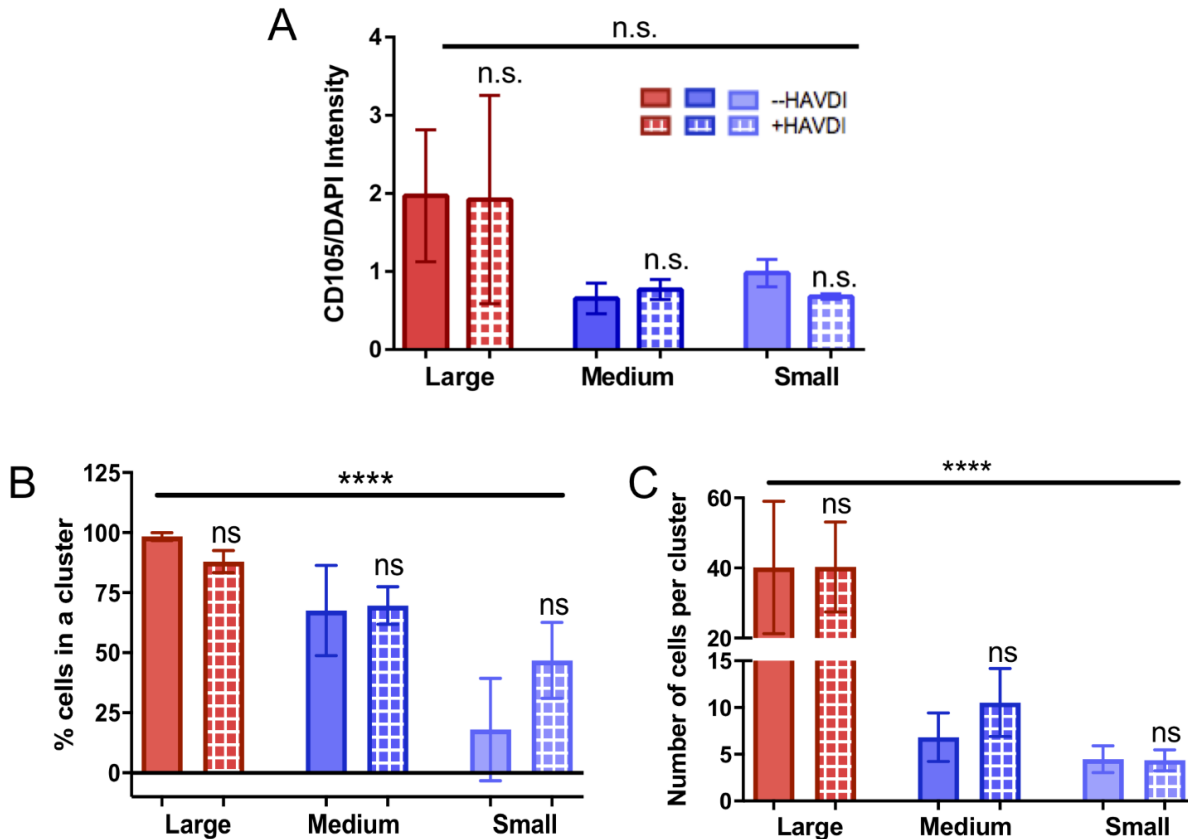
Figure 4.10 Engineered HAVDI microgels have no significant differences in hMSC behavior. (A) Average intensity of the hMSC multipotency marker CD105 in large ($190 \pm 100\mu m$) diameter (red), medium ($110 \pm 60\mu m$) diameter (blue), and small ($13 \pm 6\mu m$) diameter (light blue) microgel scaffolds without (solid color) and with (patterned) the HAVDI peptide. CD105 intensity was normalized to DAPI for each cell. (B) Percentage of hMSCs in a cluster (3 or more cells) and (C) number of cells per cluster by condition were not significantly different between HAVDI and unmodified scaffolds. Overall significant was determined using a one-way ANOVA with multiple comparisons. ****<0.0001, n.s. – not significant

4.10 References

(1)   Trounson, A. & Mcdonald, C. Cell Stem Cell Stem Cell Therapies in Clinical Trials: Progress and Challenges. *Stem Cell* **17**, 11–22 (2015).

(2)   Caplan, A. I. & Correa, D. The MSC: An Injury Drugstore. *Cell Stem Cell* **9**, 11–15 (2011).

(3)   da Silva Meirelles, L., Fontes, A. M., Covas, D. T. & Caplan, A. I. Mechanisms involved in the therapeutic properties of mesenchymal stem cells. *Cytokine Growth Factor Rev.* **20**, 419–427 (2009).

(4)   Huebsch, N. *et al.* Matrix elasticity of void-forming hydrogels controls transplanted-stem-cell-mediated bone formation. *Nat. Mater.* **14**, 1269–77 (2015).

(5)   Engler, A. J., Sen, S., Sweeney, H. L. & Discher, D. E. Matrix Elasticity Directs Stem Cell Lineage Specification. *Cell* **126**, 677–689 (2006).

(6)   Murphy, W. L., McDevitt, T. C. & Engler, A. J. Materials as stem cell regulators. *Nat. Mater.* **13**, 547–556 (2014).

(7)   Killaars, A. R. *et al.* Extended Exposure to Stiff Microenvironments Leads to Persistent Chromatin Remodeling in Human Mesenchymal Stem Cells. *Adv. Sci.* **6**, 1801483 (2019).

(8)   Caliari, S. R., an Vega, S. L., Kwon, M., Soulas, E. M. & Burdick, J. A. Dimensionality and spreading influence MSC YAP/TAZ signaling in hydrogel environments. *Biomaterials* **103**, 314–323 (2016).

(9)   Di Luca, A. *et al.* Influencing chondrogenic differentiation of human mesenchymal stromal cells in scaffolds displaying a structural gradient in pore size. *Acta Biomater.* **36**, 210–219 (2016).

(10)   Gupte, M. J. *et al.* Pore size directs bone marrow stromal cell fate and tissue regeneration in nanofibrous macroporous scaffolds by mediating vascularization. *Acta Biomater.* **82**, 1–11 (2018).

(11)   Karimi, F., O'Connor, A. J., Qiao, G. G. & Heath, D. E. Integrin Clustering Matters: A Review of Biomaterials Functionalized with Multivalent Integrin-Binding Ligands to Improve Cell Adhesion, Migration, Differentiation, Angiogenesis, and Biomedical Device Integration. *Adv. Healthc. Mater.* **1701324**, 1–28 (2018).

(12)   Burdick, J. A. & Anseth, K. S. Photoencapsulation of osteoblasts in injectable RGD-modified PEG hydrogels for bone tissue engineering. *Biomaterials* **23**, 4315–4323 (2002).

(13)   Rao, V. V., Vu, M. K., Ma, H., Killaars, A. R. & Anseth, K. S. Rescuing mesenchymal stem cell regenerative properties on hydrogel substrates post serial expansion. *Bioeng. Transl. Med.* **4**, 51–60 (2019).

(14)   Abdeen, A. A., Weiss, J. B., Lee, J. & Kilian, K. A. Matrix Composition and Mechanics Direct Proangiogenic Signaling from Mesenchymal Stem Cells. *Tissue Eng. Part A* **00**, 1–9 (2014).

(15)   Gionet-Gonzales, M. A. & Leach, J. K. Engineering principles for guiding spheroid function in the regeneration of bone, cartilage, and skin. *Biomed. Mater.* **13**, 034109 (2018).

(16)   Ho, S. S., Murphy, K. C., Binder, B. Y. K., Vissers, C. B. & Leach, J. K. Increased Survival and Function of Mesenchymal Stem Cell Spheroids Entrapped in Instructive Alginate Hydrogels. *Stem Cells Transl. Med.* **5**, 773–781 (2016).

(17)   Murphy, K. C. *et al.* Multifactorial Experimental Design to Optimize the Anti-Inflammatory and Proangiogenic Potential of Mesenchymal Stem Cell Spheroids. *Stem Cells* **35**, 1493–1504 (2017).

(18)   Qazi, T. H., Mooney, D. J., Duda, G. N. & Geissler, S. Biomaterials that promote cell-cell interactions enhance the paracrine function of MSCs. *Biomaterials* **140**, 103–114 (2017).

(19)   Caldwell, A. S., Campbell, G. T., Shekiro, K. M. T. & Anseth, K. S. Clickable Microgel Scaffolds as Platforms for 3D Cell Encapsulation. *Adv. Healthc. Mater.* **6**, 1–8 (2017).

(20)   Bian, L., Guvendiren, M., Mauck, R. L. & Burdick, J. A. Hydrogels that mimic developmentally relevant matrix and N-cadherin interactions enhance MSC chondrogenesis. **110**, 10117–10122 (2013).

(21) Deforest, C. A., Polizzotti, B. D. & Anseth, K. S. Sequential click reactions for synthesizing and patterning three-dimensional cell microenvironments. *Nat. Mater.* (2009). doi:10.1038/nmat2473

(22) Yang, C., Tibbitt, M. W., Basta, L. & Anseth, K. S. Mechanical memory and dosing influence stem cell fate. *Nat. Mater.* **113**, 645–651 (2014).

(23) Cosgrove, B. D. *et al.* N-cadherin adhesive interactions modulate matrix mechanosensing and fate commitment of mesenchymal stem cells. *Nat. Mater.* **15**, 1297–1306 (2016).

(24) Galderisi, U. & Giordano, A. The Gap Between the Physiological and Therapeutic Roles of Mesenchymal Stem Cells. *Med. Res. Rev.* **34**, 1100–1126 (2014).

(25) Ranganath, S. H., Levy, O., Inamdar, M. S. & Karp, J. M. Harnessing the Mesenchymal Stem Cell Secretome for the Treatment of Cardiovascular Disease. *Cell Stem Cell* **10**, 244–258 (2012).

(26) Lian, Q., Liang, X., Ding, Y., Zhang, Y. & Tse, H.-F. Paracrine Mechanisms of Mesenchymal Stem Cell-Based Therapy: Current Status and Perspectives. *Cell Transplant.* **23**, 1045–1059 (2014).

(27) Ferreira, J. R. *et al.* Mesenchymal Stromal Cell Secretome: Influencing Therapeutic Potential by Cellular Pre-conditioning. *Front. Immunol.* **9**, 2837 (2018).

(28) Gumbiner, B. M. Regulation of cadherin-mediated adhesion in morphogenesis. *Nat. Rev. Mol. Cell Biol.* **6**, 622–634 (2005).

(29) Galderisi, U., Squillaro, T. & Peluso, G. Clinical Trials With Mesenchymal Stem Cells: An Update. *Cell Transplant.* **25**, 829–848 (2016).

(30) Ferrara, N., Gerber, H. P. & LeCouter, J. The biology of VEGF and its receptors. *Nat. Med.* **9**, 669–676 (2003).

(31)   Pons, J. *et al.* VEGF improves survival of mesenchymal stem cells in infarcted hearts. *Biochem. Biophys. Res. Commun.* **376**, 419–422 (2008).

(32)   Tang, J. M. *et al.* VEGF/SDF-1 promotes cardiac stem cell mobilization and myocardial repair in the infarcted heart. *Cardiovasc. Res.* **91**, 402–411 (2011).

(33)   Ibáñez, C. F. & Andressoo, J.-O. Biology of GDNF and its receptors — Relevance for disorders of the central nervous system. *Neurobiol. Dis.* **97**, 80–89 (2017).

(34)   Hoban, D. B., Howard, L. & Dowd, E. GDNF-secreting mesenchymal stem cells provide localized neuroprotection in an inflammation-driven rat model of Parkinson's disease. *Neuroscience* **303**, 402–411 (2015).

(35)   Haider, H. K., Jiang, S., Idris, N. M. & Ashraf, M. Cellular Biology IGF-1-Overexpressing Mesenchymal Stem Cells Accelerate Bone Marrow Stem Cell Mobilization via Paracrine Activation of SDF-1/CXCR4 Signaling to Promote Myocardial Repair. (2008). doi:10.1161/CIRCRESAHA.108.186742

(36)   Hunt, L. C. & White, J. The Role of Leukemia Inhibitory Factor Receptor Signaling in Skeletal Muscle Growth, Injury and Disease. in *Growth Factors and Cytokines in Skeletal Muscle Development, Growth, Regeneration and Disease* (eds. White, J. & Smythe, G.) 45–59 (Springer International Publishing, 2016). doi:10.1007/978-3-319-27511-6_3

(37)   Sideris, E. *et al.* Particle Hydrogels Based on Hyaluronic Acid Building Blocks. *ACS Biomater. Sci. Eng.* **2**, 2034–2041 (2016).

(38)   Scott, E. A., Nichols, M. D., Kuntz-Willits, R. & Elbert, D. L. Modular scaffolds assembled around living cells using poly(ethylene glycol) microspheres with macroporation via a non-cytotoxic porogen. *Acta Biomater.* **6**, 29–38 (2010).

(39)   Roam, J. L. *et al.* A modular, plasmin-sensitive, clickable poly(ethylene glycol)-heparin-laminin microsphere system for establishing growth factor gradients in nerve guidance conduits. *Biomaterials* **72**, 112–124 (2015).

(40)   Truong, N. F. *et al.* Microporous annealed particle hydrogel stiffness, void space size, and adhesion properties impact cell proliferation, cell spreading, and gene transfer. *Acta Biomater.* **94**, 160–172 (2019).

(41)   Griffin, D. R., Weaver, W. M., Scumpia, P. O., Di Carlo, D. & Segura, T. Accelerated wound healing by injectable microporous gel scaffolds assembled from annealed building blocks. *Nat. Mater.* (2015). doi:10.1038/nmat4294

(42)   Imparato, G., Urciuolo, F., Casale, C. & Netti, P. A. The role of microscaffold properties in controlling the collagen assembly in 3D dermis equivalent using modular tissue engineering. *Biomaterials* **34**, 7851–7861 (2013).

(43)   Koh, J. *et al.* Enhanced In Vivo Delivery of Stem Cells using Microporous Annealed Particle Scaffolds. *Small* 1903147 (2019). doi:10.1002/smll.201903147

(44)   Yao, M.-H. *et al.* Directed self-assembly of polypeptide-engineered physical microgels for building porous cell-laden hydrogels. *Chem. Commun. (Camb).* **50**, 9405–8 (2014).

(45)   Kim, J., Li, W. A., Sands, W. & Mooney, D. J. Effect of pore structure of macroporous poly(lactide-co-glycolide) scaffolds on the in vivo enrichment of dendritic cells. *ACS Appl. Mater. Interfaces* **6**, 8505–8512 (2014).

(46)   Chen, R., Ma, H., Zhang, L. & Bryers, J. D. Precision-porous templated scaffolds of varying pore size drive dendritic cell activation. *Biotechnol. Bioeng.* **115**, 1086–1095 (2018).

(47) Vissers, C. A. B., Harvestine, J. N. & Leach, J. K. Pore size regulates mesenchymal stem cell response to Bioglass-loaded composite scaffolds. *J. Mater. Chem. B* **3**, 8650–8658 (2015).

(48) Qazi, T. H. *et al.* Extrusion Printed Sca ff olds with Varying Pore Size As Modulators of MSC Angiogenic Paracrine E ff ects. (2019). doi:10.1021/acsbiomaterials.9b00843

(49) Mao, A. S. *et al.* Programmable microencapsulation for enhanced mesenchymal stem cell persistence and immunomodulation. doi:10.1073/pnas.1819415116

(50) Hass, R., Kasper, C., Böhm, S. & Jacobs, R. Different populations and sources of human mesenchymal stem cells (MSC): A comparison of adult and neonatal tissue-derived MSC. *Cell Commun. Signal.* **9**, (2011).

(51) Pires, A. O. *et al.* Unveiling the Differences of Secretome of Human Bone Marrow Mesenchymal Stem Cells, Adipose Tissue-Derived Stem Cells, and Human Umbilical Cord Perivascular Cells: A Proteomic Analysis. *Stem Cells Dev.* **25**, 1073–1083 (2016).

Chapter 5

Evaluation of the efficacy of rMSC laden porous granular scaffolds to direct bone regeneration in critical sized rat calvarial defects

---

5.1 Abstract

Critical sized bone defects often result in delayed or non-union healing. Delivery of mesenchymal stromal cells (MSCs) can improve bone regeneration; but MSCs injected into defect sites without a carrier are not retained for more than a few hours. While delivery of MSCs encapsulated in bulk hydrogels can improve *in vivo* retention times, bulk encapsulation does not promote MSC secreted factors, which can signal to exogenous cells and spur bone deposition. In this study, we tested the bone regeneration capacity of rMSC laden porous granular scaffolds engineered to elevate secretory properties, both through pore-directed cell clustering and through the inclusion of an N-cadherin mimic peptide, HAVDI. rMSCs were cultured in microgel scaffolds with average pore lengths of ~200 µm that either contained 1 mM RGD (RGD formulations) or 1mM RGD and 1 mM HAVDI (HAVDI formulations). In both formulations, ~ 90% of rMSCs resided in a cluster containing ~45 cells on average, indicating that variations in peptides did not alter rMSC clustering phenotype. However, inclusion of HAVDI inclusion increased secretion of all measured factors from rMSCs; including key growth factors involved in bone regeneration, such as VEGF-A and PDGF-AA, and anti-inflammatory factors known to resolve inflammation, such as IL-4 and IL-13. Upon implantation into 6 mm critical-sized rat calvarial defects, microgel degradation and rMSC retention were monitored using an *in vivo* imaging system (IVIS) over 4 weeks. Neither cellularity nor HAVDI inclusion affected microgel degradation and all formulations were completely degraded over the course of 28 days. However, no differences in

intensity between acellular and rMSC laden microgels was observed, indicating Qdot labeled rMSCs were undetectable *in vivo*. Lastly, no differences in bone volume were observed with microcomputed tomography (µCT) at 4 and 8 weeks between defects with microgel formulations compared to defects without any treatment. Overall, granular scaffolds, both formulated with RGD, HAVDI, or with rMSCs, did not improve bone regeneration in critical sized rat calvarial defects. However, further research is needed to determine if rMSCs survived and if their secretory properties were in fact elevated *in vivo*.

5.2   Introduction

Critical sized craniofacial bone defects, resulting from surgery, traumatic injury, or birth defects, do not heal properly without intervention[1–3]. One study estimated the overall US market for facial bone trauma to be as high as $400 million annually[4]. The current gold stand in craniofacial repair, a bone autograft, can have major limitations including limited availability and donor site pain and morbidity[5–7]. Specifically in the case of critical size defects, large defect sizes and complicated geometries can make it impractical to remove sufficient bone for an autograft[7]. Therefore, researchers have explored regenerative medicine strategies to heal critical sized craniofacial defects[8–10].

When proper fracture healing does not occur, delivery of mesenchymal stem/stromal cells (MSCs) has been used extensively in pre-clinical and clinical settings to aid bone regeneration[10–14]. MSCs are one of the most widely used cell types in clinical trials and can easily be harvested from multiple adult tissue sources, including bone marrow and adipose deposits[15,16]. Historically, MSC multipotent abilities (i.e., their capacity to differentiate into osteoblasts, chondrocytes, and adipocytes) have been exploited for bone tissue engineering applications[8,10,17]. However, recent studies have determined that MSC secreted factors are also critical to their therapeutic

efficacy[11,12,15,18]. For example, in a critical size calvarial defect model in rats, treatment with alginate gels soaked in media conditioned with MSC secreted factors resulted in improved defect closure relative to gels soaked in media without secreted factors[19]. However, factors delivered acellularly will deplete over time. Alternatively, delivering MSCs themselves can result in a consistent stream of newly produced factors. Additionally, MSCs can temporally alter their secretory profile to respond to and aid in the various steps of wound healing.

Intravenous delivery or injection into the injury site of MSCs alone often results in poor survival and retention[20,21]. In many cases, less than 5% of delivered MSCs are present in the defect area mere hours after injection[22]. Some of these limitations can be overcome by using hydrogels to protect MSC and improve retention during delivery[23,24]. Encapsulation in bulk hydrogels, where pores are on the nanoscale and MSC reside as single cells, can increase MSC retention in the injured area from hours to weeks[24]. However, bulk encapsulation of MSCs does not promote their secretory properties[25].

Several groups have demonstrated that MSCs cultured in biomaterials with pore sizes on the microscale, where cells physically interact with each other, directly elevate their secretory properties[25–27]. Specifically, MSCs clustered together show increased N-cadherin expression and elevated global cytokine and growth factor secretion[25,27]. Additionally, N-cadherin mimicking peptides, such as HAVDI, can further enhance hMSCs secretory properties, in both clustered and single cell conditions[27]. We sought to explore the use of these material systems for bone tissue engineering applications.

This study focused on one central question: Can materials designed to elevate rMSC secretome sufficiently drive bone regeneration in a critical sized rat calvarial defect? To test this hypothesis, we utilized a granular hydrogel scaffold based on micron-sized PEG microspheres,

called microgels, to create a porous cell-laden scaffold. We designed degradable microgel scaffolds with pore dimensions optimized to promote MSC clustering, which directly elevated human MSC secretory properties through N-cadherin mediated cell-cell contacts. Additionally, we included an N-cadherin mimic peptide, HAVDI, to further elevate MSC secreted factors. We implanted these materials with rMSCs and acellular controls into 6 mm critical size rat calvarial defects and monitored microgel degradation and rMSC retention with an *in vivo* imaging system (IVIS). Lastly, bone regeneration was visualized using micro-computed tomography imaging (μCT) and histology. Overall, we hypothesized that microgel formulations designed to promote rMSC secretory properties, both through pore-directed cell clustering and the inclusion of an N-cadherin mimic peptide, would improve healing and direct bone regeneration in a critical sized calvarial defect.

5.3   Materials and methods

5.3.1   rMSC isolation and culture

rMSCs were isolated from bone marrow biopsies of 14-week-old female Sprague Dawley rats. Briefly, rMSCs were isolated from the femurs and humeri of 8 rats. After euthanasia, the ends of the long bone were cut, and their internal cavities were flushed with PBS. The bone marrow mixture was plated onto tissue culture plastic in media comprised of alpha modified Eagle medium (alpha-MEM) with nucleosides supplemented with 50 μg/mL penicillin, 50 μg/mL streptomycin, and 1 μg/mL fungizone, and 10% (vol/vol) fetal bovine serum (FBS). After 24 hours, the plates were washed with fresh media and the attached rMSCs were left to proliferate for an additional 10 days, with media changes occurring everything 3 days. P1 rMSCs were frozen down in 80% FBS with 20% DMSO. All experiments used P2 rMSCs.

5.3.2   Macromer synthesis and microgel scaffold fabrication

Multi-arm poly (ethylene glycol) (PEG) polymers, specifically 8-arm 20kDa PEG alcohol and 4-arm 10kDa PEG amine (Jenkem) were used to make PEG- dibenzocylcooctyne (DBCO) and PEG-azide (PEG-N$_3$), respectively. C6-DBCO-acid was purchased from Click Chemistry Tools. PEG-DBCO was synthesized via an esterification reaction using N-(3-Dimethylaminopropyl)-N′-ethylcarbodiimide hydrochloride (EDC, Sigma) and 4-Dimethylaminopyridine (DMAP, Sigma) overnight under argon in anhydrous dichloromethane (DCM) at RT. The resulting mixture was precipitated in cold diethyl ether, centrifuged, washed, and dried. The solid was dissolved in water, dialyzed against water for 3 days, frozen, and lyophilized. The resulting ester linked PEG-DBCO is susceptible to hydrolysis and cell secreted esterases. End-group functionalization was confirmed by ^{1}H NMR to be >85%.

4-arm PEG-azide was prepared in a two-step synthesis. First a 4-arm PEG-mesylate was synthesized in by adding triethylamine and methanesulfonyl chloride sequentially to dissolved PEG-amine in DCM and stirred overnight at RT. The next day, the reaction was diluted with DCM, washed with brine, and the organic phase dried with sodium sulfate, filtered over sand and celite, and concentrated under vacuum. The concentrated oil was precipitated into diethyl ether on ice and washed. The resulting tetra-arm PEG-mesylate was reacted with sodium azide in anhydrous DMF at 60°C for 2 days. The solution containing tetra-arm PEG-azide was dialyzed against water and lyophilized. Complete disappearance of end-group mesyl protons on ^{1}H NMR was interpreted as quantitative conversion of tetra-PEG-mesylate to tetra-PEG-azide.

An azide modified lysine analog (Fmoc-azide-L-lysine, ChemImpex) was used to synthesize an azide-labeled RGD (N$_3$-KGRGDS) and HAVDI (N$_3$-KGHAVDI) peptides using standard Fmoc chemistry and a Rink Amide MBHA resin (Chempep Inc, USA) on a Protein Technologies

Tribute Peptide Synthesizer. The peptides were purified using reverse phase High Pressure Liquid Chromatography (HPLC) and confirmed using Electrospray Ionization (ESI) mass spectroscopy.

Individual microgels were synthesized as previously described[27]. Briefly, individual microgels were created using an inverse suspension polymerization under shear (magnetic stirring) with PEG-DBCO and PEG-N_3 macromers in hexanes with Span-80 (2.25% v/v) and Tween-20 (0.75% v/v). Two distinct sets of microgels, with diameters of ~200 μm, one with excess DBCO and the other with excess azide, were prepared with 11mM excess of either functional group to allow for subsequent scaffold assembly. 1mM of N_3-GRGDS was included in all microgels, and 1mM of N_3-GRGDS and 1 mM of HAVDI were included in the HAVDI microgels. Microgels used for *in vivo* degradation experiments were labelled with 40mM azide-modified 680 nm dye (LICOR). Microgels were washed with 100% isopropanol (IPA) (4x) and placed on a shaker overnight in IPA in 15 mL conical tubes. For *in vivo* experiments, the microgels were shipped in IPA at RT to Amherst. Upon arrival, they were stored at -80°C until use. For *in vitro* use, they were used the next day without storage in the freezer.

5.3.3 rMSC microgel encapsulation

After equilibrating the conical tubes containing microgels in IPA to RT, a probe sonicator was used to break up any aggregates of microgels. The microgels were washed again with 100% IPA, centrifuged, and then washed twice with sterile PBS in a biosafety cabinet. To create rMSC-laden microgel scaffolds, 6 million rMSCs, were mixed with DBCO-excess and N_3-excess microgels (~100 μL polymer mix each) swollen in PBS. The suspension was then centrifuged at 1000 rcf for 10 minutes, followed by 3000 rcf for 3 minutes in a syringe mold (~10mm in diameter). After centrifugation, scaffolds were removed from the mold, stamped using a 6 mm biopsy punch, and immediately placed in rMSC media. This procedure created scaffolds

that were ~1-2 mm thick and 6 mm in diameter with rMSCs at a density of 10 million cells/mL or 1.5 million cells/ scaffold. After three days in media, the scaffolds were implanted into the bone defects or used for *in vitro* experiments.

For *in vivo* experiments, rMSCs were labelled with Qdot 800 before encapsulation (Qtracker Kit, Thermo Fisher) according to the manufacturer's protocols. Briefly, 15 mM of the Qdot 800 working solution was prepared and 0.2 mL of the solution was placed on a T-75 flask of ~70% confluent rMSCs for 1 hour at 37°C. The plate was washed twice with media.

5.3.4   Cluster analysis

After three days of culture, rMSC laden microgel scaffolds were fixed for 30 min with 10% formalin. Next, samples were washed with PBS 3x for 10 min each. Permeabilization and blocking were performed each for 1 hour at RT in 0.1% TritonX-100 in PBS and 5% bovine serum albumin (BSA) in PBS, respectively. Samples were incubated with DAPI (1:500) and HCS cell mask Orange (1:5000) for 1 hour at RT. Samples were washed with PBST 3x for 10 min each. Approximately 80-100 µm z-stack images (with <1 µm intervals between slices) were acquired using a Nikon Spinning Disc Confocal (40x air objective).

Cluster size and percent of cells in cluster were determined using IMARIS 3D visualization software (Bitplane). First, a 3D surface around a cluster was created using the cell mask stain. Next, the nuclei were marked using DAPI staining and the Spot Analysis feature of IMARIS. Using a pre-written Matlab code (Split into Surface Objects Xtension) within the IMARIS software, the number of nuclei within each cluster (defined as >3 nuclei) was determined.

5.3.5   Secretory Analysis

Secreted factors from rMSCs in RGD gels and HAVDI gels were measured using a Rat Cytokine Array C2 (RayBiotech). First, arrays were blocked for 30 min at RT. 1 mL of media pooled from 3 gels of each condition was incubated on arrays overnight at 4°C. The next day, the membranes were washed, incubated with a biotinylated antibody cocktail for 1.5 hours at RT, washed again, and then incubated with HRP-streptavidin for 2 hours at RT. Chemiluminescence signal from the membranes was detected using a charge-coupled device camera (ImageQuant LAS 4000 GE Healthcare). Analysis was performed using the manufacture's guidance (Raybiotech). Spot intensity values from raw images were determined using the 2D Array feature of ImageQuant (GE Healthcare). The background signal was subtracted, and average intensities were normalized first to positive spot controls on each array and then control (blank media) arrays. Additionally, the intensity values were normalized to ng DNA as determined by Quant-it Picogreen (Thermo Fisher).

5.3.6 Critical sized calvarial defect surgery

A 6 mm calvarial defect was created in 11-week-old female Sprague Dawley rats. Animals received subcutaneous injections of buprenorphine hydrochloride (0.05mg/kg) as an analgesic, cefazolin (20 mg/kg) as an antibiotic, and saline (5mL/kg) to account for fluid loss, at least 30 minutes prior to surgery. The rats were anesthetized via isoflurane inhalation, to effect (2.5%-3.5%). This was maintained via nose cone during the entire procedure. A 1 cm midline incision was made through the skin and periosteum along the sagittal suture. The periosteum was then laterally contracted to expose the calvarium. The 6 mm circular defects were made on the lateral ridge about 5 mm below the ear using a trephine operating at 1500 RPM attached to a dental drill (Saeyang KRAFIT Ki-20 Dental Implant Motor) under room temperature saline irrigation. Qdot-labelled rMSC-laden microgels or acellular controls were placed in the defects. 7 rats were used

for each condition (RGD, HAVDI, RGD+rMSCs, HAVDI+rMSCs). An empty defect control (n=7 rats) was also included. The periosteum and skin were sutured closed using 4-0 maxon sutures and wound clip staples were placed over the incision. Subcutaneous injections of buprenoprhine hydrochloride (0.05 mg/kg) were administered 12-, 24-, and 36-hours post operation as a post-analgesic.

5.3.7   IVIS imaging

To monitor rMSC retention and microgel degradation, live in vivo imaging was performed using an IVIS Spectrum CT (Perkin Elmer, Waltham, MA) on days 1, 4, 7, 10, 14, 21, and 28 post surgery. Before imaging, rats were anesthetized via isoflurane inhalation, to effect (2.5%-3.5%). For each image acquisition, a gray scale body surface image was collected, followed by an overlay of the fluorescence channels. For Qdots detection, excitation at 430 nm and emission at 800 nm was measured. For the microgel detection, excitation at 675 nm and emission at 720 nm was measured.   The average radiant efficiency ($[p/s/cm/sr]/ [\mu W/cm^2]$) was quantified using LivingImage software (Perkin Elmer, Waltham, MA).

5.3.8   Microcomputed tomography measurement (μCT)

Bone formation was analyzed by a microcomputed tomography (μCT) imaging system (Bruker SkyScan 1276) at 4 and 8 weeks after surgery. Before and during imaging, rats were anesthetized with 2.5% isoflurane. The skulls were scanned (60 kV, 125μA, 539ms exposure time) with a voxel size of 40 µm and a 1 mm aluminum filter. Images were collected every 0.8º for 360º. The selected region of interest was constrained to the height of the native bone (Figure 5.5). μCT images were reconstructed using NRecon, with a dynamic range of 0 to 0.052639, a beam hardening of 30%, a Gaussian smoothing of 2, and a ring correction of 10. Images were aligned and saved in the coronal plane using DataViewer and analyzed using CTan. All images were

thresholded from 137-255 on a grayscale of 0-255. This correlates to bone being considered any mineralized tissue >0.644 g HA/cm^3. This helps distinguish heavily mineralized tissue from poorly mineralized tissue.

5.3.9 Histological staining and analysis

For histology analysis, animals were sacrificed at 8 weeks post-surgery. Animals were anesthetized via isoflurane inhalation (3.5%) and then euthanized via cardiac exsanguination. Calvarial segments containing the defect were removed using a high speed Dremel. The segments were fixed in 10% formalin for 72 hours, decalcified in rapid acting formic acid, embedded in paraffin wax, and 5 µm thick sections were obtained from the midline of the defect using a microtome. Samples from at least 7 rats per treatment group were stained with Hematoxylin and Eosin using standard methods. Samples were imaged at 400 x total magnification using a Keyence BZ-X800 light microscope fitted with a Nikon 40x 0.6NA objective. Each imaged sample was scored on a 0-3 grading scale for the presence of bone tissue. A score of 0 indicates no tissue in the defect and score of 3 indicates extensive tissue in the defect. All samples were graded relative to each other. Two separate researchers independently defined the defect boundaries and graded samples for each tissue category. When a discrepancy in grading occurred between the two researchers, samples were looked at together and a single grade was agreed upon.

5.4 Results

5.4.1 Preparation of rMSC laden microgel scaffolds

After centrifugation in a syringe mold, rMSC laden microgel scaffolds were biopsy punched to create scaffolds that are ~1 mm in height and ~ 6 mm in diameter, the approximate size of the calvarial defect (Figure 5.1a, right). In contrast to formulations in previous chapters, these microgels were created with an ester linked PEG-DBCO, thereby rendering the scaffolds

degradable, either through cell secreted esterases or through hydrolysis (Figure 5.1a, left). Using

methods developed in Chapter 4, the microgels particles were synthesized under magnetic stirring,

resulting in scaffolds of average pore lengths of ~200 µm (Figure 4.3).
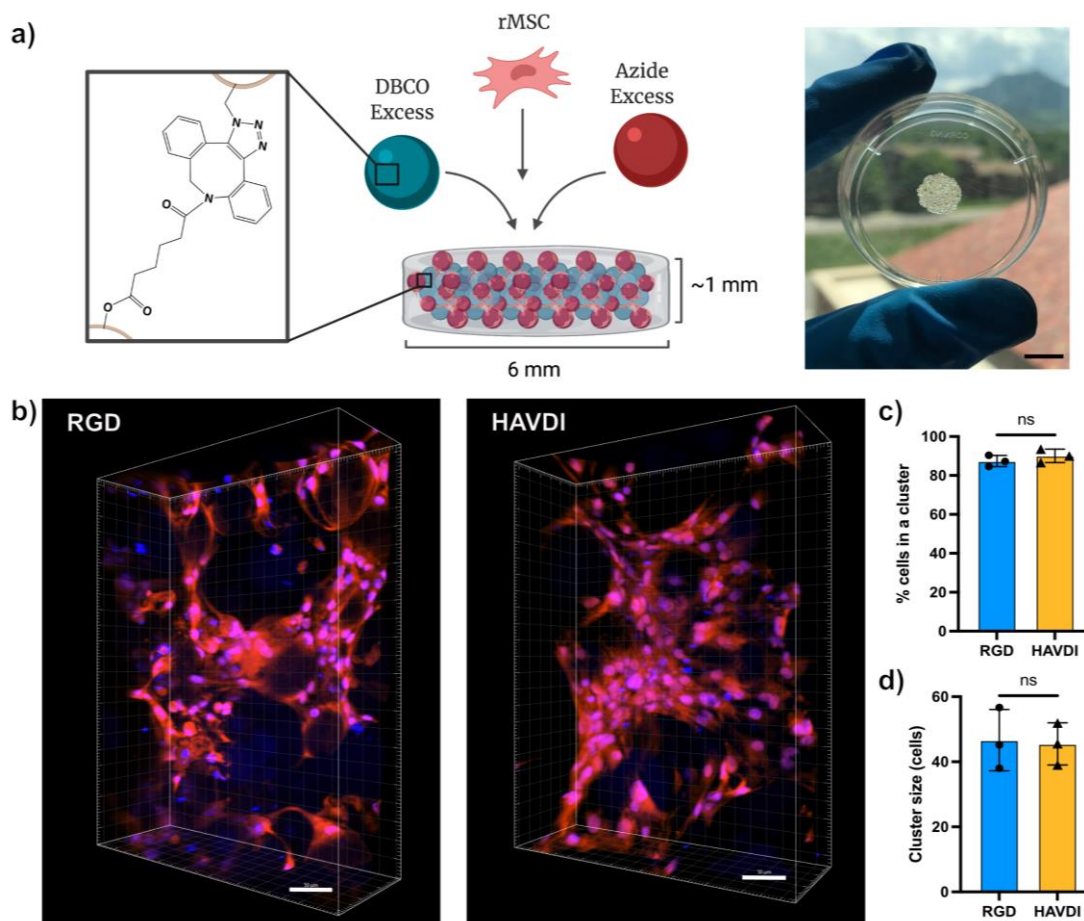
Figure 5.1 Cell clustering analysis of rMSC laden microgel scaffolds.
(a) rMSC were mixed with DBCO excess and azide excess microgels to create cell-laden porous
scaffolds that are covalently bound using SPAAC chemistry. Scaffolds were biopsy punched to
achieve dimension of a calvarial defect (~1mm height, ~ 6mm diameter) Scale bar = 6 mm. (b)
Representative images of rMSCs (10 million cells/mL) in microgel scaffold with RGD (left) and
RGD + HAVDI (right). Nuclei are labelled in blue and cytoplasm is labelled in red. Scale bar =
50 µm. Quantification of percent of cells in a cluster (c) and cells size (d) for rMSCs cultured in
RGD (blue bar, circles) and HAVDI (yellow bar, triangles) for three days. n.s. – not significant.

5.4.2 rMSC clustering is the same in RGD and HAVDI formulations

After three days in culture, we characterized the percent of rMSCs in a cluster and the size of

the cluster, in both HAVDI and RGD containing formulations. We observed similar morphologies

of rMSCs cultured in RGD and HAVDI formulations (Figure 5.1b). Using a 3D rendering software, IMARIS, we quantified the percent of cells present in a cluster (defined as more than 3 cells) (Figure 5.1c). In formulations containing only RGD, 87% ±2.9 % of cells were in a cluster. Cell clustering was not significantly altered in microgel formulations containing both RGD and HAVDI; 90%±3.5 % were present in a cluster. Additionally, the cluster size was not significantly different between RGD and HAVDI formulations (Figure 5.1d). Cluster size was ~47 ± 9 cells and ~45 ± 6 cells for RGD and HAVDI formulations, respectively. Overall, the variation in the peptides would not alter the pore directed cell clustering.

5.4.3   HAVDI inclusion increased concentrations of secreted factors from rMSCs

After confirming that the inclusion of HAVDI does not alter cell clustering phenotypes, we next measured the secretory properties of rMSCs encapsulated in microgel formulations containing only RGD or RGD and HAVDI peptides using a cytokine array (Figure 5.2a). Strikingly, concentrations of almost all measured cytokines were elevated by rMSCs encapsulated in HAVDI microgels (Figure 5.2b). Key factors known to promote bone regeneration, such as PDGF-AA and VEGF-A, were elevated in HAVDI gels. Additionally, anti-inflammatory factors, responsible for resolving inflammation and directing regenerative immune cell populations, such as IL-13, IL-4, and Fas Ligand, were elevated by rMSCs in HAVDI containing microgels relative to rMSCs in microgels containing only RGD. However, IL-10 was not secreted by rMSCs in either RGD or HAVDI formulations, potentially due to the absence of pro-inflammatory cytokines known to be required for IL-10 production from human MSCs[28]. On the other hand, pro-inflammatory cytokines, such as TNF-alpha, IFN-gamma, and IL-1, all known to drive inflammation and inhibit bone regeneration, were also elevated in HAVDI formulations. Overall, global secretion of cytokines was increased by rMSCs in the presence of HAVDI.
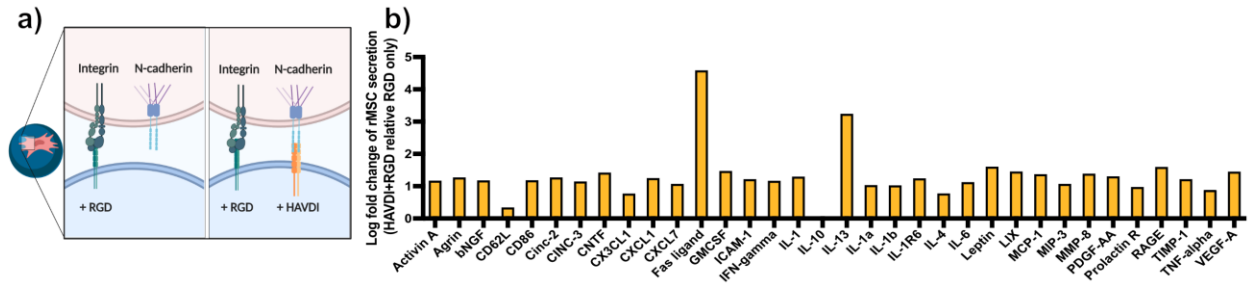
Figure 5.2 Inclusion of HAVDI increased global cytokine secretion by rMSCs.
(a) Microgels containing RGD interact with integrins only. The inclusion of HAVDI allows binding of N-cadherins on the cell surface. (b) Log fold change in secretion of rMSCs cultured in HAVDI gels relative to RGD only gels.

5.4.4 Cellularity did not alter microgel degradation in vivo

As MSC secreted factors are known to influence endogenous cell migration, potentially leading to increased local esterase concentration, we hypothesized that microgel degradation might be expedited in HAVDI+rMSCs formulations. Additionally, as this was the first time microgel scaffolds were implanted into the calvarial defect, it was important to determine the *in vivo* degradation profile. Four microgel conditions, RGD, HAVDI, RGD+rMSCs, and HAVDI+rMSCs, were labelled with an azide functionalized 680 nm fluorescent dye and implanted into a 6 mm rat calvarial defect. Live imaging using a Perkin Elmer IVIS was performed 1, 7, 14, 21, and 28 days after implantation. Representative images show no visible difference between the 4 microgels conditions over time (Figure 5.3a). Quantification of the average radiant efficiency determined that degradation profile follows an exponential decay (Figure 5.3b). All conditions at Day 7, 14, 21, and 28 timepoints were significantly different than Day 1. Days 14, 21, and 28 were significantly different than Day 7. However, no significant difference was present between average radiant efficiencies of all conditions between Day 14, 21, and Day 28 timepoints. In summary, the granular hydrogel scaffolds were completely degraded over the course of 28 days, with the majority of the degradation occurring in the first two weeks. Overall, the cellularity of the scaffolds did not significantly affect *in vivo* microgel scaffold degradation.
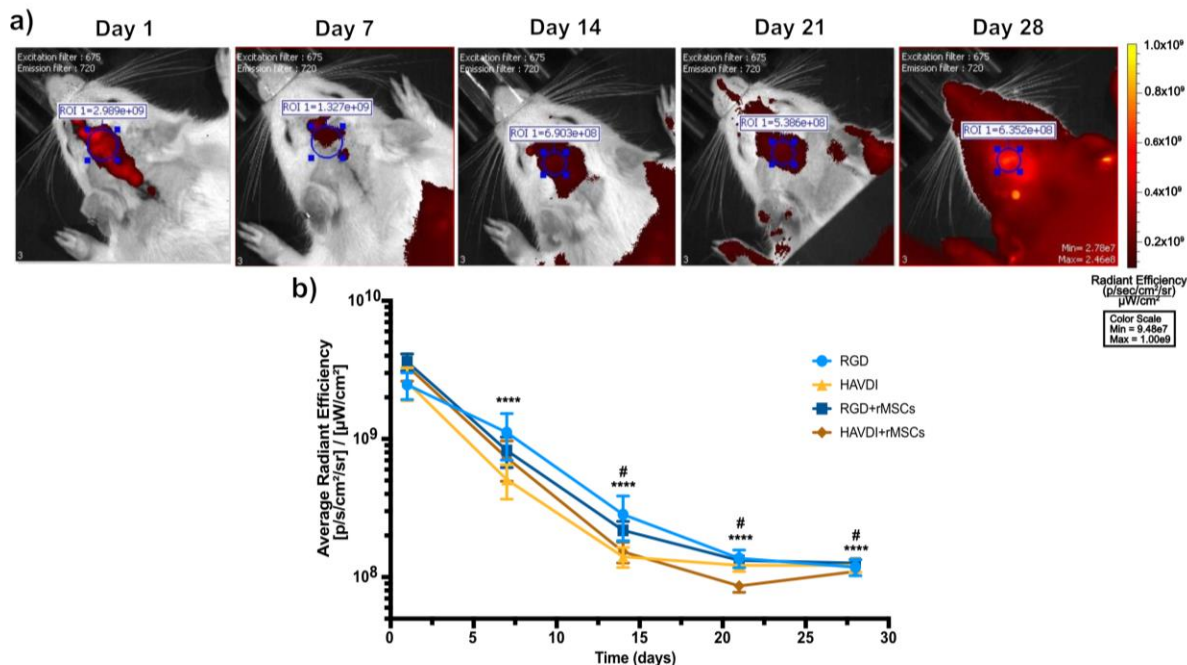
Figure 5.3 In vivo microgel degradation.
(a) Representative IVIS images over time of the 4 conditions (RGD, HAVDI, RGD+rMSCs, and HAVDI+rMSCs). Excitation (675 nm) and emission wavelength (720 nm) were optimized for microgels labelled with 680 nm dye. (b) Average radiant efficiency (([p/s/cm/sr]/ [μW/cm2]) for microgels containing RGD (light blue circle), HAVDI (yellow triangle), RGD+rMSCs (navy square), and HAVDI+rMSCs (brown diamond). n=7 rats for each condition. Error bars represent SEM. Stars represent significance relative to Day 1 and hashtag represent significance relative to Day 7. ****, # p-value <0.0001.

5.4.5   rMSCs were undetectable in vivo

In addition to monitoring microgel degradation, we monitored rMSC retention *in vivo*. We labelled the rMSCs using Qdot 800 and imaged live at 1, 4, 7, 14, 21, and 28 days post-surgery. Before implantation, we confirmed the signal from rMSCs embedded in microgel scaffold (Figure 5.7). However, even after 24 hours after implantation, average radiant efficiency values were not significantly different between acellular microgels or empty defects and rMSC laded microgels (Figure 5.4a). We observed no differences between conditions over time as well (Figure 5.4b). These results may indicate that rMSCs likely did not survive less than 1 day after implantation and might suggest the need to integrate pro-survival or proliferative queues into the scaffold. On the

142

other hand, the Qdot signal may also be too weak for detection, either due to low concentrations of dye or high background signal. Further study needs to be completed to determine the definitive cause for rMSCs not being detected.
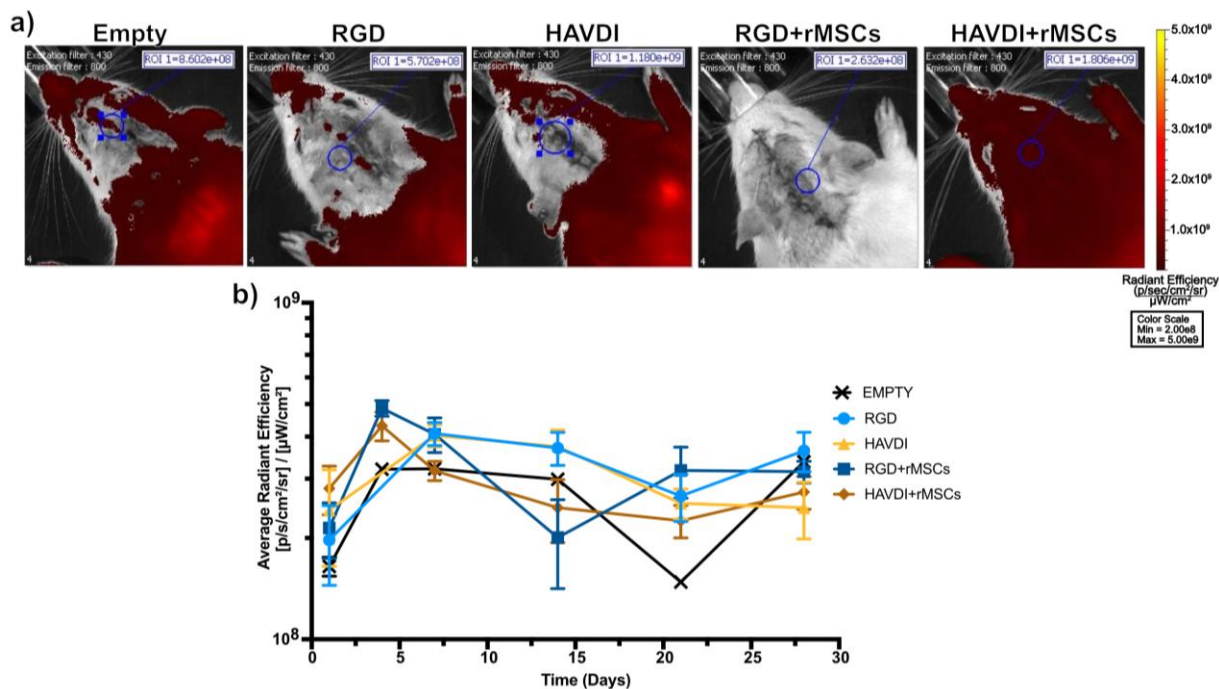
Figure 5.4 IVIS images of rMSCs *in vivo.*
(a) Representative IVIS images of Qdot-labelled rMSCs in microgel conditions (RGD, HAVDI, RGD+rMSCs, and HAVDI+rMSCs) and empty defects 1 day after implantation. Excitation (430 nm) and emission wavelength (800 nm) were optimized for rMSCs labelled with Qdot 800 nm dye. (b) Average radiant efficiency (([p/s/cm/sr]/ [µW/cm2]) for Qdot-labelled rMSCs in microgels containing RGD (light blue circle), HAVDI (yellow triangle), RGD+rMSCs (navy square), and HAVDI+rMSCs (brown diamond). n=7 rats for each condition. Error bars represent SEM.

5.4.6   Microgels scaffolds did not promote mineralized bone formation in vivo

To determine if the microgels promoted bone regeneration *in vivo*, we measured mineralized bone deposition in the calvarial defects using µCT at 4 and 8 weeks after implantation. Representative images taken at 4 and 8 weeks show no bone formation in any of the microgel conditions or empty defect controls (Figure 5.5a). We further quantified common bone regeneration parameters from a large region of interest (ROI), where the height of the ROI was not

constricted to the height of the surrounding native bone (Figure 5.6). No significant differences in percent of tissue mineral density was measured for any of the microgel conditions relative to the empty defect control (Figure 5.5b). Similarly, no significant differences were present in bone mineral density or bone volume (Figure 5.5c,d).
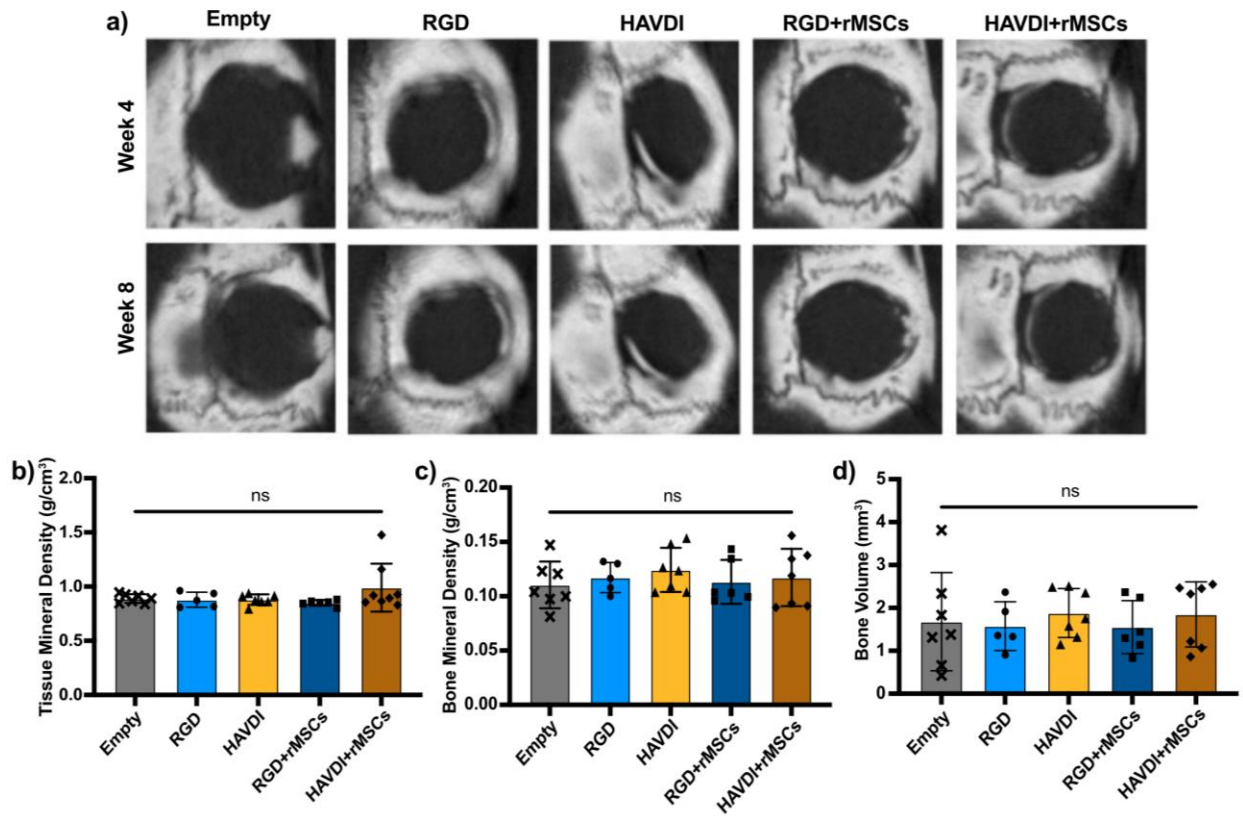
Figure 5.5 µCT analysis of microgels in critical sized rat calvarial defects.
(a) Representative µCT images of microgel formulations containing RGD, HAVDI, RGD+rMSCs, and HAVDI+rMSCs at 4 and 8 weeks post implantation. (b) Percent of bone volume to total volume (%BV/TV), (c) bone mineral density (g/cm^3), and (d) bone volume (mm^3) in the defect area (defect height restricted to the height of the surrounding native bone). ns – not significant.

5.4.7 Histological analysis

Lastly, we performed histological staining of decalcified slices from gels explanted 8 weeks in the calvarial defect. Sections stained with hematoxylin and eosin were scored on a 0-3 grading scale for the presence of bone in the detect area. Representative images are shown for a score of 0 (no bone tissue) and score of 3 (extensive bone tissue) (Figure 5.6a). Blue bars indicate areas of

bone tissue. Confirming the µCT data, we did not observe any significant bone formation in any

of the conditions relative to the empty defect (Figure 5.6b).
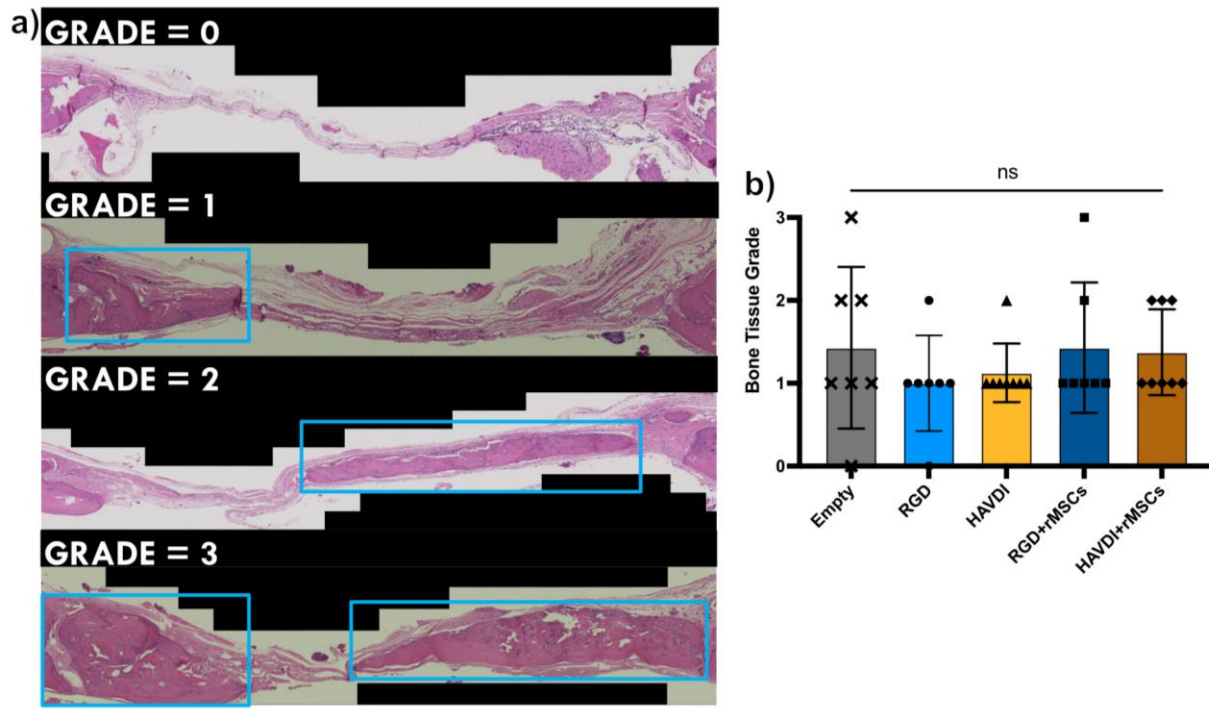
Figure 5.6 Histological analysis of bone tissue in calvarial defect at 8 weeks.
(a) Representative images for grading the extent of bone tissue at 400x total magnification. A score
of 0 indicates no tissue in the defect and score of 3 indicates extensive tissue in the defect. Blue
bars indicate areas of bone tissue. (b) Quantification of bone tissue grade. ns – not significant.

5.5   Discussion

In this study, we tested whether porous microgel scaffolds engineered to increase rMSC

secretory properties could promote bone regeneration in critical sized rat calvarial defects. RGD

was included to ensure cell adhesion and inhibit anoikis, while HAVDI was included to elevate

rMSC secretory properties. The majority of rMSCs (~90%) cultured in scaffolds with pore lengths

of ~200 µm resided in clusters with ~45 cells on average (Figure 5.1). The percent of cells in a

cluster and the cluster size was not affected but HAVDI peptide inclusion. However, HAVDI

inclusion elevated the concentrations of all measured secreted factors from rMSCs, including

factors that promote vascularization (VEGF-A), increase proliferation (PDGF-AA), and reduce

inflammation (IL-13, Fas Ligand) (Figure 5.2). Next, we implanted scaffolds designed (i) to elevate rMSC secretion (HAVDI+rMSCs), (ii) to provide a cellular control (RGD+rMSCs), (iii) to control for HAVDI effects on endogenous cells (HAVDI), and (iv) to provide an acellular control (RGD) in 6 mm rat calvarial defects. In addition to monitoring bone regeneration using μCT, we monitored rMSC retention and microgel degradation using IVIS. We chose to label rMSCs with Qdot 800 as quantum dots are relatively low cost, have high photostability, and are commercially available with optimized protocols to label millions of cells within hours. Microgels were labelled by incorporating an azide functionalized Alexafluor 680 nm dye. We hypothesized that microgel degradation might be increased in HAVDI+rMSC formulations as high concentrations of MSC secreted factors may drive cell infiltration causing increases in local esterase activity. However, the rMSCs were not detected *in vivo* (Figure 5.4) and HAVDI inclusion and cellularity did not influence microgel degradation and all formulations were degraded at 28 days (Figure 5.3). We additionally hypothesized that HAVDI+rMSC formulations would improve bone healing as increased secreted factors would promote cell infiltration, reduce inflammation, and direct endogenous osteogenic progenitors and osteoblasts. Unfortunately, bone formation (Figure 5.5, 5.6) was not observed any of the formulations.

To understand if the central hypothesis of this study was adequately tested, we must first determine if delivered rMSCs survived *in vivo*. There are several potential reasons rMSCs were undetectable with IVIS. First, the concentrations of Qdots in the microgel scaffolds might have been too low. However, as evidenced by Figure 5.7, the IVIS detected rMSCs with settings optimized for Qdot 800 detection (excitation 430 nm, emission 800 nm) *in vitro* before implantation, indicating that the Qdot concentration in the scaffold was sufficient for IVIS detection. Next, the interference from the animal itself may have been too high to detect the Qdots

in vivo. While the emission wavelengths of the Qdots are optimal for *in vivo* detection (near infrared wavelengths at 800 nm), the excitation wavelength used, 430 nm, is also highly absorbed by blood and fat[29]. Tissue absorption may have limited the excitation of the Qdots, rendering the rMSCs undetectable. However, the microgels are implanted underneath ~2mm skin on the skull, where blood and fat interference should be minimal. Another possibility is the sensitivity of the IVIS itself. While the IVIS is advantageous for longitudinal studies, the lasers and hardware are not as powerful as other microscopes. Additionally, the resolution of the IVIS may be too low to detect Qdots if they become too diffuse. Lastly, the rMSCs could have died before the first imaging timepoint (24 hours), allowing the Qdots to diffuse out of the defect and, therefore, the imaging region. However, based on the compounding interferences aforementioned; it is not possible to definitively conclude that rMSC death occurred.

Indeed, the immediate next step is to perform a short-term study to analyze rMSC survival. We aim to alter the imaging methods and fluorescent dyes used to detect and label delivered rMSCs. First, modifying the imaging would be a simple solution while still utilizing the Qdots to label the rMSCs. Confocal microscopes provide greater excitation laser power, have increased resolution, and reduced background in 3D samples. For *in vivo* applications, the calvarial defect can be opened and covered with a glass coverslip during confocal imaging. Imaging rats short time points after implantation (8 hours, 16 hours, 24 hours, 48 hours) would determine if the Qdot-labelled rMSCs survived.

If modifications to the imaging machinery are unable to detect the Qdots, rMSCs can be genetically modified to constitutively produce a near infrared fluorescent protein, either through the transfection or transduction of a plasmid or through CRISPR modifications. Out of these three methods, viral transduction has several key advantages making it most suitable. In contrast to

CRISPR, viral transduction of an IR fluorescent protein relies on commercially available plasmids and toolkits utilizing relatively simple protocols requiring minimal optimization. Additionally, as these studies typically require many millions rMSCs, the incorporation of the plasmid into the cell genome, achieved through viral transduction, would allow rMSCs to pass the genetic information to their daughter cells. Alternatively, we could isolate rMSCs from transgenic rats, engineered to produce a fluorescent protein or luciferase. Unfortunately, these rats are difficult to commercially obtain.

Regardless of rMSC survival, the results clearly indicate that delivery of the acellular microgel formulations, with or without HAVDI, is not sufficient to spur bone regeneration. There are several ways the microgels could be improved to promote bone regeneration, including incorporation of cell-instructive factors, such as growth factors or anti-inflammatory factors, or incorporation of inorganic components to act as nucleation sites for matrix mineralization. The microgel system is advantageous for delivery of multiple factors, as various populations of microgels loaded with proteins can be synthesized independently and combined in precise ratios with unmodified gels to achieve independent release profiles without impacting the structural properties of the scaffold. Firstly, we could incorporate factors, such as FGF, to improve rMSC proliferation. Additionally, due to the highly porous nature of these scaffolds, we anticipate unimpeded cell infiltration, both of osteoblast progenitors and immune cells. Therefore, we could modify microgel scaffolds with known bone promoting factors, such as BMP-2 or TGF-beta, to drive osteoblastic differentiation and matrix deposition. Alternatively, we could include anti-inflammatory factors, such as IL-4 or IL-10, to resolve inflammation and promote regenerative immune cell polarizations. Lastly, instead of delivering factors to direct endogenous cell behavior, we can directly promote mineralization by incorporating bioactive inorganic components. For

example, calcium phosphate particles, such as of hydroxyapatite or beta-tricalcium phosphate, can act as nucleation points for mineralization of matrix deposited by osteoblasts.

5.6   Conclusions

Hydrogels formulated to deliver MSCs and improve their secretory properties could aid bone regeneration in critical sized craniofacial defects. In this study, we implanted rMSC laden porous microgel scaffolds engineered to elevated rMSC secretory properties, both through pore-directed cell clustering and N-cadherin peptide inclusion, into critical sized rat calvarial defects. Overall, current microgels formulations, either modified with HAVDI or rMSCs, did not promote bone regeneration over the course of the 8-week study. However, as rMSCs were undetected *in vivo*, further experiments need to be conducted to fully understand if how microgel scaffolds need to be modified for future studies.

5.7   Supplemental Information
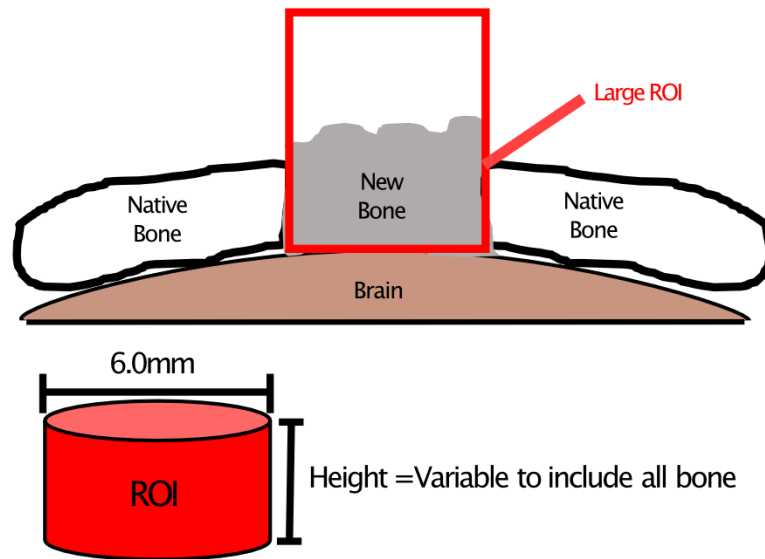
Figure 5.7 Schematic of the region on interest used to define the bone defect and determine parameters in Figure 5.5.
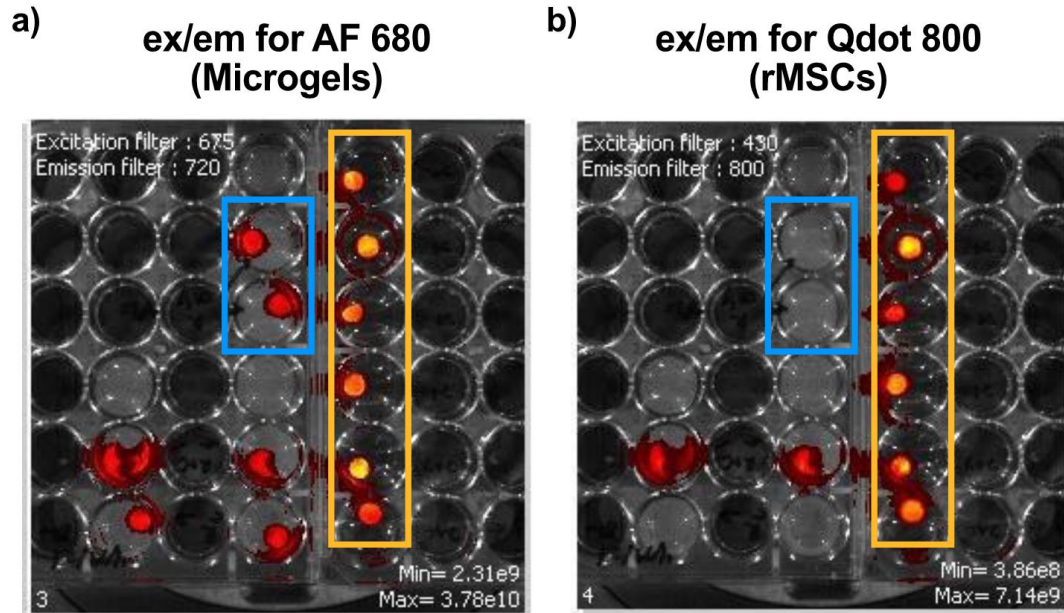
Figure 5.8 In vitro IVIS imaging of Qdot-labelled rMSCs in microgel scaffolds before implantation.
(a) Imaging with excitation (675 nm) and emission (720 nm) wavelengths optimized for Alexaflour (AF) 680 nm labelled microgels. Gels in the blue rectangles are acellular and the gels in the yellow rectangles have rMSCs. (b) Imaging with excitation (430 nm) and emission (800 nm) wavelengths optimized for Qdot 800 nm present in rMSCs. The acellular gels (blue rectangles) do not have any signal in with these imaging parameters.

5.8 References

(1) Harris, A. M.; Althausen, P. L.; Kellam, J.; Bosse, M. J.; Castillo, R. Complications Following Limb-Threatening Lower Extremity Trauma. *Journal of Orthopaedic Trauma* **2009**, *23* (1), 1–6. https://doi.org/10.1097/BOT.0B013E31818E43DD.

(2) Karladani, A. H.; Granhed, J.; Kärrholm, J.; Styf, J. The Influence of Fracture Etiology and Type on Fracture Healing: A Review of 104 Consecutive Tibial Shaft Fractures. *Archives of orthopaedic and trauma surgery* **2001**, *121* (6), 325–328. https://doi.org/10.1007/S004020000252.

(3) Bernabé, P. F. E.; Melo, L. G. N.; Cintra, L. T. A.; Gomes-Filho, J. E.; Dezan, E.; Nagata, M. J. H. Bone Healing in Critical-Size Defects Treated with Either Bone Graft, Membrane,

or a Combination of Both Materials: A Histological and Histometric Study in Rat Tibiae. *Clinical Oral Implants Research* **2012**. https://doi.org/10.1111/j.1600-0501.2011.02166.x.

(4)   Frost; Sullivan. *U.S. Trauma Fixation Markets*; 2008.

(5)   Damien, C. J.; Parsons, J. R. Bone Graft and Bone Graft Substitutes: A Review of Current Technology and Applications. *Journal of applied biomaterials : an official journal of the Society for Biomaterials* **1991**, *2* (3), 187–208. https://doi.org/10.1002/JAB.770020307.

(6)   Coventry, M. B.; Tapper, E. Pelvic Instability: Aconsequence of Removing Iliac Bone for Grafting. . *The Journal of Joint and Bone Surgery* **1972**.

(7)   Wojda, S. J.; Donahue, S. W. Parathyroid Hormone for Bone Regeneration. *Journal of Orthopaedic Research* **2018**. https://doi.org/10.1002/jor.24075.

(8)   Meijer, G. J.; Bruijn, J. D. de; Koole, R.; Blitterswijk, C. A. van. Cell-Based Bone Tissue Engineering. *PLOS Medicine* **2007**, *4* (2), e9. https://doi.org/10.1371/JOURNAL.PMED.0040009.

(9)   Bhumiratana, S.; Bernhard, J. C.; Alfi, D. M.; Yeager, K.; Eton, R. E.; Bova, J.; Shah, F.; Gimble, J. M.; Lopez, M. J.; Eisig, S. B.; Vunjak-Novakovic, G. Tissue-Engineered Autologous Grafts for Facial Bone Reconstruction. *Science translational medicine* **2016**, *8* (343), 343ra83. https://doi.org/10.1126/SCITRANSLMED.AAD5904.

(10)   Murphy, M. P.; Quarto, N.; Longaker, M. T.; Wan, D. C. Calvarial Defects: Cell-Based Reconstructive Strategies in the Murine Model. https://doi.org/10.1089/ten.tec.2017.0230.

(11)   Levy, O.; Kuai, R.; Siren, E. M. J.; Bhere, D.; Milton, Y.; Nissar, N.; de Biasio, M.; Heinelt, M.; Reeve, B.; Abdi, R.; Alturki, M.; Fallatah, M.; Almalik, A.; Alhasan, A. H.; Shah, K.; Karp, J. M. Shattering Barriers toward Clinically Meaningful MSC Therapies. *Science Advances* **2020**, *6*.

(12) Stoddart, M. J.; Salgado, A.; Presen, D. M.; Traweger, A.; Gimona, M.; Redl, H. Mesenchymal Stromal Cell-Based Bone Regeneration Therapies: From Cell Transplantation and Tissue Engineering to Therapeutic Secretomes and Extracellular Vesicles. *Frontiers in Bioengineering and Biotechnology | www.frontiersin.org* **2019**, *1*, 352. https://doi.org/10.3389/fbioe.2019.00352.

(13) Phetfong, J.; Sanvoranart, T.; Nartprayut, K.; Nimsanor, N.; Seenprachawong, K.; Prachayasittikul, V.; Supokawej, A. Osteoporosis: The Current Status of Mesenchymal Stem Cell-Based Therapy. *Cellular & Molecular Biology Letters* **2016**, *21* (1), 12. https://doi.org/10.1186/s11658-016-0013-1.

(14) Antebi, B.; Pelled, G.; Gazit, D. Stem Cell Therapy for Osteoporosis. *Current Osteoporosis Reports* **2014**, *12* (1), 41–47. https://doi.org/10.1007/s11914-013-0184-x.

(15) Wechsler, M. E.; Rao, V. v; Borelli, A. N.; Anseth, K. S. Engineering the MSC Secretome : A Hydrogel Focused Approach. **2021**, *2001948*, 1–17. https://doi.org/10.1002/adhm.202001948.

(16) Dominici, M.; Blanc, K. Le; Mueller, I.; Marini, F. C.; Krause, D. S.; Deans, R. J.; Keating, A.; Prockop, D. J.; Horwitz, E. M. Minimal Criteria for Defining Multipotent Mesenchymal Stromal Cells . The International Society for Cellular Therapy Position Statement. *Cytotherapy* **2006**, *8* (4), 315–317. https://doi.org/10.1080/14653240600855905.

(17) Shang, F.; Yu, Y.; Liu, S.; Ming, L.; Zhang, Y.; Zhou, Z.; Zhao, J.; Jin, Y. Advancing Application of Mesenchymal Stem Cell-Based Bone Tissue Regeneration. *Bioactive Materials*. KeAi Communications Co. March 1, 2021, pp 666–683. https://doi.org/10.1016/j.bioactmat.2020.08.014.

(18) Pittenger, M. F.; Discher, D. E.; Péault, B. M.; Phinney, D. G.; Hare, J. M.; Caplan, A. I. Mesenchymal Stem Cell Perspective: Cell Biology to Clinical Progress. *npj Regenerative Medicine* **2019**, *4* (22). https://doi.org/10.1038/s41536-019-0083-6.

(19) Osugi, M.; Katagiri, W.; Yoshimi, R.; Inukai, T.; Hibi, H.; Ueda, M. Conditioned Media from Mesenchymal Stem Cells Enhanced Bone Regeneration in Rat Calvarial Bone Defects. *Tissue Engineering - Part A* **2012**, *18* (13–14), 1479–1489. https://doi.org/10.1089/ten.tea.2011.0325.

(20) Levit, R. D.; Landázuri, N.; Phelps, E. A.; Brown, M. E.; García, A. J.; Davis, M. E.; Joseph, G.; Long, R.; Safley, S. A.; Suever, J. D.; Lyle, A. N.; Weber, C. J.; Taylor, W. R. Cellular Encapsulation Enhances Cardiac Repair. *Journal of the American Heart Association* **2013**. https://doi.org/10.1161/JAHA.113.000367.

(21) van der Bogt, K. E. A.; Sheikh, A. Y.; Schrepfer, S.; Hoyt, G.; Cao, F.; Ransohoff, K. J.; Swijnenburg, R. J.; Pearl, J.; Lee, A.; Fischbein, M.; Contag, C. H.; Robbins, R. C.; Wu, J. C. Comparison of Different Adult Stem Cell Types for Treatment of Myocardial Ischemia. *Circulation* **2008**. https://doi.org/10.1161/CIRCULATIONAHA.107.759480.

(22) Ishihara, A. Effect of Intra-Medullar and Intra-Venous Infusions of Mesenchymal Stem Cells on Cell Engraftment by In-Vivo Cell Tracking and Osteoinductivity in Rabbit Long Bones: A Pilot Study. *Orthopedic & Muscular System* **2014**. https://doi.org/10.4172/2161-0533.1000172.

(23) Mao, A. S.; Özkale, B.; Shah, N. J.; Vining, K. H.; Descombes, T.; Zhang, L.; Tringides, C. M.; Wong, S.-W.; Shin, J.-W.; Scadden, D. T.; Weitz, D. A.; Mooney, D. J. Programmable Microencapsulation for Enhanced Mesenchymal Stem Cell Persistence and Immunomodulation. https://doi.org/10.1073/pnas.1819415116.

(24) Rustad, K. C.; Wong, V. W.; Sorkin, M.; Glotzbach, J. P.; Major, M. R.; Rajadas, J.; Longaker, M. T.; Gurtner, G. C. Enhancement of Mesenchymal Stem Cell Angiogenic Capacity and Stemness by a Biomimetic Hydrogel Scaffold. *Biomaterials* **2012**, *33* (1), 80–90. https://doi.org/10.1016/j.biomaterials.2011.09.041.

(25) Qazi, T. H.; Mooney, D. J.; Duda, G. N.; Geissler, S. Biomaterials That Promote Cell-Cell Interactions Enhance the Paracrine Function of MSCs. *Biomaterials* **2017**, *140*, 103–114. https://doi.org/10.1016/j.biomaterials.2017.06.019.

(26) Qazi, T. H.; Mooney, D. J.; Duda, G. N.; Geissler, S. Niche-Mimicking Interactions in Peptide-Functionalized 3D Hydrogels Amplify Mesenchymal Stromal Cell Paracrine Effects. *Biomaterials* **2020**, *230*. https://doi.org/10.1016/j.biomaterials.2019.119639.

(27) Caldwell, A. S.; Rao, V. v.; Golden, A. C.; Anseth, K. S. Porous Bio-Click Microgel Scaffolds Control HMSC Interactions and Promote Their Secretory Properties. *Biomaterials* **2020**, *232* (December 2019), 119725. https://doi.org/10.1016/j.biomaterials.2019.119725.

(28) Caldwell, A. S.; Rao, V. v.; Golden, A. C.; Bell, D. J.; Grim, J. C.; Anseth, K. S. Mesenchymal Stem Cell-Inspired Microgel Scaffolds to Control Macrophage Polarization. *Bioengineering and Translational Medicine* **2021**, *6* (2). https://doi.org/10.1002/BTM2.10217/FORMAT/PDF.

(29) Rapp, T. L.; DeForest, C. A. Visible Light-Responsive Dynamic Biomaterials: Going Deeper and Triggering More. *Advanced Healthcare Materials* **2020**, *9* (7), 1901553. https://doi.org/10.1002/ADHM.201901553.

Chapter 6

Granular PEG hydrogels mediate osteoporotic mesenchymal stromal cell clustering and influence their pro-resorptive secretory profiles

Sections prepared for submittion to Acta Biomaterialia, 2021

6.1 Abstract

Postmenopausal osteoporosis, a disorder defined by decreased bone mineral density, is a result of a pro-resorptive bone marrow environment. Bone marrow derived mesenchymal stem/stromal cells (MSCs) secrete factors involved in bone homeostasis, but changes to their secretions during osteoporosis remain understudied. Herein, we examined the secretome of MSCs isolated from ovariectomized rats (OVX rMSCs) as a function of cell-cell interactions. Specifically, we controlled clustering of OVX and SHAM rMSCs by encapsulating them in granular hydrogels synthesized from poly(ethylene glycol) microgels with average diameters of ~10, 100, and 200 µm. We directed both the size of rMSC clusters (single cells to ~30 cells/cluster) and the percentages of cells within clusters (~20-90%). Large clusters of OVX rMSCs had elevated secretory properties compared to the SHAM condition. Further, the secretory profile of large clusters of OVX rMSCs had pro-resorptive bias, with increased concentrations of Activin A, CXCL1, CX3CL1, MCP-1, TIMP1, and TNF-α, compared to SHAM. As this pro-resorptive bias was only observed in large cell clusters, we characterized the expression of several cadherins, mediators of cell-cell contacts. N-cadherin expression was elevated (~4-fold) in OVX relative to SHAM rMSCs, both in clusters and in single cells. Finally, only large cell clusters of OVX rMSCs selectively decreased secretion of TIMP-1 and MCP-1 when N-cadherin interactions were blocked, highlighting the dependence of OVX rMSC secretion on N-cadherin mediated cell-cell

contacts. However, further elucidation of the OVX MSC secretome is needed to realize the full potential of MSC therapies for postmenopausal osteoporosis.

6.2   Introduction

Initiated by estrogen deficiency experienced during menopause, Type 1 or postmenopausal osteoporosis (OP) is a bone disorder that affects tens of millions of women worldwide[1,2]. OP is characterized by decreased bone mineral density, leading to bone fragility and increased fracture risk [3,4]. The loss of bone mass is a result of an imbalanced rate of bone turnover, where the rate of bone resorption outpaces the rate of bone formation. The main cell types involved in the bone turnover processes are osteoclasts, responsible for bone resorption, and osteoblasts, responsible for bone matrix deposition. In OP, the loss of estrogen leads to increased pro-inflammatory signaling, osteoclast fusion, and osteoblast apoptosis, collectively leading to a pro-resorptive bone marrow environment. In addition to lower bone density, bone marrow adiposity is increased in OP.

One key cell type implicated in OP is the bone marrow derived mesenchymal stromal cell (MSC). MSCs are a heterogenous population of multipotent and secretory cells involved in bone homeostasis and fracture healing[5–7]. In healthy environments, a multipotent subset of MSCs differentiate primarily into osteoblasts and to a lesser extent into adipocytes. However, MSCs isolated from osteoporotic environments, specifically from ovariectomized rats (OVX rMSCs), have decreased osteogenic capacity and are biased towards adipogenesis *in vitro*[8,9].

Beyond their differentiation potential, MSCs secrete a variety of factors—including cytokines, growth factors, and chemokines—that influence bone homeostasis and contribute to their therapeutic efficacy. MSCs secrete factors that can direct osteoblast differentiation and matrix deposition, osteoclast fusion and resorption activity, and macrophage and lymphocyte migration

and polarization, all functions that directly impact osteoporosis[6,10]. In addition to being involved in bone homeostasis, MSC secreted factors are used clinically as therapeutics[11–14]. Specifically relevant to bone regeneration, delivery of MSC secreted factors can enhance bone formation in critical sized bone defects[15]. While bone maintenance and fracture repair are known to be impaired in OVX models, less is known about the secretome of OVX rMSCs and how it influences the osteoporotic bone environment.

Prior work has determined that MSC secretory properties are dependent on their culturing context. *Ex vivo* expansion of MSCs using traditional culture substrates (such as tissue culture polystyrene or TCPS) is known to adversely affect their secretory properties[16]. Alternative culture systems have evolved to address this problem. For example, systems that promote MSCs cellular interactions, such as spheroid culture[17,18] and porous scaffolds[16,19], are known to promote MSC secretions, in part through N-cadherin signaling.

Herein, we used porous granular hydrogels to cluster OVX rMSCs and study their secretome. OVX rMSCs were isolated from ovariectomized rats exhibiting osteoporotic bone parameters, including decreased bone mineral density and volume. To control rMSC clustering, poly(ethylene glycol) based granular hydrogel scaffolds were synthesized from micrometer-sized hydrogel spheres (diameters ~10, 100 and 200 μm), termed microgels. Trophic factors secreted from OVX and SHAM control rMSCs were measured as a function of cell clustering and cluster size. In large clusters, we observed differences in secretion of pro-resorptive and anti-osteogenic factors between OVX and SHAM rMSCs, attributed to increased cell-cell contacts. For this reason, we investigated the gene expression of cadherin molecules (facilitators of cell-cell contacts) in OVX and SHAM rMSCs. To determine if cadherin expression was related to changes in the secretory profiles, N-cadherin interactions were blocked in large MSC clusters, and the secreted factors

measured. The results obtained suggest that differences in the OVX rMSC secretory profile are influenced by cadherin expression which may contribute to the overall pro-resorptive nature of the osteoporotic bone environment.

6.3   Materials and methods

6.3.1   Ovariectomy surgery and subsequent trabecular bone characterization

Female Sprague Dawley rats (14 weeks-old) were ovariectomized as previously described[20]. At least 30 minutes prior to surgery, animals received subcutaneous injections of buprenorphine hydrochloride (0.05mg/kg) as an analgesic, cefazolin (20 mg/kg) as an antibiotic, and saline (5mL/kg) to account for fluid loss. The rats were anesthetized via isoflurane inhalation to effect (2.5%-3.5%). An incision was made in the lower back, directly below the ribs. The ovaries were removed. For sham surgery, the ovaries were identified and replaced in the abdominal cavity.

14 weeks after Sprague-Dawley rats underwent an ovariectomy (OVX) or sham (SHAM) surgeries, animals first anesthetized via isoflurane inhalation (3.5%) and then euthanized via cardiac exsanguination. The tibias from 7 rats of each condition were removed, and microcomputed tomography was performed on the trabecular regions (Figure 6.7a). µCT images were reconstructed using NRecon, saved in the DataViewer, and analyzed using CTan. Rats that underwent the OVX surgery (OVX rats) had significantly lower bone mineral density (Figure 6.7b) and bone volume (Figure 6.7c) compared to rats that underwent a sham surgery (SHAM rats). Properties of the trabeculae were also altered. The number of trabeculae per unit length, or trabecular number, was significantly decreased in (Figure 6.7d) and the spacing between individual trabecula was increased in OVX rats (Figure 6.7e). Interestingly, no differences in trabecular thickness was observed, as both SHAM and OVX rats had 0.09 mm thick trabeculae.

6.3.2   OVX rMSC isolation

Post-surgery (14-weeks), rMSCs were isolated from the bone marrow of SHAM and OVX rats (n=7). Briefly, the humerii from each rat was removed, the ends of the bone cut, and the bone marrow flushed with PBS and plated onto tissue culture plastic plates. rMSCs were cultured in alpha modified Eagle medium (alpha-MEM) with nucleosides supplemented with 50 μg/mL penicillin, 50 μg/mL streptomycin, and 1 μg/mL fungizone) containing 10% (vol/vol) fetal bovine serum (FBS). Media was changed every 2-3 days. After 10 days, rMSCs from each individual rat were frozen down in a solution of 80% FBS and 20% DMSO. Passage 1 (P1) rMSCs from individual rats were pooled and frozen at P2 in Cell Freezing Medium (ThermoFisher). All experiments used P3 pooled SHAM and OVX rMSCs.

6.3.3   Macromer synthesis

The synthesis of tetra-arm poly(ethylene glycol) (PEG)-azide and eight-arm PEG-dibenzocyclooctyne (DBCO) was performed according to previously published procedures[21–23]. Briefly, four-arm PEG amine (Mn~10,000 Da, JenKen) was dissolved in cooled dichloromethane (DCM), followed by the sequential addition oftriethylamine and methanesulfonyl chloride. The stirring solution was purged with argon for one hour and kept overnight at room temperature. The reaction was then diluted with DCM and washed with brine. The organic phase was dried, filtered, and concentrated under vacuum. Residual oil was precipitated into diethyl ether, centrifuged, and washed with excess ether to give mesylated PEG. ^{1}H NMR analysis was used to determine end group functionalization. Next, tetra-arm PEG-mesylate and sodium azide were dissolved in anhydrous dimethylformamide (DMF) and stirred for 48 hours at 60°C. The solution was dialyzed against deionized (DI) water (MWCO 3.5 kDa) for seven days and lyophilized. Complete disappearance of end-group mesyl protons on ^{1}H NMR was interpreted as quantitative conversion of tetra-PEG-mesylate to tetra-PEG-azide.

Eight-arm PEG amine (Mn~20,000 Da, JenKem), HATU, and c6-DBCO-acid (Click Chem Tools) were dissolved in DMF. Methylmorpholine was added to this solution and the reaction was left overnight to stir under inert gas. Macromers were precipitated directly into diethyl ether, collected by centrifugation, dialyzed in the dark against DI water (MWCO 8 kDa), and lyophilized.

An azide modified lysine analog (Fmoc-azide-L-lysine, ChemImpex) was used to synthesize an azide-labeled RGD (N$_3$-KGRGDS) using standard Fmoc chemistry and a Rink Amide MBHA resin (Chempep Inc, USA) on a Protein Technologies Tribute Peptide Synthesizer. The peptides were purified using reverse phase High Pressure Liquid Chromatography (HPLC) and confirmed using Electrospray Ionization (ESI) mass spectroscopy.

6.3.4 Microgel scaffold fabrication

Microgels were synthesized as previously described[19]. Briefly, individual microgels were created using an inverse suspension polymerization with PEG-DBCO and PEG-N$_3$ macromers in hexanes with Span-80 (2.25% v/v) and Tween-20 (0.75% v/v). Two distinct sets of microgels, one with excess DBCO and the other with excess azide, were prepared with 11mM excess of either functional group in the polymer mix to allow for subsequent scaffold assembly. For DBCO excess microgels, 3mM of 8 arm 20kDa PEG-DBCO and 3mM of 4 arm 10kDa PEG-Azide were used. For azide excess formulations, 2mM of 8 arm 20kDa PEG-DBCO and 6.5mM of 4 arm 10kDa PEG-Azide. 1mM of N$_3$-GRGDS was included in all microgels. Shear force, either magnetic stirring, vortexing, or sonication respectively, was applied during polymerization to create microgels of various sizes (Figure 6.8). Specifically, stirring resulted in large microgel diameters of 210 µm ± 109 µm (~200 µm), vortexing resulted in medium microgel diameters of 102 µm ± 43 µm (~100 µm), and sonicating resulted in microgel diameters of 14 µm ± 9 µm (~10 µm).

Microgels were washed (under sterile conditions) with isopropanol (4x) and with 2x PBS before resuspension in PBS. Probe sonication was used before resuspension in PBS on occasion to break apart any aggregates. Microgels in PBS were used for rMSC encapsulation.

6.3.5 rMSC encapsulation in granular porous scaffolds

rMSC-laden microgel scaffolds were prepared by suspending cell solutions, either 1 million OVX or SHAM rMSCs, with both microgel populations, DBCO-excess and N_3-excess microgels (~50 µL polymer mix each) swollen in PBS and centrifuging. After centrifugation, scaffolds were immediately placed in rMSC culture media. The swollen scaffolds reached a final swollen volume of ~200µL, and a corresponding density of 5 million cells/ mL. Media was changed 24 hours after encapsulation.

6.3.6 Osteogenic and adipogenic differentiation of OVX and SHAM rMSCs

To confirm the adipogenic bias of rMSCs isolated from OVX rats, SHAM and OVX rMSCs were differentiated into osteogenic and adipogenic lineages using a commercially available kit following the manufacturer's instructions (R&D Systems # SC020). Briefly, rMSCs were seeded on fibronectin coated glass coverslips at a density of 4000 cells/cm^2 and cultured to ~60% and ~100% confluency for osteogenic and adipogenic differentiation conditions, respectively. Media was replaced with osteogenic and adipogenic media formulations (provided from manufacturer) every 3-4 days for up to 21 days.

After 14 days in osteogenic media, gene expression of *runx2*, a key osteogenic transcription factor, was significantly lower in OVX rMSCs (Figure 6.9a) compared to SHAM. In adipogenic media, expression of *pparγ* and *fabp4*, both markers of adipocyte differentiation, were significantly higher in OVX rMSCs compared to SHAM. Protein expression of FABP4 was also significantly increased in OVX rMSCs at Day 14 relative to SHAM (Figure 6.9b). A marker of

osteogenic differentiation, ALP activity, was significantly decreased in OVX rMSCs in osteogenic

media conditions at Day 14 (Figure 6.9c). Lastly, calcified matrix deposition, as measured by

Alizarin Red at Day 21 was also significantly decreased in OXV rMSCs relative to SHAM.

Collectively, these results confirmed the increased adipogenic potential and decreased osteogenic

potential of OVX rMSCs compared to SHAM controls.

6.3.7   RNA isolation and RT-qPCR

RNA was collected from Day 0 (24 hours after seeding) on TCPS and 4 days after culture in

microgels using the RNeasy Micro Kit (Qiagen, Cat. No. 74004). RNA quantity and purity were

determined via spectrophotometry (ND- 7 1000; NanoDrop). Complementary DNA (cDNA) was

synthesized using the iScript Synthesis kit (Bio-Rad, Cat. No. 1708841) on an Eppendorf

Mastercycler. RT-qPCR was performed using SYBR Green reagents (Bio-Rad, Cat. No. 1708884)

on an iCycler (BioRad). Relative mRNA expression levels from three technical replicates per

condition were normalized to GAPDH. Primer sequences are listed in Table 1.

Table 6.2 List of primers for RT-qPCR genes.

Gene	Forward ((5' -> 3')	Reverse ((5' -> 3')
runx2	AAGTGGCCAGGTTCAACGAT	CAAGCTTCTGTCTGTGCCTT
osteocalcin (OCN)	ATTGTGACGAGCTAGCGGAC	TCGAGTCCTGGAGAGTAGCC
pparγ	CCTGTTGACCCAGAGCATGG	GGTCCACAGAGCTGATTCCG
Fabp4	AGAAGTGGGAGTTGGCTTCG	ACTCTCTGACCGGATGACGA
Cdh1 (E-cadherin)	CCATCAACTGCCCGGAAAAT	ACCGTTGTCTCTTTGTCCCT
Chd2 (N-cadherin)	GGAGCCGATGAAGGAACCACA	ACCTGATCCTGACAAGCTCT
Chd4	CTGCGTTGATCTCCCCGAAT	TACTGCGTCCCTTTGGTGTC
Chd5 (VE-cadherin)	GATGAGAATGACAACGCCCC	TTGTGTTTACTGGCACCACG
Chd11 (OB-cadherin)	TTGTGAATGGGACTGGGACTG	TCACAGAGTCACAAAGCCAAA

Chd13 (T-cadherin)	TCAGAATGACAACCGACCCA	GGTCATCTGCATCAAACGCT
Chd15 (M-cadherin)	ATGAGTTCTGCTCTGCTCTTC	ACACACTGATGGGTGGGATG
Gapdh	GTTACCAGGGCTGCCTTCTC	GATGGTGATGGGTTTCCCGT

6.3.8 Alkaline phosphatase (ALP) detection

ALP detection was performed on OVX and SHAM rMSCs cultured in osteogenic conditions for 14 days using a commercially available kit (Sigma-Aldrich SCR004). Briefly, the samples were fixed in 4% paraformaldehyde (PFA) for 2 min and rinsed with Tris Buffered Saline (TBS) + 0.05% Tween 20 (TBST). A 2:1:1 mixed on Fast Violet Red (0.8g/L stock): Napthol AS-BI phosphate solution (4mg/mL) in AMPD buffer (2mol/L:water) was added to the samples for 15 min. After an additional wash with TBST, the samples were stored in PBS. Images were obtained using a 20x air objective Nikon Eclipse TE300 microscope and the % ALP area was quantified using ImageJ.

6.3.9 Alizarin Red staining

Alizarin Red staining was performed at Day 21 to detect the deposited mineralized extracellular matrix by SHAM and OVX rMSCs cultured in osteogenic inductive medium. Samples were fixed in 4% PFA for 15 min at RT and washed with PBS 3x. They were then incubated in a 40 mM solution of Alizarin Red (Sigma Aldrich TMS-008) in distilled water (pH 4.2) for 15 min. Samples were washed with PBS and images were obtained using a 20x with a Nikon Eclipse TE300 microscope. The % Alizarin red area was quantified using ImageJ.

6.3.10 Immunofluorescence staining

Samples were fixed for 30 min using 4% PFA or 10% formalin for rMSCs cultured on coverslips or in microgel scaffolds, respectively. Samples were washed with PBS 3x for 10 min

each. Permeabilization and blocking were performed each for 1 hour at RT in 0.1% TritonX-100 in PBS and 5% bovine serum albumin (BSA) in PBS, respectively Mouse Anti-N-cadherin (Sigma Aldrich, 10µg/mL), Goat Anti-Mouse FABP4 (R&D systems, 10µg/mL) primary antibodies in Cell Staining Buffer (Biolegend) were incubated while rocking overnight at 4°C. The next day, three washes with PBS with 0.05% Tween 20 (PBST) for 10 min each was performed. Then, secondary antibodies (specifically, goat anti-mouse Alexaflour 488 or chicken anti-goat Alexaflour 647 (1:500), DAPI (1:500), Rhodamine Phallodin (1:300)), were incubated for 1 hour at RT. Samples were washed with PBST 3x for 5-10 min. Images were acquired using either the Operetta (Perkin Elmer) for 2D samples or a Nikon Spinning Disc Confocal (40x air objective) or a Laser Scanning Confocal Microscope (20x water objective) for 3D microgel samples.

6.3.11 Image Analysis

Percent   Positive: For   %   positive analysis   (%FABP4+),   DAPI and Rhodamine Phalloidin staining were used to determine the nuclear and cytoplasmic areas using the Harmony software (Perkin Elmer). Cell number was determined by the number of nuclei. The number of positive cells were determined by the cytoplasm stained with FABP4. Percent of FABP4 was calculated for each field of view and analyzed.

N-cadherin intensity: For rMSCs cultured on 2D TCPS, N-cadherin intensity measurements were determined using Harmony software (Perkin Elmer). For rMSCs cultured in microgels, the N-cadherin intensity was determined using ImageJ. Outlier analysis was conducted using the ROUT method and Q=1%.

Cluster size and percentage: Cluster size and % of cells in cluster were determined using IMARIS 3D visualization software (Bitplane). Approximately 80-100 µm z-stack images (with <1 µm intervals between slices) were imported into the software and 3D surfaces

around a cluster was created using the F-actin stain. Next, the nuclei were marked using DAPI staining and the Spot Analysis feature of IMARIS. Using a pre-written Matlab code (Split into Surface Objects Xtension) within the IMARIS software, the number of nuclei within each cluster (defined as >3 nuclei) was determined.

6.3.12 Secretory Analysis

Global secretory profiles were measured using a Rat Cytokine Array C2 (RayBiotech) and the manufacturer's protocol was followed. Briefly, arrays were blocked for 30 min at RT and incubated overnight at 4°C with 1 mL of conditioned media collected after three days of rMSC culture in microgel scaffolds. The next day, the membranes were washed, incubated with a biotinylated antibody cocktail for 1.5 hrs at RT, washed, and then incubated with HRP-streptavidin for 2 hrs at RT. Chemiluminescence signal from the membranes was detected using a charge-coupled device camera (ImageQuant LAS 4000 GE Healthcare).

Analysis was performed using the manufacture's guidance. Spot intensity values from raw images were determined using the 2D Array feature of ImageQuant (GE Healthcare). The background signal was subtracted, and average intensities were normalized to positive spot controls on each array and control (blank media) arrays. ELISAs were performed according to the manufacturer's protocol for TIMP-1 and MCP-1 (R&D systems, rat Duo ELISA kits).

6.3.13 N-cadherin blocking

Blocking of N-cadherin cell-cell interactions were performed using an anti-N-cadherin antibody following previously published protocols[18,23]. Briefly, rMSCs were trypsinized, re-suspended in growth media containing N-cadherin blocking antibody (50 μg ml^{-1}, Sigma-Aldrich GC4), and incubated for 45 min at 4°C. The cells were then washed twice with PBS and encapsulated in microgels networks or plated on glass coverslips. It is important to note that 10

μg/mL of the N-cadherin blocking antibody was also included in the media throughout the experiments to ensure sustained blocking.

6.3.14 Statistical Analysis

Statistical analysis and data visualization was done using Graphpad v9. A two-way ANOVA with multiple comparisons were used to determine statistical significance between SHAM and OVX (Factor 1) and microgel conditions (Factor 2) for cell cluster size and %cells in a cluster (Figure 1). One-way ANOVAs with Tukey ad hoc tests were performed to determine statistical significance for secretion and gene expression data. N=3 technical replicates are plotted with standard mean error unless otherwise noted.

6.4 Results

6.4.1 Granular porous scaffolds with varied particle sizes direct rMSC clustering

After OVX and SHAM rMSCs were cultured on TCPS for four days, 97% of the secreted cytokine and growth factors measured as low or undetectable concentrations (Figure 6.10); necessitating an alternative culture platform to study their secreted factors. Prior literature has suggested that MSCs cultured in three-dimensional biomaterial scaffolds can better maintain and even increase MSC secretory properties by promoting cell-cell interactions [16,19].

For this reason, we utilized a cell-adhesive microgel scaffold with varying pore sizes to cluster and culture OVX and SHAM rMSCs in 3D. The porous scaffolds were assembled from microgels by using a SPAAC reaction between multi-arm PEG macromers end functionalized DBCO or azide under varying degrees of shear (Figure 6.1a). Upon assembly with rMSCs (~5million cells/mL), the cells become embedded in the void spaces and interact with the RGD motifs (1 mM) on the microgels (Figure 6.1b). After four days of culture, rMSCs encapsulated in scaffolds comprised of microgels with average diameters of ~10 μm reside largely as single cells

(Figure 6.1c, left). rMSCs in scaffolds comprised of microgels with increasing average diameters, ~100 μm and ~200 μm, form progressively larger clusters (Figures 6.1c, middle, right).

Using a 3D rendering software, IMARIS, the degree of cell clustering (Figure 6.1d) and cluster size (Figure 6.1e) were quantified for both SHAM and OVX rMSCS. Here, we defined a cluster as three or more nuclei (blue) contained within the same F-actin region (red). Less than 25% of SHAM and OVX rMSCs in 10 μm scaffolds resided in a cluster (~3 cells). In 100 μm scaffolds, $47.8\% \pm 17.1\%$ of SHAM rMSCs and $36.0\% \pm 2.7\%$ of OVX rMSCs resided in clusters, and these clusters contain ~5 cells. In scaffolds prepared with the 200 μm microgels, the OVX rMSCs had high degree of clustering ($95.0\% \pm 2.1\%$ with $\sim30 \pm 10$ cells) relative to SHAM cells ($84.1\% \pm 7.3\%$, $\sim20 \pm 7$ cells). A two-way ANOVA analysis revealed that both the degree of clustering and the cluster size were significantly varied between the three microgel conditions. However, there were no statistical differences between the clustering phenotypes of SHAM and OVX rMSCs in each microgel condition, ensuring that any observed secretory differences are not due to differences in the extent of clustering. For the remainder of the discussion, the conditions will be referred to as large clusters for rMSCs encapsulated in the 200 μm microgel diameter scaffolds, small clusters for rMSCs encapsulated in 100 μm microgel scaffolds, and single cells for rMSCs encapsulated in 10 μm microgel scaffolds.
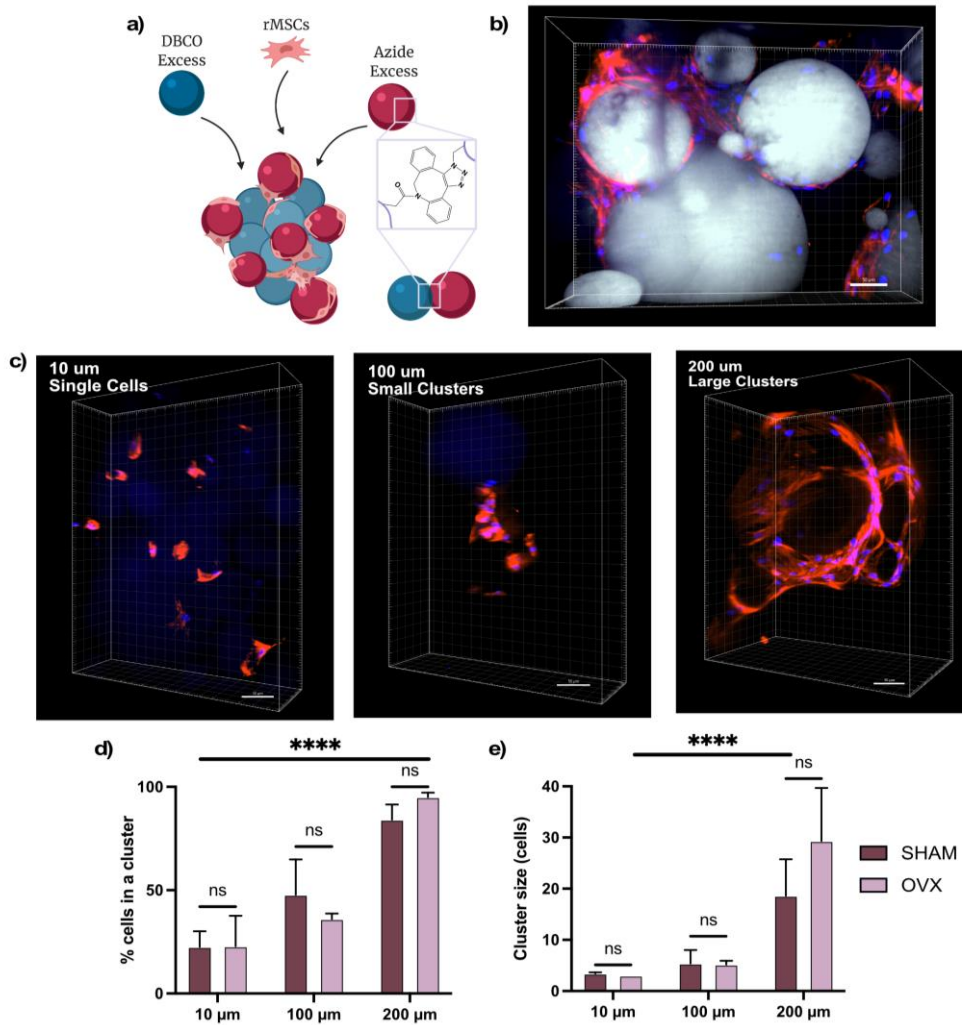
Figure 6.1 Porous granular scaffolds direct rMSC clustering.
(A) Schematic of cell-laden microgel scaffolds synthesized by combing DBCO excess microgels, azide excess microgels, and rMSCs. Individual microgels and the scaffold are covalently bound with SPAAC chemistry (B) Representative image of rMSCs in 200 µm scaffolds. (C) Representative images of rMSCs cultured in 10 µm (left), 100 µm (middle), and 200 µm (right) average diameter microgel scaffolds. Quantification of (D) % cells in clusters and (E) cluster size of SHAM (black) and OVX (grey) rMSCs. Error bars represent SEM. Scale bar = 50 µm. Microgels labeled in grey, nuclei in blue, and F-actin in red. Stars represent significance across conditions using a two-way ANOVA (**** p-value <0.0001, ns – not significant)

6.4.2   Clustering increases global cytokine secretion in both OVX and SHAM rMSCs, but

the increases are more pronounced in OVX rMSCs

After establishing three clustering phenotypes by varying the microgel pore dimensions, we

next measured the secretory properties of SHAM and OVX rMSCs cultured as large clusters (~30

cells/cluster), as small clusters (~5 cells/cluster), and as single cells using a cytokine array (RayBiotech Rat C2). Both SHAM and OVX rMSCs in large clusters had elevated secretion of a majority of the measured secreted factors (Figure 6.2a).
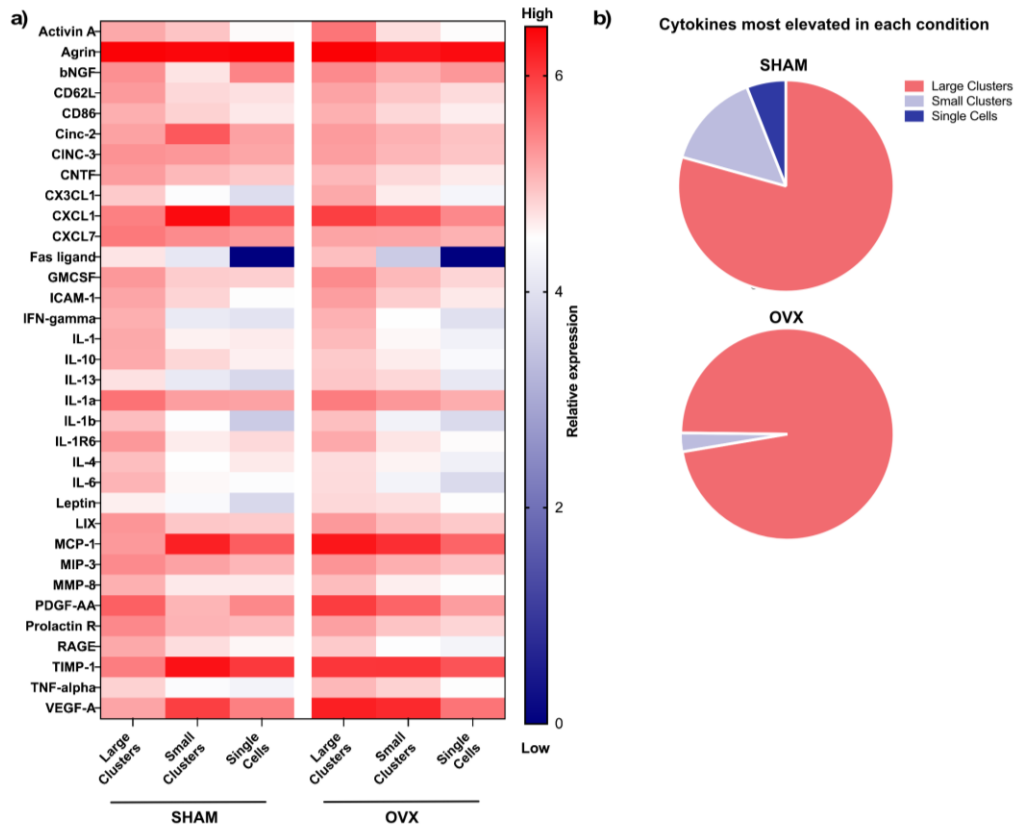
Figure 6.2 OVX and SHAM rMSCs secretory properties are increased in large clusters.
(A) Heatmap of concentration of cytokine array OVX and SHAM rMSCs cultured in large clusters, small clusters, and as single cells. Red represents high expression and blue represents low expression or no detection. (B) Distribution of factors most elevated in each clustering condition for SHAM (top) and OVX (bottom).

For SHAM rMSC conditions, out of the 34 secreted factors measured, 79% were most elevated in the large clusters, followed by ~15% in the small clusters and ~6% in the single cells (Figure 6.2b, top). For the OVX rMSCs conditions, 97% of the measured factors were most elevated in large clusters, only ~3% in small clusters, and zero in the single cells (Figure 6.2b, bottom). These results indicate that in large clusters, OVX rMSCs are more secretory than SHAM controls. Next, we

sought to analyze the differences between the SHAM and OVX rMSC secretory profiles in greater detail.

6.4.3 OVX rMSCs have elevated secretion of anti-osteogenic/pro-resorptive cytokines in large clusters relative to SHAM

To further explore whether an altered secretory profile from OVX rMSCs may be involved in their pro-resorptive bias, we identified a subset of factors deemed anti-osteogenic and/or pro-resorptive (Figure 6.3a). Also included were pro-inflammatory factors, such as, IL-1, IL-1α, IL-1, IL-6, TNF-α, and CXCL1, which are known to decrease osteogenic differentiation in progenitor cells and decrease matrix deposition of osteoblasts[24–26], and factors known to increase osteoclast maturation, such as Activin A, CX3CL1, and MCP-1[27–29]. Many of these factors can direct macrophage and lymphocyte recruitment into the bone, which initiates an inflammatory cascade that can inhibit osteoblast activity. Lastly, we included TIMP-1, which inhibits MMP activity, crucial for bone turnover and remodeling. TIMP-1 can also directly inhibit osteoblast mineralization. All these factors are labelled in red in Figure 6.3b.

Many of the pro-resorptive factors are secreted by both SHAM and OVX cells cultured as single cells or in small clusters had a similar profile (Figure 6.3a). However, in the large clusters, more significant differences are observed between the SHAM and OVX rMSCs. Large clusters of SHAM cells have decreased secretion of several key pro-resorptive factors, especially MCP1, TIMP-1, and CXCL1. In contrast, OVX rMSCs maintain or further elevate secretion of these factors and others (Figure 6.3a, large cluster panels).
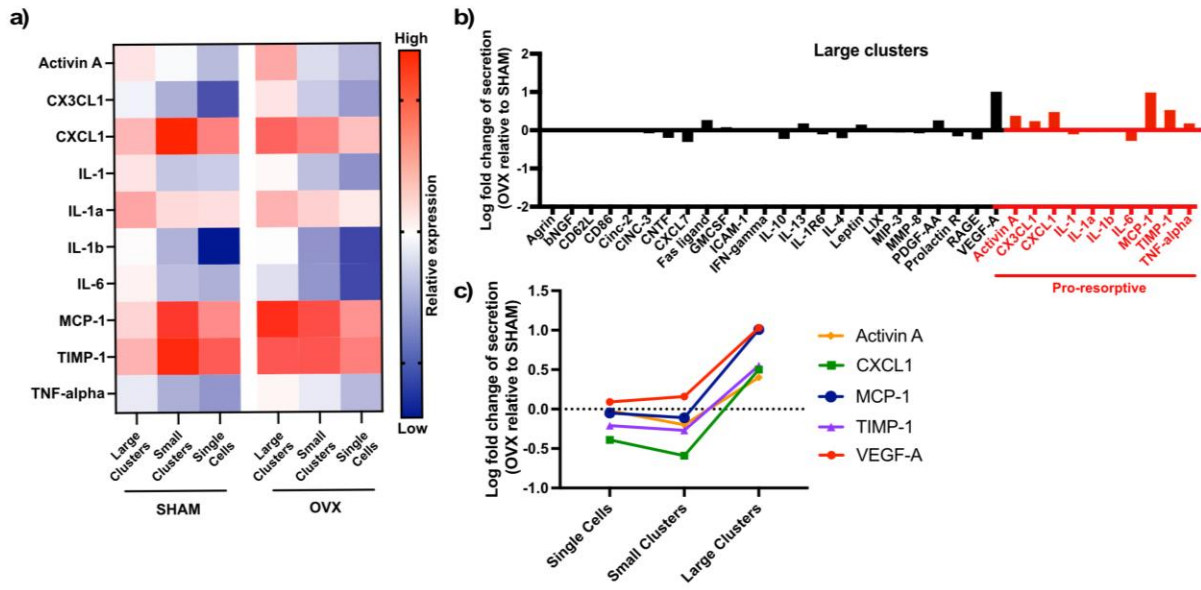
Figure 6.3 OVX rMSC secretory profile exhibits an anti-osteogenic/pro-resorptive bias.
(a) Heatmap of pro-resorptive or anti-osteogenic factor secretion from OVX and SHAM rMSC cultured as large clusters, small clusters, or single cells. (b) Log fold change of secretion of OVX rMSC in large clusters relative to SHAM rMSCs in large clusters. Factors listed in red are classified as pro-resorptive. (c) Log fold change of the top five factors most elevated by OVX rMSCs in large clusters across all clustering conditions.

Notably, 6 of the 10 pro-resorptive factors, Activin A, CXCL1, CX3CL1, MCP-1, TIMP-1, and TNF-alpha, are greatly elevated in OVX rMSC clusters relative to SHAM (Figure 6.3b). There were no differences in the secretion of IL-1, IL-1a, IL-1b, and IL-6, indicating that pro-inflammatory interleukin secretion may not be significantly altered in OVX rMSCs. Additionally, secretion of VEGF-A, an angiogenic factor present in bone marrow adipose tissue, was elevated in the OVX rMSCs compared to SHAM rMSCs[30]. Four of the top five most elevated factors in OVX compared to SHAM rMSCs are classified as pro-resorptive (Figure 6.3c). Collectively, these results indicate that the secretory profile of OVX rMSCs is biased towards a pro-resorptive and/or anti-osteogenic phenotype. However, we note that the differences in the secretory profile are not present when OVX and SHAM rMSCs are cultured in small clusters or as single cells (Figure

6.11), indicating that cell-cell contacts may be involved in the pro-resorptive cytokine production by OVX rMSCs.

6.4.4 N-cadherin expression is significantly elevated in OVX rMSCs

Given the differences observed in the secretory profiles between small and large OVX rMSC clusters, we wanted to examine the role of cadherins. Cadherins are a type of calcium dependent adherence junction that participate in intercellular homotypic binding[31,32] and further direct downstream gene expression through the force mediated formation of the cadherin catenin complex[31,33]. To begin, we first used RT-qPCR to examine the expression of a variety of cadherins in OVX and SHAM rMSCs.
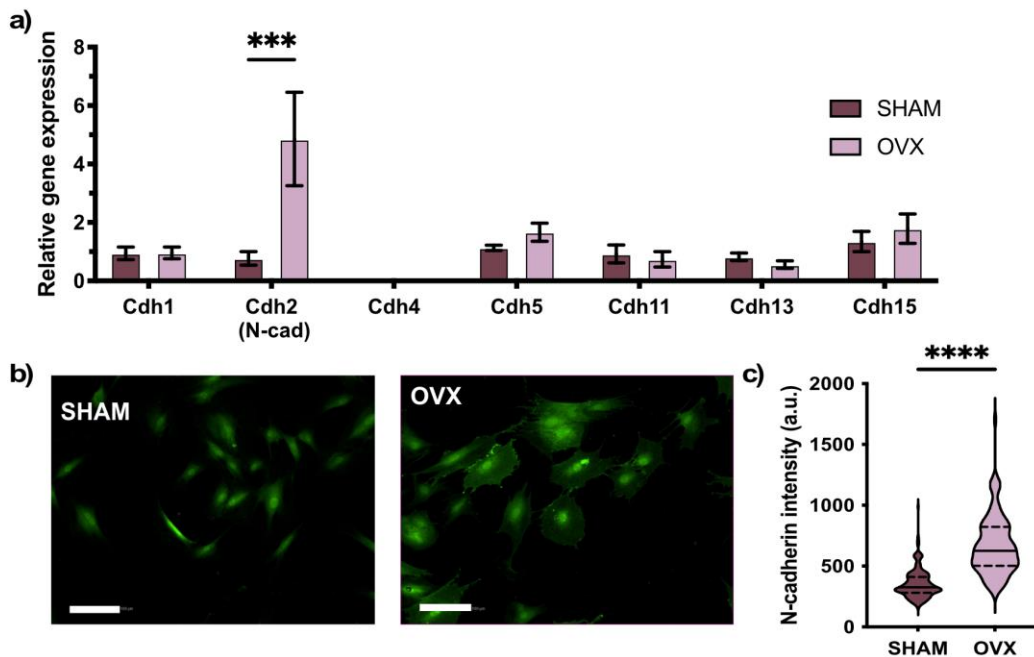
Figure 6.4 Higher expression of N-cadherin in OVX rMSCs on TCPS.
(A) Relative expression of multiple cadherins in SHAM and OVX rMSCs cultured for 24 hours on TCPS in growth media. Error bars represent SEM. (B) Representative images of N-cadherin immunostaining (green) of SHAM and OVX rMSCs on TCPS. Scale bar (white) 100 μm. (C) Quantification of N-cadherin fluorescent intensity. Stars represent significance between OVX and SHAM (**** p-value <0.0001).

After culturing SHAM and OVX rMSCs on TCPS for 4 days in growth conditions, RT-qPCR was performed for a variety of cadherin genes (Figure 6.4a). In general, both SHAM and OVX expressed *Cdh1* (E-cadherin), *Cdh2* (N-cadherin), *Cdh5* (VE-cadherin) *Cdh11* (OB-cadherin), *Cdh13* (T-cadherin), and *Cdh15* (M-cadherin) and, notably, did not express *Cdh4*. Only *Cdh2*, or N-cadherin, gene expression was ~4 fold higher in OVX rMSCs relative to SHAM, which was further observed at the protein level by immunostaining (Figure 6.4b). Image quantification confirmed an overall higher fluorescence intensity of N-cadherin by OVX rMSCs relative to SHAM (Figure 6.4c). Based on these results, we investigated N-cadherin expression in the 3D porous microgel scaffolds and as a function of rMSC clustering.
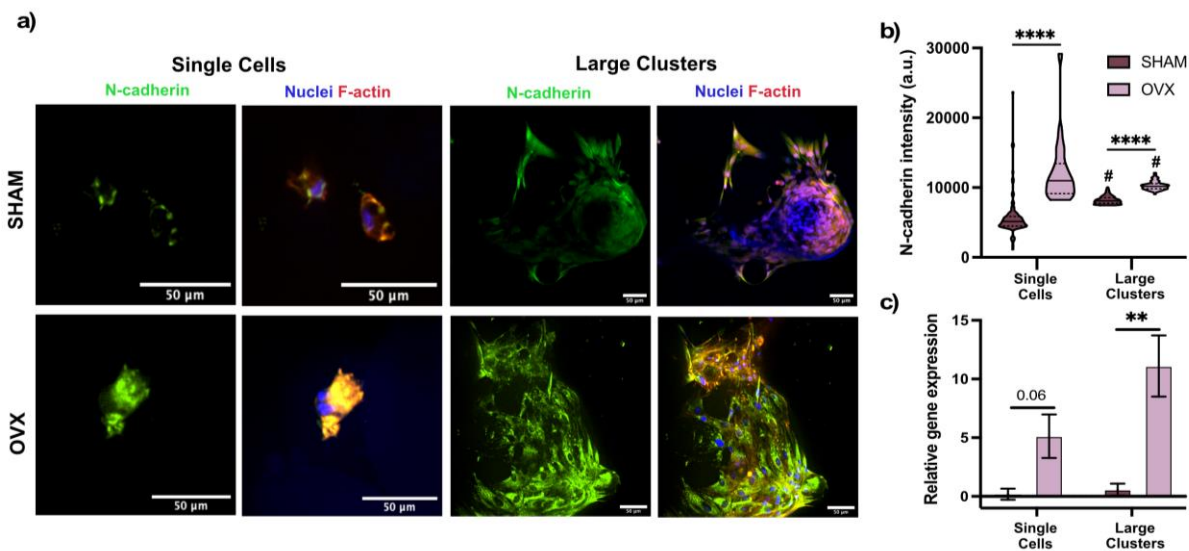
Figure 6.5 OVX rMSCs N-cadherin expression stays elevated when cultured in microgels scaffolds.
(A) Representative immunostaining images of N-cadherin (green) of SHAM and OVX rMSCs cultured as single cells and as large clusters in microgel scaffolds. Nuclei are staining with DAPI (blue) and F-actin is stained with Rhodamine Phallodin (red). (B) Quantification of N-cadherin fluorescent intensity. (C) Relative N-cadherin gene expression of SHAM and OVX rMSCs cultured in microgel scaffolds. Error bars represent SEM. Stars represent significance between SHAM (dark green) and OVX (light green) (**** p-value <0.0001, ** p-value <0.01). Hashtags represent significant between single cells and large clusters for each cell type (# p-value <0.001).

6.4.5 N-cadherin expression is elevated in clustered and single OVX rMSCs relative to SHAM rMSCs

We next measured N-cadherin expression in the 3D porous microgel scaffolds, where rMSCs were cultured as either single cells or as large clusters for both OVX and SHAM rMSCs. Representative images show increased N-cadherin expression for single OVX rMSCs cultured in the 10 μm microgel scaffolds compared to SHAM single cells (Figure 6.5a, left). This observation was quantified in Figure 6.5b. *Cdh2* gene expression was also ~4 fold higher in OVX rMSCs relative to SHAM cells (Figure 6.5c). These trends were also observed in the large rMSC clusters in ~200 μm microgel scaffolds (Figure 6.5a, right). However, the relative increase in N-cadherin protein levels in the OVX rMSCs was smaller in the large clusters (~0.2x) compared to single cells (~3x) (Figure 6.5b,c).

6.4.6 Blocking N-cadherin reduces secretion of pro-resorptive cytokines in OVX rMSCs clusters

As N-cadherin expression is higher in OVX rMSCs, both as single cells and as large clusters, we next sought to determine the specific role of N-cadherin on MSC secretory properties and profiles. To do this, we blocked N-cadherin and then encapsulated OVX and SHAM rMSCs in ~200 μm microgel scaffolds, where they reside as large cell clusters. After 4 days of culture, cytokine and growth factor secretion was measured. Results showed a significant decrease in overall secretion in OVX rMSCs relative to SHAM cells (Figure 6.6a). In contrast to the secretory profiles seen before (Figure 6.3b), when N-cadherin interactions were blocked, large clusters of OVX rMSCs no longer produced higher levels of pro-resorptive cytokines relative to SHAM cells in the same conditions. This reduction was not observed when N-cadherin was blocked in OVX rMSC cultures as single cells (Figure 6.12). Approximately no change or decreased in secretion

was observed for the previously five most elevated factors by OVX rMSCs in large clusters (Activin A, CXCL1, MCP1, TIMP1 and VEGF-A) when N-cadherin was blocked (Figure 6.6b).
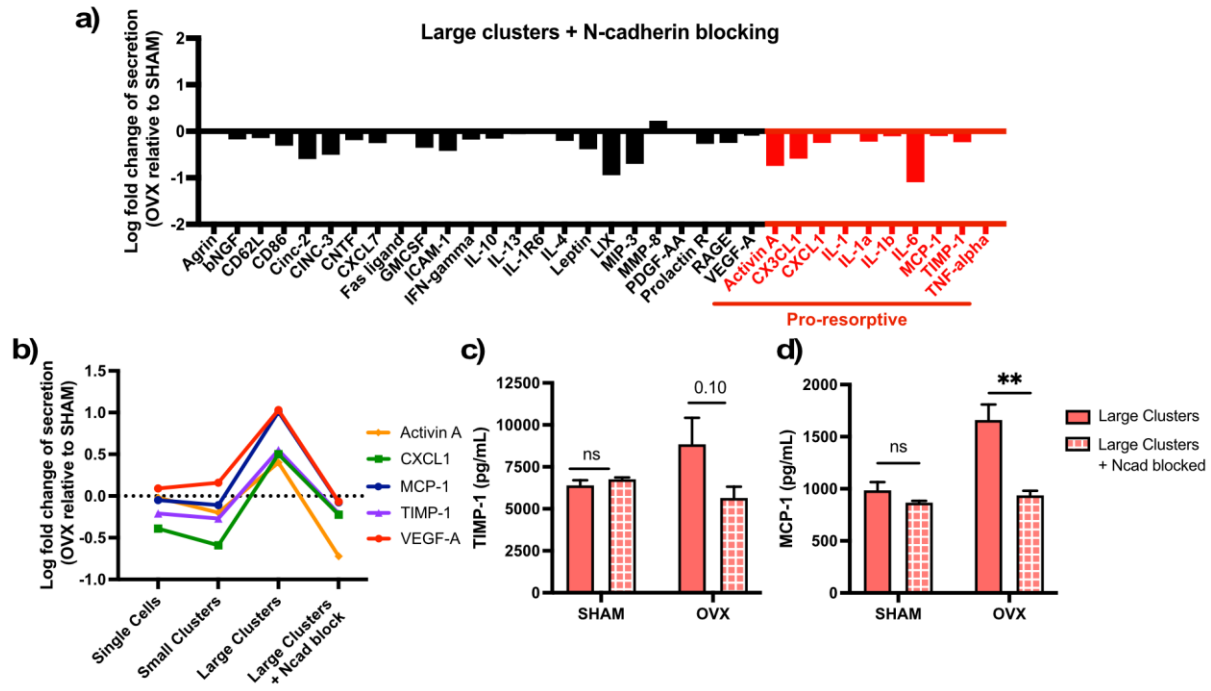
Figure 6.6 N-cadherin blocking decreased secretion of pro-resorptive factors selectively from OVX rMSCs.
(A) Log fold change in secretion between OVX and SHAM rMSCs cultured in large clusters with blocked N-cadherin is blocked. Pro-resorptive factors are labelled in red. (B) Log fold change of the top 5 five most elevated by OVX rMSCs in large clusters across all clustering conditions and with N-cadherin blocking. ELISA quantification of (C) TIMP-1 and (D) MCP-1 of SHAM and OVX rMSCs. Error bars represent SEM. Stars represent significance between SHAM (black) and OVX (gray) (** p-value <0.01, ns – not significant)

To test whether the global decreases were due to a lack of secretion from both cell types or a decrease by OVX rMSCS only, we performed ELISAs to measure the absolute concentrations of TIMP-1 (Figure 6.6c) and MCP-1 (Figure 6.6d). For both factors, blocking N-cadherin caused OVX rMSCs in large clusters to selectively decrease secretion, while SHAM rMSCs maintained their secretion at the same levels as their respective unblocked controls. Overall, these results

indicate that N-cadherin interactions are necessary for the pro-resorptive bias of the secretory profile of OVX rMSCs.

6.5 Discussion

Patients with postmenopausal osteoporosis have a higher bone resorption and higher fracture risk, potentially due to impairments in their MSCs. As factors secreted by MSCs are known to be involved with bone healing and homeostatis, we characterized the secretory profile of OVX rMSCs utilizing a porous microgel system to cluster rMSCs (single cells to ~30 cell/cluster) with varying percentages of cells within clusters (~20-90%) (Figure 6.1). Clustering increased the concentrations of factors secreted by OVX rMSCs relative to single cells (Figure 6.2), specifically pro-resorptive and anti-osteogenic factors (Figure 6.3). We further sought to understand if cadherin mediated cell-cell connections were involved. N-cadherin was highly expressed in OVX rMSCs compared to SHAM (Figure 6.4, 6.5). Blocking N-cadherin suppressed the pro-resorptive bias of the OVX rMSC secretory profile (Figure 6.6).

In addition to an altered secretory profile and elevated N-cadherin, OVX rMSCs exhibit decreased osteogenic differentiation capacities (Figure 6.9). While no studies have directly explored the influence of N-cadherin signaling on the differentiation of OVX rMSCs, research with healthy MSCs indicates that N-cadherins can influence cell fate decisions. When hMSCs were cultured on 2D hydrogels modified with N-cadherin mimic peptide, they exhibited decreased RUNX2 nuclear to cytoplasmic ratios, indicating a decrease in osteogenic differentiation potential[32]. Similarly, another study demonstrated increased hMSC osteogenic differentiation and collagenous matrix deposition when N-cadherin was inhibited, both when MSCs were cultured on TCPS and as 3D aggregates[34]. In contrast, MSCs encapsulated in hyaluronic acid hydrogels functionalized with N-cadherin mimic peptides exhibited enhanced osteogenic differentiation[35].

While we focused on the role of N-cadherin interactions on the OVX rMSC secretory profile, future studies might focus on the N-cadherin regulation of OVX rMSC osteogenic differentiation. In addition, as MSC differentiation is also affected by matrix cues, other studies could focus on exploring the role of stiffness, in addition to N-cadherin signaling, on OVX rMSC differentiation.

While the *in vivo* locations and functions of MSCs are not fully understood, MSCs likely participate in N-cadherin signaling in the bone marrow niche[36–38]. To maintain bone homeostasis, MSCs interact with bone lining cells and osteoblasts—which have high N-cadherin expression[10,12]—and can secrete factors to direct activities of nearby cells, including immune cells, osteoblasts, osteoclasts, and other MSCs. In this study, we observed that OVX rMSCs in large clusters (partially mediated through N-cadherin interactions) secrete TNF-α, TIMP1, and CXCL1 that are known to inhibitors of osteoprogenitor proliferation, differentiation, and mineralization44, 50. OVX rMSCs also have elevated secretion of factors, such as Activin A and MCP-1, that can promote osteoclast fusion, increasing rates of bone resorption[27,28]. Additionally, TNF-α, CXCL1, MCP-1, and CX3CL1 can direct macrophage and lymphocyte migration and pro-inflammatory polarization[40,41].

While the results of this study are promising, it is important to note that the OVX rMSCs isolated from seven separate wildtype outbred rats and pooled together for these in vitro experiments. As in humans, the genetic variations in rats contribute to variations in bone loss after ovariectomy, indicating degrees of bone resorption. This could potentially be influencing the pro-resorptive factor section from OVX rMSCs. Future work should analyze the secretions of OVX rMSCs from individual animals to understand how genetic differences may be influencing MSC secretions.

Interestingly, some of these factors are also known to be elevated in osteoporosis. Serum analysis demonstrated increased TFN-α in osteoporotic women compared to age matched controls[42]. Additionally, VEGF-A, MCP-1, and TNF- α levels were elevated in white adipose tissue isolated from OVX rats[30]. MCP-1 expression is also elevated in immune cells in bone marrow fat, which can contribute to an inflammatory environment52. While it is unlikely that MSCs are solely responsible for these secretions—as they are present in very few numbers *in vivo*—their role in the pathogenesis of osteoporosis requires further elucidation. However, these results highlight the ability of granular PEG hydrogels to mediate OVX rMSC clustering via N-cadherin, thus influencing the pro-resorptive bias of their secretory profile.

One potential implication from this study goes beyond the investigation of the OVX rMSC secretory profile; namely, that the binding of N-cadherin may be necessary for MSC secretome elevation. Even though OVX rMSCs cultured across multiple platforms had elevated expression of N-cadherin relative to SHAM (Figures 6.4, 6.5), their secretory properties were only elevated when in large clusters (Figure 6.2). Additionally, blocking N-cadherin interactions reduced secretion from OVX rMSCs solely in large clusters (Figure 6.6) and not in single cells (Figure 6.12). Molecularly, the homotypic binding of N-cadherin initiates the formation of the cadherin catenin complex, resulting in the sequestration of α- and β-catenin in a force-dependent manner[31]. α-catenin can bind to F-actin, thus linking the cadherin-catenin complex to the cytoskeleton, where applied tension can result in downstream gene expression[53]. Additionally, β-catenin can interact with multiple transcriptional pathways, including Wnt[45–47] and NF-kB[39,48], which both regulate transcription of multiple secreted factors. Taken together, these results indicate that overexpression of N-cadherin may not be enough to elevate MSC secretion, but rather N-cadherin binding, facilitated through cell clustering, must occur. Therefore, MSC clustering may be a necessary

strategy for cell-based therapeutics relying on their secreted factors and aid in the improvement of biomaterial delivery systems.

6.6   Conclusions

MSCs have been implicated in post-menopausal osteoporosis as their adipogenic differentiation bias may contribute to increased bone marrow adiposity. Additionally, MSC secreted factors can influence multiple cell behaviors, including bone resorption which is elevated in osteoporosis. Here, we utilized a porous microgel scaffold to cluster and elevate the secretion of OVX and SHAM rMSCs. We observed a pro-resorptive bias of the secretory profile of OVX rMSCs cultured in large cell clusters relative to SHAM rMSCs. Further, we observed elevated N-cadherin expression in OVX rMSCs compared to SHAM, when both were cultured as single cells and as large clusters. Finally, we demonstrated that N-cadherin signaling was partially responsible for the regulation of OVX rMSC secretory properties. Characterizing the secretory factors of OVX rMSCs and understanding the signaling pathways that may be involved will inform the design of future MSC therapies for healing in osteoporotic environments.

6.7 Associated content
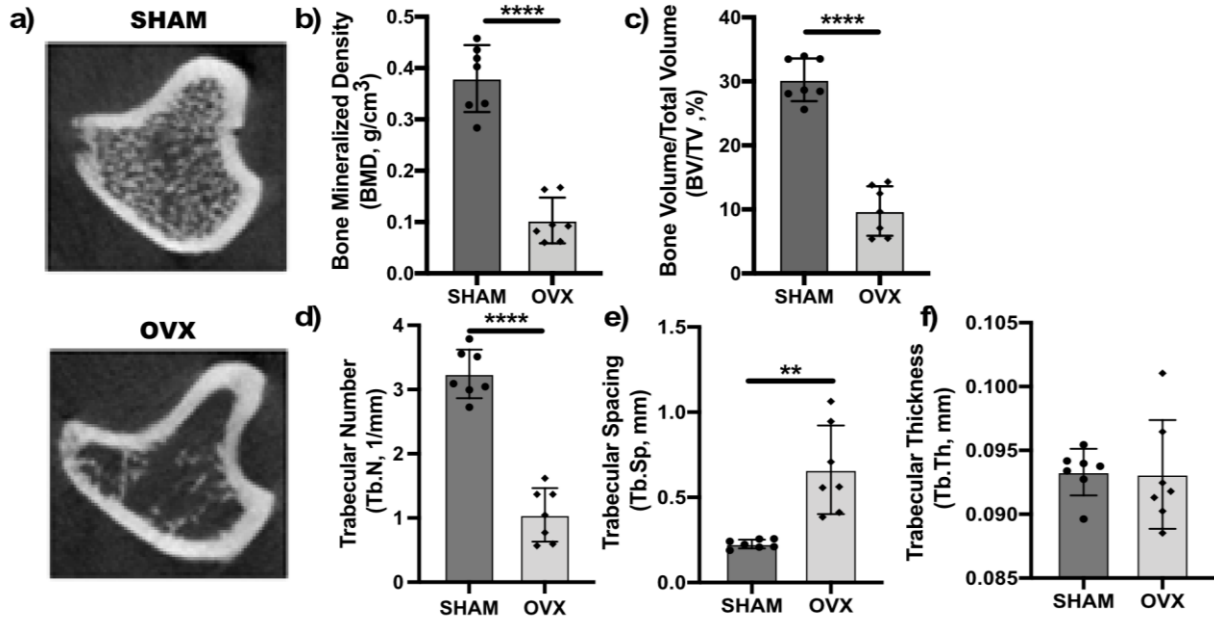
Figure 6.7 Ovariectomy (OVX) results in decreased bone mass.
(a) Representative µCT images of trabecular bone of rats 14-weeks post OVX and SHAM surgeries. Quantification of (b) bone minearlized density (g/cm^3), (c) percent of bone volume/total volume, (d) trabecular number (1/mm), trabecular spacing (mm), and (f) trabecular thickeness (mm) of OVX and SHAM rats. Stars represent significance between SHAM and OVX (**** p-value <0.0001, ** p-value <0.01).
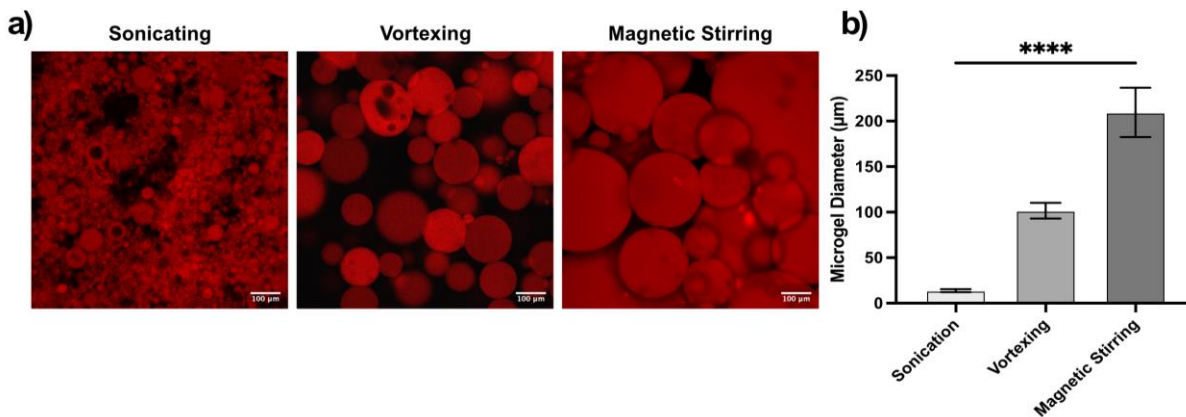
Figure 6.8 Microgel diameter characterization.
(a) Microgels of varied sizes (red) were fabricated in an inverse phase polymerization under shear.
(b) Sonication resulted in microgels with an average diameter of 14 µm $\pm$ 9 µm (~10 µm), vortexing resulted in microgels of average diameters of 102 µm $\pm$ 43 µm (~100 µm), and

sonicating resulted in microgels of average diameters of 210 µm ± 109 µm (~200 µm). Scale bar = 100 µm. Significance was determine using a one-way ANOVA (**** p-value <0.0001).
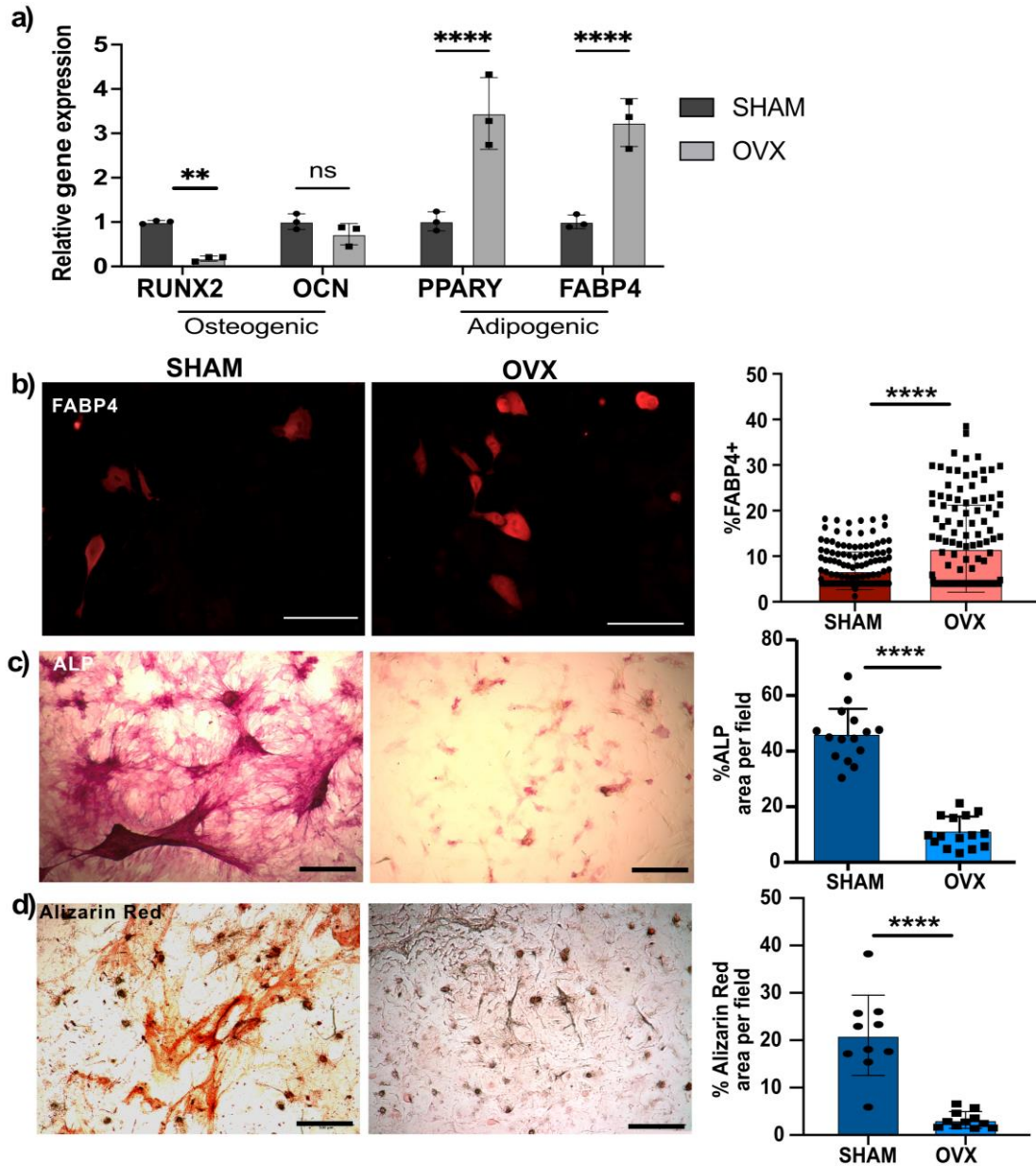
Figure 6.9 OVX rMSCs have decreased osteogenic differentiation potential and increased adipogenic differentiation potential.
(a) Gene expression of SHAM (dark gray) and OVX (light grey) rMSCs RUNX2 and OCN in osteogenic media conditions and PPARY and FABP4 in adipogenic media conditions. (b) Representative images and quantification of FABP4 positive cells per field of view. c) Representative images and quantification of % ALP area positive per field of view. d)

Representative images and quantification of % Alizarin Red area positive per field of view Significance was determine using a student's t-test (**** p-value <0.0001, ns - non significant).
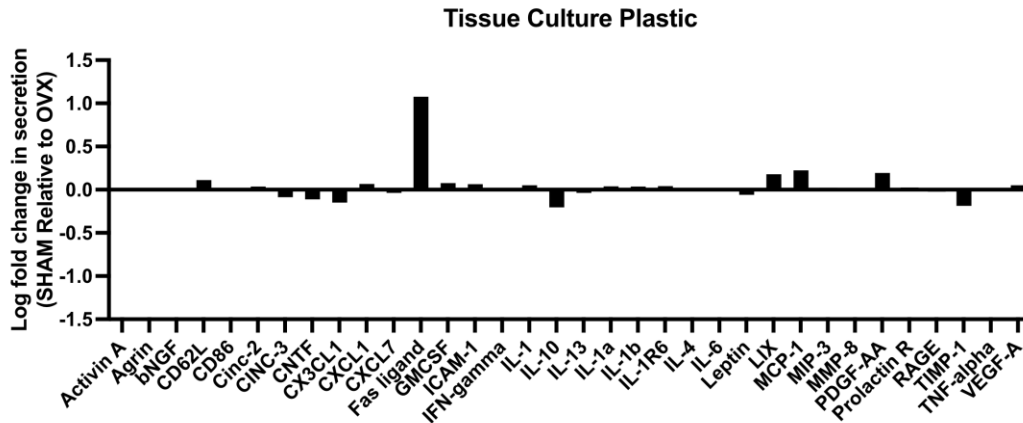
Figure 6.10 TCPS culture does not elevate OVX and SHAM rMSC secretory properties. Log fold change of secretion of SHAM rMSC on TCPS relative to OVX rMSCs on TCPS.
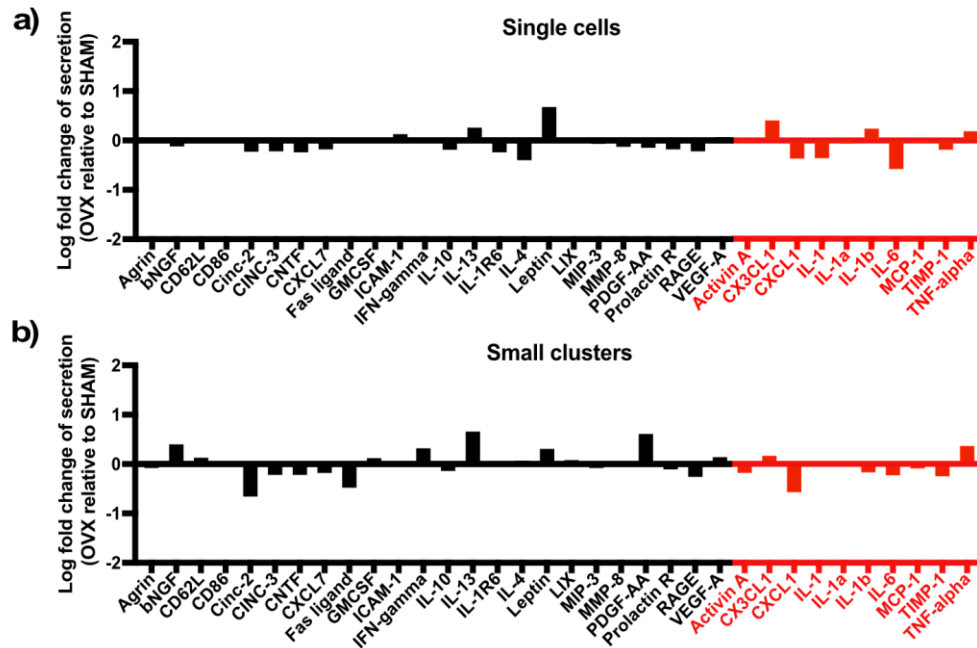
Figure 6.11 OVX rMSCs secretory profile is not biased towards pro-resorptive factors in single cells or small clusters.
Log fold change in secretion between OVX and SHAM rMSC cultured as (a) single cells and (b) small clusters. Factors listed in red are classified as pro-resorptive.
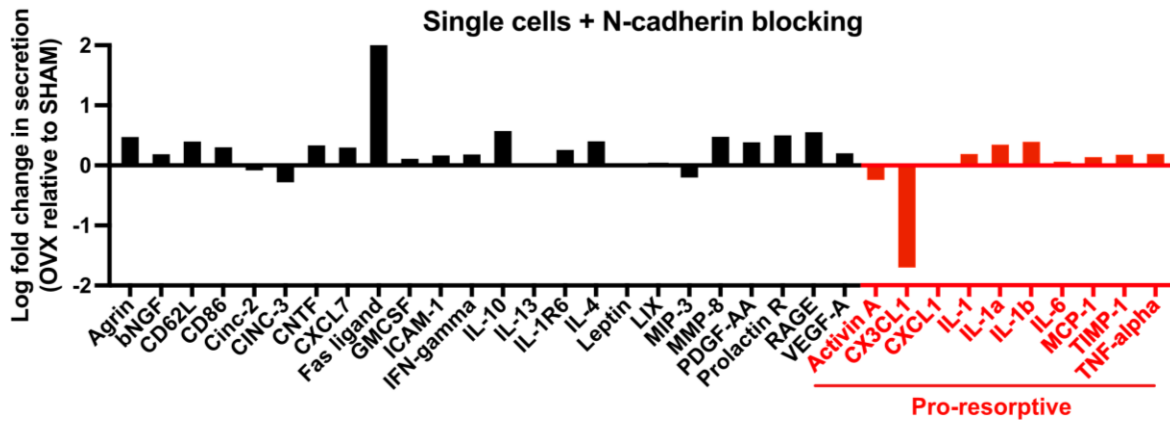
Figure 6.12 Blocking N-cadherin in single OVX rMSCs does not decrease their secretion relative to single SHAM rMSCs with N-cadherin blocking.
Log fold change in secretion between OVX and SHAM rMSC cultured as single cells with N-cadherin interaction blocked. Factors listed in red are classified as pro-resorptive.

6.8 References

(1)   Eastell, R.; O, T. W.; Hofbauer, L. C.; Langdahl, B.; Reid, I. R.; Gold, D. T.; Cummings, S. R. Postmenopausal Osteoporosis. **2016**. https://doi.org/10.1038/nrdp.2016.69.

(2)   Yu, B.; Wang, C. Y. Osteoporosis: The Result of an 'Aged' Bone Microenvironment. *Trends in Molecular Medicine* **2016**, *22* (8), 641–644. https://doi.org/10.1016/j.molmed.2016.06.002.

(3)   Eastell, R.; O, T. W.; Hofbauer, L. C.; Langdahl, B.; Reid, I. R.; Gold, D. T.; Cummings, S. R. Postmenopausal Osteoporosis. *Nature Review Primer* **2016**. https://doi.org/10.1038/nrdp.2016.69

(4)   Wu, D.; Cline-Smith, A.; Shashkova, E.; Aurora, R. *Osteoporosis: A Multifactorial Disease*.

(5)   Whitfield, J. F. How to Grow Bone to Treat Osteoporosis and Mend Fractures. *Current osteoporosis reports* **2003**, *1* (1), 32–40. https://doi.org/10.1007/s11914-003-0006-7.

(6)   Cheung, W. H.; Miclau, T.; Chow, S. K.-H.; Yang, F. F.; Alt, V. Fracture Healing in Osteoporotic Bone. *Injury* **2016**, *47*, S21–S26. https://doi.org/10.1016/S0020-1383(16)47004-X.

(7)   Park, D.; Spencer, J. A.; Koh, B. I.; Kobayashi, T.; Fujisaki, J.; Clemens, T. L.; Lin, C. P.; Kronenberg, H. M.; Scadden, D. T. Endogenous Bone Marrow MSCs Are Dynamic, Fate-Restricted Participants in Bone Maintenance and Regeneration. *Cell Stem Cell* **2012**, *10* (3), 259–272. https://doi.org/10.1016/j.stem.2012.02.003.

(8)   Tewari, M. C.; Nagar, G. K.; Vishwakarma, A. L.; Ogechukwu, O. E.; Bellare, J. R.; Gambhir, S.; Chattopadhyay, N. Ovariectomized Rats with Established Osteopenia Have Diminished Mesenchymal Stem Cells in the Bone Marrow and Impaired Homing, Osteoinduction and Bone Regeneration at the Fracture Site. *Stem Cell Reviews and Reports* **2015**, *11* (2), 309–321. https://doi.org/10.1007/s12015-014-9573-5.

(9)   Corrigan, M. A.; Coyle, S.; Eichholz, K. F.; Riffault, M.; Lenehan, B.; Hoey, D. A. Aged Osteoporotic Bone Marrow Stromal Cells Demonstrate Defective Recruitment, Mechanosensitivity, and Matrix Deposition. *Cells Tissues Organs* **2019**, *207* (2), 83–96. https://doi.org/10.1159/000503444.

(10)   Cao, X.; Frenette, P. S.; Mao, J. J.; Robey, P. G.; Simmons, P. J.; Wang, C.-Y.; Bianco, P. The Meaning, the Sense and the Significance: Translating the Science of Mesenchymal Stem Cells into Medicine. *Nature Medicine* **2013**. https://doi.org/10.1038/nm.3028.

(11)   Wechsler, M. E.; Rao, V. v; Borelli, A. N.; Anseth, K. S. Engineering the MSC Secretome: A Hydrogel Focused Approach. **2021**, *2001948*, 1–17. https://doi.org/10.1002/adhm.202001948.

(12)   Pittenger, M. F.; Discher, D. E.; Péault, B. M.; Phinney, D. G.; Hare, J. M.; Caplan, A. I. Mesenchymal Stem Cell Perspective: Cell Biology to Clinical Progress. *npj Regenerative Medicine* **2019**, *4* (22). https://doi.org/10.1038/s41536-019-0083-6.

(13)   Stoddart,   M. J.; Salgado, A .; Presen, D. M.; Traweger , A.; Gimona, M.; Redl, H. Mesenchymal Stromal Cell-Based   Bone   Regeneration   Therapies: From   Cell Transplantation and Tissue Engineering to Therapeutic Secretomes and Extracellular Vesicles. *Frontiers in Bioengineering and Biotechnology | www.frontiersin.org* **2019**, *1*, 352. https://doi.org/10.3389/fbioe.2019.00352.

(14)   Levy, O.; Kuai, R.; Siren, E. M. J.; Bhere, D.; Milton, Y.; Nissar, N.; de Biasio, M.; Heinelt, M.; Reeve, B.; Abdi, R.; Alturki, M.; Fallatah, M.; Almalik, A.; Alhasan, A. H.; Shah, K. Karp, J. M. Shattering Barriers toward Clinically Meaningful MSC Therapies. *Science Advances* **2020**, *6*.

(15)   Osugi, M.; Katagiri, W.; Yoshimi, R.; Inukai, T.; Hibi, H.; Ueda, M. Conditioned Media from Mesenchymal Stem Cells Enhanced Bone Regeneration in Rat Calvarial Bone Defects. *Tissue   Engineering - Part A* **2012**, *18* (13–14), 1479–1489. https://doi.org/10.1089/ten.tea.2011.0325.

(16)   Qazi, T. H.; Mooney, D. J.; Duda, G. N.; Geissler, S. Biomaterials That Promote Cell-Cell Interactions Enhance the Paracrine Function of MSCs. *Biomaterials* **2017**, *140*, 103–114. https://doi.org/10.1016/j.biomaterials.2017.06.019.

(17)   Gionet-Gonzales, M. A.; Leach, J. K. Engineering Principles for Guiding Spheroid Function in the Regeneration of Bone, Cartilage, and Skin. *Biomedical Materials (Bristol)* **2018**, *13* (3). https://doi.org/10.1088/1748-605X/aab0b3.

(18)   Ho, S. S.; Murphy, K. C.; Binder, B. Y. K.; Vissers, C. B.; Leach, J. K. Increased Survival and Function of Mesenchymal Stem Cell Spheroids Entrapped in Instructive Alginate Hydrogels. *Stem Cells Translational Medicine* **2016**, *5*, 773–781.

(19)   Caldwell, A. S.; Rao, V. v.; Golden, A. C.; Anseth, K. S. Porous Bio-Click Microgel Scaffolds Control hMSC Interactions and Promote Their Secretory Properties. *Biomaterials* **2020**, *232* (December 2019), 119725. https://doi.org/10.1016/j.biomaterials.2019.119725.

(20)   Helfrich, M. H.; Ralston, S. H.; Idris, A. I. Ovariectomy/Orchidectomy in Rodents. *Methods in Molecular Biology* **2012**, *816*, 545–551. https://doi.org/10.1007/978-1-61779-415-5_34.

(21)   Rossow, T.; Seiffert, S. Supramolecular Polymer Gels with Potential Model-Network Structure. *Polymer Chemistry* **2014**, *5* (8), 3018–3029. https://doi.org/10.1039/C3PY01692G.

(22)   Tang, S.; Ma, H.; Tu, H.-C.; Wang, H.-R.; Lin, P.-C.; Anseth, K. S. Adaptable Fast Relaxing Boronate-Based Hydrogels for Probing Cell–Matrix Interactions. *Advanced Science* **2018**, *5* (9), 1800638. https://doi.org/10.1002/ADVS.201800638.

(23)   Caldwell, A. S.; Campbell, G. T.; Shekiro, K. M. T.; Anseth, K. S. Clickable Microgel Scaffolds as Platforms for 3D Cell Encapsulation. *Advanced Healthcare Materials* **2017**, *6* (15), 1–8. https://doi.org/10.1002/adhm.201700254.

(24)   Du, D.; Zhou, Z.; Zhu, L.; Hu, X.; Lu, J.; Shi, C.; Chen, F.; Chen, A. TNF-α Suppresses Osteogenic Differentiation of MSCs by Accelerating P2Y2 Receptor in Estrogen-Deficiency Induced Osteoporosis. *Bone* **2018**, *117*, 161–170. https://doi.org/10.1016/j.bone.2018.09.012.

(25)   Wang, L.; Zhao, Y.; Liu, Y.; Akiyama, K.; Chen, C.; Qu, C.; Jin, Y.; Shi, S. IFN-γ and TNF-α Synergistically Induce Mesenchymal Stem Cell Impairment and Tumorigenesis via NFκB Signaling. *Stem Cells* **2013**, *31* (7), 1383–1395. https://doi.org/10.1002/stem.1388.

(26)   Chang, J.; Liu, F.; Lee, M.; Wu, B.; Ting, K.; Zara, J. N.; Soo, C.; al Hezaimi, K.; Zou, W.; Chen, X.; Mooney, D. J.; Wang, C.-Y.; Chien, S. NF-KB Inhibits Osteogenic Differentiation of Mesenchymal Stem Cells by Promoting β-Catenin Degradation. https://doi.org/10.1073/pnas.1300532110.

(27)   Ikenoue, T.; Jingushi, S.; Urabe, K.; Okazaki, K.; Iwamoto, Y. *Inhibitory Effects of Activin A on Osteoblast Differentiation During Cultures of Fetal Rat Calvarial Cells*; 1999; Vol 75.

(28)   Kajita, T.; Ariyoshi, W.; Okinaga, T.; Mitsugi, S.; Tominaga, K.; Nishihara, T. Mechanisms Involved in Enhancement of Osteoclast Formation by Activin-A. *Journal of Cellular Biochemistry* **2018**, *119* (8), 6974–6985. https://doi.org/10.1002/jcb.26906.

(29)   Mulholland, B. S.; Forwood, M. R.; Morrison, N. A. Monocyte Chemoattractant Protein-1 (MCP-1/CCL2) Drives Activation of Bone Remodelling and Skeletal Metastasis. *Current Osteoporosis Reports* **2019**, *17* (6), 538–547. https://doi.org/10.1007/s11914-019-00545-7.

(30)   Shen, H. H.; Yang, C. Y.; Kung, C. W.; Chen, S. Y.; Wu, H. M.; Cheng, P. Y.; Lam, K. K.; Lee, Y. M. Raloxifene Inhibits Adipose Tissue Inflammation and Adipogenesis through Wnt Regulation in Ovariectomized Rats and 3 T3-L1 Cells. *Journal of Biomedical Science* **2019**, *26* (1), 1–12. https://doi.org/10.1186/s12929-019-0556-3.

(31)   Barcelona-Estaje, E.; Dalby, M. J.; Cantini, M.; Salmeron-Sanchez, M. You Talking to Me? Cadherin and Integrin Crosstalk in Biomaterial Design. *Advanced Healthcare*

Materials. John Wiley and Sons Inc March 1, 2021. https://doi.org/10.1002/adhm.202002048.

(32)   Cosgrove, B. D.; Mui, K. L.; Driscoll, T. P.; Caliari, S. R.; Mehta, K. D.; Assoian, R. K.; Burdick, J. A.; Mauck, R. L. N-Cadherin Adhesive Interactions Modulate Matrix Mechanosensing and Fate Commitment of Mesenchymal Stem Cells. *Nature Materials* **2016**, *15* (12), 1297–1306. https://doi.org/10.1038/nmat4725.

(33)   Haÿ, E.; Dieudonné, F. X.; Saidak, Z.; Marty, C.; Brun, J.; da Nascimento, S.; Sonnet, P.; Marie, P. J. N-Cadherin/Wnt Interaction Controls Bone Marrow Mesenchymal Cell Fate and Bone Mass During Aging. *Journal of Cellular Physiology* **2014**, *229* (11), 1765–1775. https://doi.org/10.1002/jcp.24629.

(34)   Passanha, F. R.; Geuens, T.; Konig, S.; van Blitterswijk, C. A.; LaPointe, V. L. Cell Culture Dimensionality Influences Mesenchymal Stem Cell Fate through Cadherin-2 and Cadherin-11. *Biomaterials* **2020**, *254*. https://doi.org/10.1016/j.biomaterials.2020.120127.

(35)   Zhu, M.; Lin, S.; Sun, Y.; Feng, Q.; Li, G.; Bian, L. Biomaterials Hydrogels Functionalized with N-Cadherin Mimetic Peptide Enhance Osteogenesis of HMSCs by Emulating the Osteogenic Niche. *Biomaterials* **2016**, *77*, 44–52. https://doi.org/10.1016/j.biomaterials.2015.10.072.

(36)   Marie, P. J.; Haÿ, E.; Saidak, Z. Integrin and Cadherin Signaling in Bone: Role and Potential Therapeutic Targets. *Trends in Endocrinology and Metabolism*. Elsevier Inc. November 1, 2014, pp 567–575. https://doi.org/10.1016/j.tem.2014.06.009.

(37)   Marie, P. J. N-Cadherin-Wnt Connections and the Control of Bone Formation. **2009**, *6* (4), 150–156. https://doi.org/10.1138/20090372.

(38) Marie, P. J. Role of N-Cadherin in Bone Formation. *Journal of Cellular Physiology* **2002**, *190* (3), 297–305. https://doi.org/10.1002/JCP.10073.

(39) Chang, J.; Liu, F.; Lee, M.; Wu, B.; Ting, K.; Zara, J. N.; Soo, C.; al Hezaimi, K.; Zou, W.; Chen, X.; Mooney, D. J.; Wang, C. Y. NF-KB Inhibits Osteogenic Differentiation of Mesenchymal Stem Cells by Promoting β-Catenin Degradation. *Proceedings of the National Academy of Sciences of the United States of America* **2013**. https://doi.org/10.1073/pnas.1300532110.

(40) Zha, L.; He, L.; Liang, Y.; Qin, H.; Yu, B.; Chang, L.; Xue, L. TNF-α Contributes to Postmenopausal Osteoporosis by Synergistically Promoting RANKL-Induced Osteoclast Formation. *Biomedicine and Pharmacotherapy* **2018**, *102*, 369–374. https://doi.org/10.1016/j.biopha.2018.03.080.

(41) Mosser, D. M.; Edwards, J. P. Exploring the Full Spectrum of Macrophage Activation. *Nature Reviews Immunology*. December 2008, pp 958–969. https://doi.org/10.1038/nri2448.

(42) Pino, A. M.; Ríos, S.; Astudillo, P.; Fernández, M.; Figueroa, P.; Seitz, G.; Rodríguez, J. P. Concentration of Adipogenic and Proinflammatory Cytokines in the Bone Marrow Supernatant Fluid of Osteoporotic Women. *Journal of Bone and Mineral Research* **2010**, *25* (3), 492–498. https://doi.org/10.1359/jbmr.090802.

(43) Kim, W.-K.; Choi, E.-K.; Sul, O.-J.; Park, Y.-K.; Kim, E.-S.; Yu, R.; Suh, J.-H.; Choi, H.-S. Monocyte Chemoattractant Protein-1 Deficiency Attenuates Oxidative Stress and Protects against Ovariectomy-Induced Chronic Inflammation in Mice. *PLoS ONE* **2013**, *8* (8), e72108. https://doi.org/10.1371/journal.pone.0072108.

(44)   Killaars, A. R.; Walker, C. J.; Anseth, K. S. Nuclear Mechanosensing Controls MSC Osteogenic Potential through HDAC Epigenetic Remodeling. https://doi.org/10.1073/pnas.2006765117/-/DCSupplemental.

(45)   Hendriks, D.; Macdougald, O.; Bernkopf, D.; de Winter, T. J. J.; Nusse, R. Running Against the Wnt: How Wnt/β-Catenin Suppresses Adipogenesis. *Frontiers in Cell and Developmental Biology | www.frontiersin.org* **2021**, *9*, 627429. https://doi.org/10.3389/fcell.2021.627429.

(46)   Nelson, W. J.; Nusse, R. *Convergence of Wnt,-Catenin, and Cadherin Pathways*.

(47)   Hay, E. H.; Laplantine, E.; Geoffroy, V.; Frain, M.; Kohler, T.; Müller, R.; Marie, P. J. N Cadherin Interacts with Axin and LRP5 To Negatively Regulate Wnt/-Catenin Signaling, Osteoblast Function, and Bone Formation. *Molecular and Cellular Biology* **2009**, *29* (4), 953–964. https://doi.org/10.1128/MCB.00349-08.

(48)   Manuel Baizabal-Aguirre, V.; Tyagi, A. K.; Hottiger, M. O.; Ma, B. Crosstalk between Wnt/β-Catenin and NF-KB Signaling Pathway during Inflammation. 2016, 7, 1. https://doi.org/10.3389/fimmu.2016.00378.

Chapter 7

Conclusions and Future Directions

Sections as published in Advanced Healthcare Materials, 2021, 2001948

7.1   Summary of Findings

Factors that MSC secrete are crucial to their therapeutic efficacy[1]. However, MSCs expansion *in vitro* can decrease their regenerative properties[2]. Additionally, direct injection of MSCs (without any carrier) does not promote their survival or maintain their secretory properties during *in vivo* delivery[3]. This thesis focused on developing hydrogel platforms to direct and maintain MSC secretory phenotypes during *in vitro* expansion and *in vivo* delivery. We used PEG-based synthetic macromers reacted via bio-click reactions to create hydrogel environments to direct matrix mechanics, MSC-matrix interactions, and MSC-MSC contacts. By precisely controlling the cellular microenvironment, we developed an understanding of how biophysical factors can be tuned to influence MSC secretory properties.

To obtain clinically relevant numbers, human hMSCs are often expanded on stiff substrates (e.g., tissue culture polystyrene (TCPS) or polystyrene microcarriers), which decrease their multipotency and induce replicative senescence[4,5]. However, how TCPS expansion alters other MSC properties, such as mechanosensing capacity and secretion, are not known. In Chapter 3, we first sought to quantify how serial expansion of hMSCs on TCPS influences their proliferation, expression of cell surface markers, Yes-associated protein (YAP)-mediated mechanosensing, and secretory properties. hMSCs were cultured on TCPS and passaged every three days up to 12 passages (P12). After only 5 passages (P5), hMSCs had decreased proliferation and expression of stem cell-surface markers (e.g., CD105, CD90, CD73). Decreased YAP nuclear localization,

indicating a loss of mechanosensing ability, and decreased cytokine secretion, were observed at later passages (P11-P12). Collectively, these results show significant reduction in the functional properties of hMSCs during TCPS expansion.

We next investigated the capacity of hydrogel matrices to rescue the hMSC properties lost during expansion. hMSCs of early (P1-P2), middle (P5-P6), and late (P11-P12) passages were transferred onto poly(ethylene glycol) hydrogels (Young's modulus~1kPa) synthesized with a photoinitiated thiol-ene reaction and modified with RGD (to promote cell attachment). The drift in cell surface marker expression observed at middle passages (P5) on TCPS was reversed on hydrogels. We observed a ~50% increase in hMSCs positive for CD105, CD90, and CD73 after 9 days of hydrogel culture. Hydrogel culture also increased secretion of cytokines involved in inflammatory signaling, cell growth, and trafficking for both early and late passage hMSCs. Together, these results suggest that hydrogel interventions may be useful for rescuing secretory properties of serially expanded hMSCs.

Results from Chapter 3 supported the notion that biophysical properties of 2D hydrogels can be used to recover MSC secretion after *in vitro* expansion. However, there is still a need to design material systems to maintain MSC properties during *in vivo* delivery. To this end, in Chapter 4, we designed a granular hydrogel system, comprised of micron-scale PEG-based hydrogels, to control MSC cell-cell and cell-matrix interactions in 3D. Individual microgels were fabricated using an inverse suspension polymerization in hexanes. Microgels were created using multi-arm PEG macromers functionalized with dibenzocyclooctyne (DBCO) and azide macromers, while an applied shear force was varied to control microgel size during polymerizations. Three different microgel populations, with small (~10 µm), medium (~100 µm), and large (~200µm) diameters, were co-assembled with hMSCs to create distinct clustering phenotypes. MSCs embedded in 200

µm diameter microgel networks resided in large clusters (~40 cells), MSCs in 100 µm diameter microgels resided in small clusters (~6 cells), and MSCs in 10 µm diameter microgel networks resided primarily as single cells. Using a membrane-based cytokine array, we measured an overall increase in secretion from hMSCs cultured in scaffolds that promoted clustering; over 60% of the measured cytokines were most elevated by hMSC in the 200 µm diameter microgel networks.

Next, we sought to understand if cell-cell interactions, mediated by N-cadherin, were involved in promoting MSC secretion. N-cadherin protein expression was elevated in the large hMSC clusters present in 200 µm scaffolds. Additionally, blocking N-cadherin interactions with antibodies resulted in a global decrease of secretion from MSCs in all three clustering conditions. After identifying N-cadherin as partially mediating these differences, microgel formulations were modified with an N-cadherin epitope, HAVDI, to mimic cell-cell interactions via MSC interactions with the microgel surfaces. hMSCs cultured in HAVDI functionalized scaffolds, even the non-clustered cells in 10µm diameter microgel networks, had greatly elevated secretory properties. Over 85% of all measured cytokines had elevated concentrations across all clustering phenotypes. Together, these results describe a microgel-based granular hydrogel system to tailor hMSCs secretory properties for *in vivo* delivery.

Exploiting our understanding of the influence of pore-directed cell clustering and the inclusion of N-cadherin peptide mimetics on hMSC secretion (Chapter 4), we next tested the bone regeneration capacity of granular hydrogel scaffolds engineered to elevate rMSC secretory properties (Chapter 5). First, we designed degradable formulations of the granular hydrogel systems by synthesizing an ester-linked PEG-DBCO; a molecule susceptible to degradation by hydrolysis and cell-secreted esterase. As factors secreted by MSCs are immunomodulatory, we chose to deliver rat MSCs (rMSCs) into wild-type rats with intact immune systems instead of hMSCs

into nude rats with modified immune systems. Therefore, we conducted *in vitro* experiments to compare the influence of cell clustering and HAVDI inclusion on rMSC versus hMSCs secretome. In this study, we utilized both pore dimensions (~200 µm) and HAVDI inclusion to create scaffolds capable of achieving highly secretory rMSCs. As is seen in hMSCs, HAVDI inclusion increased secretion of all measured factors from rMSCs; including key growth factors involved in bone regeneration, such as VEGF-A and PDGF-AA, and anti-inflammatory factors known to resolve inflammation, such as IL-4 and IL-13.

The *in vivo* experimental design included four scaffold conditions: (i) to elevate rMSC secretion (HAVDI+rMSCs), (ii) to provide a non-secretory cellular control (RGD+rMSCs), (iii) to control for HAVDI effects on endogenous cells (HAVDI), and (iv) to provide an acellular control (RGD). Scaffolds were implanted into 6 mm critical-sized rat calvarial defects and microgel degradation and rMSC retention were monitored using an *in vivo* imaging system (IVIS) over 4 weeks. Neither cellularity nor HAVDI inclusion affected microgel degradation, and all formulations were completely degraded over the course of 28 days. However, Qdot labeled rMSCs were undetectable *in vivo*. Further experiments are needed to confirm if the rMSCs survived transplantation, and if so, for how long. Lastly, we observed no differences in bone volume with microcomputed tomography (µCT) at 4 and 8 weeks between defects with microgel formulations compared with defects without any treatment. Further suggesting that the rMSCs likely did not survive for any appreciable amount of time in this study. Overall, these results indicate that microgel formulations modified with only RGD and HAVDI were not sufficient to promote rMSCs retention or induce bone regeneration *in vivo*. Future *in vivo* studies with microgels modified with factors that might promote rMSC survival and proliferation are needed.

While Chapter 5 explored the use of granular hydrogels for an i*n vivo* application, Chapter 6 utilized these material systems to better understand how MSC secretory properties change with disease. Specifically, we studied factors that are secreted by MSCs isolated from osteoporotic environments—specifically from ovariectomized rats (OVX rMSCs)—as a function of cell-cell interactions. We controlled cell clustering by encapsulating OVX and SHAM control rMSCs in granular scaffolds (developed in Chapter 4) comprised of microgel with varied diameters (~10 µm, ~100 µm, and ~200 µm). OVX rMSCs residing as large clusters (~30 cells/cluster) in ~200 µm scaffolds had elevated secretory properties. About 97% of factors were elevated in rMSC large clusters compared to 79% in SHAM rMSC controls. Further, the secretory profile of OVX rMSC in large clusters had an anti-osteogenic and pro-resorptive bias. We observed higher secretion of Activin A, CXCL1, CX3CL1, MCP-1, TIMP1, TNF-α by OVX rMSCs compared to SHAM rMSCs.

Interestingly, the pro-resorptive bias was only observed in the secretory profile of OVX rMSCs in large clusters. Therefore, we hypothesized that cell-cell interactions, such as cadherin signaling, may be involved. When we measured the gene expression of 7 different cadherins, we observed an ~4-fold higher N-cadherin expression in OVX rMSCs, both as clusters and as single cells. By blocking N-cadherin binding in the large OVX rMSC clusters, the secretion of several pro-resorptive cytokines (e.g., TIMP-1, MCP-1) was selectively decreased compared to blocked SHAM rMSCs (i.e., healthy control).

Overall, this thesis work developed hydrogel microenvironments to direct and study MSC secretory properties during *in vitro* culture and *in vivo* delivery. We designed PEG-based culture platforms—with tailored matrix mechanics, porosity, and integrin and cadherin binding epitopes—to understand how biophysical cues can control MSC secretion. We also tested the efficacy of

MSC-laden granular hydrogels for bone tissue engineering applications. Lastly, we utilized these materials to improve our understanding of the molecular mechanisms involved in MSC secretion. Specifically, we characterized the influence of N-cadherin mediated cell-cell contacts on the secretome of healthy and osteoporotic MSCs.

7.2 Engineering the next generation of precision hydrogels to direct MSC secretion

7.2.1 Where we have been and where we are going?

Over the last two decades, the increased understanding of MSCs has caused a shift in their therapeutic use. Once primarily focused on identifying ideal culture conditions to induce MSC differentiation, researchers are now transitioning towards investigating microenvironments that can direct the MSC secretome. Initial reliance on TCPS and mechanical signaling cues has given way to expanding and delivering MSCs in highly controlled 2D and 3D microenvironments containing multiple biophysical and biochemical stimuli. While MSC culture on TCPS provides a simple method for expansion and characterization, other studies have revealed that continuous culture on stiff substrates can bias MSCs towards an osteogenic fate, cause loss of multipotency, and decrease their stemness.[26] In addition to identifying specific stiffness ranges, experimenters have identified specific transcription factors, genes, growth factors, and media cocktails to promote MSC commitment towards a particular lineage or pathway. These early investigations were essential for the advancement of MSC biology and identifying methods to harness the vast potential of MSCs for end use in a clinical environment.

Later, bioengineers and materials scientist began to use hydrogels as 2D and 3D culture platforms for MSCs, in some cases aiming to recapitulate the in vivo tissue environment. Hydrogel matrices allow control of the cell's surrounding microenvironment, enabling end-users to tailor material properties such as matrix modulus, viscoelasticity, porosity, and degradability. Published

work demonstrates the individual effects of the aforementioned hydrogel properties on MSC functions (see Sections 2-3). In relation to the MSC secretome, more recent studies have demonstrated the direct influence of matrix stiffness and viscoelasticity on global secretion. Additionally, hydrogel porosity and degradation have been used to direct MSC clustering and promote secretion by increasing cell-cell contacts. However, the underlying mechanisms responsible for increased MSC secretion due to specific hydrogel properties have yet to be elucidated.

To continue to understand the biophysical regulation of MSC secreted factors, sophisticated hydrogel culture platforms must be designed and employed. One critical material characteristic of the ECM found in many tissues is the viscoelasticity, or the ability to deform under constant applied strain. Viscoelastic properties in a material can direct MSC cell spreading, mechanotransduction, and cell fate.[6] However, the effects of viscoelasticity on the MSC secretome has yet to be fully explored. Additionally, the influence of temporal changes in the matrix, both locally and macroscopically, on MSC properties should be more thoroughly investigated, and many dynamic biomaterials matrices could prove beneficial. Materials allowing for in situ control over stiffening, softening, or degradation should be employed to study how temporal changes in matrix modulus and degradability can influence the MSC secretory profile. In addition, platforms utilizing photo or chemical patterning techniques to create gradients of mechanical properties or of chemical signals may prove useful to optimize the mechanical and/or chemical dosages needed to achieve a specific MSC secretory profile. As MSC secreted factors are known to influence other cell types in vivo, the development of more sophisticated in vitro co-culture platforms that allow control of the spatial proximity of cells and control of cell-cell interactions will provide insight as to how secreted factors influence cellular crosstalk. Finally, culturing methods to test the influence

of other material properties known to direct cellular behavior, such as topography, surface charge, and surface roughness, on MSC secretion should be investigated. By thoroughly understanding how specific material properties and matrix interactions influence MSC secretion, researchers will be able to design improved expansion and delivery platforms capable of improving clinical translation of MSC-based therapies.

Another advantage of using hydrogels as MSC culture environments is the ease of systematic incorporation of biochemical compounds (i.e., small molecules, peptides, growth factors, cytokines, etc.) into the material system. Bio-orthogonal conjugation methods and/or traditional adsorption and affinity methods allow MSCs to receive both biophysical and biochemical stimuli simultaneously. Receptor dynamics, local concentrations, etc. can be highly dependent on the matrix environment. Previous studies have investigated the influence of various bioactive factors such as, cytokines (i.e., IFN-γ and TNF-α), growth factors (i.e., BMP-2, TGF-β1, and VEGF), and small molecules (i.e., estradiol, purmorphamine, and kartogenin) on MSC cell fate and secretion profile. With regard to influencing MSC secretion, cell priming with biochemical cues (e.g., pro-inflammatory) can be advantageous to induce a specific secretory profile (e.g., anti-inflammatory) or increase secretion of a specific factor (e.g., IL-10). However, the altered secretion profile is often short-lived; once the appropriate cue is removed, MSCs can revert to their steady state profile. To overcome such challenges, a combinatorial approach requiring the use of hydrogels with biochemical treatments may promote sustainable alterations to the MSC secretory profile (Figure 7.1).

Designing the next generation of hydrogels for directing the MSC secretome
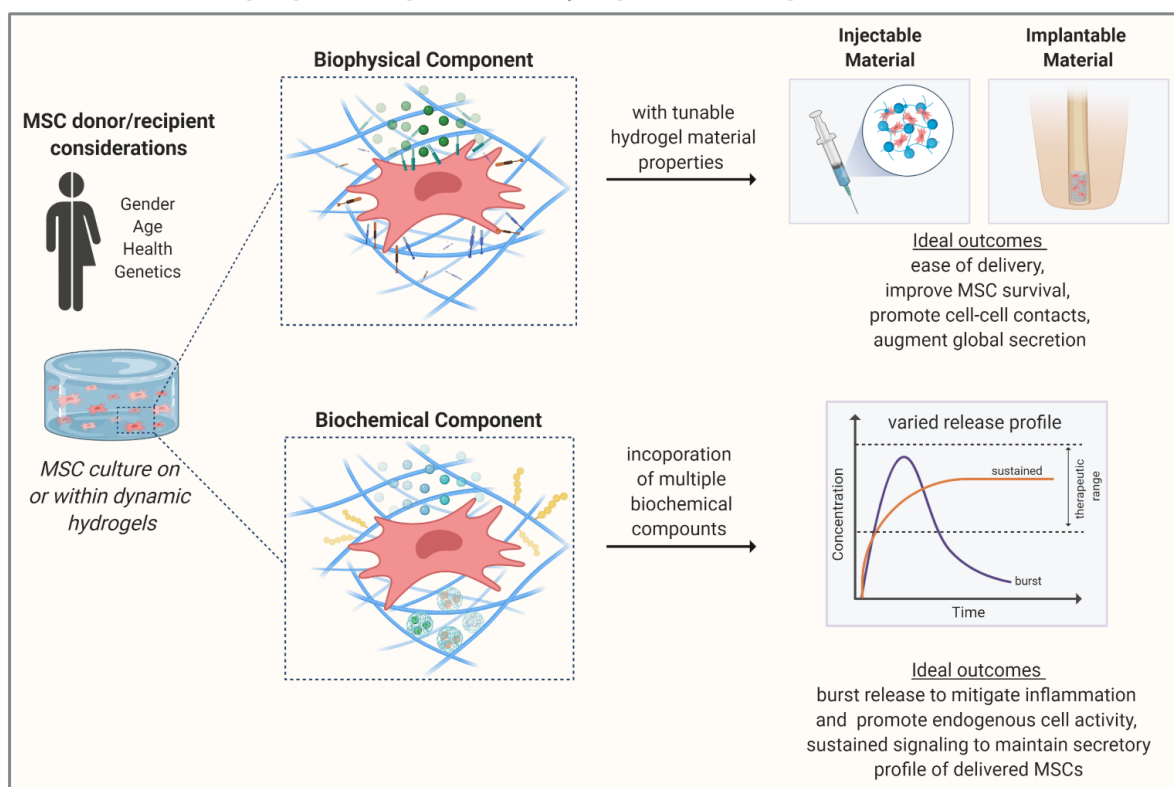
Figure 7.1 Design considerations for the next generation of hydrogels to direct the MSC secretome. Prior to hydrogel use, MSC donor characteristics, such as, gender, age, health, and genetics, must be evaluated. A hydrogel platform with specific material properties can then be utilized for MSC culture. Material characteristics should be chosen based on whether the hydrogel will be injected or implanted, in addition to how these properties will affect the MSC secretome. Furthermore, various biochemical compounds can be incorporated into the material system. Specific release profiles of bioactive factors can be obtained depending on how the molecules are incorporated into the hydrogel system.

Methods, including nanoparticle delivery, bulk adsorption, or direct tethering of bioactive factors into hydrogels, could be used to direct the secretion of encapsulated MSCs for longer time scales than what can be achieved with traditional priming methods. Several molecular signaling pathways have been implicated in governing MSC secretory activity, including NF-kB, Smad, VEGF, and β-catenin. Small molecules, genetic components, proteins, or peptide fragments could be used to either inhibit or enhance specific pathways of interest. Inclusion of biochemical compounds by matrix-immobilization (i.e., direct tethering of a molecule or loaded nanoparticle)

to hydrogels would enable sustained presentation to MSCs, whether internalized or through receptor binding. A combination of drug loading strategies, such as bulk adsorption and molecule conjugation, could be used to deliver secretory enhancing molecules sequentially or in parallel and affect not only MSCs within the hydrogel, but surrounding endogenous cells once delivered *in vivo*. The combination of biochemical signals with material design strategies has the potential to improve both the innate and altered MSC secretions.

Specifically for bone regeneration applications, MSC secretory profiles could be tuned with a combination of biochemical and biophysical regulation. Future research should focus on characterizing how exposure to routinely used osteoinductive factors—such as BMP-2, TGF-β, calcium phosphate, dexamethasone, and hydroxyapatite—influences MSC secretory profiles. Further, exploring the temporal changes to MSC secretions during osteoblastic differentiation may help illuminate alternative biochemical regulation of MSC secretory properties. In addition, biophysical cell-matrix cues, such as culture on substrates designed to mimic the bone ECM, may cause MSCs to secrete factors to promote osteoprogenitor differentiation and osteoblast matrix deposition. While stiffness is known to influence MSC osteogenic differentiation, the influence of stiffness on MSC osteoinductive factor secretion has not been fully explored. Finally, the combinatorial effects of cell-matrix cues and biochemical signaling could be used to engineer hydrogel environment to deliver MSCs with optimized secretory profile for bone regeneration applications.

While the focus of this thesis has been on measuring final outputs, i.e., proteins that MSCs are secreting, more work is needed to further understand the molecular pathways dictating the composition and concentration of the MSC secretome. Multiple studies have shown that material stiffness influences MSC secretion, which begs the question: are the often-studied rheostats

governing MSC fates, specifically YAP and TAZ, involved in regulating their secretory properties? Or is it a different mechanotransduction mechanism all together? Are there explicit stiffness ranges, ECM ligands, viscoelastic time scales, or cell cluster sizes that reliably lead to specific secretory profiles, as is observed with the specific material properties needed to direct MSC proliferation, migration, and differentiation? Additionally, multiple research groups have determined that N-cadherins are key regulators of MSC paracrine activity. However, further studies are needed to identify the downstream regulators of N-cadherin signaling that lead to improved secretory outcomes. Furthermore, are other pathways capable of facilitating cell-cell interactions, such as E-cadherins dimerization or gap junctions? This warrants further investigation pertaining to their potential involvement in regulating MSC secretion. Understanding the synergistic effects of mechanical and biochemical cues on the MSC secretome will be key in the rational design of the next generation of hydrogel platforms.

7.2.2 Importance of secretome measurement techniques

When investigating the secretome, it is important to note the differences in methods for detection. Proper characterization of the MSC secretome will aid in clinical utility once a specific profile is obtained. The identification of protein components is commonly obtained using two proteomic approaches: immunological based or shot-gun based (Figure 7.2).

Immunological-based assays offer high specificity, sensitivity, and reproducibility. These aspects are critical as secreted proteins are often present at low levels in media, ranging from picograms to nanograms. Examples of immunological-based assays include: enzyme-linked immunosorbent assays (ELISA), multi-plex antibody bead-based assays, microarrays, western blotting, and cytokine antibody arrays. While these assays are highly specific, they are limited to the detection of known proteins. However, while some of these systems, such as cytokine arrays,

are advantageous to broadly characterize the differences between experimental conditions, they

often do not provide the level of quantification needed to compare results between research groups.

	Shot-gun based proteomics: exploratory, best for identifying unknowns	Immunological-based assays: assays for testing known proteins conducted with high specificity, sensitivity, and reproducibility		
	Mass Spectrometry	Cytokine Array	Traditional ELISA	Multi-plex ELISA
Quantitative/ qualitative	quantitative	semi-quantitative	quantitative	quantitative
Sample concentration	μM	pg-ng	pg-ng	pg
Sample volume	< 10 μL	100 μL - 1 mL	100 - 200 μL	< 50 μL
Sample preparation	minimal/ exstensive	minimal	minimal	minimal
Instrumentation	mass spectrometer	CCD camera, laser scanner	plate reader	luminex
Analysis	extensive	minimal	minimal	minimal

Figure 7.2 Proteomic approaches used to detect and quantify MSC secretory components.
Shot-gun based proteomics (primarily mass spectrometry based) are used for the detection of unknown or unique proteins. Once these proteins are identified, publicly available databases and bioinformatics can be used for pathway analyses to determine specific protein roles (extensive analyses). Immunological-based assays are used for testing a broad range of known proteins. These assays are often user-friendly involving minimal sample preparation and analysis methods resulting in quantitative or semi-quantitative outcomes.

The shot-gun based proteomics approach is more exploratory and used for identification of

unknown or unique secreted proteins. Examples of such techniques include: liquid

chromatography with tandem mass spectrometry, matrix-assisted laser desorption/ionization-time

of flight, quadrupole time-of-flight mass spectrometry, and 2D gel electrophoresis. Once specific

proteins are identified, publicly available databases and bioinformatics tools can be used for

pathway analyses to determine protein roles of biological and clinical relevance. Compared to

immunological-based assays, shot-gun based proteomics approaches require more specialized instrumentation and intensive downstream data processing.

7.3 Future Directions

7.3.1 Realtime tracking of delivered MSCs in the rat calvarial defect *in vivo*

In the bone regeneration study conducted in Chapter 5, rMSCs were undetectable after 24 hours in vivo and no bone formation was observed for rMSC laden, or cell-free scaffolds delivered to into rat calvarial defects. To better understand why bone mineral deposition was not achieved in this study, we must first determine the fate, concerning both survival and differentiation, of the delivered rMSCs.

As Qdot labeled rMSCs were not detected with the IVIS, the immediate next step will be to modify the *in vivo* imaging protocol. Instead of the IVIS Spectrum (Perkin-Elmer), we will utilize a confocal imaging system with increased excitation laser power and emission sensitivity. Qdot labeled rMSC-laden microgels will be imaged *in vitro* and in rat cadavers to confirm Qdot detect and optimize imaging protocol before *in vivo* imaging. If the Qdots are still undetectable with confocal microscopy, rMSCs will be engineered to express near-infrared fluorescent proteins, optimized for IVIS detection. *In vitro* and rat cadaver experiments will be repeated with the genetically engineered rMSCs. Based on the results of these *in vitro* experiments, an optimal rMSC labeling, either Qdots or fluorescent proteins, and the corresponding imaging protocol will be established. Next, fluorescently labeled rMSCs will be encapsulated into microgels and implanted into critical-sized rat calvarial defects. Defects will be imaged at 8 hours, 24 hours, 48 hours, and 72 hours after implantation. The timepoints may be skipped or extended based on rMSC signal intensity. After this experiment is conducted, the scaffolds will be fixed, sectioned, and imaged to visualize the labeled MSCs and confirm *in vivo* imaging results. Additionally, delivered

rMSCs will be stained with primary antibodies against markers of osteogenic differentiation (ALP, OCN, Osterix) and MSC stemness (CD90, CD105, CD73) to determine their fate. In addition to establishing an optimized imaging protocol, these results will inform us of the timing of rMSC survival to better design the next microgel scaffolds for future bone regeneration studies. The outlined experiments will not only shed light on the results of the study conducted in Chapter 5 but could have broader implications on understanding the mechanism of action of MSCs in bone regeneration (i.e., secretion versus differentiation).

7.3.2 Explore the acute foreign body response to rMSC-laden granular hydrogel scaffolds

In vivo implantation of synthetic biomaterials, such as the PEG-based hydrogels developed in this thesis, elicits a foreign body response from the host immune system[7]. Upon implantation, the initial acute inflammatory phase causes dendritic cell and neutrophil recruitment to the implant site. These cells release pro-inflammatory cytokines, reactive oxygen species (ROS), and chemokines to recruit other inflammatory immune cells, such as macrophages to the implant site[8].

The initial release of pro-inflammatory factors and ROS can have detrimental effects for delivered cells. In Chapter 5, we delivered rMSC-laden scaffolds with pore dimensions on the order of ~200 µm, which allow for rapid cell infiltration. However, the rMSCs were undetectable *in vivo* after only 24 hours. We hypothesize that the acute foreign body response is the likely cause of rMSC death.

Based on the results of the studies outline in Section 7.3.1, we will have an increased understanding of the timeframe of rMSC survival. Using this timing as a guide, future studies should more thoroughly characterize the immune response to rMSC laden porous granular hydrogels in the calvarial defect. For example, hydrogels should be explanted at earlier time points (i.e., hours, 1-2 days) to understand the timing of neutrophil and macrophage infiltration.

Experimental methods like fluorescence activated cell sorting, transcriptomics, and high throughput image analysis could be used to determine the identities of infiltrating cells and characterize MSC-immune interactions across multiple timepoints.

After characterizing the cell types in involved in killing the rMSCs, future work should focus on modifying the microgel formulations to improve rMSC survival. One approach would be incorporate signals to directly inhibit the pro-inflammatory activities of immune cells. For example, we could include ligands, like TRAIL and Fas, to cause neutrophil apoptosis[9,10]. We could also release anti-inflammatory factors, such as IL-4, IL-10, or IL-13 to polarize endogenous macrophages from pro-inflammatory to anti-inflammatory phenotypes[11,12]. Alternatively, we could modify a subset of the microgel to neutralize or sequester the harmful factors directly. For example, incorporation of a TNF-α sequestering peptide (WP9QY) into hydrogels can increase the survival of encapsulated cells in challenging inflammatory environments[13]. Additionally, we could signal to the rMSCs; either including factors to increase proliferation (e.g., FGF, PDGF[14]) or promote secretion of anti-inflammatory factor (e.g., include tetrandrine to elevate PGE2 secretion[15]. Lastly, we could modify the material properties of the scaffolds itself, such as decreasing the porosity to protect MSCs from interacting physically with immune cells.

7.3.3 Investigate the influence of signaling pathways downstream of N-cadherin on MSC secretion

Throughout this thesis—in hMSCs, in healthy rMSCs, and in OVX rMSCs—increased cell clustering resulted in elevated secretory properties, specifically in an N-cadherin dependent manner. However, we did not delve deeper into the potential pathways, downstream of bound N-cadherins, that might drive the transcription of secreted factors. The binding of extracellular N-cadherins initiates the intracellular formation of the cadherin-catenin complex, which both

stabilizes the bound N-cadherins and links them to the actin cytoskeleton (Figure 7.3a)[16,17]. The key proteins present in the intracellular side of the complex are multiple catenins: p120 catenin, α-catenin, and β-catenin. Based on findings in literature, β-catenin is the most likely of the three catenins to be involved the gene transcription of MSC secreted factors[16,18,19]. Specifically, β-catenin can interfere with the NF-κB pathway, both as a suppressor and an activator[18,20]. These interactions regulate transcription of multiple cytokines and inflammatory factors, including IL-1 and TNF-α[21]. To begin to explore these relationships, we conducted a preliminary experiment characterizing β-catenin localization in OVX and SHAM rMSCs.

In Chapter 6, we measured higher N-cadherin expression in OVX rMSCs compared to SHAM rMSC controls. As β-catenin is involved in stabilizing bound N-cadherin, we next characterized β-catenin membrane localization in clusters of OVX and SHAM rMSCs cultured on TCPS using immunostaining (Figure 7.3b). Using Harmony software (Perkin-Elmer), we quantified the intensity of β-catenin in the nuclear, cytoplasmic, and membrane regions of cells in contact with one another. The nuclear to membrane ratio of β-catenin were lower in OVX rMSC compared to SHAM (Figure 7.2c), potentially indicating greater membrane bound β-catenin in OVX rMSCs. Additionally, nuclear to cytoplasmic ratios of β-catenin were also significantly lower in OVX rMSCs, potentially resulting in decreased transcriptional activity (Figure 7.3d). Next, to determine if the membrane bound β-catenin was due to the formation of cadherin-catenin complex, we blocked N-cadherin interactions and remeasured β-catenin localization (right panel Figures 7.3c,d). Interestingly, blocking N-cadherin interactions resulted in increased β-catenin nuclear to membrane ratios in OVX rMSCs cell clusters (Figure 7.3c). This decrease was because of lower levels of membrane bound β-catenin, as indicated by raw intensity values (data not shown).
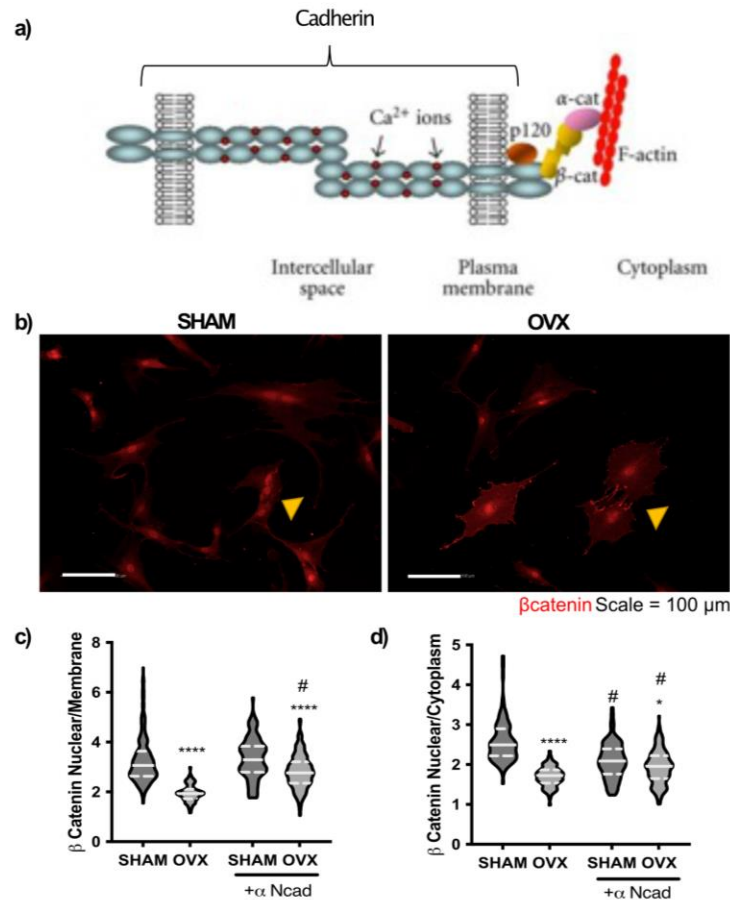
Figure 7.3 The influence of N-cadherin on β-catenin localization in SHAM and OVX rMSCs
(a) Schematic of the cadherin-catenin complex (b) Representative images of β-catenin in SHAM and OVX rMSCs cultured on TCPS. Scale bar = 100 µm. Yellow triangles indicated cells touching one another. Quantification of β-catenin nuclear to membrane ratios (c) and nuclear to cytoplasmic ratios (d). **** $p<0.0001$ between SHAM and OVX, # $p<0.0001$ between block versus unblocked.

N-cadherin blocking was also accompanied by an increased nuclear to cytoplasmic ratios of β-catenin, which may cause downstream changes to MSC secretome. As previously described, experiments in Chapter 6 determined that blocking N-cadherin in large clusters cultured in granular hydrogels reduced pro-resorptive factor secretion by OVX rMSCs (Figure 6.6). However, β-catenin experiments were conducted on 2D TCPS where MSC secretion was not measured.

These preliminary results indicate that β-catenin membrane localization is influenced by N-cadherin binding in OVX rMSCs. However, a direct causation has not been demonstrated. More research is needed to determine if OVX rMSC or healthy MSC secreted factors, specifically factors

transcribed downstream of NF-kB, are influenced by β-catenin nuclear localization. Immediate future studies should focus on analyzing β-catenin localization in 3D cell clusters. Further mechanistic experiments targeting N-cadherin binding and β-catenin expression are needed to fully understand the relationship between β-catenin/NF-kB pathways and clustered MSC secretion.

7.3.4 Precision hydrogels for MSC-based therapies

To move towards the translation of MSC-based therapies, it is important to realize a "one-size-fits-all" approach is clinically outdated. Donor/recipient characteristics such as gender, age, genetics, and overall health status (e.g., severity of disease) should be considered when developing material strategies for clinical translation. From this perspective, the evolution of 'precision biomaterials', tailored to deliver MSCs at the right dose with the right secretome for the tissue or disease, might be envisioned for personalized cell therapies[19]. The high tunability and versatility of hydrogels should enable progress towards this goal. To develop personalized MSC therapies, hydrogels could incorporate customized material chemistries, bioactive components, and patient-specific factors to promote tissue regeneration to treat disease. Once delivered, these hydrogel-based MSC therapies should acclimate to the patient's diseased microenvironment. For example, a change in the temperature, pH, or concentration of a cytokine in vivo might trigger release of a drug to stimulate MSC trophic factor secretion. In addition, in cases of autologous transplantation, precision hydrogel use during MSC expansion and delivery may have the ability to correct an undesired patient specific MSC secretory profile.

Overall, MSCs represent a cell population that can serve as an incredible source of bioactive factors. By exerting control over their microenvironment, the field is beginning to unravel the influence of both biophysical material properties and biochemical signals on the composition and

concentration of MSC trophic factor secretion. However, challenges remain with respect to the clinical translation of MSC-based therapies. MSCs lose many of their regenerative properties, such as stemness and secretion, during expansion on TCPS. Once delivered via injection, MSCs have low survival, retention, and engraftment rates in vivo. Additionally, the MSC secretion profile is rarely, intentionally directed before their clinical use. To address these challenges, we propose a precision biomaterial-based approach utilizing hydrogels with optimized biophysical properties, in combination with biochemical compound incorporation, to enhance and direct the MSC secretory profile. Once the ideal material design parameters are fully elucidated, this next generation of hydrogel based MSC-therapies will have immense clinical potential.

7.4 References

(1)   Wechsler, M. E.; Rao, V. v; Borelli, A. N.; Anseth, K. S. Engineering the MSC Secretome : A   Hydrogel   Focused   Approach. **2021**, *2001948*, 1–17. https://doi.org/10.1002/adhm.202001948.

(2)   Banfi, A.; Bianchi, G.; Notaro, R.; Luzzatto, L.; Cancedda, R.; Quarto, R. Replicative Aging and Gene Expression in Long-Term Cultures of Human Bone Marrow Stromal Cells. *TISSUE ENGINEERING* **2002**, *8* (6).

(3)   Ishihara, A. Effect of Intra-Medullar and Intra-Venous Infusions of Mesenchymal Stem Cells on Cell Engraftment by In-Vivo Cell Tracking and Osteoinductivity in Rabbit Long Bones: A Pilot Study. *Orthopedic & Muscular System* **2014**. https://doi.org/10.4172/2161-0533.1000172.

(4)   Wagner, W.; Horn, P.; Castoldi, M.; Diehlmann, A.; Bork, S.; Saffrich, R.; Benes, V.; Blake, J.; Pfister, S.; Eckstein, V.; Ho, A. D. Replicative Senescence of Mesenchymal Stem Cells:

A Continuous and Organized Process. *PLoS ONE* **2008**, *3* (5). https://doi.org/10.1371/journal.pone.0002213.

(5) Yang, C.; Tibbitt, M. W.; Basta, L.; Anseth, K. S. Mechanical Memory and Dosing Influence Stem Cell Fate. *Nature Materials* **2014**, *113*, 645–651. https://doi.org/10.1038/NMAT3889.

(6) Chaudhuri, O.; Cooper-White, J.; Janmey, P. A.; Mooney, D. J.; Shenoy, V. B. Effects of Extracellular Matrix Viscoelasticity on Cellular Behaviour. *Nature* **2020**, *584*, 535. https://doi.org/10.1038/s41586-020-2612-2.

(7) Saleh, L. S.; Bryant, S. J. The Host Response in Tissue Engineering: Crosstalk between Immune Cells and Cell-Laden Scaffolds. *Current Opinion in Biomedical Engineering* **2018**, *6* (March), 58–65. https://doi.org/10.1016/j.cobme.2018.03.006.

(8) Anderson, J. M. BIOLOGICAL RESPONSES TO MATERIALS. **2001**.

(9) Croker, B. A.; O'Donnell, J. A.; Nowell, C. J.; Metcalf, D.; Dewson, G.; Campbell, K. J.; Rogers, K. L.; Hu, Y.; Smyth, G. K.; Zhang, J. G.; White, M.; Lackovic, K.; Cengia, L. H.; O'Reilly, L. A.; Bouillet, P.; Cory, S.; Strasser, A.; Roberts, A. W. Fas-Mediated Neutrophil Apoptosis Is Accelerated by Bid, Bak,and Bax and Inhibited by Bcl-2 and Mcl-1. *Proceedings of the National Academy of Sciences of the United States of America* **2011**, *108* (32), 13135–13140. https://doi.org/10.1073/PNAS.1110358108/-/DCSUPPLEMENTAL.

(10) McGrath, E. E.; Marriott, H. M.; Lawrie, A.; Francis, S. E.; Sabroe, I.; Renshaw, S. A.; Dockrell, D. H.; Whyte, M. K. B. TNF-Related Apoptosis-Inducing Ligand (TRAIL) Regulates Inflammatory Neutrophil Apoptosis and Enhances Resolution of Inflammation. *Journal of Leukocyte Biology* **2011**, *90* (5), 855–865. https://doi.org/10.1189/JLB.0211062.

(11) Hachim, D.; LoPresti, S. T.; Yates, C. C.; Brown, B. N. Shifts in Macrophage Phenotype at the Biomaterial Interface via IL-4 Eluting Coatings Are Associated with Improved Implant Integration. *Biomaterials* **2017**, *112*, 95–107. https://doi.org/10.1016/j.biomaterials.2016.10.019.

(12) Hachim, D.; Lopresti, S. T.; Rege, R. D.; Umeda, Y.; Iftikhar, A.; Nolfi, A. L.; Skillen, C. D.; Brown, B. N. Distinct Macrophage Populations and Phenotypes Associated with IL-4 Mediated Immunomodulation at the Host Implant Interface. *Biomaterials Science* **2020**, *8* (20), 5751–5762. https://doi.org/10.1039/d0bm00568a.

(13) Lin, C. C.; Metters, A. T.; Anseth, K. S. Functional PEG-Peptide Hydrogels to Modulate Local Inflammation Induced by the Proinflammatory Cytokine TNFα. *Biomaterials* **2009**, *30* (28), 4907. https://doi.org/10.1016/J.BIOMATERIALS.2009.05.083.

(14) Farokhi, M.; Mottaghitalab, F.; Shokrgozar, M. A.; Ou, K. L.; Mao, C.; Hosseinkhani, H. Importance of Dual Delivery Systems for Bone Tissue Engineering. *Journal of Controlled Release* **2016**, *225*, 152–169. https://doi.org/10.1016/j.jconrel.2016.01.033.

(15) Yang, Z.; Concannon, J.; Ng, K. S.; Seyb, K.; Mortensen, L. J.; Ranganath, S.; Gu, F.; Levy, O.; Tong, Z.; Martyn, K.; Zhao, W.; Lin, C. P.; Glicksman, M. A.; Karp, J. M. Tetrandrine Identified in a Small Molecule Screen to Activate Mesenchymal Stem Cells for Enhanced Immunomodulation. *Scientific Reports 2016 6:1* **2016**, *6* (1), 1–10. https://doi.org/10.1038/srep30263.

(16) Nelson, W. J.; Nusse, R. *Convergence of Wnt,-Catenin, and Cadherin Pathways*.

(17) Barcelona-Estaje, E.; Dalby, M. J.; Cantini, M.; Salmeron-Sanchez, M. You Talking to Me? Cadherin and Integrin Crosstalk in Biomaterial Design. *Advanced Healthcare Materials*. John Wiley and Sons Inc March 1, 2021. https://doi.org/10.1002/adhm.202002048.

(18)   Chang, J.; Liu, F.; Lee, M.; Wu, B.; Ting, K.; Zara, J. N.; Soo, C.; al Hezaimi, K.; Zou, W.; Chen, X.; Mooney, D. J.; Wang, C.-Y.; Chien, S. NF-ΚB Inhibits Osteogenic Differentiation of Mesenchymal Stem Cells by Promoting β-Catenin Degradation. https://doi.org/10.1073/pnas.1300532110.

(19)   Imamura, A.; Kajiya, H.; Fujisaki, S.; Maeshiba, M.; Yanagi, T.; Kojima, H.; Ohno, J. Three-Dimensional Spheroids of Mesenchymal Stem/Stromal Cells Promote Osteogenesis by Activating Stemness and Wnt/β-Catenin. *Biochemical and Biophysical Research Communications* **2020**, *523* (2), 458–464. https://doi.org/10.1016/j.bbrc.2019.12.066.

(20)   Manuel Baizabal-Aguirre, V.; Tyagi, A. K.; Hottiger, M. O.; Ma, B. Crosstalk between Wnt/β-Catenin and NF-ΚB Signaling Pathway during Inflammation. **2016**, *7*, 1. https://doi.org/10.3389/fimmu.2016.00378.

(21)   Ma, B.; Fey, M.; Hottiger, M. O. WNT/β-Catenin Signaling Inhibits CBP-Mediated RelA Acetylation and Expression of Proinflammatory NF-ΚB Target Genes. **2015**. https://doi.org/10.1242/jcs.168542.

(22)   Aguado, B. A.; Grim, J. C.; Rosales, A. M.; Watson-Capps, J. J.; Anseth, K. S. Engineering Precision Biomaterials for Personalized Medicine. *Science Translational Medicine*. American Association for the Advancement of Science January 17, 2018. https://doi.org/10.1126/scitranslmed.aam8645.

Bibliography

Chapter 1

(1)   Friedenstein, A. J.; Gorskaja, U. F.; Kulagina, N. N. Fibroblast Precursors in Normal and Irradiated Mouse Hematopoietic Organs. Experimental Hematology 1976, 4 (5), 267–274.

(2)   Dominici, M.; Blanc, K. le; Mueller, I.; Marini, F. C.; Krause, D. S.; Deans, R. J.; Keating, A.; Prockop, D. J.; Horwitz, E. M. Minimal Criteria for Defining Multipotent Mesenchymal Stromal Cells . The International Society for Cellular Therapy Position Statement. Cytotherapy 2006, 8 (4), 315–317. https://doi.org/10.1080/14653240600855905.

(3)   Hass, R.; Kasper, C.; Böhm, S.; Jacobs, R. Different Populations and Sources of Human Mesenchymal Stem Cells (MSC): A Comparison of Adult and Neonatal Tissue-Derived MSC. Cell Communication and Signaling 2011, 9. https://doi.org/10.1186/1478-811X-9-12.

(4)   Pittenger, M. F.; Discher, D. E.; Péault, B. M.; Phinney, D. G.; Hare, J. M.; Caplan, A. I. Mesenchymal Stem Cell Perspective: Cell Biology to Clinical Progress. npj Regenerative Medicine. Nature Research December 1, 2019. https://doi.org/10.1038/s41536-019-0083-6.

(5)   Levy, O.; Kuai, R.; Siren, E. M. J.; Bhere, D.; Milton, Y.; Nissar, N.; De Biasio, M.; Heinelt, M.; Reeve, B.; Abdi, R.; Alturki, M.; Fallatah, M.; Almalik, A.; Alhasan, A. H.; Shah, K.; Karp, J. M. Shattering Barriers toward Clinically Meaningful MSC Therapies. Science advances. NLM (Medline) July 1, 2020, p eaba6884. https://doi.org/10.1126/sciadv.aba6884.

(6)   Murray, I. R.; Péault, B. Q&A: Mesenchymal Stem Cells - Where Do They Come from and Is It Important? BMC Biology 2015, 13 (1). https://doi.org/10.1186/s12915-015-0212-7.

(7)   Caplan, A. I. Why Are MSCs Therapeutic? New Data: New Insight. Journal of Pathology. J Pathol January 2009, pp 318–324. https://doi.org/10.1002/path.2469.

(8)   Osugi, M.; Katagiri, W.; Yoshimi, R.; Inukai, T.; Hibi, H.; Ueda, M. Conditioned Media from Mesenchymal Stem Cells Enhanced Bone Regeneration in Rat Calvarial Bone Defects. Tissue Engineering - Part A 2012, 18 (13–14), 1479–1489. https://doi.org/10.1089/ten.tea.2011.0325.

(9)   Fontaine, M. J.; Shih, H.; Schäfer, R.; Pittenger, M. F. Unraveling the Mesenchymal Stromal Cells' Paracrine Immunomodulatory Effects. Transfusion Medicine Reviews. W.B. Saunders January 1, 2016, pp 37–43. https://doi.org/10.1016/j.tmrv.2015.11.004.

(10)   English, K.; French, A.; Wood, K. J. Mesenchymal Stromal Cells: Facilitators of Successful Transplantation? Cell Stem Cell. Cell Stem Cell October 8, 2010, pp 431–442. https://doi.org/10.1016/j.stem.2010.09.009.

(11)   da Silva Meirelles, L.; Fontes, A. M.; Covas, D. T.; Caplan, A. I. Mechanisms Involved in the Therapeutic Properties of Mesenchymal Stem Cells. Cytokine & Growth Factor Reviews 2009, 20 (5–6), 419–427. https://doi.org/10.1016/j.cytogfr.2009.10.002.

(12)   da Silva Meirelles, L.; Fontes, A. M.; Covas, D. T.; Caplan, A. I. Mechanisms Involved in the Therapeutic Properties of Mesenchymal Stem Cells. Cytokine & Growth Factor Reviews 2009, 20 (5–6), 419–427. https://doi.org/10.1016/j.cytogfr.2009.10.002.

(13)   Herrera, M. B.; Bussolati, B.; Bruno, S.; Morando, L.; Mauriello-Romanazzi, G.; Sanavio, F.; Stamenkovic, I.; Biancone, L.; Camussi, G. Exogenous Mesenchymal Stem Cells

Localize to the Kidney by Means of CD44 Following Acute Tubular Injury. Kidney International 2007, 72 (4), 430–441. https://doi.org/10.1038/sj.ki.5002334.

(14)   Ogata, K.; Osugi, M.; Kawai, T.; Wakayama, Y.; Sakaguchi, K.; Nakamura, S.; Katagiri, W. Secretomes of Mesenchymal Stem Cells Induce Early Bone Regeneration by Accelerating Migration of Stem Cells. Journal of Oral and Maxillofacial Surgery, Medicine, and Pathology 2018, 30 (5), 445–451. https://doi.org/10.1016/j.ajoms.2018.04.002.

(15)   Katagiri, W.; Sakaguchi, K.; Kawai, T.; Wakayama, Y.; Osugi, M.; Hibi, H. A Defined Mix of Cytokines Mimics Conditioned Medium from Cultures of Bone Marrow-Derived Mesenchymal Stem Cells and Elicits Bone Regeneration. Cell Proliferation 2017, 50 (3), e12333. https://doi.org/10.1111/cpr.12333.

(16)   Nicola, M. Di; Carlo-Stella, C.; Magni, M.; Milanesi, M.; Longoni, P. D.; Matteucci, P.; Grisanti, S.; Gianni, A. M. Human Bone Marrow Stromal Cells Suppress T-Lymphocyte Proliferation Induced by Cellular or Nonspecific Mitogenic Stimuli. Blood 2002, 99 (10), 3838–3843. https://doi.org/10.1182/blood.V99.10.3838.

(17)   Zinöcker, S.; Vaage, J. T. Rat Mesenchymal Stromal Cells Inhibit T Cell Proliferation but Not Cytokine Production Through Inducible Nitric Oxide Synthase. Frontiers in Immunology 2012, 3 (APR), 62. https://doi.org/10.3389/fimmu.2012.00062.

(18)   Corcione, A.; Benvenuto, F.; Ferretti, E.; Giunti, D.; Cappiello, V.; Cazzanti, F.; Risso, M.; Gualandi, F.; Mancardi, G. L.; Pistoia, V.; Uccelli, A. Human Mesenchymal Stem Cells Modulate B-Cell Functions. Blood 2006. https://doi.org/10.1182/blood-2005-07-2657.

(19)   Viswanathan, S.; Shi, Y.; Galipeau, J.; Krampera, M.; Leblanc, K.; Martin, I.; Nolta, J.; Phinney, D. G.; Sensebe, L. Mesenchymal Stem versus Stromal Cells: International

Society for Cell & Gene Therapy (ISCT®) Mesenchymal Stromal Cell Committee Position Statement on Nomenclature. Cytotherapy 2019, 21 (10), 1019–1024. https://doi.org/10.1016/j.jcyt.2019.08.002.

(20) Galderisi, U.; Squillaro, T.; Peluso, G. Clinical Trials With Mesenchymal Stem Cells: An Update. Cell Transplantation 2016, 25, 829–848. https://doi.org/10.3727/096368915X689622.

(21) Chen, Y.-S. Mesenchymal Stem Cell: Considerations for Manufacturing and Clinical Trials on Cell Therapy Product. International Journal of Stem cell Research & Therapy 2016, 3 (1), 1–12. https://doi.org/10.23937/2469-570X/1410029.

(22) Squillaro, T.; Peluso, G.; Galderisi, U. Review Clinical Trials With Mesenchymal Stem Cells : An Update. Cell Transplantation 2016, 25, 829–848.

(23) Chen, Y.-S. Mesenchymal Stem Cell: Considerations for Manufacturing and Clinical Trials on Cell Therapy Product. International Journal of Stem cell Research & Therapy 2016, 3 (1), 1–12. https://doi.org/10.23937/2469-570X/1410029.

(24) Wagner, W.; Horn, P.; Castoldi, M.; Diehlmann, A.; Bork, S.; Saffrich, R.; Benes, V.; Blake, J.; Pfister, S.; Eckstein, V.; Ho, A. D. Replicative Senescence of Mesenchymal Stem Cells: A Continuous and Organized Process. PLoS ONE 2008, 3 (5). https://doi.org/10.1371/journal.pone.0002213.

(25) Jiang, T.; Xu, G.; Wang, Q.; Yang, L.; Zheng, L.; Zhao, J.; Zhang, X. In Vitro Expansion Impaired the Stemness of Early Passage Mesenchymal Stem Cells for Treatment of Cartilage Defects. Cell Death and Disease 2017, 8 (6). https://doi.org/10.1038/cddis.2017.215.

(26)   Wagner, W.; Horn, P.; Castoldi, M.; Diehlmann, A.; Bork, S.; Saffrich, R.; Benes, V.; Blake, J.; Pfister, S.; Eckstein, V.; Ho, A. D. Replicative Senescence of Mesenchymal Stem Cells: A Continuous and Organized Process. PLoS ONE 2008, 3 (5). https://doi.org/10.1371/journal.pone.0002213.

(27)   Wu, P. K.; Wang, J. Y.; Chen, C. F.; Chao, K. Y.; Chang, M. C.; Chen, W. M.; Hung, S. C. Early Passage Mesenchymal Stem Cells Display Decreased Radiosensitivity and Increased DNA Repair Activity. Stem Cells Translational Medicine 2017, 6 (6), 1504–1514. https://doi.org/10.1002/sctm.15-0394.

(28)   Banfi, A.; Bianchi, G.; Notaro, R.; Luzzatto, L.; Cancedda, R.; Quarto, R. Replicative Aging and Gene Expression in Long-Term Cultures of Human Bone Marrow Stromal Cells. Tissue Engineering 2002, 8 (6), 901–910. https://doi.org/10.1089/107632702320934001.

(29)   Rao, V. v.; Vu, M. K.; Ma, H.; Killaars, A. R.; Anseth, K. S. Rescuing Mesenchymal Stem Cell Regenerative Properties on Hydrogel Substrates Post Serial Expansion. Bioengineering & Translational Medicine 2018, No. June, 1–10. https://doi.org/10.1002/btm2.10104.

(30)   Qazi, T. H.; Mooney, D. J.; Duda, G. N.; Geissler, S. Biomaterials That Promote Cell-Cell Interactions Enhance the Paracrine Function of MSCs. Biomaterials 2017, 140, 103–114. https://doi.org/10.1016/j.biomaterials.2017.06.019.

(31)   Rao, V. V.; Vu, M. K.; Ma, H.; Killaars, A. R.; Anseth, K. S. Rescuing Mesenchymal Stem Cell Regenerative Properties on Hydrogel Substrates Post Serial Expansion. Bioengineering & Translational Medicine 2018, No. June, 1–10. https://doi.org/10.1002/btm2.10104.

(32)   Madl, C. M.; Heilshorn, S. C.; Blau, H. M. Bioengineering Strategies to Accelerate Stem Cell Therapeutics. Nature. Nature Publishing Group May 17, 2018, pp 335–342. https://doi.org/10.1038/s41586-018-0089-z.

(33)   Burdick, J. A.; Mauck, R. L.; Gerecht, S. To Serve and Protect: Hydrogels to Improve Stem Cell-Based Therapies. Cell Stem Cell 2016, 18 (1), 13–15. https://doi.org/10.1016/j.stem.2015.12.004.

(34)   Führmann, T.; Tam, R. Y.; Ballarin, B.; Coles, B.; Elliott Donaghue, I.; van der Kooy, D.; Nagy, A.; Tator, C. H.; Morshead, C. M.; Shoichet, M. S. Injectable Hydrogel Promotes Early Survival of Induced Pluripotent Stem Cell-Derived Oligodendrocytes and Attenuates Longterm Teratoma Formation in a Spinal Cord Injury Model. Biomaterials 2016. https://doi.org/10.1016/j.biomaterials.2015.12.032.

(35)   Hofmann, M.; Wollert, K. C.; Meyer, G. P.; Menke, A.; Arseniev, L.; Hertenstein, B.; Ganser, A.; Knapp, W. H.; Drexler, H. Monitoring of Bone Marrow Cell Homing into the Infarcted Human Myocardium. Circulation 2005, 111 (17), 2198–2202. https://doi.org/10.1161/01.CIR.0000163546.27639.AA.

(36)   Levit, R. D.; Landázuri, N.; Phelps, E. A.; Brown, M. E.; García, A. J.; Davis, M. E.; Joseph, G.; Long, R.; Safley, S. A.; Suever, J. D.; Lyle, A. N.; Weber, C. J.; Taylor, W. R. Cellular Encapsulation Enhances Cardiac Repair. Journal of the American Heart Association 2013, 2 (5). https://doi.org/10.1161/JAHA.113.000367.

(37)   Ullah, M.; Liu, D. D.; Thakor, A. S. Mesenchymal Stromal Cell Homing: Mechanisms and Strategies for Improvement. iScience. Elsevier Inc. May 31, 2019, pp 421–438. https://doi.org/10.1016/j.isci.2019.05.004.

(38) Kraitchman, D. L.; Tatsumi, M.; Gilson, W. D.; Ishimori, T.; Kedziorek, D.; Walczak, P.; Segars, W. P.; Chen, H. H.; Fritzges, D.; Izbudak, I.; Young, R. G.; Marcelino, M.; Pittenger, M. F.; Solaiyappan, M.; Boston, R. C.; Tsui, B. M. W.; Wahl, R. L.; Bulte, J. W. M. Dynamic Imaging of Allogeneic Mesenchymal Stem Cells Trafficking to Myocardial Infarction. Circulation 2005, 112 (10), 1451–1461. https://doi.org/10.1161/CIRCULATIONAHA.105.537480.

(39) Wagner, B.; Henschler, R. Fate of Intravenously Injected Mesenchymal Stem Cells and Significance for Clinical Application. In Advances in biochemical engineering/biotechnology; Springer, Berlin, Heidelberg, 2012; Vol. 130, pp 19–37. https://doi.org/10.1007/10_2012_155.

(40) Scarfe, L.; Taylor, A.; Sharkey, J.; Harwood, R.; Barrow, M.; Comenge, J.; Beeken, L.; Astley, C.; Santeramo, I.; Hutchinson, C.; Ressel, L.; Smythe, J.; Austin, E.; Levy, R.; Rosseinsky, M. J.; Adams, D. J.; Poptani, H.; Park, B. K.; Murray, P.; Wilm, B. Non-Invasive Imaging Reveals Conditions That Impact Distribution and Persistence of Cells after in Vivo Administration. Stem Cell Research and Therapy 2018, 9 (1). https://doi.org/10.1186/s13287-018-1076-x.

(41) Ozeki, N.; Muneta, T.; Koga, H.; Nakagawa, Y.; Mizuno, M.; Tsuji, K.; Mabuchi, Y.; Akazawa, C.; Kobayashi, E.; Matsumoto, K.; Futamura, K.; Saito, T.; Sekiya, I. Not Single but Periodic Injections of Synovial Mesenchymal Stem Cells Maintain Viable Cells in Knees and Inhibit Osteoarthritis Progression in Rats. Osteoarthritis and Cartilage 2016, 24 (6), 1061–1070. https://doi.org/10.1016/j.joca.2015.12.018.

(42) Kim, Y. H.; Jin, H. J.; Heo, J.; Ju, H.; Lee, H. Y.; Kim, S.; Lee, S.; Lim, J.; Jeong, S. Y.; Kwon, J. H.; Kim, M.; Choi, S. J.; Oh, W.; Yang, Y. S.; Hwang, H. H.; Yu, H. Y.; Ryu, C.

M.; Jeon, H. B.; Shin, D. M. Small Hypoxia-Primed Mesenchymal Stem Cells Attenuate Graft-versus-Host Disease. Leukemia 2018, 32 (12), 2672–2684. https://doi.org/10.1038/s41375-018-0151-8.

(43)   Antebi, B.; Rodriguez, L. A.; Walker, K. P.; Asher, A. M.; Kamucheka, R. M.; Alvarado, L.; Mohammadipoor, A.; Cancio, L. C. Short-Term Physiological Hypoxia Potentiates the Therapeutic Function of Mesenchymal Stem Cells. Stem Cell Research and Therapy 2018, 9 (1). https://doi.org/10.1186/s13287-018-1007-x.

(44)   Vigo, T.; Procaccini, C.; Ferrara, G.; Baranzini, S.; Oksenberg, J. R.; Matarese, G.; Diaspro, A.; Kerlero de Rosbo, N.; Uccelli, A. IFN-γ Orchestrates Mesenchymal Stem Cell Plasticity through the Signal Transducer and Activator of Transcription 1 and 3 and Mammalian Target of Rapamycin Pathways. Journal of Allergy and Clinical Immunology 2017, 139 (5), 1667–1676. https://doi.org/10.1016/j.jaci.2016.09.004.

(45)   Yang, Z.; Concannon, J.; Ng, K. S.; Seyb, K.; Mortensen, L. J.; Ranganath, S.; Gu, F.; Levy, O.; Tong, Z.; Martyn, K.; Zhao, W.; Lin, C. P.; Glicksman, M. A.; Karp, J. M. Tetrandrine Identified in a Small Molecule Screen to Activate Mesenchymal Stem Cells for Enhanced Immunomodulation. Scientific Reports 2016, 6. https://doi.org/10.1038/srep30263.

(46)   Levy, O.; Mortensen, L. J.; Boquet, G.; Tong, Z.; Perrault, C.; Benhamou, B.; Zhang, J.; Stratton, T.; Han, E.; Safaee, H.; Musabeyezu, J.; Yang, Z.; Multon, M.-C.; Rothblatt, J.; Deleuze, J.-F.; Lin, C. P.; Karp, J. M. A Small-Molecule Screen for Enhanced Homing of Systemically Infused Cells. Cell Reports 2015, 10 (8), 1261–1268. https://doi.org/10.1016/j.celrep.2015.01.057.

(47)   Noronha Nc, N. D. C.; Mizukami, A.; Caliári-Oliveira, C.; Cominal, J. G.; Rocha, J. L. M.; Covas, D. T.; Swiech, K.; Malmegrim, K. C. R. Priming Approaches to Improve the Efficacy of Mesenchymal Stromal Cell-Based Therapies. Stem Cell Research and Therapy. BioMed Central Ltd. May 2, 2019. https://doi.org/10.1186/s13287-019-1224-y.

(48)   Ranganath, S. H.; Tong, Z.; Levy, O.; Martyn, K.; Karp, J. M.; Inamdar, M. S. Controlled Inhibition of the Mesenchymal Stromal Cell Pro-Inflammatory Secretome via Microparticle Engineering. Stem Cell Reports 2016, 6 (6), 926–939. https://doi.org/10.1016/j.stemcr.2016.05.003.

(49)   Lutolf, M. P.; Hubbell, J. A. Synthetic Biomaterials as Instructive Extracellular Microenvironments for Morphogenesis in Tissue Engineering. Nature Biotechnology. Nature Publishing Group January 1, 2005, pp 47–55. https://doi.org/10.1038/nbt1055.

(50)   Hubbell, J. A. Biomaterials in Tissue Engineering. Bio/Technology. Nature Publishing Group 1995, pp 565–576. https://doi.org/10.1038/nbt0695-565.

(51)   Place, E. S.; Evans, N. D.; Stevens, M. M. Complexity in Biomaterials for Tissue Engineering. Nature Materials 2009, 8 (6), 457–470. https://doi.org/10.1038/nmat2441.

(52)   Slaughter, B. V; Khurshid, S. S.; Fisher, O. Z.; Khademhosseini, A.; Peppas, N. A. Hydrogels in Regenerative Medicine. Advanced materials (Deerfield Beach, Fla.) 2009, 21 (32–33), 3307–3329. https://doi.org/10.1002/adma.200802106.

(53)   Peppas, N. A. Hydrogels in Medicine and Pharmacy; CRC Press, 1986.

(54)   Peppas, N. A.; Hilt, J. Z.; Khademhosseini, A.; Langer, R. Hydrogels in Biology and Medicine: From Molecular Principles to Bionanotechnology. Advanced Materials 2006, 18 (11), 1345–1360. https://doi.org/10.1002/adma.200501612.

(55)   Peppas, N. A.; Bures, P.; Leobandung, W.; Ichikawa, H. Hydrogels in Pharmaceutical Formulations. European Journal of Pharmaceutics and Biopharmaceutics 2000, 50 (1), 27–46. https://doi.org/10.1016/S0939-6411(00)00090-4.

(56)   Wong, S. W.; Lenzini, S.; Cooper, M. H.; Mooney, D. J.; Shin, J. W. Soft Extracellular Matrix Enhances Inflammatory Activation of Mesenchymal Stromal Cells to Induce Monocyte Production and Trafficking. Science Advances 2020, 6 (15). https://doi.org/10.1126/sciadv.aaw0158.

(57)   Ho, S. S.; Murphy, K. C.; Binder, B. Y. K.; Vissers, C. B.; Leach, J. K. Increased Survival and Function of Mesenchymal Stem Cell Spheroids Entrapped in Instructive Alginate Hydrogels. Stem Cells Translational Medicine 2016, 5, 773–781.

(58)   Sridhar, B. V.; Brock, J. L.; Silver, J. S.; Leight, J. L.; Randolph, M. A.; Anseth, K. S. Development of a Cellularly Degradable PEG Hydrogel to Promote Articular Cartilage Extracellular Matrix Deposition. Advanced Healthcare Materials 2015, 4 (5), 702–713. https://doi.org/10.1002/adhm.201400695.

(59)   Park, K. W.; Waki, H.; Kim, W.-K.; Davies, B. S. J.; Young, S. G.; Parhami, F.; Tontonoz, P. The Small Molecule Phenamil Induces Osteoblast Differentiation and Mineralization. Molecular and Cellular Biology 2009, 29 (14), 3905–3914. https://doi.org/10.1128/MCB.00002-09.

(60)   Fan, J.; Im, C. S.; Cui, Z. K.; Guo, M.; Bezouglaia, O.; Fartash, A.; Lee, J. Y.; Nguyen, J.; Wu, B. M.; Aghaloo, T.; Lee, M. Delivery of Phenamil Enhances BMP-2-Induced Osteogenic Differentiation of Adipose-Derived Stem Cells and Bone Formation in Calvarial Defects. Tissue engineering. Part A 2015, 21 (13–14), 2053–2065. https://doi.org/10.1089/ten.tea.2014.0489.

(61) Fan, W.; Yuan, L.; Li, J.; Wang, Z.; Chen, J.; Guo, C.; Mo, X.; Yan, Z. Injectable Double-Crosslinked Hydrogels with Kartogenin-Conjugated Polyurethane Nano-Particles and Transforming Growth Factor B3 for in-Situ Cartilage Regeneration. Materials Science and Engineering C 2020, 110, 110705. https://doi.org/10.1016/j.msec.2020.110705.

(62) Chinnadurai, R.; Copland, I. B.; Patel, S. R.; Galipeau, J. IDO-Independent Suppression of T Cell Effector Function by IFN-γ–Licensed Human Mesenchymal Stromal Cells. The Journal of Immunology 2014, 192 (4), 1491–1501. https://doi.org/10.4049/jimmunol.1301828.

(63) Tsiapalis, D.; O'Driscoll, L. Mesenchymal Stem Cell Derived Extracellular Vesicles for Tissue Engineering and Regenerative Medicine Applications. Cells. NLM (Medline) April 16, 2020. https://doi.org/10.3390/cells9040991.

(64) Park, K. S.; Bandeira, E.; Shelke, G. V.; Lässer, C.; Lötvall, J. Enhancement of Therapeutic Potential of Mesenchymal Stem Cell-Derived Extracellular Vesicles. Stem Cell Research and Therapy. BioMed Central Ltd. September 23, 2019, pp 1–15. https://doi.org/10.1186/s13287-019-1398-3.

(65) Brennan, M. Á.; Layrolle, P.; Mooney, D. J. Biomaterials Functionalized with MSC Secreted Extracellular Vesicles and Soluble Factors for Tissue Regeneration. Advanced Functional Materials 2020, 1909125. https://doi.org/10.1002/adfm.201909125.

(66) Balmayor, E. R. Targeted Delivery as Key for the Success of Small Osteoinductive Molecules. Advanced Drug Delivery Reviews 2015, 94, 13–27. https://doi.org/10.1016/j.addr.2015.04.022.

(67)   Lo, K. W.-H.; Jiang, T.; Gagnon, K. A.; Nelson, C.; Laurencin, C. T. Small-Molecule Based Musculoskeletal Regenerative Engineering. Trends in biotechnology 2014, 32 (2), 74–81. https://doi.org/10.1016/j.tibtech.2013.12.002.

(68)   Wu, X.; Ding, S.; Ding, Q.; Gray, N. S.; Schultz, P. G. A Small Molecule with Osteogenesis-Inducing Activity in Multipotent Mesenchymal Progenitor Cells. Journal of the American Chemical Society 2002, 124 (49), 14520–14521. https://doi.org/10.1021/ja0283908.

(69)   Lo, K. W.-H.; Ulery, B. D.; Kan, H. M.; Ashe, K. M.; Laurencin, C. T. Evaluating the Feasibility of Utilizing the Small Molecule Phenamil as a Novel Biofactor for Bone Regenerative Engineering. Journal of Tissue Engineering and Regenerative Medicine 2014, 8 (9), 728–736. https://doi.org/10.1002/term.1573.

(70)   Johnson, K.; Zhu, S.; Tremblay, M. S.; Payette, J. N.; Wang, J.; Bouchez, L. C.; Meeusen, S.; Althage, A.; Cho, C. Y.; Wu, X.; Schultz, P. G. A Stem Cell-Based Approach to Cartilage Repair. Science 2012, 336 (6082), 717–721. https://doi.org/10.1126/science.1215157.

(71)   Wu, X.; Ding, S.; Ding, Q.; Gray, N. S.; Schultz, P. G. A Small Molecule with Osteogenesis-Inducing Activity in Multipotent Mesenchymal Progenitor Cells. Journal of the American Chemical Society 2002, 124 (49), 14520–14521. https://doi.org/10.1021/ja0283908.

(72)   Gellynck, K.; Shah, R.; Parkar, M.; Young, A.; Buxton, P.; Brett, P. Small Molecule Stimulation Enhances Bone Regeneration but Not Titanium Implant Osseointegration. Bone 2013, 57 (2), 405–412. https://doi.org/10.1016/j.bone.2013.09.012.

(73)   Park, K. W.; Waki, H.; Kim, W.-K.; Davies, B. S. J.; Young, S. G.; Parhami, F.; Tontonoz, P. The Small Molecule Phenamil Induces Osteoblast Differentiation and Mineralization. Molecular and Cellular Biology 2009, 29 (14), 3905–3914. https://doi.org/10.1128/MCB.00002-09.

(74)   Lo, K. W.-H.; Kan, H. M.; Laurencin, C. T. Short-Term Administration of Small Molecule Phenamil Induced a Protracted Osteogenic Effect on Osteoblast-like MC3T3-E1 Cells. Journal of Tissue Engineering and Regenerative Medicine 2016, 10 (6), 518–526. https://doi.org/10.1002/term.1786.

(75)   Lo, K. W.-H.; Ulery, B. D.; Kan, H. M.; Ashe, K. M.; Laurencin, C. T. Evaluating the Feasibility of Utilizing the Small Molecule Phenamil as a Novel Biofactor for Bone Regenerative Engineering. Journal of Tissue Engineering and Regenerative Medicine 2014, 8 (9), 728–736. https://doi.org/10.1002/term.1573.

(76)   Zhao, D.; Lei, L.; Wang, S.; Nie, H. Understanding Cell Homing-Based Tissue Regeneration from the Perspective of Materials. Journal of Materials Chemistry B. Royal Society of Chemistry July 22, 2015, pp 7319–7333. https://doi.org/10.1039/c5tb01188d.

(77)   Hong, L.; Zhang, G.; Sultana, H.; Yu, Y.; Wei, Z. The Effects of 17-β Estradiol on Enhancing Proliferation of Human Bone Marrow Mesenchymal Stromal Cells in Vitro. Stem Cells and Development 2011, 20 (5), 925–931. https://doi.org/10.1089/scd.2010.0125.

(78)   Zhao, Q.; Ren, H.; Han, Z. Mesenchymal Stem Cells: Immunomodulatory Capability and Clinical Potential in Immune Diseases. Journal of Cellular Immunotherapy. Shanghai Hengrun Biomedical Technology Research Institute March 2016, pp 3–20. https://doi.org/10.1016/j.jocit.2014.12.001.

(79)   Abdi, R.; Fiorina, P.; Adra, C. N.; Atkinson, M.; Sayegh, M. H. Immunomodulation by Mesenchymal Stem Cells: A Potential Therapeutic Strategy for Type 1 Diabetes. Diabetes. American Diabetes Association July 2008, pp 1759–1767. https://doi.org/10.2337/db08-0180.

(80)   Abdi, R.; Fiorina, P.; Adra, C. N.; Atkinson, M.; Sayegh, M. H. Immunomodulation by Mesenchymal Stem Cells: A Potential Therapeutic Strategy for Type 1 Diabetes. Diabetes. American Diabetes Association July 2008, pp 1759–1767. https://doi.org/10.2337/db08-0180.

(81)   Song, N.; Scholtemeijer, M.; Shah, K. Mesenchymal Stem Cell Immunomodulation: Mechanisms and Therapeutic Potential. Trends in Pharmacological Sciences. Elsevier Ltd September 1, 2020, pp 653–664. https://doi.org/10.1016/j.tips.2020.06.009.

(82)   Ghannam, S.; Bouffi, C.; Djouad, F.; Jorgensen, C.; Noël, D. Immunosuppression by Mesenchymal Stem Cells: Mechanisms and Clinical Applications. Stem Cell Research and Therapy. BioMed Central March 2010, p 2. https://doi.org/10.1186/scrt2.

(83)   Wang, M.; Yuan, Q.; Xie, L. Mesenchymal Stem Cell-Based Immunomodulation: Properties and Clinical Application. Stem Cells International. Hindawi Limited 2018. https://doi.org/10.1155/2018/3057624.

(84)   Cicchese, J. M.; Evans, S.; Hult, C.; Joslyn, L. R.; Wessler, T.; Millar, J. A.; Marino, S.; Cilfone, N. A.; Mattila, J. T.; Linderman, J. J.; Kirschner, D. E. Dynamic Balance of Pro- and Anti-Inflammatory Signals Controls Disease and Limits Pathology. Immunological Reviews 2018, 285 (1), 147–167. https://doi.org/10.1111/imr.12671.

(85)   Saldaña, L.; Bensiamar, F.; Vallés, G.; Mancebo, F. J.; García-Rey, E.; Vilaboa, N. Immunoregulatory Potential of Mesenchymal Stem Cells Following Activation by

Macrophage-Derived Soluble Factors. Stem Cell Research & Therapy 2019, 10 (1), 58. https://doi.org/10.1186/s13287-019-1156-6.

(86)   Kyurkchiev, D. Secretion of Immunoregulatory Cytokines by Mesenchymal Stem Cells. World Journal of Stem Cells 2014, 6 (5), 552. https://doi.org/10.4252/wjsc.v6.i5.552.

(87)   Sivanathan, K. N.; Gronthos, S.; Rojas-Canales, D.; Thierry, B.; Coates, P. T. Interferon-Gamma Modification of Mesenchymal Stem Cells: Implications of Autologous and Allogeneic Mesenchymal Stem Cell Therapy in Allotransplantation. Stem Cell Reviews and Reports 2014, 10 (3), 351–375. https://doi.org/10.1007/s12015-014-9495-2.

(88)   Bartosh, T. J.; Ylöstalo, J. H.; Mohammadipoor, A.; Bazhanov, N.; Coble, K.; Claypool, K.; Lee, R. H.; Choi, H.; Prockop, D. J. Aggregation of Human Mesenchymal Stromal Cells (MSCs) into 3D Spheroids Enhances Their Antiinflammatory Properties. Proceedings of the National Academy of Sciences of the United States of America 2010, 107 (31), 13724–13729. https://doi.org/10.1073/pnas.1008117107.

(89)   Krampera, M.; Cosmi, L.; Angeli, R.; Pasini, A.; Liotta, F.; Andreini, A.; Santarlasci, V.; Mazzinghi, B.; Pizzolo, G.; Vinante, F.; Romagnani, P.; Maggi, E.; Romagnani, S.; Annunziato, F. Role for Interferon-γ in the Immunomodulatory Activity of Human Bone Marrow Mesenchymal Stem Cells. Stem Cells 2006, 24 (2), 386–398. https://doi.org/10.1634/stemcells.2005-0008.

(90)   Ghannam, S.; Bouffi, C.; Djouad, F.; Jorgensen, C.; Noël, D. Immunosuppression by Mesenchymal Stem Cells: Mechanisms and Clinical Applications. Stem Cell Research and Therapy. BioMed Central March 2010, p 2. https://doi.org/10.1186/scrt2.

(91)   Idriss, H. T.; Naismith, J. H. TNFα and the TNF Receptor Superfamily: Structure-Function Relationship(s). Microscopy Research and Technique 2000, 50 (3), 184–195. https://doi.org/10.1002/1097-0029(20000801)50:3<184::AID-JEMT2>3.0.CO;2-H.

(92)   Tu, Z.; Li, Q.; Bu, H.; Lin, F. Mesenchymal Stem Cells Inhibit Complement Activation by Secreting Factor h. Stem Cells and Development 2010, 19 (11), 1803–1809. https://doi.org/10.1089/scd.2009.0418.

(93)   François, M.; Romieu-Mourez, R.; Li, M.; Galipeau, J. Human MSC Suppression Correlates with Cytokine Induction of Indoleamine 2,3-Dioxygenase and Bystander M2 Macrophage Differentiation. Molecular Therapy 2012, 20 (1), 187–195. https://doi.org/10.1038/mt.2011.189.

(94)   Redondo-Castro, E.; Cunningham, C.; Miller, J.; Martuscelli, L.; Aoulad-Ali, S.; Rothwell, N. J.; Kielty, C. M.; Allan, S. M.; Pinteaux, E. Interleukin-1 Primes Human Mesenchymal Stem Cells towards an Anti-Inflammatory and pro-Trophic Phenotype in Vitro. Stem Cell Research and Therapy 2017, 8 (1). https://doi.org/10.1186/s13287-017-0531-4.

(95)   Madrigal, M.; Rao, K. S.; Riordan, N. H. A Review of Therapeutic Effects of Mesenchymal Stem Cell Secretions and Induction of Secretory Modification by Different Culture Methods. Journal of Translational Medicine. BioMed Central Ltd. December 11, 2014, p 260. https://doi.org/10.1186/s12967-014-0260-8.

(96)   Gnecchi, M.; Zhang, Z.; Ni, A.; Dzau, V. J. Paracrine Mechanisms in Adult Stem Cell Signaling and Therapy. Circulation Research. Lippincott Williams & Wilkins November 21, 2008, pp 1204–1219. https://doi.org/10.1161/CIRCRESAHA.108.176826.

(97)   Song, N.; Scholtemeijer, M.; Shah, K. Mesenchymal Stem Cell Immunomodulation: Mechanisms and Therapeutic Potential. Trends in Pharmacological Sciences. Elsevier Ltd September 1, 2020, pp 653–664. https://doi.org/10.1016/j.tips.2020.06.009.

(98)   Li, J. H.; Zhang, N.; Wangi, J. A. Improved Anti-Apoptotic and Anti-Remodeling Potency of Bone Marrow Mesenchymal Stem Cells by Anoxic Pre-Conditioning in Diabetic Cardiomyopathy. Journal of Endocrinological Investigation 2008, 31 (2), 103–110. https://doi.org/10.1007/BF03345575.

(99)   Hawkins, K. E.; Sharp, T. V.; Mckay, T. R. The Role of Hypoxia in Stem Cell Potency and Differentiation. Regenerative Medicine. Regen Med November 2013, pp 771–782. https://doi.org/10.2217/rme.13.71.

(100) Murphy, K. C.; Hung, B. P.; Browne-Bourne, S.; Zhou, D.; Yeung, J.; Genetos, D. C.; Leach, J. K. Measurement of Oxygen Tension within Mesenchymal Stem Cell Spheroids. Journal of the Royal Society Interface 2017, 14 (127). https://doi.org/10.1098/rsif.2016.0851.

(101) Ho, S. S.; Hung, B. P.; Heyrani, N.; Lee, M. A.; Leach, J. K. Hypoxic Preconditioning of Mesenchymal Stem Cells with Subsequent Spheroid Formation Accelerates Repair of Segmental Bone Defects. Stem Cells 2018, 36 (9), 1393–1403. https://doi.org/10.1002/stem.2853.

(102) Kyburz, K. A.; Anseth, K. S. Synthetic Mimics of the Extracellular Matrix: How Simple Is Complex Enough? Annals of Biomedical Engineering 2015, 43 (3), 489–500. https://doi.org/10.1007/s10439-015-1297-4.

(103) Humphrey, J. D.; Dufresne, E. R.; Schwartz, M. A. Mechanotransduction and Extracellular Matrix Homeostasis. Nature Reviews Molecular Cell Biology. Nature Publishing Group December 11, 2014, pp 802–812. https://doi.org/10.1038/nrm3896.

(104) Tibbitt, M. W.; Anseth, K. S. Hydrogels as Extracellular Matrix Mimics for 3D Cell Culture. Biotechnology and Bioengineering 2009, 103 (4), 655–663. https://doi.org/10.1002/bit.22361.

(105) Karimi, F.; O'Connor, A. J.; Qiao, G. G.; Heath, D. E. Integrin Clustering Matters: A Review of Biomaterials Functionalized with Multivalent Integrin-Binding Ligands to Improve Cell Adhesion, Migration, Differentiation, Angiogenesis, and Biomedical Device Integration. Advanced Healthcare Materials 2018, 1701324, 1–28. https://doi.org/10.1002/adhm.201701324.

(106) De Lisio, M.; Jensen, T.; Sukiennik, R. A.; Huntsman, H. D.; Boppart, M. D. Substrate and Strain Alter the Muscle-Derived Mesenchymal Stem Cell Secretome to Promote Myogenesis. Stem Cell Research and Therapy 2014, 5 (3), 74. https://doi.org/10.1186/scrt463.

(107) Abdeen, A. A.; Weiss, J. B.; Lee, J.; Kilian, K. A. Matrix Composition and Mechanics Direct Proangiogenic Signaling from Mesenchymal Stem Cells. Tissue engineering. Part A 2014, 20 (19–20), 2737–2745. https://doi.org/10.1089/ten.tea.2013.0661.

(108) Ogle, M. E.; Doron, G.; Levy, M. J.; Temenoff, J. S. Hydrogel Culture Surface Stiffness Modulates Mesenchymal Stromal Cell Secretome and Alters Senescence. Tissue Engineering Part A 2020, ten.tea.2020.0030. https://doi.org/10.1089/ten.tea.2020.0030.

(109) Clark, A. Y.; Martin, K. E.; García, J. R.; Johnson, C. T.; Theriault, H. S.; Han, W. M.; Zhou, D. W.; Botchwey, E. A.; García, A. J. Integrin-Specific Hydrogels Modulate

Transplanted Human Bone Marrow-Derived Mesenchymal Stem Cell Survival, Engraftment, and Reparative Activities. Nature Communications 2020, 11 (1). https://doi.org/10.1038/s41467-019-14000-9.

(110) Wu, P. K.; Wang, J. Y.; Chen, C. F.; Chao, K. Y.; Chang, M. C.; Chen, W. M.; Hung, S. C. Early Passage Mesenchymal Stem Cells Display Decreased Radiosensitivity and Increased DNA Repair Activity. Stem Cells Translational Medicine 2017, 6 (6), 1504–1514. https://doi.org/10.1002/sctm.15-0394.

(111) Liu, F. D.; Pishesha, N.; Poon, Z.; Kaushik, T.; Van Vliet, K. J. Material Viscoelastic Properties Modulate the Mesenchymal Stem Cell Secretome for Applications in Hematopoietic Recovery. ACS Biomaterials Science and Engineering 2017, 3 (12), 3292–3306. https://doi.org/10.1021/acsbiomaterials.7b00644.

(112) Cai, L.; Dewi, R. E.; Goldstone, A. B.; Cohen, J. E.; Steele, A. N.; Woo, Y. J.; Heilshorn, S. C. Regulating Stem Cell Secretome Using Injectable Hydrogels with In Situ Network Formation. Advanced Healthcare Materials 2016, 5 (21), 2758–2764. https://doi.org/10.1002/adhm.201600497.

(113) Cosgrove, B. D.; Mui, K. L.; Driscoll, T. P.; Caliari, S. R.; Mehta, K. D.; Assoian, R. K.; Burdick, J. A.; Mauck, R. L. N-Cadherin Adhesive Interactions Modulate Matrix Mechanosensing and Fate Commitment of Mesenchymal Stem Cells. Nature Materials 2016, 15 (12), 1297–1306. https://doi.org/10.1038/nmat4725.

(114) Caldwell, A. S.; Rao, V. V.; Golden, A. C.; Anseth, K. S. Porous Bio-Click Microgel Scaffolds Control HMSC Interactions and Promote Their Secretory Properties. Biomaterials 2020, 232 (December 2019), 119725. https://doi.org/10.1016/j.biomaterials.2019.119725.

(115) Caldwell, A. S.; Campbell, G. T.; Shekiro, K. M. T.; Anseth, K. S. Clickable Microgel Scaffolds as Platforms for 3D Cell Encapsulation. Advanced Healthcare Materials 2017, 6 (15), 1–8. https://doi.org/10.1002/adhm.201700254.

(116) Gionet-Gonzales, M. A.; Leach, J. K. Engineering Principles for Guiding Spheroid Function in the Regeneration of Bone, Cartilage, and Skin. Biomedical Materials (Bristol) 2018, 13 (3). https://doi.org/10.1088/1748-605X/aab0b3.

(117) Gionet-Gonzales, M. A.; Leach, J. K. Engineering Principles for Guiding Spheroid Function in the Regeneration of Bone, Cartilage, and Skin. Biomedical Materials (Bristol) 2018, 13 (3). https://doi.org/10.1088/1748-605X/aab0b3.

(118) Murphy, K. C.; Whitehead, J.; Falahee, P. C.; Zhou, D.; Simon, S. I.; Leach, J. K. Multifactorial Experimental Design to Optimize the Anti-Inflammatory and Proangiogenic Potential of Mesenchymal Stem Cell Spheroids. Stem Cells 2017, 35 (6), 1493–1504. https://doi.org/10.1002/stem.2606.

(119) Murphy, K. C.; Whitehead, J.; Zhou, D.; Ho, S. S.; Leach, J. K. Engineering Fibrin Hydrogels to Promote the Wound Healing Potential of Mesenchymal Stem Cell Spheroids. Acta Biomaterialia 2017, 64, 176–186. https://doi.org/10.1016/j.actbio.2017.10.007.

(120) Peyton, S. R.; Kalcioglu, Z. I.; Cohen, J. C.; Runkle, A. P.; Van Vliet, K. J.; Lauffenburger, D. A.; Griffith, L. G. Marrow-Derived Stem Cell Motility in 3D Synthetic Scaffold Is Governed by Geometry along with Adhesivity and Stiffness. Biotechnology and Bioengineering 2011, 108 (5), 1181–1193. https://doi.org/10.1002/bit.23027.

(121) Madden, L. R.; Mortisen, D. J.; Sussman, E. M.; Dupras, S. K.; Fugate, J. A.; Cuy, J. L.; Hauch, K. D.; Laflamme, M. A.; Murry, C. E.; Ratner, B. D. Proangiogenic Scaffolds as Functional Templates for Cardiac Tissue Engineering. Proceedings of the National

Academy of Sciences of the United States of America 2010, 107 (34), 15211–15216. https://doi.org/10.1073/pnas.1006442107.

(122) Golden, A. P.; Tien, J. Fabrication of Microfluidic Hydrogels Using Molded Gelatin as a Sacrificial Element. Lab on a Chip 2007, 7 (6), 720–725. https://doi.org/10.1039/b618409j.

(123) Lutolf, M. P.; Weber, F. E.; Schmoekel, H. G.; Schense, J. C.; Kohler, T.; Müller, R.; Hubbell, J. A. Repair of Bone Defects Using Synthetic Mimetics of Collagenous Extracellular Matrices. Nature Biotechnology 2003, 21 (5), 513–518. https://doi.org/10.1038/nbt818.

(124) Qazi, T. H.; Tytgat, L.; Dubruel, P.; Duda, G. N.; Van Vlierberghe, S.; Geissler, S. Extrusion Printed Scaffolds with Varying Pore Size As Modulators of MSC Angiogenic Paracrine Effects. ACS Biomaterials Science and Engineering 2019, 5 (10), 5348–5358. https://doi.org/10.1021/acsbiomaterials.9b00843.

(125) de Rutte, J. M.; Koh, J.; Di Carlo, D. Scalable High-Throughput Production of Modular Microgels for In Situ Assembly of Microporous Tissue Scaffolds. Advanced Functional Materials 2019, 29 (25), 1900071. https://doi.org/10.1002/adfm.201900071.

(126) Zhang, L.; Chen, K.; Zhang, H.; Pang, B.; Choi, C.-H.; Mao, A. S.; Liao, H.; Utech, S.; Mooney, D. J.; Wang, H.; Weitz, D. A. Microfluidic Templated Multicompartment Microgels for 3D Encapsulation and Pairing of Single Cells. Small 2018, 14 (9), 1702955. https://doi.org/10.1002/smll.201702955.

(127) Caldwell, A. S.; Campbell, G. T.; Shekiro, K. M. T.; Anseth, K. S. Clickable Microgel Scaffolds as Platforms for 3D Cell Encapsulation. Advanced Healthcare Materials 2017, 6 (15), 1–8. https://doi.org/10.1002/adhm.201700254.

(128) Qazi, T. H.; Tytgat, L.; Dubruel, P.; Duda, G. N.; Van Vlierberghe, S.; Geissler, S. Extrusion Printed Scaffolds with Varying Pore Size As Modulators of MSC Angiogenic Paracrine Effects. ACS Biomaterials Science and Engineering 2019, 5 (10), 5348–5358. https://doi.org/10.1021/acsbiomaterials.9b00843.

(129) Williams, E.; Williams, G.; Gour, B. J.; Blaschuk, O. W.; Doherty, P. A Novel Family of Cyclic Peptide Antagonists Suggests That N-Cadherin Specificity Is Determined by Amino Acids That Flank the HAV Motif*; 2000.

(130) Cosgrove, B. D.; Mui, K. L.; Driscoll, T. P.; Caliari, S. R.; Mehta, K. D.; Assoian, R. K.; Burdick, J. A.; Mauck, R. L. N-Cadherin Adhesive Interactions Modulate Matrix Mechanosensing and Fate Commitment of Mesenchymal Stem Cells. Nature Materials 2016, 15 (12), 1297–1306. https://doi.org/10.1038/nmat4725.

(131) Qazi, T. H.; Mooney, D. J.; Duda, G. N.; Geissler, S. Niche-Mimicking Interactions in Peptide-Functionalized 3D Hydrogels Amplify Mesenchymal Stromal Cell Paracrine Effects. Biomaterials 2020, 230. https://doi.org/10.1016/j.biomaterials.2019.119639.

(132) Mao, A. S.; Özkale, B.; Shah, N. J.; Vining, K. H.; Descombes, T.; Zhang, L.; Tringides, C. M.; Wong, S. W.; Shin, J. W.; Scadden, D. T.; Weitz, D. A.; Mooney, D. J. Programmable Microencapsulation for Enhanced Mesenchymal Stem Cell Persistence and Immunomodulation. Proceedings of the National Academy of Sciences of the United States of America 2019, 116 (31), 15392–15397. https://doi.org/10.1073/pnas.1819415116.

(133) Murphy, K. C.; Hung, B. P.; Browne-Bourne, S.; Zhou, D.; Yeung, J.; Genetos, D. C.; Leach, J. K. Measurement of Oxygen Tension within Mesenchymal Stem Cell Spheroids. Journal of the Royal Society Interface 2017, 14 (127). https://doi.org/10.1098/rsif.2016.0851.

(134) Zimmermann, J. A.; Mcdevitt, T. C. Pre-Conditioning Mesenchymal Stromal Cell Spheroids for Immunomodulatory Paracrine Factor Secretion. Cytotherapy 2014, 16 (3), 331–345. https://doi.org/10.1016/j.jcyt.2013.09.004.

(135) Frost; Sullivan. U.S. Trauma Fixation Markets; 2008.

(136) Levy, O.; Kuai, R.; Siren, E. M. J.; Bhere, D.; Milton, Y.; Nissar, N.; de Biasio, M.; Heinelt, M.; Reeve, B.; Abdi, R.; Alturki, M.; Fallatah, M.; Almalik, A.; Alhasan, A. H.; Shah, K.; Karp, J. M. Shattering Barriers toward Clinically Meaningful MSC Therapies. Science Advances 2020, 6.

(137) Stoddart, M. J.; Salgado, A.; Presen, D. M.; Traweger, A.; Gimona, M.; Redl, H. Mesenchymal Stromal Cell-Based Bone Regeneration Therapies: From Cell Transplantation and Tissue Engineering to Therapeutic Secretomes and Extracellular Vesicles. Frontiers in Bioengineering and Biotechnology | www.frontiersin.org 2019, 1, 352. https://doi.org/10.3389/fbioe.2019.00352.

(138) Phetfong, J.; Sanvoranart, T.; Nartprayut, K.; Nimsanor, N.; Seenprachawong, K.; Prachayasittikul, V.; Supokawej, A. Osteoporosis: The Current Status of Mesenchymal Stem Cell-Based Therapy. Cellular & Molecular Biology Letters 2016, 21 (1), 12. https://doi.org/10.1186/s11658-016-0013-1.

(139) Antebi, B.; Pelled, G.; Gazit, D. Stem Cell Therapy for Osteoporosis. Current Osteoporosis Reports 2014, 12 (1), 41–47. https://doi.org/10.1007/s11914-013-0184-x.

(140) Murphy, M. P.; Quarto, N.; Longaker, M. T.; Wan, D. C. Calvarial Defects: Cell-Based Reconstructive Strategies in the Murine Model. https://doi.org/10.1089/ten.tec.2017.0230.

(141) Cao, X.; Frenette, P. S.; Mao, J. J.; Robey, P. G.; Simmons, P. J.; Wang, C.-Y.; Bianco, P. The Meaning, the Sense and the Significance: Translating the Science of Mesenchymal Stem Cells into Medicine. Nature Medicine 2013. https://doi.org/10.1038/nm.3028.

(142) Cheung, W. H.; Miclau, T.; Chow, S. K.-H.; Yang, F. F.; Alt, V. Fracture Healing in Osteoporotic Bone. Injury 2016, 47, S21–S26. https://doi.org/10.1016/S0020-1383(16)47004-X.

(143) Caldwell, A. S.; Rao, V. v.; Golden, A. C.; Bell, D. J.; Grim, J. C.; Anseth, K. S. Mesenchymal Stem Cell-Inspired Microgel Scaffolds to Control Macrophage Polarization. Bioengineering and Translational Medicine 2021, 6 (2). https://doi.org/10.1002/BTM2.10217/FORMAT/PDF.

(144) Gionet-Gonzales, M.; Casella, A.; Diloretto, D.; Ginnell, C.; Griffin, K. H.; Bigot, A.; Leach, J. K. Sulfated Alginate Hydrogels Prolong the Therapeutic Potential of MSC Spheroids by Sequestering the Secretome. Advanced Healthcare Materials 2021, 2101048. https://doi.org/10.1002/ADHM.202101048.

(145) Ando, Y.; Matsubara, K.; Ishikawa, J.; Fujio, M.; Shohara, R.; Hibi, H.; Ueda, M.; Yamamoto, A. Stem Cell-Conditioned Medium Accelerates Distraction Osteogenesis through Multiple Regenerative Mechanisms. 2014. https://doi.org/10.1016/j.bone.2013.12.029.

(146) Abdeen, A. A.; Weiss, J. B.; Lee, J.; Kilian, K. A. Matrix Composition and Mechanics Direct Proangiogenic Signaling from Mesenchymal Stem Cells. Tissue Engineering Part A 2014, 00 (00), 1–9. https://doi.org/10.1089/ten.tea.2013.0661.

(147) Ho, S. S.; Hung, B. P.; Heyrani, N.; Lee, M. A.; Leach, J. K. Hypoxic Preconditioning of Mesenchymal Stem Cells with Subsequent Spheroid Formation Accelerates Repair of

Segmental Bone Defects. Stem Cells 2018, 36 (9), 1393–1403. https://doi.org/10.1002/STEM.2853.

(148) Clark, A. Y.; Martin, K. E.; García, J. R.; Johnson, C. T.; Theriault, H. S.; Han, W. M.; Zhou, D. W.; Botchwey, E. A.; García, A. J. Integrin-Specific Hydrogels Modulate Transplanted Human Bone Marrow-Derived Mesenchymal Stem Cell Survival, Engraftment, and Reparative Activities. Nature Communications 2020, 11 (1). https://doi.org/10.1038/s41467-019-14000-9.

Chapter 2

(1) Pittenger, M. F.; Discher, D. E.; Péault, B. M.; Phinney, D. G.; Hare, J. M.; Caplan, A. I. Mesenchymal Stem Cell Perspective: Cell Biology to Clinical Progress. *npj Regenerative Medicine* **2019**, *4* (22). https://doi.org/10.1038/s41536-019-0083-6.

(2) Trounson, A.; Mcdonald, C. Cell Stem Cell Stem Cell Therapies in Clinical Trials: Progress and Challenges. *Stem Cell* **2015**, *17*, 11–22. https://doi.org/10.1016/j.stem.2015.06.007.

(3) Wechsler, M. E.; Rao, V. v; Borelli, A. N.; Anseth, K. S. Engineering the MSC Secretome : A Hydrogel Focused Approach. **2021**, *2001948*, 1–17. https://doi.org/10.1002/adhm.202001948.

(4) da Silva Meirelles, L.; Fontes, A. M.; Covas, D. T.; Caplan, A. I. Mechanisms Involved in the Therapeutic Properties of Mesenchymal Stem Cells. *Cytokine & Growth Factor Reviews* **2009**, *20* (5–6), 419–427. https://doi.org/10.1016/j.cytogfr.2009.10.002.

(5)   Lian, Q.; Liang, X.; Ding, Y.; Zhang, Y.; Tse, H.-F. Paracrine Mechanisms of Mesenchymal Stem Cell-Based Therapy: Current Status and Perspectives. *Cell Transplantation* **2014**, *23*, 1045–1059. https://doi.org/10.3727/096368913X667709.

(6)   Caplan, A. I.; Correa, D. The MSC: An Injury Drugstore. *Cell Stem Cell* **2011**, *9* (1), 11–15. https://doi.org/10.1016/j.stem.2011.06.008.

(7)   Caplan, A. I.; Correa, D. THE MSC: AN INJURY DRUGSTORE The Mesenchymal Stem Cell (MSC). **2011**. https://doi.org/10.1016/j.stem.2011.06.008.

(8)   Chen, L.; Tredget, E. E.; Wu, P. Y. G.; Wu, Y.; Wu, Y. Paracrine Factors of Mesenchymal Stem Cells Recruit Macrophages and Endothelial Lineage Cells and Enhance Wound Healing. *PLoS ONE* **2008**. https://doi.org/10.1371/journal.pone.0001886.

(9)   Kusuma, G. D.; Carthew, J.; Lim, R.; Frith, J. E. Effect of the Microenvironment on Mesenchymal Stem Cell Paracrine Signaling: Opportunities to Engineer the Therapeutic Effect. https://doi.org/10.1089/scd.2016.0349.

(10)   da Silva Meirelles, L.; Fontes, A. M.; Covas, D. T.; Caplan, A. I. Mechanisms Involved in the Therapeutic Properties of Mesenchymal Stem Cells. *Cytokine & Growth Factor Reviews* **2009**, *20* (5–6), 419–427. https://doi.org/10.1016/j.cytogfr.2009.10.002.

(11)   Phetfong, J.; Sanvoranart, T.; Nartprayut, K.; Nimsanor, N.; Seenprachawong, K.; Prachayasittikul, V.; Supokawej, A. Osteoporosis: The Current Status of Mesenchymal Stem Cell-Based Therapy. **2016**. https://doi.org/10.1186/s11658-016-0013-1.

(12)   Stoddart, M. J.; Salgado, A.; Presen, D. M.; Traweger, A.; Gimona, M.; Redl, H. Mesenchymal Stromal Cell-Based Bone Regeneration Therapies: From Cell Transplantation and Tissue Engineering to Therapeutic Secretomes and Extracellular

Vesicles. *Frontiers in Bioengineering and Biotechnology | www.frontiersin.org* **2019**, *1*, 352. https://doi.org/10.3389/fbioe.2019.00352.

(13)   Lambrechts, T.; Sonnaert, M.; Schrooten, J.; Luyten, F. P.; Aerts, J.-M.; Papantoniou, I. Large-Scale Mesenchymal Stem/Stromal Cell Expansion: A Visualization Tool for Bioprocess Comparison. *Tissue engineering. Part B, Reviews* **2016**, *22* (6), 485–498. https://doi.org/10.1089/ten.teb.2016.0111.

(14)   Panchalingam, K. M.; Jung, S.; Rosenberg, L.; Behie, L. A. Bioprocessing Strategies for the Large-Scale Production of Human Mesenchymal Stem Cells: A Review. *Stem Cell Research & Therapy* **2015**, *6* (1), 225. https://doi.org/10.1186/s13287-015-0228-5.

(15)   Trounson, A.; Mcdonald, C. Cell Stem Cell Stem Cell Therapies in Clinical Trials: Progress and Challenges. **2015**. https://doi.org/10.1016/j.stem.2015.06.007.

(16)   Ma, T.; Tsai, A. C.; Liu, Y. Biomanufacturing of Human Mesenchymal Stem Cells in Cell Therapy: Influence of Microenvironment on Scalable Expansion in Bioreactors. *Biochemical Engineering Journal* **2016**, *108*, 44–50. https://doi.org/10.1016/j.bej.2015.07.014.

(17)   A, I.; K, O.; SE, W.; AL, B. Effect of Intra-Medullar and Intra-Venous Infusions of Mesenchymal Stem Cells on Cell Engraftment by *In-Vivo* Cell Tracking and Osteoinductivity in Rabbit Long Bones: A Pilot Study. *Orthopedic & Muscular System : Current Research* **2014**, *3* (3), 172. https://doi.org/10.4172/2161-0533.1000172.

(18)   Engler, A. J.; Sen, S.; Sweeney, H. L.; Discher, D. E. Matrix Elasticity Directs Stem Cell Lineage Specification. *Cell* **2006**, *126* (4), 677–689. https://doi.org/10.1016/j.cell.2006.06.044.

(19)   Yang, C.; Tibbitt, M. W.; Basta, L.; Anseth, K. S. Mechanical Memory and Dosing Influence Stem Cell Fate. *Nature Materials* **2014**, *113*, 645–651. https://doi.org/10.1038/NMAT3889.

(20)   Ho, S. S.; Murphy, K. C.; Binder, B. Y. K.; Vissers, C. B.; Leach, J. K. Increased Survival and Function of Mesenchymal Stem Cell Spheroids Entrapped in Instructive Alginate Hydrogels. *Stem Cells Translational Medicine* **2016**, *5*, 773–781.

(21)   Murphy, K. C.; Whitehead, J.; Falahee, P. C.; Zhou, D.; Simon, S. I.; Leach, J. K. Multifactorial Experimental Design to Optimize the Anti-Inflammatory and Proangiogenic Potential of Mesenchymal Stem Cell Spheroids. *Stem Cells* **2017**, *35* (6), 1493–1504. https://doi.org/10.1002/stem.2606.

Chapter 3

(1)   Dominici M, Blanc K Le, Mueller I, et al. Minimal criteria for defining multipotent mesenchymal stromal cells . The International Society for Cellular Therapy position statement. *Cytotherapy*. 2006;8(4):315-317. doi:10.1080/14653240600855905

(2)   Billing AM, Ben Hamidane H, Dib SS, et al. Comprehensive transcriptomic and proteomic characterization of human mesenchymal stem cells reveals source specific cellular markers. *Sci Rep*. 2016;6(February):1-15. doi:10.1038/srep21507

(3)   Bunpetch V, Zhang Z-Y, Zhang X, et al. Strategies for MSC expansion and MSC-based microtissue for bone regeneration. *Biomaterials*. 2017:1-13. doi:10.1016/j.biomaterials.2017.11.023

(4)   Trounson A, Mcdonald C. Cell Stem Cell Stem Cell Therapies in Clinical Trials: Progress and Challenges. 2015. doi:10.1016/j.stem.2015.06.007

(5)   Lambrechts T, Sonnaert M, Schrooten J, Luyten FP, Aerts J-M, Papantoniou I. Large-Scale Mesenchymal Stem/Stromal Cell Expansion: A Visualization Tool for Bioprocess Comparison. *Tissue Eng Part B Rev*. 2016;22(6):485-498. doi:10.1089/ten.teb.2016.0111

(6)   Panchalingam KM, Jung S, Rosenberg L, Behie LA. Bioprocessing strategies for the large-scale production of human mesenchymal stem cells: a review. *Stem Cell Res Ther*. 2015;6(1):225. doi:10.1186/s13287-015-0228-5

(7)   Ma T, Tsai AC, Liu Y. Biomanufacturing of human mesenchymal stem cells in cell therapy: Influence of microenvironment on scalable expansion in bioreactors. *Biochem Eng J*. 2016;108:44-50. doi:10.1016/j.bej.2015.07.014

(8)   Squillaro T, Peluso G, Galderisi U. Review Clinical Trials With Mesenchymal Stem Cells : An Update. *Cell Transplant*. 2016;25:829-848.

(9)   Chen Y-S. Mesenchymal Stem Cell: Considerations for Manufacturing and Clinical Trials on Cell Therapy Product. *Int J Stem cell Res Ther*. 2016;3(1):1-12. doi:10.23937/2469-570X/1410029

(10)   Madrigal M, Rao KS, Riordan NH. A review of therapeutic effects of mesenchymal stem cell secretions and induction of secretory modification by different culture methods. *J Transl Med*. 2014;12:260. doi:10.1186/s12967-014-0260-8

(11)   Cheleuitte D, Mizuno S, Glowacki J. *In Vitro* Secretion of Cytokines by Human Bone Marrow: Effects of Age and Estrogen Status. *J Clin Endocrinol Metab*. 1998;83(6):2043-2051. doi:10.1210/jcem.83.6.4848

(12) Zhukareva V, Obrocka M, Houle JD, Fischer I, Neuhuber B. Secretion profile of human bone marrow stromal cells: Donor variability and response to inflammatory stimuli. *Cytokine*. 2010;50:317-321. doi:10.1016/j.cyto.2010.01.004

(13) Kyurkchiev D, Bochev I, Ivanova-Todorova E, et al. Secretion of immunoregulatory cytokines by mesenchymal stem cells. *World J Stem Cells J Stem Cells*. 2014;6(65):552-570. doi:10.4252/wjsc.v6.i5.552

(14) Li C, Li G, Liu M, Zhou T, Zhou H. Paracrine effect of inflammatory cytokine-activated bone marrow mesenchymal stem cells and its role in osteoblast function. *J Biosci Bioeng*. 2016;121(2):213-219. doi:10.1016/j.jbiosc.2015.05.017

(15) Bone RC. Sepsis: A New Hypothesis for Pathogenesis of the Disease Process*. *Chest*. 1997;112(1):235-243. doi:10.1378/chest.112.1.235

(16) Rustad KC, Wong VW, Sorkin M, et al. Enhancement of mesenchymal stem cell angiogenic capacity and stemness by a biomimetic hydrogel scaffold. *Biomaterials*. 2012;33(1):80-90. doi:10.1016/J.BIOMATERIALS.2011.09.041

(17) Kwon HM, Hur SM, Park KY, et al. Multiple paracrine factors secreted by mesenchymal stem cells contribute to angiogenesis. *Vascul Pharmacol*. 2014;63(1):19-28. doi:10.1016/j.vph.2014.06.004

(18) Dupont S, Morsut L, Aragona M, et al. Role of YAP/TAZ in mechanotransduction. *Nature*. 2011;474(7350):179-183. doi:10.1038/nature10137

(19) Engler AJ, Sen S, Sweeney HL, Discher DE. Matrix Elasticity Directs Stem Cell Lineage Specification. *Cell*. 2006;126(4):677-689. doi:10.1016/j.cell.2006.06.044

(20) Yang C, Tibbitt MW, Basta L, Anseth KS. Mechanical memory and dosing influence stem cell fate. *Nat Mater*. 2014;113:645-651. doi:10.1038/NMAT3889

(21)   Mammoto A, Connor KM, Mammoto T, et al. A mechanosensitive transcriptional mechanism that controls angiogenesis. *Nature*. 2009;457(7233):1103-1108. doi:10.1038/nature07765

(22)   Chen Xi Li1†, Nilesh P. Talele1†, Stellar Boo1†, et al. MicroRNA-21 preserves the fibrotic mechanical memory of mesenchymal stem cells. *Nat Mater*. 2016;16(3).

(23)   Wagner W, Horn P, Castoldi M, et al. Replicative Senescence of Mesenchymal Stem Cells: A Continuous and Organized Process. *PLoS One*. 2008;3(5). doi:10.1371/journal.pone.0002213

(24)   Jiang T, Xu G, Wang Q, et al. In vitro expansion impaired the stemness of early passage mesenchymal stem cells for treatment of cartilage defects. *Nat Publ Gr*. 2017;8. doi:10.1038/cddis.2017.215

(25)   Wu PK, Wang JY, Chen CF, et al. Early passage mesenchymal stem cells display decreased radiosensitivity and increased DNA repair activity. *Stem Cells Transl Med*. 2017;6(6):1504-1514. doi:10.1002/sctm.15-0394

(26)   Wagner W, Horn P, Castoldi M, et al. Replicative Senescence of Mesenchymal Stem Cells: A Continuous and Organized Process. *PLoS One*. 2008;3(5). doi:10.1371/journal.pone.0002213

(27)   Banfi A, Bianchi G, Notaro R, Luzzatto L, Cancedda R, Quarto R. Replicative Aging and Gene Expression in Long-Term Cultures of Human Bone Marrow Stromal Cells. *TISSUE Eng*. 2002;8(6).

(28)   Blasco MA. Telomere length, stem cells and aging. *Nat Chem Biol*. 2007. doi:10.1038/nchembio.2007.38

(29)   Lech W, Figiel-Dabrowska A, Sarnowska A, et al. Phenotypic, Functional, and Safety Control at Preimplantation Phase of MSC-Based Therapy. *Stem Cells Int*. 2016;2016. doi:10.1155/2016/2514917

(30)   Fairbanks BD, Schwartz MP, Halevi AE, Nuttelman CR, Bowman CN, Anseth KS. A Versatile Synthetic Extracellular Matrix Mimic via Thiol- Norbornene Photopolymerization. *Adv Mater*. 2009;21(48):5005-5010. doi:10.1002/adma.200901808

(31)   Gould ST, Darling NJ, Anseth KS. Small peptide functionalized thiol–ene hydrogels as culture substrates for understanding valvular interstitial cell activation and de novo tissue deposition. *Acta Biomater*. 2012;8:3201-3209. doi:10.1016/j.actbio.2012.05.009

(32)   Fairbanks BD, Schwartz MP, Bowman CN, Anseth KS. Photoinitiated polymerization of PEG-diacrylate with lithium phenyl-2,4,6-trimethylbenzoylphosphinate: polymerization rate and cytocompatibility. *Biomaterials*. 2009;30(35):6702-6707. doi:10.1016/j.biomaterials.2009.08.055

(33)   Lin C-C, Anseth KS. Cell-cell communication mimicry with poly(ethylene glycol) hydrogels for enhancing beta-cell function. *Proc Natl Acad Sci U S A*. 2011;108(16):6380-6385. doi:10.1073/pnas.1014026108

(34)   Fiedler CI, Aisenbrey EA, Wahlquist JA, et al. Enhanced mechanical properties of photo-clickable thiol–ene PEG hydrogels through repeated photopolymerization of in-swollen macromer. *Soft Matter*. 2016;12(44):9095-9104. doi:10.1039/C6SM01768A

(35)   Sawicki LA, Kloxin AM. Design of thiol–ene photoclick hydrogels using facile techniques for cell culture applications. *Biomater Sci*. 2014;2(11):1612-1626. doi:10.1039/C4BM00187G

(36)   Chen VJ, Ma PX. *Scaffolding In Tissue Engineering*.; 2006. doi:10.1007/s13398-014-0173-7.2

(37)   Shin J-W, Buxboim A, Spinler KR, et al. Contractile Forces Sustain and Polarize Hematopoiesis from Stem and Progenitor Cells. *Cell Stem Cell*. 2014;14(1):81-93. doi:10.1016/J.STEM.2013.10.009

(38)   Ivanovska IL, Shin J-W, Swift J, Discher DE. Stem cell mechanobiology: diverse lessons from bone marrow. *Trends Cell Biol*. 2015;25(9):523-532. doi:10.1016/J.TCB.2015.04.003

(39)   Griffith JW, Sokol CL, Luster AD. Chemokines and Chemokine Receptors: Positioning Cells for Host Defense and Immunity. *Annu Rev Immunol*. 2014;32:659-702. doi:10.1146/annurev-immunol-032713-120145

(40)   Corwin EJ. Understanding Cytokines Part I: Physiology and Mechanism of Action Cytokine Physiology. *Biol Res Nurs Corwin / Underst Cytokines Part I*. 2000;2(1). http://journals.sagepub.com/doi/pdf/10.1177/109980040000200104. Accessed April 9, 2018.

(41)   Chen Q, Shou P, Zhang L, et al. An osteopontin-integrin interaction plays a critical role in directing adipogenesis and osteogenesis by mesenchymal stem cells. *Stem Cells*. 2014;32(2):327-337. doi:10.1002/stem.1567

(42)   Kloxin AM, Kasko AM, Salinas CN, Anseth KS. Photodegradable hydrogels for dynamic tuning of physical and chemical properties. *Science*. 2009;324(5923):59-63. doi:10.1126/science.1169494

(43)   Martin C, Olmos É, Collignon M-L, et al. Revisiting MSC expansion from critical quality attributes to critical culture process parameters. *Process Biochem*. 2017;59:231-243. doi:10.1016/j.procbio.2016.04.017

(44)   Pourgholaminejad A, Aghdami N, Baharvand H, Moazzeni SM. The effect of pro-inflammatory cytokines on immunophenotype, differentiation capacity and immunomodulatory functions of human mesenchymal stem cells. *Cytokine*. 2016;85:51-60. doi:10.1016/j.cyto.2016.06.003

(45)   Gnecchi M, Danieli P, Malpasso G, Ciuffreda MC. Paracrine Mechanisms of Mesenchymal Stem Cells in Tissue Repair. In: *Methods in Molecular Biology (Clifton, N.J.)*. Vol 1416. ; 2016:123-146. doi:10.1007/978-1-4939-3584-0_7

(46)   Chen X, Shao H, Zhi Y, et al. CD73 Pathway Contributes to the Immunosuppressive Ability of Mesenchymal Stem Cells in Intraocular Autoimmune Responses. *Stem Cells Dev*. 2016;25(4):337-346. doi:10.1089/scd.2015.0227

(47)   Kaku H, Cheng KF, Al-Abed Y, Rothstein TL. A Novel Mechanism of B Cell–Mediated Immune Suppression through CD73 Expression and Adenosine Production. *J Immunol*. 2014;193(12):5904-5913. doi:10.4049/jimmunol.1400336

(48)   Na T, Liu J, Zhang K, Ding M, Yuan B-Z. The Notch Signaling Regulates CD105 Expression, Osteogenic Differentiation and Immunomodulation of Human Umbilical Cord Mesenchymal Stem Cells. *PLoS One*. 2015:1-19. doi:10.1371/journal.pone.0118168

(49)   Hocking AM. The Role of Chemokines in Mesenchymal Stem Cell Homing to Wounds. *Adv Wound Care*. 2015;4(11):623-630. doi:10.1089/wound.2014.0579

Chapter 4

(1)   Trounson, A. & Mcdonald, C. Cell Stem Cell Stem Cell Therapies in Clinical Trials: Progress and Challenges. *Stem Cell* **17**, 11–22 (2015).

(2)   Caplan, A. I. & Correa, D. The MSC: An Injury Drugstore. *Cell Stem Cell* **9**, 11–15 (2011).

(3)   da Silva Meirelles, L., Fontes, A. M., Covas, D. T. & Caplan, A. I. Mechanisms involved in the therapeutic properties of mesenchymal stem cells. *Cytokine Growth Factor Rev.* **20**, 419–427 (2009).

(4)   Huebsch, N. *et al.* Matrix elasticity of void-forming hydrogels controls transplanted-stem-cell-mediated bone formation. *Nat. Mater.* **14**, 1269–77 (2015).

(5)   Engler, A. J., Sen, S., Sweeney, H. L. & Discher, D. E. Matrix Elasticity Directs Stem Cell Lineage Specification. *Cell* **126**, 677–689 (2006).

(6)   Murphy, W. L., McDevitt, T. C. & Engler, A. J. Materials as stem cell regulators. *Nat. Mater.* **13**, 547–556 (2014).

(7)   Killaars, A. R. *et al.* Extended Exposure to Stiff Microenvironments Leads to Persistent Chromatin Remodeling in Human Mesenchymal Stem Cells. *Adv. Sci.* **6**, 1801483 (2019).

(8)   Caliari, S. R., an Vega, S. L., Kwon, M., Soulas, E. M. & Burdick, J. A. Dimensionality and spreading influence MSC YAP/TAZ signaling in hydrogel environments. *Biomaterials* **103**, 314–323 (2016).

(9)   Di Luca, A. *et al.* Influencing chondrogenic differentiation of human mesenchymal stromal cells in scaffolds displaying a structural gradient in pore size. *Acta Biomater.* **36**, 210–219 (2016).

(10)   Gupte, M. J. *et al.* Pore size directs bone marrow stromal cell fate and tissue regeneration in nanofibrous macroporous scaffolds by mediating vascularization. *Acta Biomater.* **82**, 1–11 (2018).

(11)   Karimi, F., O'Connor, A. J., Qiao, G. G. & Heath, D. E. Integrin Clustering Matters: A Review of Biomaterials Functionalized with Multivalent Integrin-Binding Ligands to Improve Cell Adhesion, Migration, Differentiation, Angiogenesis, and Biomedical Device Integration. *Adv. Healthc. Mater.* **1701324**, 1–28 (2018).

(12)   Burdick, J. A. & Anseth, K. S. Photoencapsulation of osteoblasts in injectable RGD-modified PEG hydrogels for bone tissue engineering. *Biomaterials* **23**, 4315–4323 (2002).

(13)   Rao, V. V., Vu, M. K., Ma, H., Killaars, A. R. & Anseth, K. S. Rescuing mesenchymal stem cell regenerative properties on hydrogel substrates post serial expansion. *Bioeng. Transl. Med.* **4**, 51–60 (2019).

(14)   Abdeen, A. A., Weiss, J. B., Lee, J. & Kilian, K. A. Matrix Composition and Mechanics Direct Proangiogenic Signaling from Mesenchymal Stem Cells. *Tissue Eng. Part A* **00**, 1–9 (2014).

(15)   Gionet-Gonzales, M. A. & Leach, J. K. Engineering principles for guiding spheroid function in the regeneration of bone, cartilage, and skin. *Biomed. Mater.* **13**, 034109 (2018).

(16)   Ho, S. S., Murphy, K. C., Binder, B. Y. K., Vissers, C. B. & Leach, J. K. Increased Survival and Function of Mesenchymal Stem Cell Spheroids Entrapped in Instructive Alginate Hydrogels. *Stem Cells Transl. Med.* **5**, 773–781 (2016).

(17)   Murphy, K. C. *et al.* Multifactorial Experimental Design to Optimize the Anti-Inflammatory and Proangiogenic Potential of Mesenchymal Stem Cell Spheroids. *Stem Cells* **35**, 1493–1504 (2017).

(18)   Qazi, T. H., Mooney, D. J., Duda, G. N. & Geissler, S. Biomaterials that promote cell-cell interactions enhance the paracrine function of MSCs. *Biomaterials* **140**, 103–114 (2017).

(19)   Caldwell, A. S., Campbell, G. T., Shekiro, K. M. T. & Anseth, K. S. Clickable Microgel Scaffolds as Platforms for 3D Cell Encapsulation. *Adv. Healthc. Mater.* **6**, 1–8 (2017).

(20)   Bian, L., Guvendiren, M., Mauck, R. L. & Burdick, J. A. Hydrogels that mimic developmentally relevant matrix and N-cadherin interactions enhance MSC chondrogenesis. **110**, 10117–10122 (2013).

(21)   Deforest, C. A., Polizzotti, B. D. & Anseth, K. S. Sequential click reactions for synthesizing and patterning three-dimensional cell microenvironments. *Nat. Mater.* (2009). doi:10.1038/nmat2473

(22)   Yang, C., Tibbitt, M. W., Basta, L. & Anseth, K. S. Mechanical memory and dosing influence stem cell fate. *Nat. Mater.* **113**, 645–651 (2014).

(23)   Cosgrove, B. D. *et al.* N-cadherin adhesive interactions modulate matrix mechanosensing and fate commitment of mesenchymal stem cells. *Nat. Mater.* **15**, 1297–1306 (2016).

(24)   Galderisi, U. & Giordano, A. The Gap Between the Physiological and Therapeutic Roles of Mesenchymal Stem Cells. *Med. Res. Rev.* **34**, 1100–1126 (2014).

(25)   Ranganath, S. H., Levy, O., Inamdar, M. S. & Karp, J. M. Harnessing the Mesenchymal Stem Cell Secretome for the Treatment of Cardiovascular Disease. *Cell Stem Cell* **10**, 244–258 (2012).

(26)   Lian, Q., Liang, X., Ding, Y., Zhang, Y. & Tse, H.-F. Paracrine Mechanisms of Mesenchymal Stem Cell-Based Therapy: Current Status and Perspectives. *Cell Transplant.* **23**, 1045–1059 (2014).

(27)   Ferreira, J. R. *et al.* Mesenchymal Stromal Cell Secretome: Influencing Therapeutic Potential by Cellular Pre-conditioning. *Front. Immunol.* **9**, 2837 (2018).

(28)   Gumbiner, B. M. Regulation of cadherin-mediated adhesion in morphogenesis. *Nat. Rev. Mol. Cell Biol.* **6**, 622–634 (2005).

(29)   Galderisi, U., Squillaro, T. & Peluso, G. Clinical Trials With Mesenchymal Stem Cells: An Update. *Cell Transplant.* **25**, 829–848 (2016).

(30)   Ferrara, N., Gerber, H. P. & LeCouter, J. The biology of VEGF and its receptors. *Nat. Med.* **9**, 669–676 (2003).

(31)   Pons, J. *et al.* VEGF improves survival of mesenchymal stem cells in infarcted hearts. *Biochem. Biophys. Res. Commun.* **376**, 419–422 (2008).

(32)   Tang, J. M. *et al.* VEGF/SDF-1 promotes cardiac stem cell mobilization and myocardial repair in the infarcted heart. *Cardiovasc. Res.* **91**, 402–411 (2011).

(33)   Ibáñez, C. F. & Andressoo, J.-O. Biology of GDNF and its receptors — Relevance for disorders of the central nervous system. *Neurobiol. Dis.* **97**, 80–89 (2017).

(34)   Hoban, D. B., Howard, L. & Dowd, E. GDNF-secreting mesenchymal stem cells provide localized neuroprotection in an inflammation-driven rat model of Parkinson's disease. *Neuroscience* **303**, 402–411 (2015).

(35)   Haider, H. K., Jiang, S., Idris, N. M. & Ashraf, M. Cellular Biology IGF-1-Overexpressing Mesenchymal Stem Cells Accelerate Bone Marrow Stem Cell Mobilization via Paracrine

Activation of SDF-1/CXCR4 Signaling to Promote Myocardial Repair. (2008). doi:10.1161/CIRCRESAHA.108.186742

(36)   Hunt, L. C. & White, J. The Role of Leukemia Inhibitory Factor Receptor Signaling in Skeletal Muscle Growth, Injury and Disease. in *Growth Factors and Cytokines in Skeletal Muscle Development, Growth, Regeneration and Disease* (eds. White, J. & Smythe, G.) 45–59 (Springer International Publishing, 2016). doi:10.1007/978-3-319-27511-6_3

(37)   Sideris, E. *et al.* Particle Hydrogels Based on Hyaluronic Acid Building Blocks. *ACS Biomater. Sci. Eng.* **2**, 2034–2041 (2016).

(38)   Scott, E. A., Nichols, M. D., Kuntz-Willits, R. & Elbert, D. L. Modular scaffolds assembled around living cells using poly(ethylene glycol) microspheres with macroporation via a non-cytotoxic porogen. *Acta Biomater.* **6**, 29–38 (2010).

(39)   Roam, J. L. *et al.* A modular, plasmin-sensitive, clickable poly(ethylene glycol)-heparin-laminin microsphere system for establishing growth factor gradients in nerve guidance conduits. *Biomaterials* **72**, 112–124 (2015).

(40)   Truong, N. F. *et al.* Microporous annealed particle hydrogel stiffness, void space size, and adhesion properties impact cell proliferation, cell spreading, and gene transfer. *Acta Biomater.* **94**, 160–172 (2019).

(41)   Griffin, D. R., Weaver, W. M., Scumpia, P. O., Di Carlo, D. & Segura, T. Accelerated wound healing by injectable microporous gel scaffolds assembled from annealed building blocks. *Nat. Mater.* (2015). doi:10.1038/nmat4294

(42)   Imparato, G., Urciuolo, F., Casale, C. & Netti, P. A. The role of microscaffold properties in controlling the collagen assembly in 3D dermis equivalent using modular tissue engineering. *Biomaterials* **34**, 7851–7861 (2013).

(43)   Koh, J. *et al.* Enhanced In Vivo Delivery of Stem Cells using Microporous Annealed Particle Scaffolds. *Small* 1903147 (2019). doi:10.1002/smll.201903147

(44)   Yao, M.-H. *et al.* Directed self-assembly of polypeptide-engineered physical microgels for building porous cell-laden hydrogels. *Chem. Commun. (Camb).* **50**, 9405–8 (2014).

(45)   Kim, J., Li, W. A., Sands, W. & Mooney, D. J. Effect of pore structure of macroporous poly(lactide-co-glycolide) scaffolds on the in vivo enrichment of dendritic cells. *ACS Appl. Mater. Interfaces* **6**, 8505–8512 (2014).

(46)   Chen, R., Ma, H., Zhang, L. & Bryers, J. D. Precision-porous templated scaffolds of varying pore size drive dendritic cell activation. *Biotechnol. Bioeng.* **115**, 1086–1095 (2018).

(47)   Vissers, C. A. B., Harvestine, J. N. & Leach, J. K. Pore size regulates mesenchymal stem cell response to Bioglass-loaded composite scaffolds. *J. Mater. Chem. B* **3**, 8650–8658 (2015).

(48)   Qazi, T. H. *et al.* Extrusion Printed Sca ff olds with Varying Pore Size As Modulators of MSC Angiogenic Paracrine E ff ects. (2019). doi:10.1021/acsbiomaterials.9b00843

(49)   Mao, A. S. *et al.* Programmable microencapsulation for enhanced mesenchymal stem cell persistence and immunomodulation. doi:10.1073/pnas.1819415116

(50)   Hass, R., Kasper, C., Böhm, S. & Jacobs, R. Different populations and sources of human mesenchymal stem cells (MSC): A comparison of adult and neonatal tissue-derived MSC. *Cell Commun. Signal.* **9**, (2011).

(51)   Pires, A. O. *et al.* Unveiling the Differences of Secretome of Human Bone Marrow Mesenchymal Stem Cells, Adipose Tissue-Derived Stem Cells, and Human Umbilical Cord Perivascular Cells: A Proteomic Analysis. *Stem Cells Dev.* **25**, 1073–1083 (2016).

Chapter 5

(1)   Harris, A. M.; Althausen, P. L.; Kellam, J.; Bosse, M. J.; Castillo, R. Complications Following Limb-Threatening Lower Extremity Trauma. *Journal of Orthopaedic Trauma* **2009**, *23* (1), 1–6. https://doi.org/10.1097/BOT.0B013E31818E43DD.

(2)   Karladani, A. H.; Granhed, J.; Kärrholm, J.; Styf, J. The Influence of Fracture Etiology and Type on Fracture Healing: A Review of 104 Consecutive Tibial Shaft Fractures. *Archives of orthopaedic and trauma surgery* **2001**, *121* (6), 325–328. https://doi.org/10.1007/S004020000252.

(3)   Bernabé, P. F. E.; Melo, L. G. N.; Cintra, L. T. A.; Gomes-Filho, J. E.; Dezan, E.; Nagata, M. J. H. Bone Healing in Critical-Size Defects Treated with Either Bone Graft, Membrane, or a Combination of Both Materials: A Histological and Histometric Study in Rat Tibiae. *Clinical Oral Implants Research* **2012**. https://doi.org/10.1111/j.1600-0501.2011.02166.x.

(4)   Frost; Sullivan. *U.S. Trauma Fixation Markets*; 2008.

(5)   Damien, C. J.; Parsons, J. R. Bone Graft and Bone Graft Substitutes: A Review of Current Technology and Applications. *Journal of applied biomaterials : an official journal of the Society for Biomaterials* **1991**, *2* (3), 187–208. https://doi.org/10.1002/JAB.770020307.

(6)   Coventry, M. B.; Tapper, E. Pelvic Instability: Aconsequence of Removing Iliac Bone for Grafting. . *The Journal of Joint and Bone Surgery* **1972**.

(7)   Wojda, S. J.; Donahue, S. W. Parathyroid Hormone for Bone Regeneration. *Journal of Orthopaedic Research* **2018**. https://doi.org/10.1002/jor.24075.

(8)   Meijer, G. J.; Bruijn, J. D. de; Koole, R.; Blitterswijk, C. A. van. Cell-Based Bone Tissue Engineering. *PLOS Medicine* **2007**, *4* (2), e9. https://doi.org/10.1371/JOURNAL.PMED.0040009.

(9)   Bhumiratana, S.; Bernhard, J. C.; Alfi, D. M.; Yeager, K.; Eton, R. E.; Bova, J.; Shah, F.; Gimble, J. M.; Lopez, M. J.; Eisig, S. B.; Vunjak-Novakovic, G. Tissue-Engineered Autologous Grafts for Facial Bone Reconstruction. *Science translational medicine* **2016**, *8* (343), 343ra83. https://doi.org/10.1126/SCITRANSLMED.AAD5904.

(10)   Murphy, M. P.; Quarto, N.; Longaker, M. T.; Wan, D. C. Calvarial Defects: Cell-Based Reconstructive Strategies in the Murine Model. https://doi.org/10.1089/ten.tec.2017.0230.

(11)   Levy, O.; Kuai, R.; Siren, E. M. J.; Bhere, D.; Milton, Y.; Nissar, N.; de Biasio, M.; Heinelt, M.; Reeve, B.; Abdi, R.; Alturki, M.; Fallatah, M.; Almalik, A.; Alhasan, A. H.; Shah, K.; Karp, J. M. Shattering Barriers toward Clinically Meaningful MSC Therapies. *Science Advances* **2020**, *6*.

(12)   Stoddart, M. J.; Salgado, A.; Presen, D. M.; Traweger, A.; Gimona, M.; Redl, H. Mesenchymal Stromal Cell-Based Bone Regeneration Therapies: From Cell Transplantation and Tissue Engineering to Therapeutic Secretomes and Extracellular Vesicles. *Frontiers in Bioengineering and Biotechnology | www.frontiersin.org* **2019**, *1*, 352. https://doi.org/10.3389/fbioe.2019.00352.

(13)   Phetfong, J.; Sanvoranart, T.; Nartprayut, K.; Nimsanor, N.; Seenprachawong, K.; Prachayasittikul, V.; Supokawej, A. Osteoporosis: The Current Status of Mesenchymal Stem Cell-Based Therapy. *Cellular & Molecular Biology Letters* **2016**, *21* (1), 12. https://doi.org/10.1186/s11658-016-0013-1.

(14)   Antebi, B.; Pelled, G.; Gazit, D. Stem Cell Therapy for Osteoporosis. *Current Osteoporosis Reports* **2014**, *12* (1), 41–47. https://doi.org/10.1007/s11914-013-0184-x.

(15)   Wechsler, M. E.; Rao, V. v; Borelli, A. N.; Anseth, K. S. Engineering the MSC Secretome : A Hydrogel Focused Approach. **2021**, *2001948*, 1–17. https://doi.org/10.1002/adhm.202001948.

(16)   Dominici, M.; Blanc, K. Le; Mueller, I.; Marini, F. C.; Krause, D. S.; Deans, R. J.; Keating, A.; Prockop, D. J.; Horwitz, E. M. Minimal Criteria for Defining Multipotent Mesenchymal Stromal Cells . The International Society for Cellular Therapy Position Statement. *Cytotherapy* **2006**, *8* (4), 315–317. https://doi.org/10.1080/14653240600855905.

(17)   Shang, F.; Yu, Y.; Liu, S.; Ming, L.; Zhang, Y.; Zhou, Z.; Zhao, J.; Jin, Y. Advancing Application of Mesenchymal Stem Cell-Based Bone Tissue Regeneration. *Bioactive Materials*. KeAi Communications Co. March 1, 2021, pp 666–683. https://doi.org/10.1016/j.bioactmat.2020.08.014.

(18)   Pittenger, M. F.; Discher, D. E.; Péault, B. M.; Phinney, D. G.; Hare, J. M.; Caplan, A. I. Mesenchymal Stem Cell Perspective: Cell Biology to Clinical Progress. *npj Regenerative Medicine* **2019**, *4* (22). https://doi.org/10.1038/s41536-019-0083-6.

(19)   Osugi, M.; Katagiri, W.; Yoshimi, R.; Inukai, T.; Hibi, H.; Ueda, M. Conditioned Media from Mesenchymal Stem Cells Enhanced Bone Regeneration in Rat Calvarial Bone Defects. *Tissue Engineering - Part A* **2012**, *18* (13–14), 1479–1489. https://doi.org/10.1089/ten.tea.2011.0325.

(20)   Levit, R. D.; Landázuri, N.; Phelps, E. A.; Brown, M. E.; García, A. J.; Davis, M. E.; Joseph, G.; Long, R.; Safley, S. A.; Suever, J. D.; Lyle, A. N.; Weber, C. J.; Taylor, W. R.

Cellular Encapsulation Enhances Cardiac Repair. *Journal of the American Heart Association* **2013**. https://doi.org/10.1161/JAHA.113.000367.

(21) van der Bogt, K. E. A.; Sheikh, A. Y.; Schrepfer, S.; Hoyt, G.; Cao, F.; Ransohoff, K. J.; Swijnenburg, R. J.; Pearl, J.; Lee, A.; Fischbein, M.; Contag, C. H.; Robbins, R. C.; Wu, J. C. Comparison of Different Adult Stem Cell Types for Treatment of Myocardial Ischemia. *Circulation* **2008**. https://doi.org/10.1161/CIRCULATIONAHA.107.759480.

(22) Ishihara, A. Effect of Intra-Medullar and Intra-Venous Infusions of Mesenchymal Stem Cells on Cell Engraftment by In-Vivo Cell Tracking and Osteoinductivity in Rabbit Long Bones: A Pilot Study. *Orthopedic & Muscular System* **2014**. https://doi.org/10.4172/2161-0533.1000172.

(23) Mao, A. S.; Özkale, B.; Shah, N. J.; Vining, K. H.; Descombes, T.; Zhang, L.; Tringides, C. M.; Wong, S.-W.; Shin, J.-W.; Scadden, D. T.; Weitz, D. A.; Mooney, D. J. Programmable Microencapsulation for Enhanced Mesenchymal Stem Cell Persistence and Immunomodulation. https://doi.org/10.1073/pnas.1819415116.

(24) Rustad, K. C.; Wong, V. W.; Sorkin, M.; Glotzbach, J. P.; Major, M. R.; Rajadas, J.; Longaker, M. T.; Gurtner, G. C. Enhancement of Mesenchymal Stem Cell Angiogenic Capacity and Stemness by a Biomimetic Hydrogel Scaffold. *Biomaterials* **2012**, *33* (1), 80–90. https://doi.org/10.1016/j.biomaterials.2011.09.041.

(25) Qazi, T. H.; Mooney, D. J.; Duda, G. N.; Geissler, S. Biomaterials That Promote Cell-Cell Interactions Enhance the Paracrine Function of MSCs. *Biomaterials* **2017**, *140*, 103–114. https://doi.org/10.1016/j.biomaterials.2017.06.019.

(26) Qazi, T. H.; Mooney, D. J.; Duda, G. N.; Geissler, S. Niche-Mimicking Interactions in Peptide-Functionalized 3D Hydrogels Amplify Mesenchymal Stromal Cell Paracrine Effects. *Biomaterials* **2020**, *230*. https://doi.org/10.1016/j.biomaterials.2019.119639.

(27) Caldwell, A. S.; Rao, V. v.; Golden, A. C.; Anseth, K. S. Porous Bio-Click Microgel Scaffolds Control HMSC Interactions and Promote Their Secretory Properties. *Biomaterials* **2020**, *232* (December 2019), 119725. https://doi.org/10.1016/j.biomaterials.2019.119725.

(28) Caldwell, A. S.; Rao, V. v.; Golden, A. C.; Bell, D. J.; Grim, J. C.; Anseth, K. S. Mesenchymal Stem Cell-Inspired Microgel Scaffolds to Control Macrophage Polarization. *Bioengineering and Translational Medicine* **2021**, *6* (2). https://doi.org/10.1002/BTM2.10217/FORMAT/PDF.

(29) Rapp, T. L.; DeForest, C. A. Visible Light-Responsive Dynamic Biomaterials: Going Deeper and Triggering More. *Advanced Healthcare Materials* **2020**, *9* (7), 1901553. https://doi.org/10.1002/ADHM.201901553.

Chapter 6

(1)   Eastell, R.; O, T. W.; Hofbauer, L. C.; Langdahl, B.; Reid, I. R.; Gold, D. T.; Cummings, S. R. Postmenopausal Osteoporosis. **2016**. https://doi.org/10.1038/nrdp.2016.69.

(2)   Yu, B.; Wang, C. Y. Osteoporosis: The Result of an 'Aged' Bone Microenvironment. *Trends in Molecular Medicine* **2016**, *22* (8), 641–644. https://doi.org/10.1016/j.molmed.2016.06.002.

(3)   Eastell, R.; O, T. W.; Hofbauer, L. C.; Langdahl, B.; Reid, I. R.; Gold, D. T.; Cummings, S. R. Postmenopausal Osteoporosis. *Nature Review Primer* **2016**. https://doi.org/10.1038/nrdp.2016.69

(4)   Wu, D.; Cline-Smith, A.; Shashkova, E.; Aurora, R. *Osteoporosis: A Multifactorial Disease*.

(5)   Whitfield, J. F. How to Grow Bone to Treat Osteoporosis and Mend Fractures. *Current osteoporosis reports* **2003**, *1* (1), 32–40. https://doi.org/10.1007/s11914-003-0006-7.

(6)   Cheung, W. H.; Miclau, T.; Chow, S. K.-H.; Yang, F. F.; Alt, V. Fracture Healing in Osteoporotic Bone. *Injury* **2016**, *47*, S21–S26. https://doi.org/10.1016/S0020-1383(16)47004-X.

(7)   Park, D.; Spencer, J. A.; Koh, B. I.; Kobayashi, T.; Fujisaki, J.; Clemens, T. L.; Lin, C. P.; Kronenberg, H. M.; Scadden, D. T. Endogenous Bone Marrow MSCs Are Dynamic, Fate-Restricted Participants in Bone Maintenance and Regeneration. *Cell Stem Cell* **2012**, *10* (3), 259–272. https://doi.org/10.1016/j.stem.2012.02.003.

(8)   Tewari, M. C.; Nagar, G. K.; Vishwakarma, A. L.; Ogechukwu, O. E.; Bellare, J. R.; Gambhir, S.; Chattopadhyay, N. Ovariectomized Rats with Established Osteopenia Have

Diminished Mesenchymal Stem Cells in the Bone Marrow and Impaired Homing, Osteoinduction and Bone Regeneration at the Fracture Site. *Stem Cell Reviews and Reports* **2015**, *11* (2), 309–321. https://doi.org/10.1007/s12015-014-9573-5.

(9)   Corrigan, M. A.; Coyle, S.; Eichholz, K. F.; Riffault, M.; Lenehan, B.; Hoey, D. A. Aged Osteoporotic Bone Marrow Stromal Cells Demonstrate Defective Recruitment, Mechanosensitivity, and Matrix Deposition. *Cells Tissues Organs* **2019**, *207* (2), 83–96. https://doi.org/10.1159/000503444.

(10)   Cao, X.; Frenette, P. S.; Mao, J. J.; Robey, P. G.; Simmons, P. J.; Wang, C.-Y.; Bianco, P. The Meaning, the Sense and the Significance: Translating the Science of Mesenchymal Stem Cells into Medicine. *Nature Medicine* **2013**. https://doi.org/10.1038/nm.3028.

(11)   Wechsler, M. E.; Rao, V. v; Borelli, A. N.; Anseth, K. S. Engineering the MSC Secretome: A Hydrogel Focused Approach. **2021**, *2001948*, 1–17. https://doi.org/10.1002/adhm.202001948.

(12)   Pittenger, M. F.; Discher, D. E.; Péault, B. M.; Phinney, D. G.; Hare, J. M.; Caplan, A. I. Mesenchymal Stem Cell Perspective: Cell Biology to Clinical Progress. *npj Regenerative Medicine* **2019**, *4* (22). https://doi.org/10.1038/s41536-019-0083-6.

(13)   Stoddart,   M. J.; Salgado, A .; Presen, D. M.; Traweger , A.; Gimona, M.; Redl, H. Mesenchymal Stromal Cell-Based Bone Regeneration Therapies: From Cell Transplantation and Tissue Engineering to Therapeutic Secretomes and Extracellular Vesicles. *Frontiers in Bioengineering and Biotechnology | www.frontiersin.org* **2019**, *1*, 352. https://doi.org/10.3389/fbioe.2019.00352.

(14)   Levy, O.; Kuai, R.; Siren, E. M. J.; Bhere, D.; Milton, Y.; Nissar, N.; de Biasio, M.; Heinelt, M.; Reeve, B.; Abdi, R.; Alturki, M.; Fallatah, M.; Almalik, A.; Alhasan, A. H.; Shah, K.

Karp, J. M. Shattering Barriers toward Clinically Meaningful MSC Therapies. *Science Advances* **2020**, *6*.

(15) Osugi, M.; Katagiri, W.; Yoshimi, R.; Inukai, T.; Hibi, H.; Ueda, M. Conditioned Media from Mesenchymal Stem Cells Enhanced Bone Regeneration in Rat Calvarial Bone Defects. *Tissue Engineering - Part A* **2012**, *18* (13–14), 1479–1489. https://doi.org/10.1089/ten.tea.2011.0325.

(16) Qazi, T. H.; Mooney, D. J.; Duda, G. N.; Geissler, S. Biomaterials That Promote Cell-Cell Interactions Enhance the Paracrine Function of MSCs. *Biomaterials* **2017**, *140*, 103–114. https://doi.org/10.1016/j.biomaterials.2017.06.019.

(17) Gionet-Gonzales, M. A.; Leach, J. K. Engineering Principles for Guiding Spheroid Function in the Regeneration of Bone, Cartilage, and Skin. *Biomedical Materials (Bristol)* **2018**, *13* (3). https://doi.org/10.1088/1748-605X/aab0b3.

(18) Ho, S. S.; Murphy, K. C.; Binder, B. Y. K.; Vissers, C. B.; Leach, J. K. Increased Survival and Function of Mesenchymal Stem Cell Spheroids Entrapped in Instructive Alginate Hydrogels. *Stem Cells Translational Medicine* **2016**, *5*, 773–781.

(19) Caldwell, A. S.; Rao, V. v.; Golden, A. C.; Anseth, K. S. Porous Bio-Click Microgel Scaffolds Control hMSC Interactions and Promote Their Secretory Properties. *Biomaterials* **2020**, *232* (December 2019), 119725. https://doi.org/10.1016/j.biomaterials.2019.119725.

(20) Helfrich, M. H.; Ralston, S. H.; Idris, A. I. Ovariectomy/Orchidectomy in Rodents. *Methods in Molecular Biology* **2012**, *816*, 545–551. https://doi.org/10.1007/978-1-61779-415-5_34.

(21)   Rossow, T.; Seiffert, S. Supramolecular Polymer Gels with Potential Model-Network Structure. *Polymer Chemistry* **2014**, *5* (8), 3018–3029. https://doi.org/10.1039/C3PY01692G.

(22)   Tang, S.; Ma, H.; Tu, H.-C.; Wang, H.-R.; Lin, P.-C.; Anseth, K. S. Adaptable Fast Relaxing Boronate-Based Hydrogels for Probing Cell–Matrix Interactions. *Advanced Science* **2018**, *5* (9), 1800638. https://doi.org/10.1002/ADVS.201800638.

(23)   Caldwell, A. S.; Campbell, G. T.; Shekiro, K. M. T.; Anseth, K. S. Clickable Microgel Scaffolds as Platforms for 3D Cell Encapsulation. *Advanced Healthcare Materials* **2017**, *6* (15), 1–8. https://doi.org/10.1002/adhm.201700254.

(24)   Du, D.; Zhou, Z.; Zhu, L.; Hu, X.; Lu, J.; Shi, C.; Chen, F.; Chen, A. TNF-α Suppresses Osteogenic Differentiation of MSCs by Accelerating P2Y2 Receptor in Estrogen-Deficiency Induced Osteoporosis. *Bone* **2018**, *117*, 161–170. https://doi.org/10.1016/j.bone.2018.09.012.

(25)   Wang, L.; Zhao, Y.; Liu, Y.; Akiyama, K.; Chen, C.; Qu, C.; Jin, Y.; Shi, S. IFN-γ and TNF-α Synergistically Induce Mesenchymal Stem Cell Impairment and Tumorigenesis via NFκB Signaling. *Stem Cells* **2013**, *31* (7), 1383–1395. https://doi.org/10.1002/stem.1388.

(26)   Chang, J.; Liu, F.; Lee, M.; Wu, B.; Ting, K.; Zara, J. N.; Soo, C.; al Hezaimi, K.; Zou, W.; Chen, X.; Mooney, D. J.; Wang, C.-Y.; Chien, S. NF-KB Inhibits Osteogenic Differentiation of Mesenchymal Stem Cells by Promoting β-Catenin Degradation. https://doi.org/10.1073/pnas.1300532110.

(27)   Ikenoue, T.; Jingushi, S.; Urabe, K.; Okazaki, K.; Iwamoto, Y. *Inhibitory Effects of Activin A on Osteoblast Differentiation During Cultures of Fetal Rat Calvarial Cells*; 1999; Vol 75.

(28)   Kajita, T.; Ariyoshi, W.; Okinaga, T.; Mitsugi, S.; Tominaga, K.; Nishihara, T. Mechanisms Involved in Enhancement of Osteoclast Formation by Activin-A. *Journal of Cellular Biochemistry* **2018**, *119* (8), 6974–6985. https://doi.org/10.1002/jcb.26906.

(29)   Mulholland, B. S.; Forwood, M. R.; Morrison, N. A. Monocyte Chemoattractant Protein-1 (MCP-1/CCL2) Drives Activation of Bone Remodelling and Skeletal Metastasis. *Current Osteoporosis Reports* **2019**, *17* (6), 538–547. https://doi.org/10.1007/s11914-019-00545-7.

(30)   Shen, H. H.; Yang, C. Y.; Kung, C. W.; Chen, S. Y.; Wu, H. M.; Cheng, P. Y.; Lam, K. K.; Lee, Y. M. Raloxifene Inhibits Adipose Tissue Inflammation and Adipogenesis through Wnt Regulation in Ovariectomized Rats and 3 T3-L1 Cells. *Journal of Biomedical Science* **2019**, *26* (1), 1–12. https://doi.org/10.1186/s12929-019-0556-3.

(31)   Barcelona-Estaje, E.; Dalby, M. J.; Cantini, M.; Salmeron-Sanchez, M. You Talking to Me? Cadherin and Integrin Crosstalk in Biomaterial Design. *Advanced Healthcare Materials*. John Wiley and Sons Inc March 1, 2021. https://doi.org/10.1002/adhm.202002048.

(32)   Cosgrove, B. D.; Mui, K. L.; Driscoll, T. P.; Caliari, S. R.; Mehta, K. D.; Assoian, R. K.; Burdick, J. A.; Mauck, R. L. N-Cadherin Adhesive Interactions Modulate Matrix Mechanosensing and Fate Commitment of Mesenchymal Stem Cells. *Nature Materials* **2016**, *15* (12), 1297–1306. https://doi.org/10.1038/nmat4725.

(33)   Haÿ, E.; Dieudonné, F. X.; Saidak, Z.; Marty, C.; Brun, J.; da Nascimento, S.; Sonnet, P.; Marie, P. J. N-Cadherin/Wnt Interaction Controls Bone Marrow Mesenchymal Cell Fate and Bone Mass During Aging. *Journal of Cellular Physiology* **2014**, *229* (11), 1765–1775. https://doi.org/10.1002/jcp.24629.

(34)   Passanha, F. R.; Geuens, T.; Konig, S.; van Blitterswijk, C. A.; LaPointe, V. L. Cell Culture Dimensionality Influences Mesenchymal Stem Cell Fate through Cadherin-2 and Cadherin-11. *Biomaterials* **2020**, *254*. https://doi.org/10.1016/j.biomaterials.2020.120127.

(35)   Zhu, M.; Lin, S.; Sun, Y.; Feng, Q.; Li, G.; Bian, L. Biomaterials Hydrogels Functionalized with N-Cadherin Mimetic Peptide Enhance Osteogenesis of HMSCs by Emulating the Osteogenic Niche. *Biomaterials* **2016**, *77*, 44–52. https://doi.org/10.1016/j.biomaterials.2015.10.072.

(36)   Marie, P. J.; Haÿ, E.; Saidak, Z. Integrin and Cadherin Signaling in Bone: Role and Potential Therapeutic Targets. *Trends in Endocrinology and Metabolism*. Elsevier Inc. November 1, 2014, pp 567–575. https://doi.org/10.1016/j.tem.2014.06.009.

(37)   Marie, P. J. N-Cadherin-Wnt Connections and the Control of Bone Formation. **2009**, *6* (4), 150–156. https://doi.org/10.1138/20090372.

(38)   Marie, P. J. Role of N-Cadherin in Bone Formation. *Journal of Cellular Physiology* **2002**, *190* (3), 297–305. https://doi.org/10.1002/JCP.10073.

(39)   Chang, J.; Liu, F.; Lee, M.; Wu, B.; Ting, K.; Zara, J. N.; Soo, C.; al Hezaimi, K.; Zou, W.; Chen, X.; Mooney, D. J.; Wang, C. Y. NF-KB Inhibits Osteogenic Differentiation of Mesenchymal Stem Cells by Promoting β-Catenin Degradation. *Proceedings of the National Academy of Sciences of the United States of America* **2013**. https://doi.org/10.1073/pnas.1300532110.

(40)   Zha, L.; He, L.; Liang, Y.; Qin, H.; Yu, B.; Chang, L.; Xue, L. TNF-α Contributes to Postmenopausal Osteoporosis by Synergistically Promoting RANKL-Induced Osteoclast Formation. *Biomedicine and Pharmacotherapy* **2018**, *102*, 369–374. https://doi.org/10.1016/j.biopha.2018.03.080.

(41)   Mosser, D. M.; Edwards, J. P. Exploring the Full Spectrum of Macrophage Activation. *Nature Reviews Immunology*. December 2008, pp 958–969. https://doi.org/10.1038/nri2448.

(42)   Pino, A. M.; Ríos, S.; Astudillo, P.; Fernández, M.; Figueroa, P.; Seitz, G.; Rodríguez, J. P. Concentration of Adipogenic and Proinflammatory Cytokines in the Bone Marrow Supernatant Fluid of Osteoporotic Women. *Journal of Bone and Mineral Research* **2010**, *25* (3), 492–498. https://doi.org/10.1359/jbmr.090802.

(43)   Kim, W.-K.; Choi, E.-K.; Sul, O.-J.; Park, Y.-K.; Kim, E.-S.; Yu, R.; Suh, J.-H.; Choi, H.-S. Monocyte Chemoattractant Protein-1 Deficiency Attenuates Oxidative Stress and Protects against Ovariectomy-Induced Chronic Inflammation in Mice. *PLoS ONE* **2013**, *8* (8), e72108. https://doi.org/10.1371/journal.pone.0072108.

(44)   Killaars, A. R.; Walker, C. J.; Anseth, K. S. Nuclear Mechanosensing Controls MSC Osteogenic Potential through HDAC Epigenetic Remodeling. https://doi.org/10.1073/pnas.2006765117/-/DCSupplemental.

(45)   Hendriks, D.; Macdougald, O.; Bernkopf, D.; de Winter, T. J. J.; Nusse, R. Running Against the Wnt: How Wnt/β-Catenin Suppresses Adipogenesis. *Frontiers in Cell and Developmental Biology / www.frontiersin.org* **2021**, *9*, 627429. https://doi.org/10.3389/fcell.2021.627429.

(46)   Nelson, W. J.; Nusse, R. *Convergence of Wnt,-Catenin, and Cadherin Pathways*.

(47)   Hay, E. H.; Laplantine, E.; Geoffroy, V.; Frain, M.; Kohler, T.; Müller, R.; Marie, P. J. N Cadherin Interacts with Axin and LRP5 To Negatively Regulate Wnt/-Catenin Signaling, Osteoblast Function, and Bone Formation. *Molecular and Cellular Biology* **2009**, *29* (4), 953–964. https://doi.org/10.1128/MCB.00349-08.

(48) Manuel Baizabal-Aguirre, V.; Tyagi, A. K.; Hottiger, M. O.; Ma, B. Crosstalk between Wnt/β-Catenin and NF-KB Signaling Pathway during Inflammation. 2016, 7, 1. https://doi.org/10.3389/fimmu.2016.00378.

Chapter 7

(1) Wechsler, M. E.; Rao, V. v; Borelli, A. N.; Anseth, K. S. Engineering the MSC Secretome : A Hydrogel Focused Approach. **2021**, *2001948*, 1–17. https://doi.org/10.1002/adhm.202001948.

(2) Banfi, A.; Bianchi, G.; Notaro, R.; Luzzatto, L.; Cancedda, R.; Quarto, R. Replicative Aging and Gene Expression in Long-Term Cultures of Human Bone Marrow Stromal Cells. *TISSUE ENGINEERING* **2002**, *8* (6).

(3) Ishihara, A. Effect of Intra-Medullar and Intra-Venous Infusions of Mesenchymal Stem Cells on Cell Engraftment by In-Vivo Cell Tracking and Osteoinductivity in Rabbit Long Bones: A Pilot Study. *Orthopedic & Muscular System* **2014**. https://doi.org/10.4172/2161-0533.1000172.

(4) Wagner, W.; Horn, P.; Castoldi, M.; Diehlmann, A.; Bork, S.; Saffrich, R.; Benes, V.; Blake, J.; Pfister, S.; Eckstein, V.; Ho, A. D. Replicative Senescence of Mesenchymal Stem Cells: A Continuous and Organized Process. *PLoS ONE* **2008**, *3* (5). https://doi.org/10.1371/journal.pone.0002213.

(5) Yang, C.; Tibbitt, M. W.; Basta, L.; Anseth, K. S. Mechanical Memory and Dosing Influence Stem Cell Fate. *Nature Materials* **2014**, *113*, 645–651. https://doi.org/10.1038/NMAT3889.

(6)   Chaudhuri, O.; Cooper-White, J.; Janmey, P. A.; Mooney, D. J.; Shenoy, V. B. Effects of Extracellular Matrix Viscoelasticity on Cellular Behaviour. *Nature* **2020**, *584*, 535. https://doi.org/10.1038/s41586-020-2612-2.

(7)   Saleh, L. S.; Bryant, S. J. The Host Response in Tissue Engineering: Crosstalk between Immune Cells and Cell-Laden Scaffolds. *Current Opinion in Biomedical Engineering* **2018**, *6* (March), 58–65. https://doi.org/10.1016/j.cobme.2018.03.006.

(8)   Anderson, J. M. BIOLOGICAL RESPONSES TO MATERIALS. **2001**.

(9)   Croker, B. A.; O'Donnell, J. A.; Nowell, C. J.; Metcalf, D.; Dewson, G.; Campbell, K. J.; Rogers, K. L.; Hu, Y.; Smyth, G. K.; Zhang, J. G.; White, M.; Lackovic, K.; Cengia, L. H.; O'Reilly, L. A.; Bouillet, P.; Cory, S.; Strasser, A.; Roberts, A. W. Fas-Mediated Neutrophil Apoptosis Is Accelerated by Bid, Bak,and Bax and Inhibited by Bcl-2 and Mcl-1. *Proceedings of the National Academy of Sciences of the United States of America* **2011**, *108* (32), 13135–13140. https://doi.org/10.1073/PNAS.1110358108/-/DCSUPPLEMENTAL.

(10)   McGrath, E. E.; Marriott, H. M.; Lawrie, A.; Francis, S. E.; Sabroe, I.; Renshaw, S. A.; Dockrell, D. H.; Whyte, M. K. B. TNF-Related Apoptosis-Inducing Ligand (TRAIL) Regulates Inflammatory Neutrophil Apoptosis and Enhances Resolution of Inflammation. *Journal of Leukocyte Biology* **2011**, *90* (5), 855–865. https://doi.org/10.1189/JLB.0211062.

(11)   Hachim, D.; LoPresti, S. T.; Yates, C. C.; Brown, B. N. Shifts in Macrophage Phenotype at the Biomaterial Interface via IL-4 Eluting Coatings Are Associated with Improved Implant Integration. *Biomaterials* **2017**, *112*, 95–107. https://doi.org/10.1016/j.biomaterials.2016.10.019.

(12)   Hachim, D.; Lopresti, S. T.; Rege, R. D.; Umeda, Y.; Iftikhar, A.; Nolfi, A. L.; Skillen, C. D.; Brown, B. N. Distinct Macrophage Populations and Phenotypes Associated with IL-4 Mediated Immunomodulation at the Host Implant Interface. *Biomaterials Science* **2020**, *8* (20), 5751–5762. https://doi.org/10.1039/d0bm00568a.

(13)   Lin, C. C.; Metters, A. T.; Anseth, K. S. Functional PEG-Peptide Hydrogels to Modulate Local Inflammation Induced by the Proinflammatory Cytokine TNFα. *Biomaterials* **2009**, *30* (28), 4907. https://doi.org/10.1016/J.BIOMATERIALS.2009.05.083.

(14)   Farokhi, M.; Mottaghitalab, F.; Shokrgozar, M. A.; Ou, K. L.; Mao, C.; Hosseinkhani, H. Importance of Dual Delivery Systems for Bone Tissue Engineering. *Journal of Controlled Release* **2016**, *225*, 152–169. https://doi.org/10.1016/j.jconrel.2016.01.033.

(15)   Yang, Z.; Concannon, J.; Ng, K. S.; Seyb, K.; Mortensen, L. J.; Ranganath, S.; Gu, F.; Levy, O.; Tong, Z.; Martyn, K.; Zhao, W.; Lin, C. P.; Glicksman, M. A.; Karp, J. M. Tetrandrine Identified in a Small Molecule Screen to Activate Mesenchymal Stem Cells for Enhanced Immunomodulation. *Scientific Reports 2016 6:1* **2016**, *6* (1), 1–10. https://doi.org/10.1038/srep30263.

(16)   Nelson, W. J.; Nusse, R. *Convergence of Wnt,-Catenin, and Cadherin Pathways*.

(17)   Barcelona-Estaje, E.; Dalby, M. J.; Cantini, M.; Salmeron-Sanchez, M. You Talking to Me? Cadherin and Integrin Crosstalk in Biomaterial Design. *Advanced Healthcare Materials*. John Wiley and Sons Inc March 1, 2021. https://doi.org/10.1002/adhm.202002048.

(18)   Chang, J.; Liu, F.; Lee, M.; Wu, B.; Ting, K.; Zara, J. N.; Soo, C.; al Hezaimi, K.; Zou, W.; Chen, X.; Mooney, D. J.; Wang, C.-Y.; Chien, S. NF-KB Inhibits Osteogenic

Differentiation of Mesenchymal Stem Cells by Promoting β-Catenin Degradation. https://doi.org/10.1073/pnas.1300532110.

(19)   Imamura, A.; Kajiya, H.; Fujisaki, S.; Maeshiba, M.; Yanagi, T.; Kojima, H.; Ohno, J. Three-Dimensional Spheroids of Mesenchymal Stem/Stromal Cells Promote Osteogenesis by Activating Stemness and Wnt/β-Catenin. *Biochemical and Biophysical Research Communications* **2020**, *523* (2), 458–464. https://doi.org/10.1016/j.bbrc.2019.12.066.

(20)   Manuel Baizabal-Aguirre, V.; Tyagi, A. K.; Hottiger, M. O.; Ma, B. Crosstalk between Wnt/β-Catenin and NF-KB Signaling Pathway during Inflammation. **2016**, *7*, 1. https://doi.org/10.3389/fimmu.2016.00378.

(21)   Ma, B.; Fey, M.; Hottiger, M. O. WNT/β-Catenin Signaling Inhibits CBP-Mediated RelA Acetylation and Expression of Proinflammatory NF-KB Target Genes. **2015**. https://doi.org/10.1242/jcs.168542.

(22)   Aguado, B. A.; Grim, J. C.; Rosales, A. M.; Watson-Capps, J. J.; Anseth, K. S. Engineering Precision Biomaterials for Personalized Medicine. *Science Translational Medicine*. American Association for the Advancement of Science January 17, 2018. https://doi.org/10.1126/scitranslmed.aam8645.